

Hazy 2

a brief introduction
to Cloudy 96

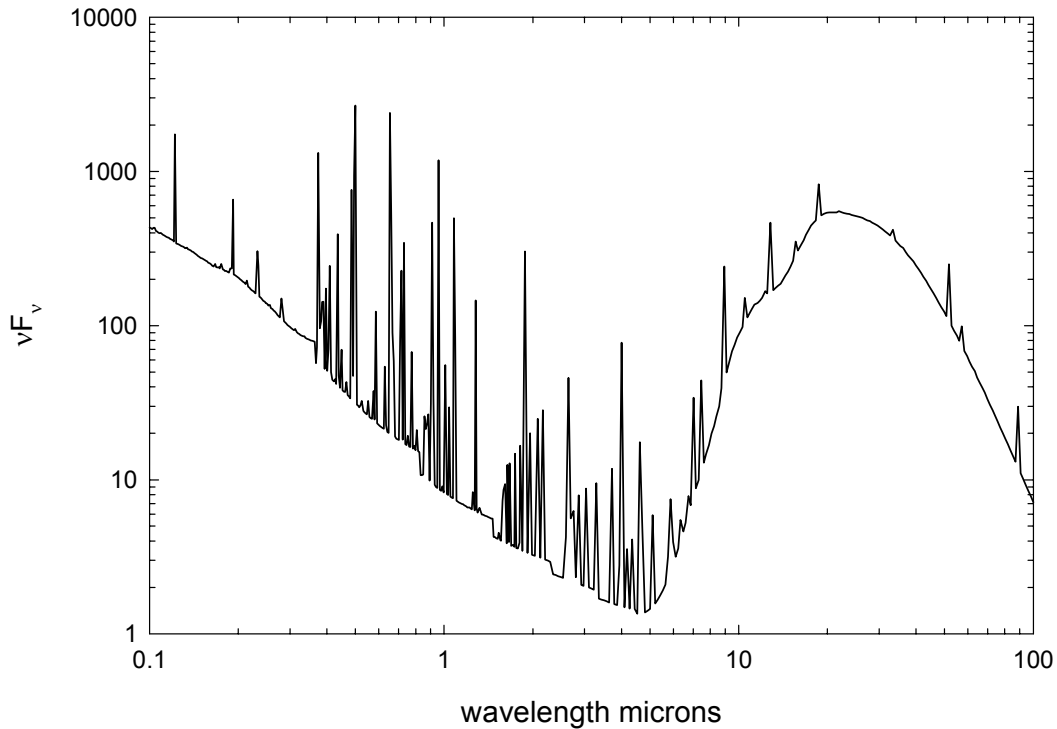
computational methods

G.J. Ferland

Department of Physics and Astronomy

University of Kentucky, Lexington

<http://www.pa.uky.edu/~gary/cloudy>



Use of this program is not restricted provided each use is acknowledged upon publication. The bibliographic reference to this version of Cloudy is Ferland, G.J., 2002, *Hazy, a Brief Introduction to Cloudy 96*, University of Kentucky Department of Physics and Astronomy Internal Report.

Portions of this document have been published, and are copyrighted by, the American Astronomical Society, the Astronomical Society of the Pacific, and the Royal Astronomical Society. The remainder of this document, and the code Cloudy, are copyright 1978-2003 by Gary J. Ferland.

Cloudy is an evolving code. Updates are made on a roughly quarterly basis, while major revisions occur roughly every three years. You should confirm that you have the most recent version of the code by checking the web site <http://www.pa.uky.edu/~gary/cloudy> or asking to be placed on the Cloudy mailing list.

CLOUDY 96

G. J. Ferland

Department of Physics and Astronomy

University of Kentucky

Lexington

Table of Contents

1 INTRODUCTION.....	201
2 LIMITS, ASSUMPTIONS, AND RELIABILITY	202
2.1 Overview	202
2.2 Time Steady	202
2.3 Atomic Database	203
2.3.1 Collisional processes	203
2.3.2 Photoionization cross sections	203
2.3.3 Recombination rate coefficients	203
2.3.4 Charge transfer.....	204
2.4 Continuous Opacity	204
2.5 Hydrogenic isoelectronic sequence	204
2.6 Helium-like isoelectronic sequence	204
2.7 Atoms and Ions of the Heavy Elements	205
2.8 Molecules.....	205
2.9 Temperature Range	205
2.10 Density Range.....	205
2.11 Radiative Transfer.....	206
2.12 Helium radiative transfer	206
2.13 Reliability	207
2.14 The Future.....	208
3 THE CONTINUUM MESH.....	209
3.1 Overview	209
3.2 Continuum Range.....	209
3.3 The Continuum Mesh.....	209
3.3.1 Defining the continuum energy mesh	209
3.3.2 Changing the energy resolution of the mesh.....	209
3.3.3 Array indices within the continuum mesh	210
3.4 Continuum Arrays.....	210
3.4.1 Continuum definition	210
3.4.2 Continuum vectors	211
3.4.3 Continuum optical depth arrays	212
3.5 Continuum Generation	212
3.5.1 Photon occupation number	213
3.5.2 Blackbody emission.....	213
3.6 Energy Units; the Rydberg	213

3.7 Conversion Factors.....	214
4 CONTINUUM INTERACTIONS.....	216
4.1 Attenuation of the Incident Continuum.....	216
4.2 Recombination Equilibrium.....	216
4.2.1 On-the-spot approximation	216
4.2.2 Outward only approximation	217
4.3 Continuous Opacities.....	217
4.3.1 Total opacity arrays.....	217
4.3.2 Cross-section array	217
4.3.3 Photoionization rates	218
4.3.4 Attenuation within the zone	218
4.3.5 Rayleigh scattering.....	219
4.3.6 Free-free opacity	219
4.3.7 Bound-free opacity	220
4.3.8 Plasma frequency	220
4.3.9 Pressure lowering of ionization potential.....	221
5 LINE DETAILS	222
5.1 Overview.....	222
5.2 Line Boltzmann Factors	222
5.3 Optical Depths, Opacities, and Transition Probabilities.....	222
5.3.1 Optical depths.....	222
5.3.2 Oscillator strengths	222
5.3.3 Absorption cross section	222
5.3.4 Velocities in a thermal distribution	223
5.3.5 The Doppler b parameter	223
5.3.6 Line Widths	223
5.3.7 Voigt function	224
5.3.8 Mean vs. line center optical depths	224
5.4 The Einstein Coefficients	224
5.5 Air vs Vacuum Wavelengths	226
5.6 The Line Source Function.....	226
5.7 The Line Escape Probability Functions	226
5.7.1 Incomplete redistribution.....	227
5.7.2 Damping constant	227
5.7.3 Background opacity and Destruction probability	227
5.7.4 Complete redistribution	227
5.7.5 Masing lines	228
5.7.6 Continuum fluorescence	228
5.7.7 Stark broadening	229
5.7.8 Net escape probability	230
5.8 Optical Depths and the Geometry	230
5.8.1 Open geometry	230
5.8.2 Closed geometry overview	230
5.8.3 Wind	230
5.9 Collision Strengths	231
5.10 Born Approximation	231

5.11 The g-bar Approximation	232
5.11.1 The g-bar implementation	232
5.12 The Critical Density	232
5.13 Line Thermalization Length	233
5.14 Averaging Levels into Terms	233
5.14.1 Collision strengths	233
5.14.2 Transition probabilities	233
5.15 Level Populations	234
5.16 The EmLine Structure	235
5.16.1 Overview	235
5.16.2 The main line structures	235
5.16.3 Evaluation of stored quantities	235
5.16.4 Contents of the EmLine structure	235
5.16.5 Dumping the line array	237
5.16.6 Generating a line label	237
5.16.7 Line excitation temperature	237
5.16.8 A Simple Two Level Atom	237
5.16.9 Adding lines to the level 1 line arrays	238
6 THE MODEL ATOM FOR ISO-SEQUENCES	241
6.1 Overview	241
6.2 Departure Coefficients	241
6.3 Level Energies and Boltzmann Factors	242
6.3.1 Pressure lowering of the ionization potential	242
6.4 Recombination Rates and Cooling	242
6.4.1 Formalism	242
6.4.2 Results	243
6.4.3 Recombination coefficients	244
6.5 The Collisional Rate Equations	244
6.6 The Radiative Rate Equations	246
6.6.1 Photoionization - recombination	246
6.6.2 Derivation of radiative balance equations	246
6.6.3 Final radiative equations	246
7 THE HYDROGENIC ISO-SEQUENCE	249
7.1 Recombination Rates and Cooling	249
7.1.1 Rational approximations	249
7.2 Effective Transition Probabilities	251
7.2.1 Einstein As	251
7.3 Collisional contributions to hydrogen lines	252
7.4 Continuous Thermal Emission	252
8 HELIUM ISO-SEQUENCE	255
8.1 Overview	255
8.2 Energy levels	255
8.3 Collisional data	256
8.4 Net emission	256
8.5 The Helium Triplets	256

8.6 Collapsed versus resolved levels	257
8.7 Ionization Equilibria.....	257
9 H⁻ AND MOLECULES	261
9.1 Overview.....	261
9.2 The Saha Equation for Arbitrary Systems.....	261
9.3 The Hydrogen Network	263
9.4 LTE Populations of Hydrogen Molecules.....	263
9.5 The H ⁻ Balance; Radiative Processes	264
9.5.1 Radiative attachment	264
9.5.2 Photodetachment.....	265
9.5.3 Photodetachment by hard photons	265
9.5.4 The approach to LTE; high radiation densities.....	266
9.6 The H ⁻ Balance; Collisional Processes	267
9.6.1 Associative detachment.....	267
9.6.2 Electron collisional detachment	267
9.6.3 Collisional ionization by suprathermal electrons.....	267
9.6.4 Mutual neutralization.....	268
9.6.5 Charge neutralization with heavy elements.....	268
9.6.6 Neglected processes	268
9.6.7 The approach to LTE; high hydrogen densities.....	268
9.7 The HeH ⁺ Molecular Ion	269
9.8 The H ₂ Molecule.....	269
9.8.1 Associative detachment of H ⁻	269
9.8.2 Catalysis on grain surfaces.....	270
9.8.3 Excited atom radiative association	270
9.8.4 Excited molecular dissociation.....	270
9.8.5 Discrete absorption into Lyman and Werner bands	271
9.8.6 Photo-ionization to H ₂ ⁺	271
9.8.7 Collisional dissociation by H ⁰ , He ⁰ , and e ⁻	271
9.8.8 H ₂ cooling.....	272
9.8.9 H ₂ heating	272
9.9 Heavy Element Molecules.....	272
9.9.1 Collisional Processes	273
9.9.2 Photochemical processes and heating.....	273
9.9.3 Cooling.....	273
9.9.4 CO Lines	273
10 THE HEAVY ELEMENTS.....	275
10.1 Overview.....	275
10.2 Solar System Abundances	276
10.3 Periodic Table.....	276
10.4 Ionization Balance	276
10.4.1 Photoionization cross sections.....	276
10.4.2 Auger multi-electron ejection	276

10.4.3 Compton scattering ionization of bound electrons	277
10.4.4 Collisional ionization rate coefficients.....	277
10.4.5 Radiative recombination rate coefficients	277
10.4.6 Low temperature dielectronic recombination.....	277
10.4.7 Charge transfer.....	278
10.5 Ionization Potentials.....	278
10.5.1 Ionization potential array indices.....	278
10.6 Heavy Element Variables.....	280
10.6.1 Atomic weights	280
10.6.2 Ionic and total abundances.....	280
10.6.3 Element names	280
10.6.4 Photoionization rates.....	281
10.6.5 Fluorescence yields.....	281
10.6.6 Ionization potential pointers.....	281
10.7 Isoelectronic Sequences.....	281
10.8 Be-sequence.....	282
10.9 Carbon	282
10.10 Nitrogen	284
10.11 Oxygen.....	284
10.11.1 The O I model atom.....	285
10.12 Neon.....	285
10.13 Magnesium	285
10.14 Aluminum.....	286
10.15 Calcium.....	286
10.15.1 The Ca II model atom.....	286
10.16 Iron.....	287
10.16.1 The FeII model atom.....	287
10.16.2 The FeIV model atom.....	287
10.16.3 Fe K α emission.....	287
10.17 Heavy Element Opacities.....	288
10.18 Overall Reliability	288
10.19 The Bi-Diagonal Matrix.....	291
10.20 Ionization stage trimming.....	291
11 THERMAL EQUILIBRIUM.....	292
11.1 Overview	292
11.2 Thermal Stability	292
11.3 Compton Energy Exchange.....	292
11.4 Bound Compton Ionization, Heating.....	296
11.5 Expansion Cooling.....	296
11.6 Free-free Heating-Cooling	296
11.7 Photoelectric Heating, Recombination Cooling	297
11.8 Collisional Ionization - Three-Body Recombination.....	297
11.9 H $^-$ Heating and Cooling.....	298
11.9.1 H $^-$ bound-free.....	298
11.9.2 H $^-$ free-free.....	298

11.10 Line Heating and Cooling	298
11.10.1 Overview	298
11.10.2 Two level atoms	299
11.10.3 Three level atoms	299
11.10.4 N level atoms	301
11.10.5 Li Sequence	301
11.10.6 Boron Sequence	302
11.10.7 Beryllium sequence atoms	302
11.11 Evaluation of the Cooling Function	303
11.11.1 Total cooling	303
11.11.2 The cooling derivative	303
11.12 Evaluation of the Heating Function	304
11.13 Equilibrium Calculations	304
11.13.1 Hydrogen only	304
11.13.2 Helium-only gas	305
11.13.3 Metal rich gas	305
12 GRAIN PHYSICS	307
12.1 Overview	307
12.2 Grain Opacity	307
12.2.1 ISM grains	307
12.2.2 Orion grains	307
12.2.3 PN grains	308
12.2.4 Extinction	308
12.3 Photoelectric Emission	308
12.4 Collisional Charging of a Grain	310
12.5 Grain Potential	311
12.6 Grain Drift Velocity	311
12.7 Radiative Heating and Cooling of a Grain	311
12.8 Collisional Heating of a Grain	311
12.9 Grain Temperature	312
12.10 Photoelectric Heating of the Gas	312
12.11 Collisional Cooling of the Gas	312
12.12 Grain Sublimation	313
12.13 Ionic Recombination on Grain Surfaces	313
12.14 Grain Variables	313
13 OTHER PHYSICAL PROCESSES	315
13.1 Overview	315
13.2 Magnetic fields	315
13.3 Cosmic Ray Interactions	316
13.4 Line Radiation Pressure	318
13.4.1 Formalism	318
13.4.2 Line width	320
13.4.3 Background opacity and thermalization	320
13.5 Radiative Acceleration	321
13.6 Pressure Laws	321
13.6.1 Units	321

13.6.2 Ideal gas laws	322
13.6.3 Equation of state.....	322
13.6.4 Turbulent pressure?.....	322
13.6.5 Ram or dynamic pressure.....	322
13.6.6 Pressure variables and routines.....	323
13.7 Wind Geometry	323
13.8 Secondary Ionization.....	325
13.8.1 Ionization, heating, and cooling	325
13.8.2 Evaluation of rate of hot electron energy input	325
13.8.3 Secondary rates per atom	325
13.8.4 Total interaction rates.....	326
13.8.5 Rates during the hydrogen balance solution.....	326
13.8.6 Molecules and Suprathermal Electrons.....	326
13.9 Eddington Limit.....	327
13.10 Jeans Length and Mass.....	327
13.11 Luminosity Distance.....	327
14 GLOSSARY OF SYMBOLS	329
15 REFERENCES	333
16 INDEX	343

List of Figures

Free-free gaunt factors.....	220
Hydrogen level populations vs density.....	245
Hydrogen level populations vs radiation density	247
Hydrogen recombination cooling.....	250
Collisional contributions to hydrogen lines.....	252
Thermal emission from nebular gas.....	253
Thermal emission near LTE.....	254
He-iso sequence atom.....	255
He I energies compared with hydrogen.....	256
He-iso sequence wavelengths	256
l-mixing vs quantum number	257
Net atomic He emission	260
H- departure coefficients vs radiation density	266
H- associative detachment formation of molecular hydrogen.....	267
H- departure coefficients vs density	269
Solar System Abundances	275
Iron photoionization cross sections.....	277
Density of Ionization Potentials.....	280
Grotrian diagrams.....	282
Be-like model atom	285
The O I model atom.....	285
The Ca II model atom.....	286
Fe II IR model atom	287

Fe IV model atom	287
Fe $K\alpha$ fluorescence yield and energy	288
Opacity of neutral gas at high energies	289
Thermal equilibria in the Compton limit	294
Thermal equilibria near the Compton limit	295
Beryllium sequence model atom	302
Boron Sequence	302
The approach to thermodynamic equilibrium	305
Thermal equilibrium of metal-rich gas	306
Wind velocity vs depth	324

List of Tables

Conversion Factors	215
Line Boltzmann Factors	222
Needed Line Parameters	239
Hydrogen recombination coefficients	243
Recombination cooling coefficients	250
He $n=2$ emission lines	258
Helium levels	259
CO rotation lines	273
Ionization Potentials of the Elements	278
Isoelectronic Sequences	283
Ionization Balance Reliability	288
Lithium Sequence Lines	302
Secondary Ionization Efficiencies	326

1 INTRODUCTION

This section outlines the physical processes incorporated into version 96 of Cloudy. Parts are modified from Ferland and Mushotzky (1984), Ferland and Rees (1988), Ferland and Persson (1989), Rees, Netzer, and Ferland (1989), Baldwin et al. (1991), Ferland, Fabian, and Johnstone (1994), Ferland et al. (1992), Ferland (1992) and Ferland et al. (1998). The code has been designed to be as general as possible, but limited to non-relativistic regimes which are not Compton-thick.

The development of Cloudy is resource limited, and updating this volume of the documentation has received a low priority. Parts that were badly out of synch with the current code have been removed, but some parts of this document don't reflect the current status of the code. Sorry.

Good reviews of the processes that are important in these environments are given by Davidson & Netzer (1978) and Osterbrock (1989). I helped organize two meetings, *Quasars and Cosmology* (1999; ASP Conf Volume 162; Ferland & Baldwin, editors) and *Spectroscopic Challenges of Photoionized Plasmas* (ASP Conf Volume 247; Ferland & Savin, editors). The articles in these books discuss many aspects of the plasma codes, photoionization equilibrium, and their application to astronomical spectroscopy.

2 LIMITS, ASSUMPTIONS, AND RELIABILITY

2.1 Overview

This section outlines some of the assumptions and limits that define the range of validity of Cloudy. The code is designed to check that these limits are not exceeded during a calculation. This self-checking is a central feature of the code since it is designed to be used to compute large grids with thousands of models, where the examination of individual results would not be possible. Cloudy should print a warning after the last zone results if any aspects of the calculation are on thin ice.

2.2 Time Steady

Cloudy makes no assumptions that the gas is in equilibrium. In most cases it does, however, assume that atomic processes occur on timescales that are much faster than other changes in the system, so that atomic rates have had time to become time-steady. Although it is possible to follow the time-dependent recombination and cooling of an optically thin cell of gas with the **time** command, and advection is included when wind solutions are done, most cases assume that the cloud is old enough for atomic processes to have become time steady. The **age** command (described in Part I of this document) should be used to specify the age of the cloud. If the cloud age is set then the code will confirm that the time-steady assumption is valid by comparing the system's age with a host of rates and timescales, and will generate a warning if the environment is not time-steady.

Various time scales characterize the approach to equilibrium of an ionized gas (see Spitzer, 1962, and Ferland 1979 for a specific application). Generally, for an ionized gas with nebular temperatures ($\approx 10^4$ K), the longest is the H^+ recombination time scale,

$$T_{rec} = \frac{1}{\alpha_A(T_e)n_e} = 7.6 t_4^{0.8} n_4^{-1} \text{ years} = 0.66 t_4^{0.8} n_9^{-1} \text{ hours} \quad (1)$$

where t_4 is the temperature in units of 10^4 K, and n_9 is the electron density in units of 10^9 cm^{-3} , and case A recombination is assumed.

For situations where molecules are important the time scales are usually far more ponderous. Generally among the longer of the time scales is the time to form H^- , an important pacesetter for H_2 formation in grain-free environments. This time scale is roughly given by

$$T_{molecule} = \frac{1}{\alpha_{rad}(T_e)n_e} = 0.3 t_3^{-0.8} n_9^{-1} \text{ years} \quad (2)$$

where t_3 is the temperature in units of 10^3 K.

Cloudy is not appropriate for the treatment of environments where conditions change more rapidly than the slowest of the equilibrium time scales.

Use the **age** command to be safe.

2.3 Atomic Database

This section outlines some of the atomic and molecular physics issues that affect the reliability of numerical simulations of nebulae. These uncertainties were extensively discussed in the Lexington Plasma 2000 meeting (ASP Conf series 247, *Spectroscopic challenges of photoionized plasmas*, Gary Ferland & Daniel Savin, editors) and they underscore the importance of atomic and molecular physics for the interpretation of astrophysical spectroscopy.

2.3.1 Collisional processes

By its nature, the electron temperature of a photoionized gas is low compared with the ionization temperature of the mixture of atoms and ions, as defined by the Saha equation (if the two were comparable, the gas would be collisionally ionized). Because of this, the rate coefficients describing collisional effects, such as the production of cooling emission lines, are often dominated by the cross sections near threshold. This is where laboratory experiments are difficult and *ab initio* quantum theory must often be used. As a result, the collision strengths undergo constant revision, towards better and more reliable values.

To cite one extreme example, the collision strength for transitions within the 3P ground term of Ne^{+4} underwent three revisions between 1984 and 1991, each by a factor of 10, because of theoretical uncertainties in positions of autoionizing states with unknown energies (Lennon and Burke 1991). The intensities of all emission lines can be affected by major changes in the atomic data for only one line for some conditions. This is because (in this case) the infrared fine structure lines of Ne^{+4} can be important coolants in low-density high-ionization gasses such as planetary nebulae, and changing their cooling rate alters the thermal structure of the entire nebula. Such changes often give even models of time-steady objects such as planetary nebulae certain time-dependent characteristics.

At present, there are fairly reliable calculations of collision strengths and transition probabilities for the majority of the strong optical and ultraviolet lines in moderate ionization nebulae. A series of papers by Oliva and collaborators (see Oliva et al. 1996 and also van Hoof et al. 2000) outline observational evidence concerning accuracies in collision strengths of moderate ionization far infrared lines. This is clearly an area of uncertainty and concern.

2.3.2 Photoionization cross sections

The photoionization cross-section database has undergone a dramatic improvement with the completion of the Opacity Project (Seaton 1987) and its fitting with analytic approximations (Verner et al., 1996). These are the photoionization cross sections used by Cloudy and they should be as accurate as 10%. All inner shell multi-electron processes are included (Kaastra and Mewe 1993) using distorted wave cross sections (referenced in Verner et al.). This part of the data base is in fairly good shape, although greater accuracy is always desired.

2.3.3 Recombination rate coefficients

Recombination from closed shell species is accurately known (Verner and Ferland 1996) since these are dominated by radiative recombination. Reliable dielectronic

recombination coefficients do not now exist for most other stages of ionization. Currently there is no theory that can reproduce the best experiments (Savin et al. 1999). For these, Cloudy uses the guestamates described in Part I of this document. This is clearly the greatest single gap in the atomic data base today. Savin (2000) shows an example where this uncertainty has a direct impact on cosmological studies.

2.3.4 Charge transfer

The rate coefficients for charge transfer are another uncertainty in the atomic and molecular database. This process is sometimes the dominant neutralization mechanism for singly or doubly ionized heavy elements. At present many charge exchange rate coefficients are the result of Landau-Zenner calculations using semi-empirical potential curves (Kingdon and Ferland 1996; 1999). These are thought to be no more accurate than a factor of three. Even the best quantal calculations are not thought to have an accuracy much better than 50 percent. Unpublished tests suggest that these uncertainties affect some line intensities at the ~20% level, and a few by more than this.

2.4 Continuous Opacity

All significant continuous opacity sources are treated for the energy range considered by the code, 1.001×10^{-8} Ryd to 7.354×10^6 Ryd. These opacity sources include inverse bremsstrahlung, grains (when present), H^- absorption, electron scattering, the damping wings of strong resonance lines (i.e., Rayleigh scattering), pair production, photoelectric absorption by the ground and excited states of all ions of the lightest 30 elements, and photoabsorption by molecules. This treatment should be adequate as long as the optical depths to electron scattering are not large. Cloudy is not now designed to simulate Compton-thick regimes. (A warning will be issued after the last zone calculation if the nebula is very optically thick to electron scattering.)

2.5 Hydrogenic isoelectronic sequence

The 30 atoms and ions of the hydrogenic iso-electronic sequence (H^0 , He^+ , through Zn^{+29}) are treated as complete multi-level atoms. The $2s$ and $2p$ states are treated separately, so $L\alpha$ and 2-photon emission are computed properly in low-density nebulae. Higher levels are assumed to be well l-mixed. Up to 400 levels can be included. Tests show that the hydrogen line emissivity predicted by Cloudy agrees with Hummer and Storey's (1987) case B $H\beta$ emissivity predictions to a few percent for all densities and temperatures (Ferguson & Ferland 1997). Details are given in Part II, and in Ferguson and Ferland (1997).

2.6 Helium-like isoelectronic sequence

The 29 atoms and ions of the helium-like isoelectronic sequence (He^0 , Li^+ , through Zn^{+28}) are treated as many-level systems. All ns levels are resolved, and there is no limit to the number of levels that can be considered. Details will be presented in a future paper (Porter et al. in preparation).

2.7 Atoms and Ions of the Heavy Elements

Most ions of the remaining heavy elements are treated as two-level systems (ground term and continuum) although photoionization from excited states is included for those cases where it is sometimes important (O^{++} and N^+ are two examples). Charge transfer, radiative and dielectronic recombination, collisional ionization, and three-body recombination processes are included in the ionization balance.

The treatment of the heavy element ionization balance should be exact in the nebular limit, but approximate for very high photon or particle densities because of the two-level atom approximation.

2.8 Molecules

At the present time a major effort is being made to complete the treatment of the heavy-element molecular equilibria and cooling in the code. The treatment of the hydrogen molecules/ions H , H_2 , H_2^+ , H_3^+ , and HeH^+ are now fairly complete and these go to LTE at high densities. The equilibrium of the heavy-element molecules OH , OH^+ , CH , CH^+ , O_2 , O_2^+ , CO , CO^+ , H_2O , H_2O^+ , H_3O^+ , and CH_2^+ is treated following Hollenbach and McKee (1979, 1989). The predictions are thought to be correct for nebular ($n < 10^8 \text{ cm}^{-3}$) conditions, but do not now go to LTE in the high nucleon-photon limits. The code may have convergence problems in the fully molecular limit.

Ferland, Fabian, & Johnstone (1994; 2002) discuss applications to grain-free molecular environments, showing how the gas goes from the fully ionized, to fully molecular, limits.

2.9 Temperature Range

Cloudy assumes that the electrons are non-relativistic, which limits it to temperatures below roughly 10^9 K . Tests presented in Parts II and III show that Cloudy goes to the Compton temperature of the radiation field to great accuracy in the limit of very high levels of ionization for blackbody radiation fields with temperatures between 2.8 K and 10^{10} K . There is no formal lower temperature limit to its validity. Note that very cold gas is rarely in steady state, however.

The present range of validity of the code is approximately from 10 K to 10^9 K . Temperatures outside this range can still be treated, although with greater uncertainty. The code will not permit temperatures below 2.8 K or above 10^{10} K .

2.10 Density Range

There is no formal lower limit to the density that Cloudy can treat. The set of heavy element fine structure lines, which dominate cooling at low densities, is complete for astrophysically abundant elements, and fine structure line optical depths, continuum pumping, and maser effects are fully treated using the escape probability formalism.

There is no formal high-density limit, although the simulation is less complete at high densities. The biggest concerns are the (inexact) treatment of radiative transfer

(see Avrett and Loeser 1988) and the approximate treatment of the collisional-radiative ionization processes for excited levels of the heavy elements. All species of H-like and He-like isoelectronic sequences are treated as many-level atoms, including all of the physical processes that allow the approach to LTE (see, for example, Mihalas 1978). Tests with a hydrogen density of 10^{19} cm^{-3} show that the hydrogen and helium atoms and the hydrogen molecules go to LTE at high densities. The treatment of Stark broadening for hydrogen lines follows Puetter (1981), so radiative transfer is treated correctly (in the context of the escape probability formalism) for densities above $\sim 10^{10} \text{ cm}^{-3}$.

The treatment of the other 28 isoelectronic sequences is presently not as complete as the H and He-like sequences. Three-body recombination is included as a general recombination process, so the treatment of these elements is approximately correct at high densities.

Cloudy has been tested at densities of 10^{-8} cm^{-3} and 10^{19} cm^{-3} on 32-bit machines. The numerical (not physical) limit to the density will actually be set by the limits to the range of the floating point numbers allowed by the machine in use. The physics incorporated in the code imposes no lower limit to the density. The physical high-density limit is roughly 10^{13} cm^{-3} , and is set by the approximate treatment of three-body recombination - collisional ionization for the heavy elements and line transfer. Non-LTE ionization, thermal equilibria, and line transfer at high densities are areas of on-going research.

2.11 Radiative Transfer

Line intensities are predicted with stellar atmosphere conditions in mind. Radiative transfer effects, including continuum pumping and possible maser emission, are treated. Nebular approximations, such as the approximation that all atoms are in the ground state, are not made. Collisional effects, including excitation and de-excitation, continuum fluorescence, recombination, etc, are all included as general line excitation mechanisms. The treatment of level populations is designed to go to LTE in the high particle or photon density cases.

Line and continuum transfer is currently treated using escape probabilities. This is probably the weakest assumption in the present prediction of the spectrum. Work is now underway to begin the conversion to formally correct transport methods. There is no way to judge the error introduced by the escape probability approximation, although it is known to be exact if the conditions do not vary across the line forming region (Elitzur 1982).

2.12 Helium radiative transfer

The helium line and continuum transfer problems are ones whose importance in determining the intensities of many ultraviolet lines is generally underestimated (see, for example, the discussion by Netzer and Ferland 1983). Recombinations to the He⁺ ground and first excited state, and He II $L\alpha$, all ionize hydrogen, and the He II $L\alpha$ line undergoes Bowen fluorescence (Osterbrock 1989; Netzer, Elitzur, and Ferland 1985). Unfortunately these continua, and especially the Bowen lines, can be the main source of photoelectric heating in the He⁺⁺ zone of some high-ionization nebulae.

Fundamental uncertainties in the treatment of the Bowen problem introduce substantial uncertainties in the local heating rate, and hence in the intensities of some ultraviolet lines, such as C III] $\lambda 1909$ and C IV $\lambda 1549$, because these lines are very temperature sensitive. My experience is that minor changes in the treatment of the Bowen problem typically results in $\sim 20\%$ changes in the intensities of these ultraviolet lines in certain low density nebulae, and in the near ultraviolet [Ne V] lines.

2.13 Reliability

Several issues affect the general question of the reliability of the code. The first is the effects of the bugs that surely must exist in a code the size of Cloudy. I have seldom found bugs in sections of the code older than roughly two to three years. Younger sections of the code sometimes contain bugs that only manifest themselves in exceptional situations. It is my belief that the issue of reliability in the face of complexity will increasingly be the single major problem limiting the development of large-scale numerical simulations (Ferland 2001b). New methods of writing code will have to be developed if we are to take full advantage of the power of future machines. Machines are getting faster more quickly than people are getting smarter.

The second issue is the validity of the numerical methods used to simulate conditions in the plasma. Fundamental uncertainties arise for cases where the density is high ($n \gg 10^{10} \text{ cm}^{-3}$). The radiative transfer techniques used by Cloudy are approximate (see the discussion by Avrett and Loeser 1988). Unfortunately, no definitive calculation now exists for the complete non-LTE equilibrium and emission for an intermediate density ($\sim 10^{13} \text{ cm}^{-3}$) cloud. For less extreme conditions ($n < 10^{10} \text{ cm}^{-3}$) nebular approximations are valid, and the comparisons presented in Part III show good agreement between Cloudy and other codes designed to work in this limit. Test cases that are designed to exercise the code in well-posed limits and for certain standard nebulae are also presented in Part III. The code is well behaved and agrees with predictions of similar codes in these limits. The discussion presented in Ferland et al. (1995) and Péquignot et al. (2001) suggests that 10% accuracy can be reached for the intensities of the stronger lines.

Uncertainties in the atomic database are a third concern. A great deal of progress will result over the next few years with the completion of the Opacity Project (Seaton 1987) and its extensions to the "Iron Project" (Hummer et al. 1993). Charge transfer, a collision process normally treated on a molecular basis, remains an uncertainty, and the current status of dielectronic recombination theory is a problem (Savin 2000).

In the end the uncertainties can probably best be judged by looking at both the dispersions among the various photoionization calculations presented in Part III and Ferland et al. (1995) and Péquignot et al. (2001), and the changes that have occurred in the predictions made by Cloudy itself over the past few years (see also Part III). Much of the dispersion is due to improvements in the atomic database.

There can be little better way to close a discussion of reliability than to quote the warning included in Kurucz's (1970, page xiii) description of ATLAS5, a code more than an order of magnitude smaller than Cloudy:

WARNING

“There is no way to guarantee that ATLAS5 does not contain errors. In fact, it is almost certain that it does, since the code is so long. There also may be truncation or underflow problems on computers like an IBM 360, even though all those known at present have been allowed for. We also point out that the computation of a model atmosphere should be considered a physical experiment. The program may not be able to calculate a model for conditions that do not occur in real stars or for conditions that violate the initial assumptions on which the program is based.”

The comparisons presented by Ferland et al. (1995) and Péquignot et al. (2001) show that predictions by the best photoionization codes agree within 10% of one another. It is not significant to try to reproduce a spectrum to better than this.

2.14 The Future

The eventual goal is for Cloudy to give reliable results for all extremes of conditions between and including the intergalactic medium and stellar atmospheres. I estimate that the code is now well over halfway complete.

Current work centers on making the code formally correct in the optically thin limit for all extremes of radiation and matter densities. Much has already been done, and present efforts center on molecules and the heavy elements.

Line transfer is now treated with escape probabilities, an approximation that is not formally correct when conditions vary across the line-forming region. A major change, to be completed within the next few years, is to transfer $L\alpha$ correctly, using the proper redistribution function, using an approach similar to that of Hummer and Kunasz (1980). The two major remaining concerns will be the continuum transport (especially in the infrared) and line transfer (complete redistribution is a good approximation for most lines). Both can be treated straightforwardly using standard radiative transfer techniques, especially the accelerated lambda operator (ALO) methods now being developed, and expanded to do higher-order geometries.

By the time this work is complete, the Opacity and Iron Projects, and their extensions to recombination, should also be finished, and attention will return to the heavy elements. An approach similar to that now used for helium (employing several pseudo-states to allow the model atom to correctly approach LTE) will be used to ensure that the treatment of the heavy elements is correct for all densities and temperatures.

An effort is now underway with Robin Williams, Will Henney, and Jane Arthur, to incorporate sufficient hydrodynamics into the code to solve the D-critical ionization front problem. This impacts any calculation that extends from an H II region into the background PDR. Doing such simulations are a high priority for the near future.

3 THE CONTINUUM MESH

3.1 Overview

Under most circumstances the continuum produced by the central object is the only source of heat and ionization for the emission-line clouds. This section describes how this continuum is treated.

Variables dealing with the continuum mesh are contained within the structure *rfield*, defined in the header file *rfield.h*. The following sections refer to parts of that structure.

3.2 Continuum Range

The energy interval 1.001×10^{-8} Ryd – 7.354×10^6 Ryd is divided into ~130000 energy bins with nearly logarithmically increasing widths. This number is stored as the code variable *NCELL*, and it will be necessary to increase it if more continuum bins are needed.

enum This is the low-energy limit to the continuum array. It can only be changed by modifying the statement where its value is set. Its current value is 1.001×10^{-8} Ryd.

egamry This is the high energy limit to the continuum array. The current value is 7.354×10^6 Ryd.

nupper This is the number of cells needed to define the continuum from the low energy limit, up to its high energy limit of 7.354×10^6 Ryd. It does not depend on the continuum shape but does depend on how fine the continuum mesh is. Array indices within the continuum arrays can be defined up through an energy of *egamry*, and they will have the value *nupper*. A particular continuum source may not extend this high, as discussed next.

nflux Each of the continuum intensity vectors is defined up to the high-energy limit for the particular continuum generated. The array index for this higher energy limit is the variable *nflux*. *nflux* is chosen so that, for the highest energy considered, $v_{\text{high}} = \text{anu}(\text{nflux})$, $v_f(v_{\text{high}})/v_f(v_{\text{peak}}) < \text{FluxFaint}$, where v_{peak} is the frequency where the continuum reaches its maximum v_f . *FluxFaint* is normally 10^{-10} and is reset with the `set flxfnt` command.

3.3 The Continuum Mesh

3.3.1 Defining the continuum energy mesh

The array *anu* gives the energy of the center of each continuum cell, in Rydbergs. This energy scale is defined in routine *ContCreatePointers*.

3.3.2 Changing the energy resolution of the mesh

The file *continuum_mesh.dat* contains ordered pairs of continuum energies and resolutions that are read by *ContCreatePointers* to set the continuum mesh when calling *fill*. Change the contents of *continuum_mesh.dat* to change the resolution of the continuum mesh. The first number on each line is the upper bound of a continuum energy interval, and the second number is the fractional resolution $\delta v/v$, where v is the photon frequency. Comments within the file explain its parameters.

If the energy resolution is increased then the code will require more mesh points to cover the full continuum and will run more slowly, but the predicted continuum will have greater detail.

3.3.3 Array indices within the continuum mesh

After the continuum energy scale is defined, one of the following routines is used to find the array index corresponding to a given energy.

ipoint This function converts energies (Rydbergs) into array indices for the cell in *anu* containing the specified energy. It has a single argument, the energy in Rydbergs, and returns the index for the appropriate cell. *ipoint* will stop if the energy does not lie within the continuum bounds of the code.

In most cases the previous routine is not used, but rather one of the following routines used instead (they call *ipoint*). The difference is that the following routines take two arguments, the energy in Rydbergs and a four-character null terminated string that identifies the line or continuum. An index for an emission line should be generated with a call to *ipLineEnergy* and a continuum edge to *ipContEnergy*.

ipLineEnergy This routine calls *ipoint* and generates an index for the energy of an emission line. Line labels are stored in the four-character array *chLineLabel*. In some cases it is important that a line index not exceed a certain value. For instance, energy would not be conserved if a Lyman line overlapped with the Lyman continuum. This routine has a third argument, an array index. If this is greater than zero then this routine will guarantee that the returning index does not equal or exceed this value.

ipContEnergy This routine calls *ipoint* and generates an index to the energy of a continuum edge. Continuum labels are stored in the four-character array *chContLabel*.

There are two arrays of character strings that identify lines (*rfield.chLineLabel[ip]*) and continuum (*rfield.chContLabel[ip]*) edges throughout the continuum arrays. The array index is the index for the energy within the continuum mesh.

3.4 Continuum Arrays

Several vectors deal with aspects of the attenuated incident and diffuse continua. All fluxes are stored in units photons cm⁻² s⁻¹ cell⁻¹ and they all map one-to-one with one another.

3.4.1 Continuum definition

anu The energy (in Rydbergs) of the center of each cell is stored in the vector *anu*. There are *nupper* cells with defined energies. This energy grid *does* have a weak dependence on continuum shape since the center of the cell is defined by a weighted average over the incident continuum.

AnuOrg This array saves the initial frequency array, so that it may be reset when the code is initialized during computations of many grid models. The opacity array is defined using this energy array.

ContBoltz Continuum Boltzmann factors, the ratio $\exp(-h\nu/kT)$, are stored in the vector *ContBoltz*.

widflx The width of each cell (Rydbergs) is stored in the vector *widflx*. There are *nupper* cells with defined widths. This energy grid does not depend on the continuum shape.

3.4.2 Continuum vectors

These store information relevant to the local radiation field. All are members of the structure *rfield*.

Outward continua:

ConOutNoInter This is a continuum that is carried outward, but does not interact with the gas. It contains mainly continua whose gas interactions are included by other methods, such as OTS. This does not affect the ionization of the gas directly, but is included in the punched continuum.

ConOutRecInter This contains ground state recombination continua that are carried outward.

ConOutInter stores the continua that are carried outward and treated as sources of ionizing radiation. This continuum is the local outward continuum at the current position within the nebula, with correction for the r^{-2} dilution of radiation.

outlin stores the many lines that are carried outward and treated as sources of ionizing radiation.

Reflected continua:

ConRefIncid This is the reflected incident continuum.

ConRefDiff This is the diffuse continuum emitted in the inward direction.

reflin The “reflected” lines (that emergent from the illuminated face of the cloud) are stored in the vector *reflin*. Throughout the calculation the reflected continuum and lines are stored relative to the inner radius of the cloud. This is only computed for an open geometry.

Local diffuse continua

Continuous diffuse emission is evaluated in routine *RTDiffuse*.

ConLocInter This stores the local diffuse continuum (total local emission due to all processes, *per unit volume* with no filling factor).

ConLocNoInter This is the non-interacting local continua.

flux The attenuated incident continuum is stored in the vector *flux*. The actual contents of *flux* are given by

$$flux(\nu) = 4\pi J_{inc} \frac{\Delta\nu}{h\nu} \text{ [photons cm}^{-2} \text{ s}^{-1}] \quad (100)$$

where the cell width $\Delta\nu$ is *widflx*.

Continuum occupation numbers

OccNumbDiffCont and *OccNumbIncidCont* The photon occupation number (see page 213 below) associated with the attenuated incident continuum is stored in the vector *OccNumbIncidCont*. The occupation number associated with the diffuse continuum is given by *OccNumbDiffCont*.

On the Spot arrays

otscon and *otslin* Two vectors, *otscon* and *otslin*, store the local on-the-spot (OTS) photon fluxes for continua and lines. Both are totally local rates.

Summed continua:

Several continua are summed together to speed up the evaluation of the local interaction rates. This is done in routine *SumContinuum*.

SummedDif This is summed diffuse continua.

SummedCon This is the sum of *SummedDif* and *flux*, the attenuated incident continuum.

SummedOcc This is the continuum occupation number (defined on page 213 below) corresponding to *SummedCon*.

3.4.3 Continuum optical depth arrays

These arrays define the gas opacity and are members of the *opac* structure.

TauAbsFace, *TauScatFace* These are the arrays containing the absorption and scattering optical depths from the current position to the illuminated face of the cloud.

TauAbsFace, *TauScatFace*, *TauTotalGeo* Total absorption, scattering, and total (absorption plus scattering) optical depths are stored in three arrays, *TauAbsFace[2][ncell]*, and *TauScatFace[2][ncell]*, *TauTotalGeo[2][ncell]*, respectively. These map one-to-one with the *anu* that give the photon energy.

The first element of the first dimension of the array gives the optical depth from the illuminated face to the current position. The second element gives the total optical depth determined in the previous iteration. For an open geometry this optical depth is only the optical depth of the computed structure. For a closed geometry the optical depth at the illuminated face is set equal to the computed optical depth.

ExpTau The vector *ExpTau* contains the attenuation term $\exp(-\tau_\nu)$ for each frequency in *anu*. This is the attenuation from the current position to the illuminated face of the cloud.

e2TauAbs The vector *e2TauAbs* contains the term $E_2(\tau)$ where τ is the absorption optical depth from the current position to the illuminated face of the cloud.

ExpZone This is the term $\exp(-d\tau)$ for the current zone.

opac This is the array of continuous absorption opacities (with units cm^{-1}). It is evaluated in *addopc*.

scatop This is the array of continuous scattering opacities (units cm^{-1}). It is evaluated in *addopc*.

3.5 Continuum Generation

The continuum is generated by the function *ffun*. *ffun* has a single argument, the energy in Rydbergs, and it returns the number of photons per unit area, time, and Rydberg, at that energy. *ffun* sums over all the specified continua and applies the appropriate normalization factors. Another function, *ffun1*, evaluates each individual continuum, and is normally called only by *ffun*.

The units, and their conversion to other measures of the continuum, are given below. The photon flux density is:

$$\varphi_\nu(\nu) = \text{ffun}(\nu) \text{ [photons cm}^{-2} \text{ s}^{-1} \text{ Ryg}^{-1}] . \quad (101)$$

This is stored in the photon array:

$$\text{flux}(\nu_i) = \varphi_\nu(\nu) \delta\nu_i = \text{ffun}(\nu_i) \times \text{widflx}(\nu) \text{ [photons cm}^{-2} \text{ s}^{-1}] . \quad (102)$$

Finally, the energy flux density is given by

$$f_\nu(\nu) = \text{ffun}(\nu) h \left(\frac{\nu}{\nu_{912}} \right) \text{ [erg cm}^{-2} \text{ s}^{-1} \text{ Hz}^{-1}] \quad (103)$$

and

$$\nu f_\nu(\nu) = \text{ffun}(\nu) h \left(\frac{\nu}{\nu_{912}} \right) \nu_{912} h \nu_{\text{Ryd}} \text{ [erg cm}^{-2} \text{ s}^{-1}] . \quad (104)$$

3.5.1 Photon occupation number

The dimensionless occupation number at a frequency ν is defined as

$$\eta_\nu \equiv J_\nu / (2h\nu^3 / c^2) = [\exp(h\nu / kT_{ex}) - 1]^{-1} . \quad (105)$$

Here J_ν is the mean intensity of the continuum at the frequency (erg cm⁻² s⁻¹ Hz⁻¹ sr⁻¹), and T_{ex} is the excitation temperature of the continuum at the frequency.

3.5.2 Blackbody emission

For reference, the Planck function is given by

$$B_\nu = I_\nu = \frac{F_\nu}{\pi} = \frac{2h\nu^3}{c^2} \frac{1}{\exp(h\nu / kT) - 1} \text{ [erg cm}^{-2} \text{ s}^{-1} \text{ sr}^{-1} \text{ Hz}^{-1}] \quad (106)$$

where F_ν is the single-hemisphere emittance from an opaque surface. Function *plankf* evaluates the Planck function for the current electron temperature. It has a single argument, a pointer to the desired continuum energy. It returns the photon flux for that cell. The photon occupation number of a blackbody is then

$$\eta_\nu = \frac{1}{\exp(h\nu / kT) - 1} \quad (107)$$

3.6 Energy Units; the Rydberg

Continuum energies are usually given in Rydbergs. One Rydberg is approximately equal to the ionization potential of hydrogen, which is

$$R_H \equiv 2.178728 \times 10^{-11} \text{ erg} = 13.59842 \text{ eV} = 91.176340 \text{ nm} = 109677.576 \text{ cm}^{-1} \quad (108)$$

This was the Rydberg unit used by Cloudy before 1988, and *is not* the more commonly used R_∞ for infinite mass nuclei.

The energy scale is now in terms of R_∞ using the 1998 CODATA revision of the fundamental constants (see Cohen and Taylor 1987; Mohr & Taylor 1998). In these units, the wavenumber corresponding to R_∞ is

$$R_\infty \equiv \frac{2\pi^2 m_e q_e^4}{ch^3} = 109737.315 \text{ cm}^{-1} , \quad (109)$$

the wavelength in vacuum is

$$1/R_\infty = 91.126732 \text{ nm}, \quad (110)$$

the frequency is

$$c R_\infty = 3.289842 \times 10^{15} \text{ s}^{-1} , \quad (111)$$

and this corresponds to an energy

$$1 \text{ Ryd} = chR_\infty = 2.179874 \times 10^{-11} \text{ erg} = 13.605698 \text{ eV} = 1.5788866 \times 10^5 \text{ K} . \quad (112)$$

Thus the ionization potential of hydrogen is actually 0.99946 Ryd. The difference between the H and infinite mass constants is significant since it enters as the third power in the photon phase-space conversion factor $2h\nu^3/c^2$.

Another commonly used unit is the “atomic unit”, also called the Hartree, which is equal to *two* Rydbergs (i.e., $2R_\infty$).

3.7 Conversion Factors

Table 16 gives conversion factors between various common units. The last column of the table gives the variable names for constants that occur within the code. Most are defined as macros within the header file **physconst.h**. These should be used instead of entering the constant directly. In the following all Rydbergs are for infinite mass nuclei.

The fundamental constants now used by the code are from the 1998 CODATA recommended values (see <http://physics.nist.gov/cuu/Constants/index.html>) and are in the header file *physconst.h*. Derived quantities should be formed from the fundamental quantities given there, so that any future changes will trickle down into all parts of the code.

Table 16 Conversion Factors

To convert from	Variable	to	multiply by	Parameter
phot/s/cm ²	flux	f _v	v _{Ryd} hv ₁ (erg)	
phot/Ryd/s/cm ²	flux/widflx	vf _v	v _{Ryd} ² hv ₁ (erg)	
phot/Ryd/s/cm ²	flux/widflx	J _v	v _{Ryd} h	
optical depth	tautot	A _V (mag)	1.08574	
energy (eV)		ergs	1.602192(-12)	
energy (eV)		K	1.1604448(4)	<i>eVdegK</i>
keV		Frequency Hz	2.41799(+17)	
energy (Ryd)	anu	Kelvin	1.5788866(5)	<i>te1ryd</i>
energy (Ryd)	anu	ergs	2.179874(-11)	<i>en1ryd</i>
energy (Ryd)	anu	cm ⁻¹	109737.315	<i>1/WavNRyd</i>
energy (Ryd)	anu	eV	13.6056981	<i>evRyd</i>
energy (Ryd)	anu	Å	911.6	<i>rydlam</i>
energy (Ryd), T	anu, Te	hv /kT	1.5788866(5)*anu/Te	<i>te1ryd</i>
temperature (K)	Te	eV	8.617385(-5)	
temperature (K)	Te	ergs	1.38063(-16)	<i>boltzmann</i>
temperature (K)	Te	Rydbergs	1/1.5788866(5)	<i>1/te1ryd</i>
wavelength (Å)		Ergs	1.9864(-8)/λ(Å)	
wavelength (Å)		degree K	1.43877(+8)/λ(Å)	
wavelength (cm)		microns	1(+4)	
wavelength (cm)		Å	1(+8)	
wavelength (cm)		degree K	1.43877/λ(cm)	
wavelength (micron)		degree K	1.43877(+4)/λ(μ)	
wavelength (micron)		ergs	1.9864(-12)/λ(μ)	
wavenumbers (cm ⁻¹)		ergs	1.98648(-16)	
wavenumbers (cm ⁻¹)		degree K	1.43877	<i>WavNKelv</i>
wavenumbers (cm ⁻¹)		Rydbergs	9.1126732(-6)	<i>WavNRyd</i>

4 CONTINUUM INTERACTIONS

4.1 Attenuation of the Incident Continuum

In an open geometry scattering is assumed to attenuate the incident continuum as

$$I = I_o (1 + 0.5 d\tau_{scat})^{-1} . \quad (113)$$

Scattering does not affect the continuum in a closed geometry. Absorption is assumed to attenuate the incident continuum as

$$I = I_o \exp(-d\tau_{abs}) . \quad (114)$$

for both geometries.

4.2 Recombination Equilibrium

4.2.1 On-the-spot approximation

A modified version of the “on-the-spot” (OTS) approximation is used in the treatment of sources of diffuse ionizing radiation when the **diffuse OTS** command is used. Were no other opacity sources present, then, for a closed geometry that is optically thick in the Lyman continuum, all recombinations of hydrogen or helium to the ground state would produce ionizing photons. Other atoms of the recombined species would quickly absorb these. In this case OTS is an excellent approximation (Van Blerkom and Hummer 1967; Bässgen, Bässgen, and Grewing 1988). However, other opacity sources are present, and these compete in absorbing photons produced by recombinations, making the recombination process more efficient than the OTS approximation would suggest.

The recombination coefficients are modified by the presence of all other opacity sources, such as grains, free-free or H⁻ absorption, and the heavy element opacities, in the following manner. The net effective recombination rate coefficient (cm³ s⁻¹) to level n , $\hat{\alpha}(T_e, n)$, is written in terms of the spontaneous radiative recombination rate coefficient $\alpha(T_e, n)$, and the opacities (cm⁻¹) κ_n and κ_o for the level n and other opacity sources respectively, as

$$\hat{\alpha}(T_e, n) = \alpha(T_e, n) \left\{ P_c(n) + [1 - P_c(n)] \left[\frac{\kappa_o}{\kappa_o + \kappa_n} \right] \right\} , \quad (115)$$

where $P_c(n)$ is the continuum escape probability. In general, $P_c(n)$ varies between 0 and 0.5 for an optically thick open geometry (see, for example Davidson 1977), $P_c \sim 1$ if the gas is optically thin, and $P_c \sim 0$ for ground states if the gas is optically thick and the geometry is closed. All computed opacity sources are included in κ_o .

These recombination continua produce a flux of local on-the-spot photons, ϕ_{OTS} (cm⁻² s⁻¹). The OTS photoabsorption rate Γ_{OTS} (s⁻¹), used to determine the ionization or heating rate for the gas or grain constituents, is then $\Gamma_{OTS} = \alpha_\nu \phi_{OTS}$ where α_ν is the absorption cross section at frequency ν . The OTS flux is related to the spontaneous recombination rate coefficient by

$$\varphi_{OTS} = \alpha(T_e, n) n_e n_{ion} \left[\frac{1 - P_c(\tau)}{\kappa_o + \kappa_n} \right] \text{cm}^{-2} \text{s}^{-1} \quad (116)$$

where n_{ion} is the density of the ion in question. These are stored in the vectors *otscon* and *otslin*, which map one-to-one onto the vectors *flux* and *anu*.

4.2.2 Outward only approximation

A composite “outward-only”-“on-the-spot” approximation is used in the treatment of sources of diffuse ionizing radiation when the **diffuse outward** command is used. This is the default assumption. The escaping radiation is then propagated in the outward direction (all for the spherical case, and half for an open geometry).

4.3 Continuous Opacities

The cloud is divided into a large number of concentric shells (zones) and the attenuated and diffuse continua and physical conditions are then determined within each.

The main opacity sources in the ultraviolet continuum are generally photoelectric and free-free (inverse brems) absorption, grain opacity, electron scattering (of both bound and free electrons), and the damping wings of Lyman lines (Rayleigh scattering). The main reemission mechanisms are generally free-free (bremsstrahlung), grain emission, free-bound, and two-photon emission. Grains are not present by default but can be added as an option. Continuous absorption and reemission by all ground states, and many excited states, of all ionization stages of the 30 elements in the calculation are explicitly included. Great care is taken to ensure that each absorption mechanism is balanced by a reemission process, and vice versa, so that energy balance in the strict thermodynamic equilibrium limit can be achieved.

4.3.1 Total opacity arrays

Total absorption opacities (cm^{-1}) are stored in the vector *opac*. Total scattering opacities (cm^{-1}) are stored in *scatop*. The opacities are evaluated in routine *ConvIonizeOpacityDo* and are within the *opac* structure (defined in *opacity.h*).

4.3.2 Cross-section array

Storage. The cross sections per particle (cm^2) for individual species (atoms, ions, molecules, etc) are stored within the array *OpacStack*, a stack array with a single dimension. These cross sections are evaluated when the code is initialized in routine *OpacityCreateAll*.

Array indices. Each species has an associated array index that defines the offset between the origin of *OpacStack*, the frequency array *anu*, and the opacity at the threshold. If this offset has the name *ioff*, for instance, then the cross section at threshold will be given by array element *OpacStack[ioff]*. If *ip* is the index to the threshold energy within *anu*, then the array index to the cross section at energy *i* will be *i-ip+ioff*.

Individual cross-sections. The function *csphot* returns the cross section at a specific frequency for any species. It has three arguments, 1) the pointer to the frequency in *anu* where the cross section is to be evaluated, 2) the pointer to the threshold for the species, and 3) the *ioff* offset described above. All are integer variables.

4.3.3 Photoionization rates

Photoionization rates (units s^{-1}) can be computed by several functions. Which is used at a particular time is determined by circumstances.

GammaK This computes the photoionization rate with allowance for an arbitrary fluorescence yield. This routine is a major pacesetter for the code since it is used to evaluate the continuum rates in the majority of the cases. The photoionization rate is given by

$$\Gamma_n = 4\pi \int_{\nu_o}^{\infty} \frac{J_\nu}{h\nu} \alpha_\nu d\nu \quad [s^{-1}]. \quad (117)$$

where α_ν is the photoionization cross section (cm^{-2}). The routine has three integer arguments, the *anu* pointers to the lower and upper energies, and the offset to the opacity array *ioff* (described above).

GammaPrt This is a special version of **GammaK** that writes (on any open file) the step by step results of the integration. The output lists the product of the photon flux and the cross section, the photon flux, and the opacity.

GammaBn This is a special version of **GammaK** that is used when the correction for stimulated emission or induced recombination is important. The photoionization rate is given by

$$\Gamma_n = 4\pi \int_{\nu_o}^{\infty} \frac{J_\nu}{h\nu} \alpha_\nu d\nu \quad [s^{-1}] \quad (118)$$

and the rate for induced recombination and its associated cooling is computed as

$$\alpha(ind) = P_n^* 4\pi \int_{\nu_o}^{\infty} \frac{J_\nu}{h\nu} \alpha_\nu \exp(-h\nu/kT) d\nu \quad [cm^3 s^{-1}]. \quad (119)$$

where P^* is the LTE population.

GammaPrtRate will print photo rates for all shells of an ion and element. It is called with three arguments, a file handle, followed by the ionization stage and element number on the C scale (0 for H or atoms, etc).

4.3.4 Attenuation within the zone

A correction must be made to account for the attenuation of the continuum across the zone (Netzer and Ferland 1983). Assuming that the continuum varies across the zone as

$$\frac{I(\nu, \delta r)}{I_o(\nu)} = \exp(-\kappa(\nu) f(r) \delta r) \quad (120)$$

then the intensity averaged over a zone with thickness δr is

$$\left\langle \frac{I(\nu, \delta r)}{I_o(\nu)} \right\rangle = \frac{1 - \exp(-\kappa(\nu) f(r) \delta r)}{\kappa(\nu) f(r) \delta r} \quad (121)$$

where $\kappa(\nu)$ is the absorption opacity and $f(r)$ is the filling factor. The coefficients giving this ratio as a function of energy are stored in the vector *tmn*, and are evaluated in subroutine *radinc*. The continuum stored in *flux* is multiplied by these factors in the same subroutine.

4.3.5 Rayleigh scattering

Clouds with neutral hydrogen column densities greater than $\sim 10^{23}$ cm⁻² are optically thick to Rayleigh scattering at wavelengths near $L\alpha$, and this process is a major scattering opacity source at short wavelengths for grain-free environments.

Rayleigh scattering cross sections given by Gavril (1967) are used, joined with expressions for the radiative damping wings of Lyman lines (Mihalas 1978). For wavelengths longward of 1410 Å a power-law fit to Gavril's quantal calculations is used;

$$\sigma_{Ray} = 8.41 \times 10^{-25} \varepsilon^4 + 3.37 \times 10^{-24} \varepsilon^6 + 4.71 \times 10^{-22} \varepsilon^{14} \quad \text{cm}^2 \quad (122)$$

where $\varepsilon \equiv \nu/cR_\infty$ is the photon energy in Rydbergs. This fit is accurate to typically a percent, with occasional errors as large as 4 percent.

For wavelengths between 1410 Å and the Lyman limit, radiative broadening of the Lyman lines is assumed (Mihalas 1978);

$$\sigma_{Ray} = \sum_{i=2}^4 \left(\frac{q_e^2 f_{1,i}}{m_e c} \right) \frac{\Gamma / 4\pi}{(\nu - \nu_{1,i})^2} \quad \text{cm}^2 \quad (123)$$

where Γ is the reciprocal lifetime of the upper level i and the sum is over the first four Lyman lines. This expression gives cross sections in excellent agreement with Gavril (1967) for these wavelengths.

4.3.6 Free-free opacity

The main opacity source in the infrared-radio spectral region for many conditions is free-free opacity with a cross section given by

$$\alpha_\nu(ff) = 3.69 \times 10^8 \bar{g}_{III}(\nu, T) f(r) \nu^{-3} T^{-1/2} \{1 - \exp(-h\nu/kT)\} \sum_A \sum_z z^2 n_A^{+z} \quad [\text{cm}^{-2}] \quad (124)$$

(see, for example, Mihalas 1978). The sum is over all ions n^{+z} of element A and over all elements. The temperature averaged gaunt factor $\bar{g}_{III}(\nu, T)$ is taken from Hummer (1988; see also Karzas and Latter 1961) and are evaluated in routine *gffsub* that was originally written by D. Hummer.

This routine did not extend to energies that could be treated by asymptotic expansions of the gaunt factor. *gffsub* was modified by J. Ferguson to extend over the full temperature and energy range considered by Cloudy, and later extensively rewritten by Ryan Porter. Figure 1 shows the gaunt factors as functions of photon energy and temperature.

4.3.7 Bound-free opacity

Continuum optical depths for photoabsorption from level l are given by

$$d\tau_l(\nu) = \alpha_\nu(n) n_l [1 - \exp(-h\nu / kT) / b_l] f(r) \delta r \quad (125)$$

where b_l is the departure coefficient for level l and α_ν is the absorption cross section [cm^2].

4.3.8 Plasma frequency

The plasma frequency, the energy where the index of refraction of an ionized medium goes to zero, is given by

$$\nu_{pl} = \left(\frac{n_e q_e^2}{\pi m_e} \right)^{1/2} = 8.978 \times 10^3 n_e^{1/2} \text{ s}^{-1} = 2.729 \times 10^{-12} n_e^{1/2} \text{ Ryd}. \quad (126)$$

An ionized gas will reflect the incident continuum for energies smaller than this. This shielding becomes important for the energy range considered by Cloudy for electron densities greater than $\sim 10^7 \text{ cm}^{-3}$. For higher densities this process is treated

free free gaunt factors

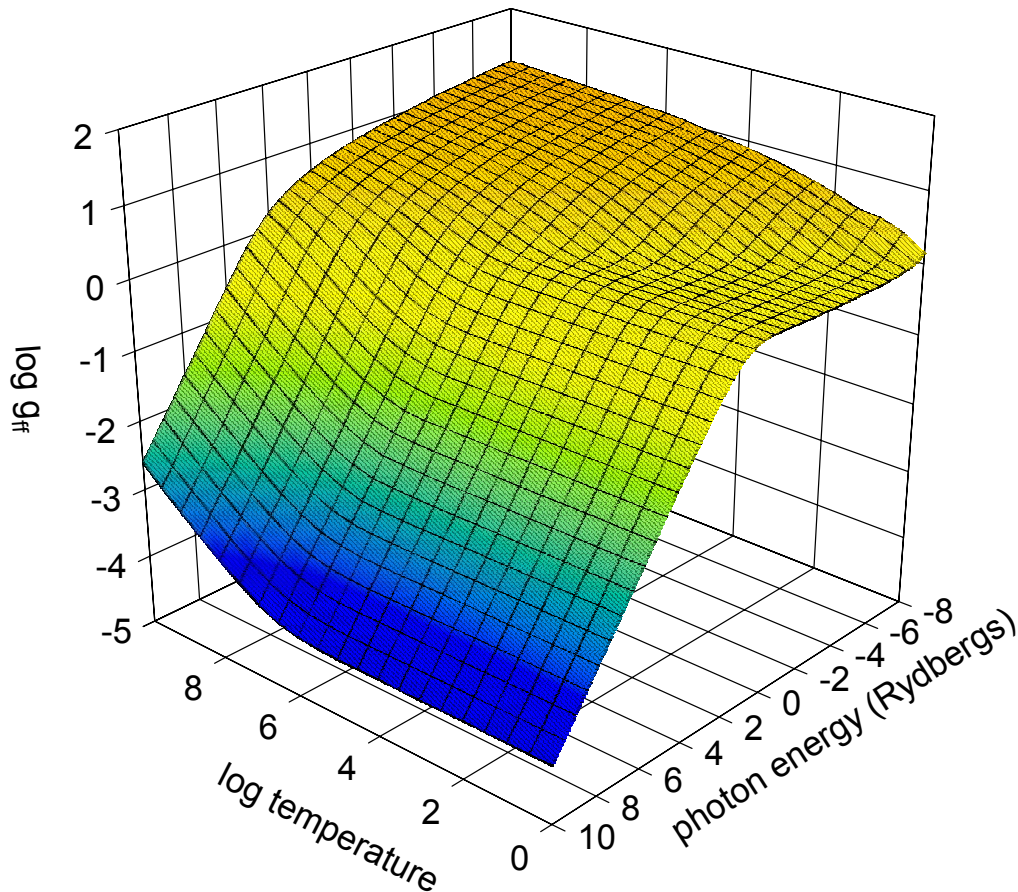


Figure 1 Thermally averaged free-free gaunt factor. The gaunt factor is shown as a function of photon energy and temperature. gaunt recoil

by setting the intensity of the incident continuum to zero for energies below the plasma frequency, adding this portion of the incident continuum to the reflected continuum, and not allowing emission or absorption for any processes that occur below the plasma frequency.

4.3.9 Pressure lowering of ionization potential

The electric field of nearby charges in the continuum acts to lower the ionization potential. The amount by which it is lowered is determined by the electron density. This is considered for all species treated with the iso-electronic model atoms (see 241 below).

5 LINE DETAILS

5.1 Overview

The effects of optical depths, continuum pumping, collisions, and destruction by background opacity, are computed for *all* permitted and intercombination lines. The cooling is usually distributed among many lines in high-density models, and these lines are usually optically thick.

5.2 Line Boltzmann Factors

The Boltzmann factor $h\nu/kT$ for a line with a known wavelength or energy is given by Table 17. The table lists the ratio $h\nu/k$ for various units of the line energy. Vacuum, not air, wavelengths, must be used for all quantities involving wavelengths.

Line Energy Units	$h\nu/k$ (K)
Angstroms	$1.43877(+8)/\lambda(\text{\AA})$
microns	$1.43877(+4)/\lambda(\mu)$
wavenumbers	$1.43877 \times \sigma$
Rydbergs	$1.5788866(+5) \times E$

5.3 Optical Depths, Opacities, and Transition Probabilities

5.3.1 Optical depths

The line center optical depth for a transition $u-l$, where u and l are the upper and lower levels, is given by

$$d\tau_{l,u} = \alpha_\nu (n_l - n_u g_l / g_u) f(r) dr \text{ [Napier]}. \quad (127)$$

Here $f(r)$ is the filling factor and α_ν the absorption cross section (cm^2).

The term in parenthesis is the population of the lower level, with correction for stimulated emission. This term is the only place where stimulated emission enters in the radiative balance equations (Elitzur et al. 1983).

5.3.2 Oscillator strengths

The absorption (f_{abs} , called $f_{l,u}$ here) and emission (f_{em} , called $f_{u,l}$) oscillator strengths are related by

$$g_l f_{l,u} = -g_u f_{u,l} \quad (128)$$

where the g 's are the statistical weights. This product is symmetric, neglecting sign, and the code tries to use g^l s throughout. The convention is the emission lines have a negative oscillator strength.

5.3.3 Absorption cross section

The line-center absorption cross section α_ν (cm^2) is related to the dimensionless absorption oscillator strength f_{lu} or f_{abs} by

$$\alpha_\nu = \frac{\pi^{1/2} q_e^2 \lambda f_{abs}}{m_e c u_{Dop}} \varphi_\nu(x) = 0.014974 f_{abs} \frac{\lambda_{cm}}{u_{Dop}} \varphi_\nu(x) = 1.4974 \times 10^{-6} f_{abs} \frac{\lambda_{\mu m}}{u_{Dop}} \varphi_\nu(x) \text{ [cm}^{-2}\text{]} \quad (129)$$

with the relative line displacement given by

$$x \equiv \frac{\nu - \nu_0}{\Delta\nu_{Dop}} \quad (130)$$

and $\varphi_\nu(x)$ is the Voigt function and u_{Dop} is the Doppler velocity width, the point where the line profile falls to $1/e$ of its peak. With this definition of the relative line displacement, the line profile due to thermal motions alone is $\exp(-x^2)$. Equation 129 is evaluated in routine *abscf*.

5.3.4 Velocities in a thermal distribution

There are three mean speeds in a thermal velocity distribution. The *most probable speed* is the peak of the velocity distribution, with a value

$$u_{mean}^2 = 2kT / m_A \text{ [cm}^2 \text{ s}^{-2}\text{]}. \quad (131)$$

This is found by setting the derivative of the Maxwell-Boltzmann function to zero (Novotny 1973, p 122). The *average speed* is obtained by averaging over this function and is given by

$$u_{average}^2 = 8kT / \pi m_A \text{ [cm}^2 \text{ s}^{-2}\text{]}. \quad (132)$$

The *Doppler velocity width*, sometimes referred to as the *velocity dispersion*, is the velocity averaged over the projected line of sight, given by (Novotny 1973; p 204)

$$u_{Doppler}^2 = 2kT / m_A \text{ [cm}^2 \text{ s}^{-2}\text{]}. \quad (133)$$

This is the distance from line center in velocity units where the line profile falls to e^{-1} of its central value. So it turns out that the most probable speed is equal to the Doppler velocity width.

5.3.5 The Doppler *b* parameter

Much of the literature will refer to the Doppler *b* parameter. This is the Doppler velocity width or velocity dispersion. For gas with purely thermal motions,

$$b^2 = u_{Doppler}^2 = 2kT / m_A \text{ [cm}^2 \text{ s}^{-2}\text{]}. \quad (134)$$

5.3.6 Line Widths

In equation 129 the Doppler velocity width (cm s^{-1}), including turbulence, is given by

$$u_{Dop}^2 = 2kT / m_A + u_{turb}^2 \text{ [cm}^2 \text{ s}^{-2}\text{]} \quad (135)$$

as determined by the local electron temperature. The micro-turbulent velocity u_{turb} is assumed to be zero unless it is reset with the **turbulence** command¹. The Doppler width (cm s^{-1}) for each element and molecule is computed in routine *velset*, and values are stored in the array *doppler*. The array *doppler*, part of the structure

¹ Note that the turbulence command enters u_{turb} in km/s , but converts it into cm/s , the units used throughout the code.

$DoppVel$, gives the velocity width of each element extending from hydrogen through the value of $limelm$, currently 30.

In $velset$ the Doppler velocity width is evaluated as

$$u_{Dop} = \sqrt{2kT / m_A + u_{turb}^2} = \sqrt{1.651 \times 10^8 T / m_{AMU} + u_{turb}^2} \quad [\text{cm s}^{-1}]. \quad (136)$$

The atomic weight in atomic mass units, m_{AMU} , is stored in the vector $AtomicWeight$, which contains m_{AMU} for the first 30 elements.

The Doppler velocity width is related to the half width at half maximum by (Novotny 1973, eqns 5-18; p 205)

$$\Delta u_{1/2} = (\ln 2)^{1/2} u_{Dop} = 0.832555 u_{Dop} \quad [\text{cm s}^{-1}] \quad (137)$$

and the FWHM is given by

$$\Delta u_{FWHM} = 2(\ln 2)^{1/2} u_{Dop} \quad [\text{cm s}^{-1}]. \quad (138)$$

With these definitions

$$b = u_{Dop} = \Delta u_{FWHM} / [2(\ln 2)^{1/2}] \quad [\text{cm s}^{-1}]. \quad (139)$$

5.3.7 Voigt function

Optical depths a relative displacement x away from line center are related to the line center optical depth τ_0 by

$$\tau(x) = \tau_0 \varphi_\nu(x) \quad . \quad (140)$$

The relative displacement is given by equation 130 above.

The Voigt function is normalized to unity at line center and is approximately given by

$$\varphi_\nu(x) \approx \exp(-x^2) + a / (\pi^{1/2} x^2) \quad (141)$$

where a is the damping constant.

5.3.8 Mean vs. line center optical depths

Cloudy tries to work with line center optical depths throughout (see, for example, Mihalas 1978). In many places routines or approximations using *mean* optical depths are encountered (e.g., Hummer and Kunasz 1980). The difference is in how equation 141 is normalized. For comparison, the line center optical depth is $\pi^{1/2}$ times *smaller* than the mean optical depth.

5.4 The Einstein Coefficients

The dimensionless oscillator strength gf is related to the transition probability A_{ul} [s^{-1}] by

$$g_l f_{abs} = \frac{mc\lambda_{cm}^2}{8\pi^2 q_e^2} g_u A_{u,l} = 1.4992 g_u A_{u,l} \lambda_{cm}^2 = 1.499 \times 10^{-8} g_u A_{u,l} \lambda_{\mu m}^2 \quad (142)$$

where $\lambda_{\mu m}$ is the wavelength in microns and λ_{cm} the wavelength in centimeters. The absorption oscillator strength is related to the transition probability by

$$f_{abs} = \frac{mc\lambda_{cm}^2}{8\pi^2 q_e^2} \frac{g_u}{g_l} A_{u,l} = 1.4992 \times 10^{-8} A_{u,l} \lambda_{\mu m}^2 \frac{g_u}{g_l} \quad (143)$$

or

$$A_{u,l} = \frac{8\pi^2 q_e^2}{mc\lambda_{cm}^2} \frac{g_l}{g_u} f_{abs} = \frac{f_{abs}}{1.4992 \times 10^{-8}} \lambda_{\mu m}^{-2} \frac{g_l}{g_u} . \quad (144)$$

Equation 144 is evaluated in routine *ena*. Combining equations 129 and 143 we obtain an expression relating the transition probability and the absorption cross section;

$$\begin{aligned} \alpha_\nu &= \frac{c^2 g_u}{8\pi\nu^2 g_l} \frac{\varphi_\nu(x)}{\pi^{1/2} \mathbf{v}_{Dop}} A_{u,l} \\ &= \frac{\lambda^2 g_u}{8\pi g_l} \frac{\varphi_\nu(x)}{\pi^{1/2} \mathbf{v}_{Dop}} A_{u,l} \quad [\text{cm}^{-2}] . \\ &= 2.24484 \times 10^{-14} A_{u,l} \lambda_{\mu m}^3 \frac{g_u}{g_l} \frac{\varphi_\nu(x)}{\mathbf{v}_{Dop}} \end{aligned} \quad (145)$$

The coefficient for induced emission, B_{ul} , is related to A_{ul} by the phase space factor $2h\nu^3 / c^2$;

$$A_{u,l} = \frac{2h\nu^3}{c^2} B_{ul} \quad (146)$$

and the induced emission and absorption probabilities are related by

$$g_l B_{l,u} = g_u B_{u,l} \quad (147)$$

so that the rate of induced radiative excitation (continuum pumping) is given by

$$r_{l,u} = n_l B_{l,u} J_{l,u} = n_l A_{u,l} \frac{J}{2h\nu^3 / c^2} \frac{g_u}{g_l} = n_l A_{u,l} \eta_{l,u} \frac{g_u}{g_l} [\text{cm}^{-3} \text{s}^{-1}] \quad (148)$$

where η is the continuum occupation number at the line energy, defined as

$$\eta_{i,j} \equiv J_\nu(i,j) / (2h\nu_{ij}^3 / c^2) = (\exp(h\nu / kT_{ex}) - 1)^{-1} . \quad (149)$$

Here $J_\nu(i,j)$ is the mean intensity of the net continuum at the line frequency, and T_{ex} is the excitation temperature of the continuum at the level frequency. Similarly the rate of induced radiative de-excitation is related by detailed balance,

$$r_{u,l} = r_{l,u} \frac{g_l}{g_u} . \quad (150)$$

The absorption cross section α_ν is related to $B_{l,u}$ by

$$\alpha_\nu = \frac{h\nu}{4\pi} B_{l,u} \text{ [cm}^2\text{]}.$$

In these terms the optical depth increment (equation 127) is given by

$$d\tau_{l,u} = \alpha_\nu (n_l - n_u g_l / g_u) f(r) dr = B_{l,u} \frac{h\nu}{4\pi} (n_l - n_u g_l / g_u) f(r) dr . \quad (151)$$

5.5 Air vs Vacuum Wavelengths

The convention across physics and astronomy is to give line wavelengths in vacuum for $\lambda \leq 2000 \text{ \AA}$ and in air for $\lambda > 2000 \text{ \AA}$. There is no discretion in the matter – if you observe visible light with HST the wavelengths must be quoted in air.

Air wavelengths are smaller than vacuum wavelengths because the wavefronts are crushed as they enter the denser medium, with its higher index of refraction. The frequency is unchanged.

Routine *RefIndex* computes the index of refraction for an emission line in the standard format (described below). The code will automatically convert a line of known energy into either air or vacuum wavelengths, whichever is appropriate.

5.6 The Line Source Function

The source function for a line is defined as

$$S_\nu(T_{exc}) \equiv B_\nu(T_{exc}) \equiv \frac{j_\nu}{\kappa_\nu} = \frac{A_{u,l} n_u}{B_{l,u} (n_l - n_u g_l / g_u)} \text{ [erg Hz}^{-1} \text{ sr}^{-1} \text{ s}^{-1}\text{]} \quad (152)$$

where T_{exc} is the line excitation temperature (see equation 194, page 237), and $B_\nu(T_{exc})$ is the Planck function at the line excitation temperature. Combining with the definitions of the Einstein relations we find the relation

$$S_\nu(T_{exc}) = \frac{2h\nu^3}{c^2} \frac{n_u / g_u}{(n_l / g_l - n_u / g_u)} . \quad (153)$$

5.7 The Line Escape Probability Functions

At low densities, line scattering for a two-level atom is coherent in the atom's reference frame, and the line profile function is described by the incomplete redistribution function. At high densities the Stark effect can broaden the line. When the radiation density is high, scattering within excited states can inhibit the broadening of resonance lines such as L β (line interlocking), destroying the coherence of the scattering process. In these cases complete redistribution in a Doppler core more closely describes the scattering process. Cloudy uses several escape probability functions to take these processes into account. Strong resonance lines are treated with partial redistribution with a Voigt profile. Subordinate lines are treated with complete redistribution in a Doppler core.

5.7.1 Incomplete redistribution

Incomplete redistribution is assumed for resonance transitions such as C IV $\lambda 1549$ and the $L\alpha$ transitions of hydrogen and helium. Two studies of line formation using this approximation are those of Bonilha et al. (1979) and Hummer and Kunasz (1980). Both studies suggest escape probabilities of the form

$$P_l(\tau) = \{1 + b(\tau)\tau\}^{-1} \quad (154)$$

but there is substantial disagreement in the form and value of the factor $b(\tau)$, sometimes by more than a factor of 2. (This is after due allowance for the different definitions of line opacities in the two papers.) Cloudy uses the Hummer and Kunasz (1980) results for H I, He I, and He II $L\alpha$ and strong resonance lines such as C IV $\lambda 1549$. Their tabulated values were fitted by interpolation.

5.7.2 Damping constant

The damping constant a is given by

$$a = \frac{\Gamma}{4\pi \Delta\nu_D} = \frac{\lambda_{cm} \sum A}{4\pi u_{Dop}} = \frac{\lambda_{cm} 7.958 \times 10^{-2} \sum A}{u_{Dop}} = \frac{\lambda_{\mu m} 7.958 \times 10^{-6} \sum A}{u_{Dop}} \quad (155)$$

where Γ is the lifetime of the level (the sum of the A 's from the upper level), $\Delta\nu_D$ is the Doppler width in frequency units (Mihalas 1978), λ_{cm} and $\lambda_{\mu m}$ are the wavelengths in cm and microns respectively, and u_{Dop} is the Doppler width in cm s^{-1} . The ratio $\Gamma\lambda/4\pi$ is stored in the line vectors and the a 's are evaluated using this ratio and the current Doppler width.

5.7.3 Background opacity and Destruction probability

The ratio of continuous to total opacity is X_c parameterized as

$$X_c = \frac{\sum \kappa_c n_c}{\kappa_l n_l + \sum \kappa_c n_c} \quad (156)$$

where the κ_l 's are the line center absorption opacities and the n 's the number of absorbers.

5.7.4 Complete redistribution

Lines arising from excited states (hydrogen Balmer, Paschen, etc.) and Lyman lines with $n_u > 2$ are treated assuming complete redistribution in a Doppler core (i.e., the damping constant a is assumed to be zero). This assumption can be changed with the **atom xxx redistribution** command. In this case, if the total optical depth of the slab is T , then the escape probability at a depth τ from the illuminated face is given by;

$$P_{u,l}(\tau, T, X_c) = [1 - X_c F(X_c)] \frac{1}{2} [K_2(\tau, X_c) + K_2(T - \tau, X_c)] \quad , \quad (157)$$

and the destruction probability is

$$D_{u,l}(X_c) = X_c F(X_c) \quad (158)$$

The function is

$$F(X_c) = \int_{-\infty}^{\infty} \frac{\varphi(x)}{X_c + \varphi(x)} dx , \quad (159)$$

where in these expressions (and in this part of the code) the *mean opacity is used*, and $\varphi(x) \approx \pi^{1/2} \exp(-x^2)$ is the Voigt function. $F(X_c)$ is interpolated from the tables presented by Hummer (1968). The function

$$K_2(\tau, X_c) \equiv \frac{1}{1 - X_c F(X_c)} \int_{-\infty}^{\infty} \frac{\varphi^2(x)}{X_c + \varphi(x)} E_2[(X_c + \varphi(x))\tau] d\tau \quad (160)$$

is evaluated numerically.

5.7.5 Masing lines

A line mases when its optical depth is negative. Routine *escmase* evaluates this escape probability as (Elitzur 1992; p 32)

$$\beta(\tau) = \frac{1 - \exp(-\tau)}{\tau} . \quad (161)$$

The code will generate a comment if strong maser action occurs for any transition.

5.7.6 Continuum fluorescence

Continuum fluorescence is treated as in Ferland and Rees (1988) and Ferland (1992).

Consider the case of a continuum that has been attenuated by photoelectric (and all other) opacity sources. The transmitted continuum has a flux of photons φ_ν (photons $\text{cm}^{-2} \text{s}^{-1} \text{Ryd}^{-1}$). Continuum pumping is included among the general line excitation processes for all lines considered by the code.

The photon occupation number of the attenuated continuum is given by equation Photon occupation above, here written as

$$\eta_\nu = \varphi_\nu \frac{c^2}{8\pi \nu_1^3 \nu_{Ryd}^2} \quad (162)$$

where ν_{Ryd} is the frequency in Rydbergs, ν_1 is the frequency of 1 Rydberg, and the other symbols have their usual meaning. The rate ions are excited from a lower level with population n_l (cm^{-3}) is then given by

$$r_{l,u} = A_{u,l} \frac{g_u}{g_l} \eta_\nu \gamma_{l,u} n_l \quad (163)$$

where $A_{u,l}$ is the transition probability and the g 's are the statistical weights. In this expression $\gamma_{l,u}$ is the probability that continuum photons penetrate a line-center distance τ_0 and are then absorbed by an atom:

$$\gamma_{l,u} = \int_0^\infty \varphi_\nu \exp(-\tau_0 \varphi_\nu) d\nu / \int_0^\infty \varphi_\nu d\nu . \quad (164)$$

where, in this expression only, φ_ν is the Voigt function. Figure 2 shows $\gamma_{l,u}$ for a wide variety of values of the damping constant a .

5.7.7 Stark broadening

Distant collisions with charged particles broaden the upper levels of lines, and in the limit of very high densities this will make the scattering process completely non-coherent even for $L\alpha$ (i.e., complete redistribution obtains). Cloudy closely follows the treatment of Puetter (1981) in treating Stark broadening. For transitions described by incomplete redistribution a total escape probability $P_{l,tot}$ given by

$$P_{u,l} = \min(P_{inc} + P_{Stark}, P_{com}) \quad (165)$$

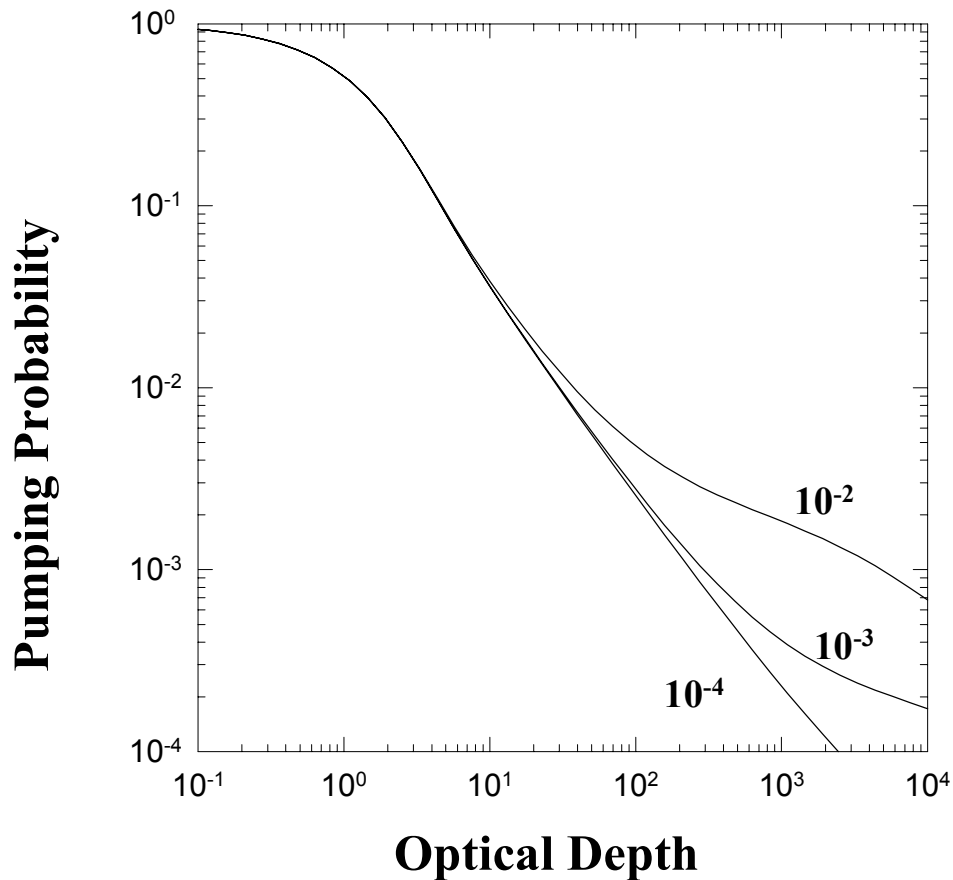


Figure 2 This figure shows the probability that a photon will penetrate to the line center optical depth shown on the x-axis, and then be absorbed by the line. The curves are for various values of the damping constant a (the ratio of damping width to Doppler width), as indicated on the figure. ppump

is defined, where the escape probabilities are those for incomplete, Stark, and complete redistribution respectively. The total effective escape probability is not allowed to exceed the complete redistribution value for $\tau > a^{-1}$.

5.7.8 Net escape probability

If τ is the optical depth in the direction towards the source of ionizing radiation and T is the total optical depth computed in a previous iteration, then the escape probability entering the balance equations is

$$P_{u,l}(\tau, T) = \{P_{u,l}(\tau) + P_{u,l}(T - \tau)\} / 2 \quad (166)$$

In general the total optical depth T is only known after the first iteration, so more than one iteration must be performed when radiative transfer is important.

5.8 Optical Depths and the Geometry

The terms open and closed geometry are defined in a section in Part I. The treatment of transfer in these two limits is described here.

5.8.1 Open geometry

This is the default. During the first iteration the line optical depth is defined using only optical depths accumulated in the inward direction. This optical depth is initialized to a very small number, at the start of the calculation. At the end of the first iteration the total optical depth is set to the optical depth accumulated in the inward direction in routine *RTOptDepthReset*. At the end of subsequent iterations the total optical depth is defined as a mean of the new and old inward optical depths.

5.8.2 Closed geometry overview

Continuum photons are assumed to interact with gas fully covering the continuum source. At the end of the first iteration the total continuum optical depths are set equal to twice the computed optical depths, and the inner optical depths reset to the computed optical depths. The same recipe is followed on subsequent iterations, except that means of old and newly computed optical depths are used.

Closed expanding geometry This is the default if the **sphere** command is entered. In this case it is assumed that line photons do not interact with lines on the “other” side of the expanding spherical nebula. The treatment of the optical depths is entirely analogous to that described for an open geometry, since the presence of the distant material has no effect on line transfer.

Closed static geometry This is assumed if the **sphere static** command is entered. In this case line photons from all parts of the spherical shell do interact. As a result the optical depth scale is poorly defined on the first iteration, and more than one iteration is required. On second and later iterations the total line optical depth is set to twice the optical depth of the computed structure, and the optical depth at the illuminated face of the shell is set to half of this. The optical depth scale is only reliably defined after at least a second iteration.

5.8.3 Wind

The model is a large velocity gradient ($v \propto R$ Sobolev approximation) wind. This is described further on page 323.

5.9 Collision Strengths

I have tried to follow the Opacity Project notation throughout this document (Lanzafame et al. 1993). The energy-specific collision strength Ω_{lu} for a transition between upper and lower levels u and l is related to the excitation cross section Q_{lu} by

$$Q_{lu} = \frac{\pi\Omega_{lu}}{g_l k_{lu}^2} \text{ [cm}^2\text{]} \quad (167)$$

where k_{lu}^2 is the wavenumber of the collision energy. If the collisions are with thermal electrons having a Maxwellian velocity distribution $f(u)$ and velocity u then the rate coefficient q_{lu} is given by

$$q_{lu} = \int_0^\infty f(u)uQ_{lu} du = \frac{2\pi^{1/2}\hbar^2}{g_l m_e} a_o \left(\frac{R_\infty}{kT}\right) \Upsilon_{lu} \exp\left(-\frac{E_{lu}}{kT}\right) \sqrt{\frac{2kT}{m_e}} \text{ [cm}^3 \text{ s}^{-1}\text{]}. \quad (168)$$

E_{ul} is the transition energy in Rydbergs, a_o is the Bohr radius,

$$a_o = \frac{\hbar^2}{m_e q_e^2} = 0.529177249 \times 10^{-8} \text{ cm} \quad (169)$$

and R_∞ is the Rydberg energy. Then the thermally-averaged collision strength is given by

$$\Upsilon_{lu} = \int_0^\infty \Omega_{lu} \exp\left(-\frac{\varepsilon}{kT}\right) d\left(\frac{\varepsilon}{kT}\right). \quad (170)$$

The rate coefficient for collisional de-excitation is then given by

$$q_{ul} = \frac{\Upsilon}{g_u \sqrt{T_e}} \left(\frac{2\pi}{k}\right)^{1/2} \frac{\hbar^2}{m_e^{3/2}} = \frac{\Upsilon 8.6291 \times 10^{-6}}{g_u \sqrt{T_e}} \text{ [cm}^3 \text{ s}^{-1}\text{]}. \quad (171)$$

The rate coefficient for excitation follows from detailed balance:

$$q_{lu} = q_{ul} \frac{g_u}{g_l} \exp(-\chi) = \frac{\Upsilon 8.6291 \times 10^{-6}}{g_l \sqrt{T_e}} \exp(-\chi) \text{ [cm}^3 \text{ s}^{-1}\text{]}. \quad (172)$$

5.10 Born Approximation

For energies much larger than the excitation energy of the transition, the Born approximation is valid and the energy specific collision strength is given by Bethe (1930)

$$\Omega_{lu} \approx \frac{4g_l f_{lu}}{E_{lu}} \ln\left(\frac{4\varepsilon}{E_{lu}}\right) \quad (173)$$

where f_{lu} is the absorption oscillator strength of the permitted transition.

5.11 The g-bar Approximation

The g-bar or van Regemorter (1962) approximation relates the collision strength to the transition probability A_{ul} and wavelength λ (in microns). Here, the collision strength for the downward transition Υ_{ul} is approximately given by

$$\begin{aligned}\Upsilon_{u,l} &= \frac{2\pi}{\sqrt{3}} \frac{m^2 e^2}{h^3} \lambda_{\mu m}^3 10^{-12} g_u A_{u,l} \bar{g} \\ &\approx 2.388 \times 10^{-6} \lambda_{\mu m}^3 g_u A_{u,l} \bar{g} \\ &\approx 159 \lambda_{\mu m} g_l f_{abs} \bar{g}\end{aligned}\tag{174}$$

where g_u and g_l are the statistical weights of the upper and lower levels and f_{abs} is the absorption oscillator strength. For energies of interest in astrophysical plasmas, where $kT < h\nu$, \bar{g} is approximately given by

$$\bar{g} \approx \begin{cases} 0.2; & \text{positive ions} \\ (kT/h\nu)/10; & \text{neutrals} \end{cases}\tag{175}$$

(van Regemorter 1962). These approximations are generally accurate to better than 1 dex.

5.11.1 The g-bar implementation

Far better collision data are available today. Dima Verner's routine, *ColStrGBar*, uses the best available data to generate collision strengths for the transferred emission lines, using data stored in the line array. The array element *ipLnCS1* points to stored information identifying the type of transition.

5.12 The Critical Density

The critical density is defined as the density at which the radiative de-excitation rate $A_{ul} P_{ul}$ (where A is the transition probability and P is the escape probability) equals the collisional de-excitation rate $q_{ul} n_e$. Setting

$$A_{ul} P_{ul} = C_{ul} = q_{ul} n_e = \Upsilon \frac{8.629 \times 10^{-6}}{g_u \sqrt{T_e}} n_e \quad [\text{s}^{-1}]\tag{176}$$

where Υ is the thermally averaged collision strength, the critical density is given by

$$n_{crit} \sim \frac{A_{ul} P_{ul} g_u \sqrt{T_e}}{\Upsilon 8.629 \times 10^{-6}} \quad [\text{cm}^{-3}].\tag{177}$$

For an optically allowed transition, in which the g-bar approximation may apply, this density is approximately given by

$$n_{crit} = \frac{4.8 \times 10^{10} \sqrt{T_e}}{\lambda_{\mu m}^3 \bar{g}} \quad [\text{cm}^{-3}].\tag{178}$$

5.13 Line Thermalization Length

Line radiative transfer will affect the thermal equilibrium of the gas when the collision time scale approaches an effective lifetime $\tau \sim (A_{ul}/n_{scat})^{-1}$, where A_{ul} is the transition probability and n_{scat} is the number of scatterings a line photon undergoes before escape. For permitted metal lines (which often have optical depths $\sim 10^4 - 10^6$) line thermalization becomes important at densities $n_e > 10^{15} / \tau \sim 10^{10} \text{ cm}^{-3}$. These effects are important for hydrogen at considerably lower densities due to its greater abundance. Additionally, continuum transfer affects the ionization and thermal equilibrium of the gas at all densities.

5.14 Averaging Levels into Terms

5.14.1 Collision strengths

Often cases are encountered in which a multiplet consisting of many lines can be treated as the equivalent two-level atom with a single transition. In these cases it is necessary to define “effective” collision strengths and transition probabilities. If the collision strength from an individual level i is Υ_i , and the statistical weights of the level and term are g_i and g_{tot} respectively, then the effective collision strength Υ_{eff} is related to Υ_i by a simple argument. The collision rate q_i is proportional to the ratio

$$n_i q_i \propto n_i \frac{\Upsilon_i}{g_i} \quad [\text{s}^{-1}] \quad (179)$$

so that

$$n_{tot} q_{tot} = \sum_i n_i q_i \propto \sum_i n_i \frac{\Upsilon_i}{g_i} \quad [\text{s}^{-1}]. \quad (180)$$

In many cases it is valid to assume that the levels within the term are populated according to their statistical weight, viz.,

$$n_i = n_{tot} \frac{g_i}{g_{tot}} \quad [\text{cm}^{-3}]. \quad (181)$$

Then, the effective collision strength Υ_{tot} is operationally defined by the relations

$$n_{tot} \frac{\Upsilon_{tot}}{g_{tot}} = \sum_i n_i \frac{\Upsilon_i}{g_i} = n_{tot} \sum_i \frac{g_i}{g_{tot}} \frac{\Upsilon_i}{g_i} = n_{tot} \frac{\sum_i \Upsilon_i}{g_{tot}} \quad (182)$$

So, the effective collision strength of the entire multiplet is

$$\Upsilon_{tot} = \sum_i \Upsilon_i \quad (183)$$

5.14.2 Transition probabilities

Under similar circumstances an effective transition probability A_{eff} may be defined as

$$n_{tot} A_{tot} = \sum_i n_i A_i = n_{tot} \sum_i \frac{g_i}{g_{tot}} A_i \quad (184)$$

so that the effective transition probability is

$$A_{tot} = \sum_i \frac{g_i}{g_{tot}} A_i \quad (185)$$

So collision strengths are added, and transition probabilities averaged.

5.15 Level Populations

Both escape and destruction probabilities enter in the calculation of a level population and line emissivity. The escape probability $P_{u,l}$ is the probability that a line photon will escape in a single scattering (Elitzur et al. 1983; Elitzur 1984). The destruction probability $D_{u,l}$ is the probability that a line photon will be destroyed in a single scattering.

The line de-excitation rate is given by

$$\left(\frac{dn_u}{dt} \right)_{rad} = n_u A_{u,l} (P_{u,l} + D_{u,l}) - n_l A_{u,l} \eta \gamma_{u,l} + n_u C_{ul} - n_l C_{lu} \quad [\text{cm}^{-3} \text{ s}^{-1}] \quad (186)$$

where η is the photon occupation number of the attenuated external radiation field, C is the collision rate (s^{-1}), and $\gamma_{u,l}$ is the fluorescence probability.

The net emission from a transition between the level n to a lower level l is then simply

$$4\pi j(n,l) = n_n A_{n,l} h\nu_{n,l} P_{u,l}(\tau_{n,l}) f(r) \quad [\text{erg cm}^{-3} \text{ s}^{-1}] \quad (187)$$

where $f(r)$ is the filling factor. The local cooling rate ($\text{erg cm}^{-3} \text{ s}^{-1}$) due to the line is related to the level populations by

$$\Lambda_{u,l} = (n_l C_{l,u} - n_u C_{u,l}) f(r) h\nu \quad [\text{erg cm}^{-3} \text{ s}^{-1}] \quad (188)$$

and the local flux ($\text{cm}^{-2} \text{ s}^{-1}$) of “on-the-spot” (OTS) photons caused by line loss (used to compute heating or photoionization rates for the sources of the background opacity) is

$$\varphi_{OTS} = \frac{n_u A_{u,l} D_{u,l}(X_c)}{\sum_c \kappa_c n(c)} \quad (189)$$

The ratio of inward to total line intensity is then given by

$$\frac{4\pi j(in)}{4\pi j(total)} = \frac{P_{u,l}(\tau)}{[P_{u,l}(\tau) + P_{u,l}(T - \tau)]} \quad (190)$$

5.16 The EmLine Structure

5.16.1 Overview

Each emission line is represented as an *EmLine* structure containing all the details needed to transfer a line and predict its intensity. This structure will evolve into an object in C++. The goal is for there to be only one emission line in Cloudy, but millions of instances of it. This *EmLine* structure is defined in *cddefines.h*. There are arrays of *EmLine* structures to contain the level 1 and level 2 lines (defined below), and the hydrogenic, He-like, molecular, and FeII atoms.

5.16.2 The main line structures

Level 1 Lines: *TauLines* This array contains the lines with high-quality atomic data. Atomic data for these lines are contained in the files *level1.dat*.

Level 2 Lines: *TauLine2* This is the large group of lines brought in by Dima Verner. These lines have Opacity Project wavelengths, generally accurate to about 10%. All have g-bar collision strengths (Gaetz & Salpeter 1983; Mewe 1972; van Regemorter 1962), generally thought to be accurate to $\sim 0.5 - 1.0$ dex. Both the wavelengths and intensities of these lines are more approximate than those of the level 1 lines.

The unified iso-electronic sequences: *EmisLines* contains the lines of the ions treated as a unified isoelectronic sequence. The array indices give the isoelectronic sequence (0 for H-like, 1 for He-like, etc), the atomic number (0 for H, 1 for He, etc), and upper and lower levels of the transition.

The long-term goal is to remove the level 1 and 2 lines, moving all ions to an iso-sequence formulation.

5.16.3 Evaluation of stored quantities

The line structures store information dealing with the solution of the equations of statistical equilibrium, and rates related to the line transfer. Quantities dealing with the populations are evaluated in the routine that computes the level populations, and this depends on the individual lines. Quantities dealing with the line transfer are evaluated in routine *RTMake*, which calls either *RTMakeStat* (for static solutions) or *RTMakeWind* (for a large velocity gradient model).

5.16.4 Contents of the EmLine structure

The structure is defined in *cddefines.h*, which describes what each member of the structure does.

int iRedisFun; This is a flag indicating the type of line redistribution function to be used.

int ipCont; This is the array index that locates the line within the continuum array

int IonStg; ion stage of element, 1 for atom, 2 ion, etc

int nelem; atomic number of element, 1 for H, 2 for He, etc

float TauCon ; The line optical depth to the continuum source.

float ColUL; Collision rate from upper to lower level.

float TauIn, TauTot; The inward and total line optical depths through the cloud. *TauTot* was computed in the previous iteration and is not defined on the first iteration.

float *FracInwd*; The *fraction* of the line escaping in the inward direction. This is between 0 and 1.

float *pump*; This is the local rate of lower to upper continuum pumping for the transition. It is the product of the local continuum and the pumping probability, given by

$$\text{TauArray.ipLnPump} = A_{u,l} \left(\frac{g_u}{g_l} \right) P \eta \quad (191)$$

where η is the occupation number of the attenuated continuum and P is the line pumping probability.

double *xIntensity*; line intensity

float *phots*; number of photons emitted per sec in the line

float *gf*; The *gf* value

float *Pesc, Pdest*; The escape and destruction probabilities for the line.

float *dampXvel*; The damping constant, and a number related to it. The ratio $\Gamma\lambda/4\pi$, used to derive the damping constant. For a two level system this is just $A_{ul}\lambda/4\pi$. This is given by

$$\begin{aligned} \text{dampXvel} &= \frac{\Gamma}{4\pi} \\ a &= \frac{\text{dampXvel}}{u_{Dop}} \end{aligned} \quad (192)$$

float *dTau*; total opacity (cm^{-1}) in transition

double *cool, heat*; cooling and heating due to collisional excitation

float *ColOvTot*; ratio of collisional to radiative excitation

float *cs*; collision strength for transition

float *WLang*; The wavelength (\AA) of the line as used in the print out of the line optical. This number is only a label and can be an air wavelength.

float *EnergyK*; transition energy in degrees kelvin

float *EnergyRyd*; transition energy in Rydberg

float *EnergyErg*; ergs

float *EnergyWN*; transition energy in wavenumbers

float *opacity*; line opacity

float *gLo, gHi*; These are the statistical weights of the lower and upper levels.

float *PopLo, PopHi*; These are the lower and upper level populations (cm^{-3}) for the transition.

float *PopOpc* The correction for stimulated emission is included in the optical depth scale for all lines of the heavy elements. The effective population determining the optical depth scale is given by the population stored here, computed as

$$n_l^{\text{eff}} = n_l - n_u \frac{g_l}{g_u} . \quad (193)$$

float Aul; transition probability, Einstein A upper to lower

float AovTot; ratio $A_{21}/(A_{21}+C_{21})$

float CS1, CS2 These indicate the type of transition, and are used when the Mewe or Verner g-bar routines are used as the source of the collision strengths. If *CS1* is zero then the line is a “high quality” or “level 1” transition, and has its own pointer to the OTS line array. If *CS1* is not zero, (a “level 2” transition) then the collision strength is generated from the contents of *CS1* and *CS2*.

float ots; ots rate

5.16.5 Dumping the line array.

The contents of the line array can be printed by calling routine *DumpLine*, with the single argument being a pointer to the line optical depth array.

5.16.6 Generating a line label

Two functions can be used to generate a designation for an emission line using the information stored in the line arrays. A 10-character function, *chLineLbl*, will generate a label for an emission line. This label is the spectroscopic designation for a line, such as C 4 1549Å. It is called with a single argument, the line array.

The spectroscopic designation of the ion by itself (“C 4”, “O 6”, etc) can be obtained from the 4 character function *chIonLbl*. It is called with a single argument, a pointer to the line array.

chLineLbl is surprisingly slow and should be used as sparingly as possible.

5.16.7 Line excitation temperature

Routine *TexcLine* will use the contents of the line array to generate the line excitation temperature. The line excitation temperature T_{exc} is operationally defined from the relative level populations n_u and n_l and the line energy $h\nu$ as

$$\frac{n_u / g_u}{n_l / g_l} = \exp(-h\nu / kT_{\text{exc}}) . \quad (194)$$

Routine *TexcLine* uses the contents of the line arrays to evaluate T_{exc} . The routine returns an excitation temperature of zero if either population is non-positive.

5.16.8 A Simple Two Level Atom

The following code fragment uses the information in the line optical depth arrays to compute the population of a two-level atom. The treatment includes pumping by the attenuated external radiation field, collisional excitation and deexcitation, and photon escape and destruction by background opacity. To see more examine routine *level2* within the code.

```
#include "cddefines.h"
/* following includes variables te and eden, the electron
 * temperature and electron density*/
#include "phycon.h"
/* following contains abundances of all ions
 * following includes sqrte, the square root of te*/
void ComputeIt( EmLine *t )
```

```

{
    /* net rate down A21*(escape + destruction) */
    Aul = t->Aul*(t->Pesc + t->Pdest);

    /* statistical weights of upper and lower levels */
    gl = t->gLo;
    gu = t->gHi;

    /* get Boltzmann factor */
    boltz = sexp(t->EnergyK/phycon.te);

    /* upward pumping by external continuum */
    PumpLU = t->pump;
    /* downward pumping by external continuum */
    PumpUL = PumpLU * gl / gu;

    /* collisions from lower to upper, and upper to lower */

    /* collisions from upper to lower */
    Cul = 8.629E-6 / phycon.sqrte * t->cs * phycon.eden / gu;

    /* collisional excitation
     * sexp is special form of exp that sets zero if very small,
     * but note that it has an implicit negative sign */
    Clu = Cul * gu/gl * sexp(boltz);

    /* xIonFrac(nelem,i) is density of ith ionization stage (cm^-3) */
    Abun = xIonFrac[ t->nelem -1][t->IonStg];

    /* this is ratio of upper to lower level population
    ratio = (Clu+PumpLU) / ( Cul+PumpUL+Aul )
    /* upper level population */
    upper = Abun / (1. + 1./ratio);
}

```

5.16.9 Adding lines to the level 1 line arrays

The file level1.dat. The list of level 1 lines is contained in the file *level1.dat*, which lives in the main data directory. This file contains the information needed to set up all the level 1 lines, and is edited to add more files. Comments may be entered anywhere within the file, and are indicated by a sharp symbol (“#”) in the first column. The order of the parameters for each line is described in the file.

The file begins with a magic number that must be changed when the file is changed. If the contents of the data file are changed then both this magic number and the parallel code in *CreateData* must be changed.

Routine *CreateData* reads the file *level1.dat*. This routine first counts how many level 1 lines are contained in the file and then allocates space for the emission line structure.

Array elements for the TauLines array. The level 1 lines are contained in *TauLines*, an array of structures of type *EmLine*. The header file *cddefines.h* contains the declaration for a long list of integer indices that are used to address elements of the *TauLines* array. The definition of this set of integers is in routine *CreateData*.

MakeLevLines After *CreateData* reads in the contents of the *level1.dat* data file, it calls *MakeLevLines* to establish the array indices. This routine uses the line wavelength, chemical element, and ionization stage to associate an array index with each line.

Follow these steps:

- **Add the line to the file level1.dat that lives in the data directory.** All level 1 lines are contained in the file *level1.dat*. The file describes the format of the

data. Each emission line is contained on a single line, which has a line label, wavelength, excitation energy, statistical weights of the upper and lower levels, either the gf or A for the transition, and the type of redistribution function. The code will count how many emission lines are present in *level1.dat* and allocate the appropriate space.

- **Enter the line in routine CreateData.** The level 1 lines are an array of structures that are defined in *createdata.c* and declared in *cddefines.h*. A series of integer variables give the array index for each line. Initially these indices are set to very large negative values.
- **Associate the line with an array index in MakeLevLines.** This routine has a series of calls to *ipFindLevLine*, which takes the line wavelength, ionization stage, and element number as arguments. *ipFindLevLine* returns the index to the emission line with the array of level 1 lines. *MakeLevLines* confirms that all array indices entered in *CreateData* are given valid indices here.
- **Compute the line intensity and cooling.** This is done by calling one of the line cooling routines, *level2*, *level3*, etc. It will be necessary to assign a collision strength to the transition. This can be done by calling *PutCS*, a routine with two arguments, the collision strength and the line vector.
- **Add the line to the line output routine.** This is done in one of the members of the *lines* family of routines. A call to routine *PutLine*, which has as a single argument the line structure, will enter all of the needed information about the line production in the current zone.
- **Recompile Cloudy**

Table 18 Needed Line Parameters

Label	λ	g_l	g_u	gf	$E(\sigma)$	Ion	Nelem	Redis	A_{ul}
	ipLnWIAng	ipLnGl	ipLnGu	ipLnGF	ipLnEnrWN	ipLnIonStg	ipLnNelem	ipLnRedis	ipLnAul

label a four character string that will identify the line in the printout.

λ This is the line wavelength in Ångstroms or microns, and is only used as a line label. It can be an air wavelength.

g_l, g_u Lower and upper statistical weights.

gf, A It is only necessary to specify either the gf or A . If the transition probability is to be entered instead of the gf , the gf must be assigned a value of zero. If gf is specified then A does not need to be set.

$E(\sigma)$ This is the line energy in wavenumbers, and is used to generate Boltzmann factors.

Redis This must be non-zero. Negative values indicate complete redistribution with a Doppler core, and positive values incomplete redistribution.

6 THE MODEL ATOM FOR ISO-SEQUENCES

6.1 Overview

Cloudy is designed to model environments that range from the low-density limit to LTE. Eventually all isoelectronic series will be treated as a multi-level atom plus continuum.

All emission lines of the isoelectronic sequences are a single four-dimensional structure of type *EmLine*. The array indices, from left to right, indicate the isoelectronic sequence, the atomic number, and the upper and lower levels. In all these the array starts from 0. The header file `cddefines.h` contains many macros that make it possible to address this array in a physically meaningful way. So, for instance, the hydrogen $L\alpha$ transition would be `EmisLines[ipH_LIKE][ipHYDROGEN][ipH2p][ipH1s]`.

6.2 Departure Coefficients

Departure coefficient is the ratio of the actual population of a state to its population in thermodynamic equilibrium. They are useful since they allow direct comparison of a population to its asymptotic equilibrium limit.

The LTE relative population density for level n is given by

$$\begin{aligned}
 P_n^* &= \frac{n_n^*}{n_e n_{ion}} = \frac{g_n}{g_e g_{ion}} \left(\frac{m_n^*}{m_e m_{ion}} \frac{h^2}{2\pi kT} \right)^{3/2} \exp(+\chi_n) \\
 &\approx \frac{g_n}{g_e g_{ion}} \left(\frac{h^2}{2\pi m_e kT} \right)^{3/2} \exp(+\chi_n) \quad [\text{cm}^3] \quad (195) \\
 &= \frac{g_n}{g_e g_{ion}} 4.1412957 \times 10^{-16} T^{-3/2} \exp(+\chi_n)
 \end{aligned}$$

where the electron statistical weight is $g_e = 2$, the ion statistical weights are 1 and 2 for H-like and He-like species, all nuclear statistical weights are ignored, and $g_n = 2n^2$ is the statistical weight of hydrogenic level n (see the discussion starting on page 261 below). n_n^* is the LTE population of level n (cm^{-3}), and the other symbols have their usual meaning, and the . Here

$$\chi_n = \frac{I_n}{kT} = \frac{15.7807 \times 10^4 Z^2}{n^2 T} \quad (196)$$

where I_n is the ionization threshold for level n and Z is the nuclear charge, the exponent in equation 195 is positive, and the last term holds for hydrogenic systems. The departure coefficients are related to the LTE relative population density by

$$b_n = \frac{n_n}{P_n^* n_e n_{ion}} \quad (197)$$

where n_n is the actual population of the level.

6.3 Level Energies and Boltzmann Factors

Boltzmann factors for transitions between levels are defined as

$$\text{iso.Boltzmann[ipISO][nelem][nu][nl]} \equiv \exp(\chi_u - \chi_l). \quad (198)$$

The energy sign convention is such that the Boltzmann factor is less than unity, decreasing with increasing temperature. Boltzmann factors for levels relative to the continuum are stored in the vector

$$\text{iso.ConBoltz[ipISO][nelem][n]} \equiv \exp(-\chi_n). \quad (199)$$

6.3.1 Pressure lowering of the ionization potential

Not yet

6.4 Recombination Rates and Cooling

State-specific rates for radiative recombination and radiative recombination cooling are needed for the temperature range $2.8 \text{ K} \leq T \leq 10^{10} \text{ K}$. The methods and assumptions used to derive these for hydrogenic ions are described here.

6.4.1 Formalism

The Milne relation for the state-specific radiative recombination rate coefficient ($\text{cm}^3 \text{ s}^{-1}$) to a level n can be expressed as (Brown and Mathews 1974; Gould 1978; Mihalas 1978);

$$\begin{aligned} \alpha_n(T) &= \left(\frac{2\pi m_e k}{h^2} \right)^{-3/2} \frac{8\pi}{c^2} \frac{g_n}{g_e g_{ion}} T^{-3/2} \int_{h\nu_o}^{\infty} \nu^2 \alpha_\nu(n) \exp(-h(\nu - \nu_o)/kT) d\nu \\ &= 4.12373 \times 10^{11} \frac{g_n}{g_e g_{ion}} T^{-3/2} \int_{h\nu_o}^{\infty} \nu_{Ryd}^2 \alpha_\nu(n) \exp(-h(\nu - \nu_o)/kT) d\nu_{Ryd} \end{aligned} \quad (200)$$

where the g 's are the statistical weights of the constituents, $h\nu_{Ryd}$ is the photon energy in Rydbergs, $h\nu_o \sim z^2/n^2$ is the ionization potential in Rydbergs, $\alpha_\nu(n)$ is the photoionization cross section, and the other symbols have their usual meanings.

In implementing this formalism the fact that, for hydrogen itself, the energy scale is shifted by the ratio of the reduced mass of the nucleus to an infinite mass was explicitly taken into account. If the energy of level n of hydrogen is $n^{-2} R_H$, then the temperature corresponding to 1 Rydberg, appearing in the exponential, is 157807 K, not the commonly quoted 157890 K. This does affect the results slightly since the energy scale enters as an exponential in equation 200.

Hydrogenic photoionization cross sections are required over a very wide range of energy since recombination coefficients over a wide range of temperature are needed. Cross sections $\alpha_\nu(n)$ were calculated using a program based on routines developed by Hummer (1988) and Storey and Hummer (1991, and private communication). The program generates the cross section values at arbitrary photon energies for all hydrogenic (n,l) states, as well as for the total n , employing analytic expressions and some very accurate expansions and numerical procedures. The

Table 19 State Specific and Case B Recombination Coefficients

log(T _e)	1	2	3	4	5	6	case B
0.5	9.258-12	5.087-12	3.512-12	2.684-12	2.172-12	1.825-12	5.758-11
1.0	5.206-12	2.860-12	1.974-12	1.508-12	1.220-12	1.025-12	2.909-11
1.5	2.927-12	1.608-12	1.109-12	8.465-13	6.842-13	5.737-13	1.440-11
2.0	1.646-12	9.028-13	6.216-13	4.732-13	3.811-13	3.183-13	6.971-12
2.5	9.246-13	5.055-13	3.460-13	2.613-13	2.084-13	1.720-13	3.282-12
3.0	5.184-13	2.805-13	1.888-13	1.395-13	1.085-13	8.717-14	1.489-12
3.5	2.890-13	1.517-13	9.779-14	6.884-14	5.099-14	3.912-14	6.430-13
4.0	1.582-13	7.699-14	4.555-14	2.965-14	2.053-14	1.487-14	2.588-13
4.5	8.255-14	3.461-14	1.812-14	1.076-14	6.953-15	4.775-15	9.456-14
5.0	3.882-14	1.316-14	6.059-15	3.314-15	2.022-15	1.331-15	3.069-14
5.5	1.545-14	4.196-15	1.736-15	8.918-16	5.219-16	3.335-16	8.793-15
6.0	5.058-15	1.146-15	4.392-16	2.160-16	1.229-16	7.694-17	2.245-15
6.5	1.383-15	2.760-16	1.005-16	4.807-17	2.685-17	1.660-17	5.190-16
7.0	3.276-16	6.031-17	2.129-17	1.000-17	5.523-18	3.385-18	1.107-16
7.5	7.006-17	1.227-17	4.251-18	1.976-18	1.083-18	6.606-19	2.221-17
8.0	1.398-17	2.377-18	8.139-19	3.759-19	2.052-19	1.248-19	4.267-18
8.5	2.665-18	4.455-19	1.515-19	6.970-20	3.796-20	2.303-20	7.960-19
9.0	4.940-19	8.175-20	2.769-20	1.271-20	6.913-21	4.190-21	1.457-19
9.5	9.001-20	1.481-20	5.005-21	2.294-21	1.247-21	7.552-22	2.636-20
10.0	1.623-20	2.662-21	8.985-22	4.116-22	2.235-22	1.354-22	4.737-21

calculations were carried out at a number of different mesh sizes to check for convergence. The results are typically accurate to better than 0.1 percent.

The recombination cooling rate coefficient (erg cm³ s⁻³) is given by

$$kT\beta(t,n) = \left(\frac{2\pi m_e k}{h^2} \right)^{-3/2} \frac{8\pi}{c^2} \frac{g_n}{g_e g_{ion}} T^{-3/2} \int_{h\nu_0}^{\infty} \nu^2 \alpha_{\nu}(n) h(\nu - \nu_0) \exp(-h(\nu - \nu_0)/kT) d\nu \quad (201)$$

6.4.2 Results

The numerical results are presented in Tables 19 and 20. The first column of the table gives the log of the temperature. Columns 2 through 7 give the total recombination coefficient for $1 \leq n \leq 6$ summed over l states. The last column gives the case B sum, $2 \leq n \leq 1000$. A very large temperature range is considered for completeness; actually, at very low temperatures three-body recombination predominates for most densities (Bates et al. 1963), while at very high temperatures other processes (i.e., Compton scattering, collisions) dominate the balance and the neutral fraction is vanishingly small.

As tests, these predictions of the recombination rate coefficients are compared with those of Seaton (1959), Ferland (1980), Hummer and Storey (1987), and Martin (1988). (Note that the total recombination rate given by Hummer and Storey is the sum of radiative and net three-body recombination. For this comparison their results for a density of 10² cm⁻³ were used to minimize the contribution of the second process.) The agreement with all of these results is good, usually much better than 1 percent. Seaton (1959) calculates the recombination cooling coefficients. The present results agree with his to better than 5 percent. Figure 5 shows the recombination-cooling coefficient for several states.

6.4.3 Recombination coefficients

Recombination coefficients for the iso-electronic sequences are stored in the four-dimensional vectors *RadRecomb*. The first dimension gives the charge, the next indicates the level of the model atom – *RadRecomb[ipH_LIKE][ipHYDROGEN][0][xx]* would refer to the ground level of hydrogen. The last dimension points to several quantities related to computation of the effective recombination coefficient.

RadRecomb[ipH_LIKE][ipHYDROGEN][n][0] This is the radiative recombination rate coefficient to level n (units $\text{cm}^3 \text{s}^{-1}$), the term $\alpha(T,n)$ in equation 115.

RadRecomb[ipH_LIKE][ipHYDROGEN][n][1] This is the dimensionless OTS effective recombination efficiency, given by the term

$$\left\{ P_c(n) + [1 - P_c(n)] \left(\frac{\kappa_o}{\kappa_o + \kappa_n} \right) \right\} \quad (202)$$

This term is zero deep in the cloud, and unity for an optically thin region.

RadRecomb[ipH_LIKE][ipHYDROGEN][n][2] This is the continuum escape probability $P_c(n)$.

ConOpacRatio[ipH_LIKE][ipHYDROGEN][n][2] These are the vectors containing the ratio of “other” to “total” opacities, which appears as the term $\kappa_o/(\kappa_o + \kappa_n)$ in equation 202.

6.5 The Collisional Rate Equations

The collision rates between two terms in strict TE are related by detailed balance². Then

$$n_l^* C_{l,u} = n_u^* C_{u,l} \quad (203)$$

and we get the usual relation between collisional excitation and de-excitation rates,

$$C_{l,u} = \left(n_u^* / n_l^* \right) C_{u,l} = (g_u / g_l) \exp(-\chi / kT) C_{u,l} . \quad (204)$$

Considering only collisional terms, the departure coefficient for level n is given by

$$\frac{db_n}{dt} = \sum_l b_l C_{n,l} + \sum_u \frac{P_u^*}{P_n^*} b_u C_{u,n} - b_n \left\{ \sum_l C_{n,l} + \sum_u \frac{P_u^*}{P_n^*} C_{u,n} + C_{n,k} (1 - b_n^{-1}) \right\} \quad (205)$$

² In version 96 the bound-bound collision rate coefficients for H were updated to Anderson et al. (2000) and to Bray et al. (2000) for He.

where the sums are over upper and lower levels. The collision rates (s^{-1}) from level i to level j are denoted by C_{ij} . The first term on the RHS represents collisional excitation to n from lower levels, the second is collisional deexcitation to n from higher levels, and the last term accounts for destruction processes. These include collisions to lower levels, upper levels, and the continuum. The factor multiplying the collisional ionization rate $C_{n\kappa}$ accounts for collisional ionization less three-body recombination. Note that this is often a net recombination process for the atom since, under many circumstances, $b_n < 1$.

Figure 3 shows a test case where collisional processes are dominant. All of the radiative processes discussed below are actually included, but the intensity of the external continuum is set to a very low (and hence negligible) value.

As a result collisional and spontaneous radiative processes are dominant. The electrons are given a temperature of 50,000 K, and the level populations and ionization of the gas are determined by solving the full set of equations of statistical

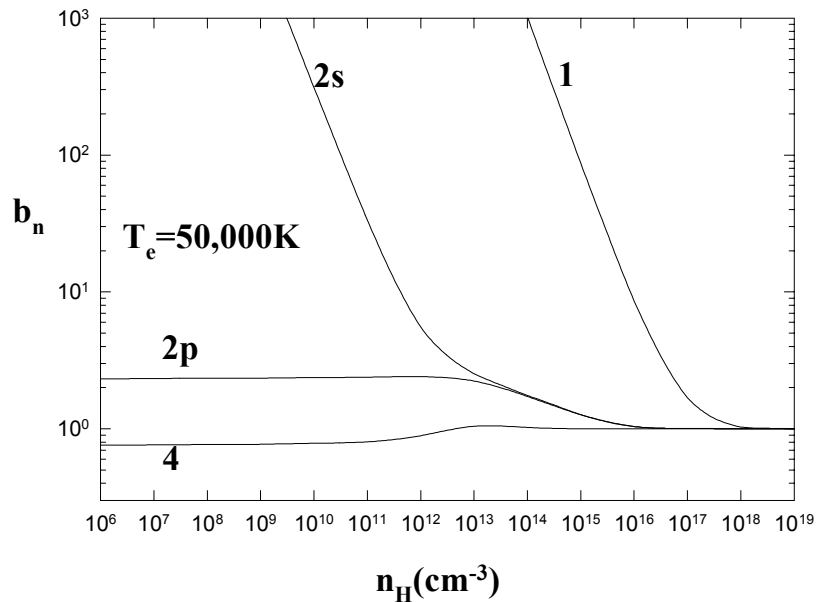


Figure 3 The equilibrium populations of the ground state and levels 2s, 2p, and 4 of the model hydrogen atom are shown as a function of the total hydrogen density n_H .

equilibrium. The model is of a very thin cell of gas that is optically thin in the lines and continuum. Departure coefficients for the ground state, 2s, 2p, and 4 are shown.

The radiation field is set to a very low intensity, and the column density is kept small enough for optical depth effects to be negligible. A constant electron temperature of 5×10^4 K is assumed, so the gas is primarily collisionally ionized and excited. Levels 2s and 2p do not mix until a density of nearly 10^{14} cm^{-3} is reached, and do not come into LTE until the density is nearly 100 times higher. The entire atom is nearly in LTE at densities greater than 10^{18} cm^{-3} .

The ground state is overpopulated relative to its LTE value when upward collisional processes are much slower than downward radiative processes. It is only when the collisional rates approach the radiative rates that b_1 approaches unity. The 2s level also has a large overpopulation for much the same reason. It is highly metastable and accumulates a large overpopulation until 2s - 2p collisions become fast enough to mix the two l levels. The more highly excited levels ($n \geq 3$) have a behavior very similar to that of $n=4$, which is shown in the figure. They are under populated relative to their LTE value when radiative decays to lower levels are

competitive with collisional processes. It is only at a density of $n_H > 10^{18} \text{ cm}^{-3}$ that collisional processes completely dominate the rate equations and the atom reaches LTE. The mean departure coefficient at a density of 10^{19} cm^{-3} is $\bar{b}_i = 1.0007 \pm 0.0022$ for the entire atom, and the largest single deviation from unity is 0.7% (for the ground level).

6.6 The Radiative Rate Equations

6.6.1 Photoionization - recombination

The photoionization rate (s^{-1}) from level n , element $nelem$, and iso-electronic sequence $ipISO$, stored in the vector $gamnc[ipISO][nelem][n]$, is given by

$$\Gamma_n = 4\pi \int_{\nu_o}^{\infty} \frac{J_\nu}{h\nu} \alpha_\nu d\nu \text{ [s}^{-1}\text{]} \quad (206)$$

and the induced recombination rate coefficient by

$$\alpha(ind) = P_n^* 4\pi \int_{\nu_o}^{\infty} \frac{J_\nu}{h\nu} \alpha_\nu \exp(-h\nu/kT) d\nu \text{ [cm}^3 \text{ s}^{-1}\text{]}. \quad (207)$$

This is evaluated at each zone by direct integration.

The ground level also includes destruction due to bound Compton scattering.

6.6.2 Derivation of radiative balance equations

Consider the balance for a level n of a three level system, with upper and lower levels u and l .

$$n_n (B_{n,u} \bar{J} + B_{n,l} \bar{J} + A_{n,l}) = n_u (B_{u,n} \bar{J} + A_{u,n}) + n_l B_{l,n} \bar{J}. \quad (208)$$

Converting densities n_i into departure coefficients, $n_i = b_i P_i^*$, we obtain

$$P_n^* b_n (B_{n,u} \bar{J} + B_{n,l} \bar{J} + A_{n,l}) = P_u^* b_u (B_{u,n} \bar{J} + A_{u,n}) + P_l^* b_l B_{l,n} \bar{J}. \quad (209)$$

Gathering LTE densities we find

$$b_n (B_{n,u} \bar{J} + B_{n,l} \bar{J} + A_{n,l}) = \frac{P_u^*}{P_n^*} b_u (B_{u,n} \bar{J} + A_{u,n}) + \frac{P_l^*}{P_n^*} b_l B_{l,n} \bar{J}. \quad (210)$$

Writing $B_{ln} = B_{nl} g_n / g_l$, we obtain the final form

$$b_n \left(\frac{g_u}{g_n} B_{u,n} \bar{J} + B_{n,l} \bar{J} + A_{n,l} \right) = \frac{P_u^*}{P_n^*} b_u (B_{u,n} \bar{J} + A_{u,n}) + \frac{P_l^*}{P_n^*} b_l \frac{g_n}{g_l} B_{n,l} \bar{J}. \quad (211)$$

6.6.3 Final radiative equations

The full set of radiative balance equations can be written as

$$\frac{db_n}{dt} = \sum_l \frac{P_l^*}{P_n^*} b_l A_{n,l} \frac{g_n}{g_l} \eta_{n,l} \gamma_{n,l} + \sum_u \frac{P_u^*}{P_n^*} b_u (A_{u,n} P_{u,n} + A_{u,n} \eta_{u,n} \gamma_{u,n}) + [\alpha(rad) + \alpha(ind)] / P_n^* - b_n \left(\sum_l (A_{n,l} P_{n,l} + A_{n,l} \eta_{n,l} \gamma_{n,l}) + \sum_u A_{u,n} \frac{g_u}{g_n} \eta_{u,n} \gamma_{u,n} + \Gamma_n \right) \quad (212)$$

where the η is the continuum occupation number in the transition ij (see page 213 above).

Figure 4 shows a test case that, in contrast to that shown in Figure 3, is dominated by radiative transitions.

Again, the full set of equations coupling the levels are solved, but spontaneous and induced processes are more important than collisions for many values

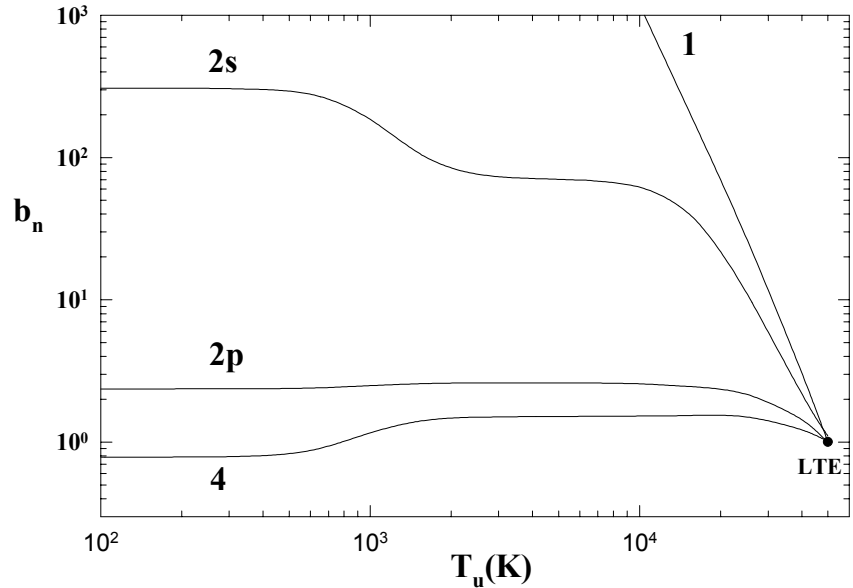


Figure 4 The calculations are for a constant temperature ($T = 5 \times 10^4$ K) optically thin gas exposed to black body radiation with a color temperature of $T_{color} = 5 \times 10^4$ K, but with various values of the energy density, parameterized as $T_u = (u/a)^{1/4}$, where u is the actual radiation density. hbnvsu

of the radiation density. The model is of a very thin cell of gas, so that all lines and continua are optically thin, has a density of $n(H) = 10^{10} \text{ cm}^{-3}$, and an electron temperature of 5×10^4 K. The gas is exposed to a black body continuum with a color temperature of $T_{color} = 5 \times 10^4$ K, but the intensity of this continuum is varied. This intensity is parameterized by an energy density temperature defined by $T_u \equiv (u/a)^{1/4}$ where u and a are, respectively, the actual radiation energy density and Stefan's radiation density constant.

A radiation field given by Planck's law (i.e., $T_u \equiv T_{color}$) forces the ionization and level population of an atom or ion to LTE in much the same way that high electron densities do. As Figure 4 shows, at very low values of T_u (low photon densities) the ground and $n = 2$ states are overpopulated for much the same reason that this occurs at low electron densities; the downward spontaneous radiative rates are fast relative to the induced (upward and downward) rates. At very low T_u (< 500 K), $n \geq 3$ levels are under populated since they decay at a rate much faster than the induced rates (for $T = 5 \times 10^4$ K these levels have $h\nu \ll kT$, so induced processes will be fast relative

to spontaneous rates when $T_u = T_{color}$ and the atom is in LTE). As T_u increases, fluorescence from the ground state over-populates excited states (because the ground state is itself overpopulated) and b_4 exceeds unity. Finally, in the limit where $T_u = T_{color}$, the departure coefficients reach unity and the atom goes to LTE. (The actual mean departure coefficient for the entire atom is $\bar{b}_i = 1.013 \pm 0.029$). Note that the vast majority of the neutral hydrogen population is in excited states when the atom approaches LTE at these temperatures.

The hydrogen density ($n(H) = 10^{10} \text{ cm}^{-3}$) is low enough for radiation to be the main agent affecting level populations for most values of T_u . Fluorescence from the ground state drives the population of $n=4$ above its LTE value for many radiation densities. Induced processes, mainly transitions between adjacent levels, drive the atom to LTE when T_u reaches $5 \times 10^4 \text{ K}$.

7 The Hydrogenic iso-sequence

Tests in the low-density, or nebular, limit show that the model atom predicts level populations and emissivities that are in much better than 1% agreement with Seaton (1959), and with the Storey and Hummer (1995) results. The atom goes to LTE in the high radiation or matter density limits.

7.1 Recombination Rates and Cooling

7.1.1 Rational approximations

It is not numerically expedient to compute these rate coefficients on-the-fly in large scale ionization/thermal structure calculations. The rate coefficients were fitted with a high-order rational approximation. The recombination rate coefficient is expressed as

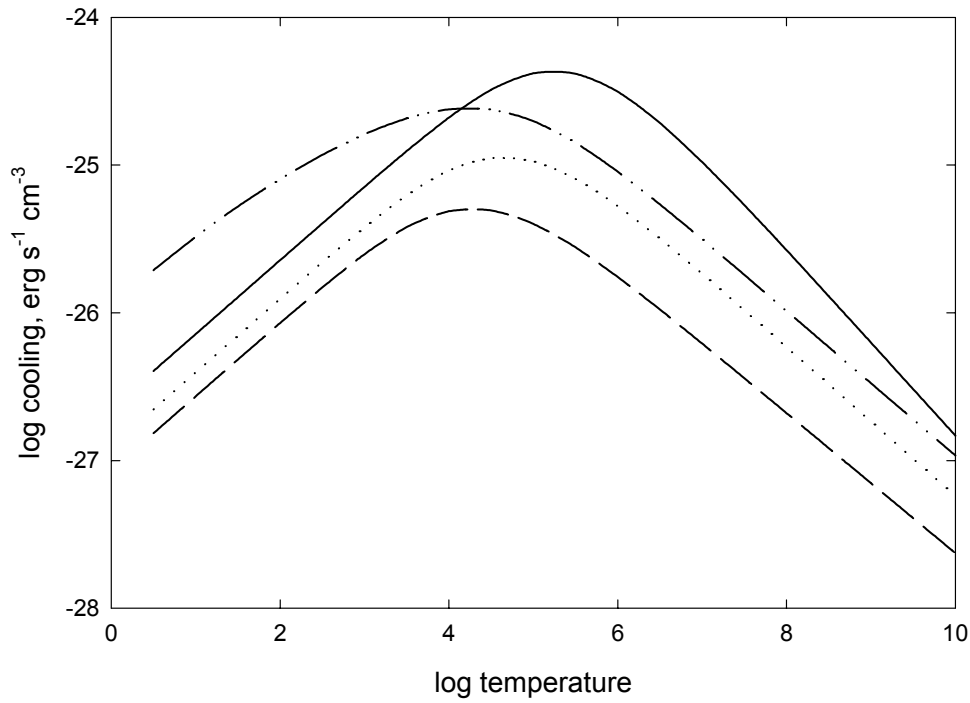


Figure 5 The recombination cooling for several states is shown as a function of temperature.

recool	3.0	7.099-26	3.785-26	2.488-26	1.784-26	1.341-26	1.039-26	1.629-25
3.5	1.241-25	6.245-26	3.796-26	2.505-26	1.740-26	1.255-26	2.082-25	
4.0	2.094-25	9.195-26	4.856-26	2.845-26	1.795-26	1.198-26	2.395-25	
4.5	3.234-25	1.112-25	4.923-26	2.557-26	1.483-26	9.305-27	2.376-25	
5.0	4.173-25	1.056-25	3.990-26	1.891-26	1.034-26	6.240-27	1.981-25	
5.5	4.149-25	7.981-26	2.698-26	1.208-26	6.389-27	3.771-27	1.390-25	
6.0	3.121-25	4.961-26	1.572-26	6.827-27	3.549-27	2.073-27	8.316-26	
6.5	1.843-25	2.616-26	8.015-27	3.429-27	1.768-27	1.028-27	4.307-26	
7.0	9.016-26	1.204-26	3.628-27	1.541-27	7.917-28	4.591-28	1.967-26	
7.5	3.847-26	4.978-27	1.487-27	6.296-28	3.229-28	1.870-28	8.109-27	
8.0	1.490-26	1.897-27	5.644-28	2.385-28	1.222-28	7.077-29	3.092-27	
8.5	5.397-27	6.811-28	2.023-28	8.541-29	4.375-29	2.533-29	1.115-27	
9.0	1.867-27	2.346-28	6.959-29	2.937-29	1.504-29	8.706-30	3.872-28	
9.5	6.261-28	7.849-29	2.327-29	9.820-30	5.028-30	2.910-30	1.316-28	
10.0	2.057-28	2.575-29	7.633-30	3.220-30	1.649-30	9.543-31	4.436-29	

$$\alpha(n, T) = 10^{F(n, T)} T^{-1} \quad (213)$$

with

$$F(n, T) = \frac{a_n + c_n x + e_n x^2 + g_n x^3 + i_n x^4}{1 + b_n x + d_n x^2 + f_n x^3 + h_n x^4} \quad (214)$$

and $x \equiv \log(T)$. The coefficients for the expansion are given in routine *hrcf*, which evaluates the rate. These approximations reproduce the numerical results with a mean error well below 0.1 percent. For levels below $n=20$ the largest error is also under 0.1 percent, although errors as large as 1.4 percent occur for the highest sum at temperatures below 100 K.

Recombination cooling coefficients were fitted to equations of the form

$$kT\beta(n, T) = 10^{F(n, T)} \quad (215)$$

where $F(T, n)$ is given above, and the fitting coefficients are given in the code. The errors in fitting these coefficients are larger, typically 0.5 percent, but sometimes as large as several percent.

7.2 Effective Transition Probabilities

7.2.1 Einstein As

Two routines are used to compute hydrogenic transition probabilities, in the limit of a completely *l*-mixed atom. The routine *fosc*(*u*, *l*) returns the absorption oscillator strength of the transition. Routine *EinstA* (*u*, *l*) drives *fosc* to actually obtain the transition probability. These routines were coded by Jason Ferguson, using algorithms given by Johnson (1972).

Note that the code considers the 2s and 2p as two separate levels. These routines return transition probabilities for a well *l*-mixed atom, and cannot be applied directly to the separate 2s and 2p levels.

7.3 Collisional contributions to hydrogen lines

Figure 6, taken from Ferland & Osterbrock (1985), shows the effects of collisional excitation on hydrogen lines. This process can be significant relative to recombination when the gas temperature is high (perhaps due to low metallicity) or in partially neutral gas that is exposed to x-rays. The lines marked “external” are reddening curves due to external dust, and “internal” tracks the effects of internal dust. The band of solutions that go across the top of the figure shows the expected hydrogen line spectrum, as set by the collision strengths of the Lyman lines.

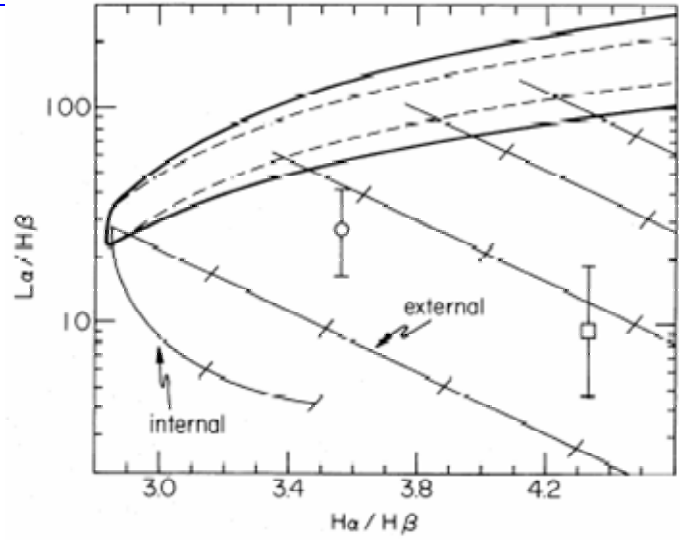


Figure 6 This figure, taken from Ferland & Osterbrock 1985, shows the effects of collisional excitation upon two ratios of hydrogen lines. The largest effects are to enhance $L\alpha$ and $H\alpha$ by large amounts.

7.4 Continuous Thermal Emission

Diffuse emission (free-free and free-bound) by all atoms is computed using the stored photoabsorption cross sections and detailed balance (i.e., the Milne relation; see Mihalas 1978).

Free-bound continua of all levels of hydrogen and helium are treated as follows. The Milne relation for the emissivity $4\pi j$ ($\text{erg cm}^3 \text{ Hz}^{-1} \text{ s}^{-1}$) can be expressed as (Brown and Mathews 1970)

$$4\pi j_\nu = h\nu \left(\frac{2\pi m_e k}{h^2} \right)^{-3/2} \frac{8\pi}{c^2} \frac{g_n}{g_e g_{ion}} T^{-3/2} \nu^2 \alpha_\nu(n) \exp(-h(\nu - \nu_o)/kT) \quad (216)$$

where the statistical weight of level n is $g_n = 2n^2$ for H^0 and He^+ , and $g_n = n^2$ for helium singlets.

The code actually works with units similar to photons $\text{Ryd}^{-1} \text{ s}^{-1} \text{ cm}^{-2}$. The photon emissivity (photons $\text{cm}^3 \text{ s}^{-1} \text{ Ryd}^{-1}$) is then

$$\begin{aligned} \varphi_\nu(T, n) &= \left(\frac{2\pi m_e k}{h^2} \right)^{-3/2} \frac{8\pi}{c^2} \frac{g_n}{g_e g_{ion}} T^{-3/2} \nu^2 \alpha_\nu(n) \exp(-h(\nu - \nu_o)/kT) \\ &= 4.12373 \times 10^{11} \frac{g_n}{g_e g_{ion}} T^{-3/2} \nu_{\text{Ryd}}^2 \alpha_\nu(n) \exp(-h(\nu - \nu_o)/kT) \end{aligned} \quad (217)$$

where the g 's are the statistical weights of the constituents, ν_{Ryd} is the photon energy in Rydbergs, $h\nu_o \sim z^2/n^2$ is the ionization potential in Rydbergs, $\alpha_\nu(n)$ is the photoionization cross section, and the other symbols have their usual meanings. Equation 217 is evaluated directly using the stored photoionization cross sections. A similar approach is used for all absorption opacities. Detailed balancing between absorption and emission mechanisms is necessary if LTE is to be achieved.

A test case with an ionized hydrogen plasma at a temperature of 10^4 K and a density of 10^7 cm^{-3} (to suppress two photon emission) was computed, and is shown in Figure 7.

The input stream used to derive the figure is given as **hemis.in** in the test suite. As can be seen from the figure, the predicted diffuse continuum is generally within a percent of the exact value (given in Ferland 1980).

Figure 8 shows another series of test cases in which a very high density gas with cosmic abundances is irradiated with a 50,000 K blackbody radiation field in strict thermodynamic equilibrium. As can be seen from the figure, the predicted continuum goes to the blackbody limit.

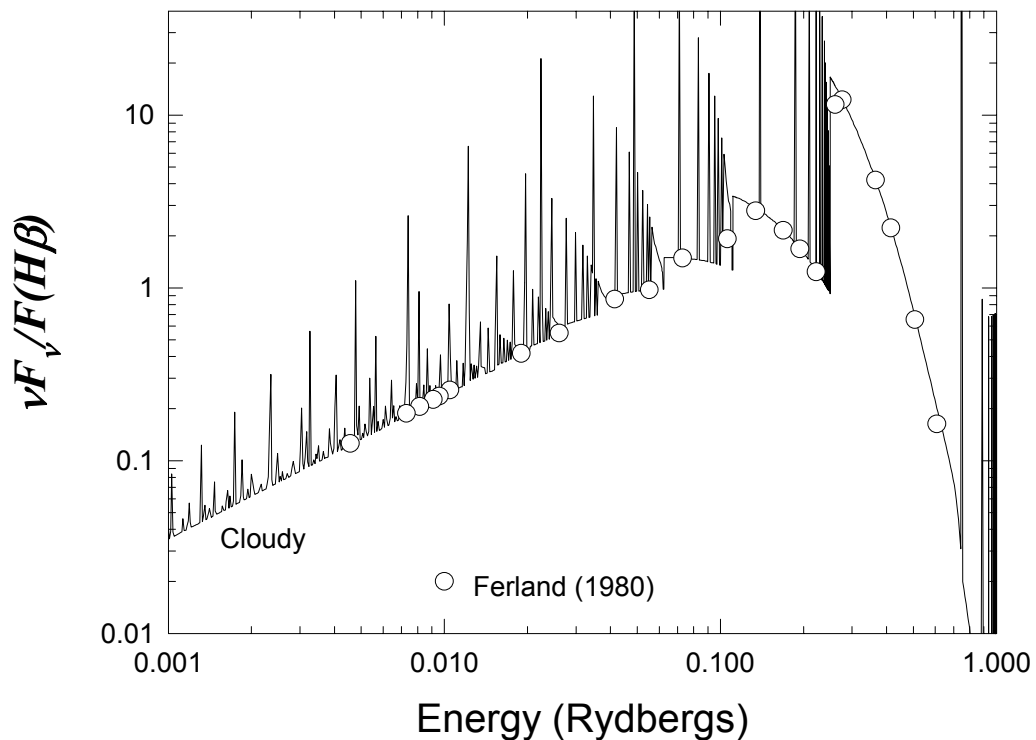


Figure 7 The emission from a slab of gas is compared with the predictions of Ferland (1980).
hemis

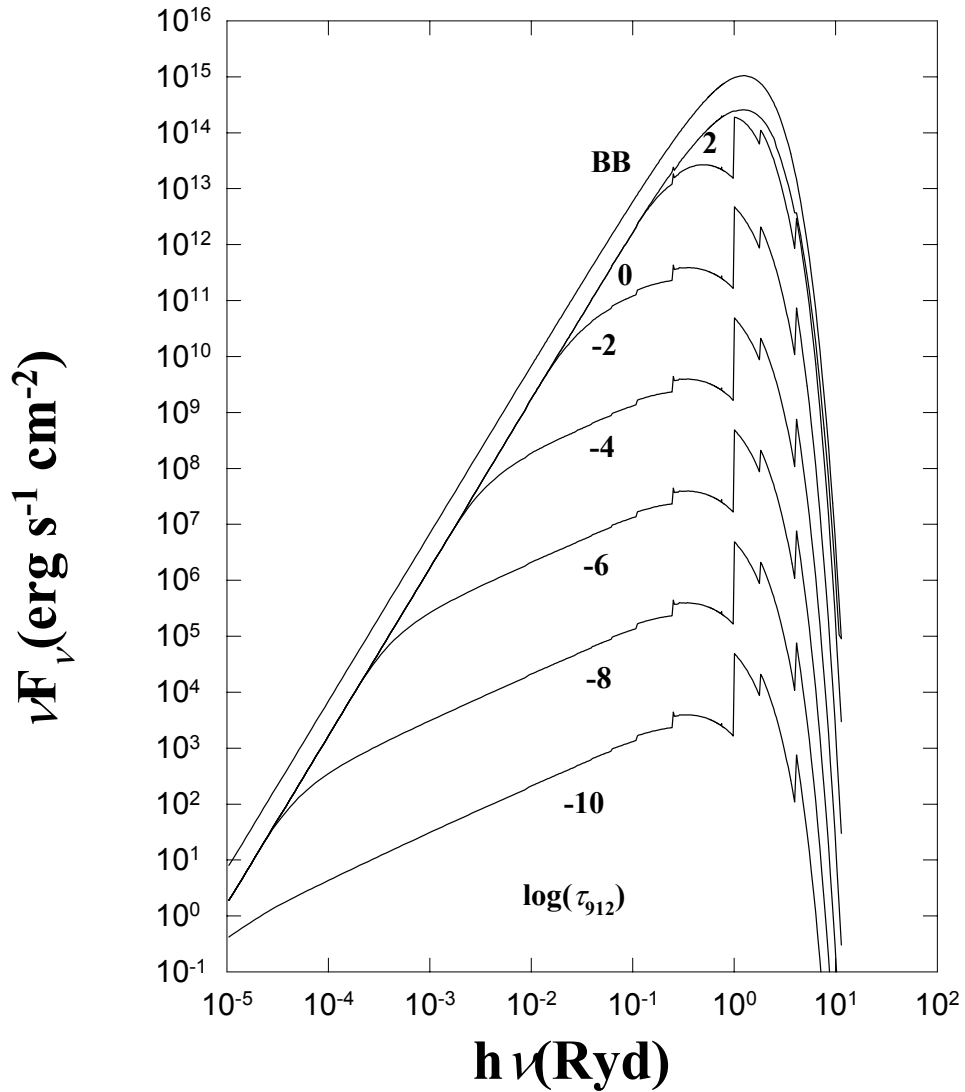


Figure 8 The emission from a dense slab of gas with cosmic abundances is shown as a function of the optical depth at the Lyman limit. The log of this optical depth is indicated on the figure. The top curve is for emission given by Planck's law. The continuous emission goes to the blackbody limit in the case of large continuum optical depths. conlte

8 HELIUM ISO-SEQUENCE

8.1 Overview

The helium-like isoelectronic sequence is treated with a single unified approach.

8.2 Energy levels

Figure 9 shows a partial Grotrian diagram for He-like ions.

The order of the J levels within $2p P^o$ is reversed for the atom; the energy levels shown in Figure 9 are for astrophysically abundant ions. In the code the energies associated with a particular J level are always correct, but for He I these occur out of order in the vector of energy levels. This is ok since the levels are so close to having the same energy.

Figure 10 compares the energies of the levels within a high- n complex of He I. For comparison, the equivalent hydrogenic energies is drawn as a dotted line. The $1P$ level is actually above the hydrogenic level but all other He I levels are below, and their energies approach the hydrogen case as the angular momentum increases. Singlets always have higher energies than triplets.

Wavelengths for lines coming from the $n = 2$ complex are listed in Table 21. These also give the letter nomenclature that is common in the X-Ray community (Porquet & Dubau 2000). Energies for lower levels of some elements are given in Table 22. The figures shows how the wavelengths of these lines changes with atomic number.

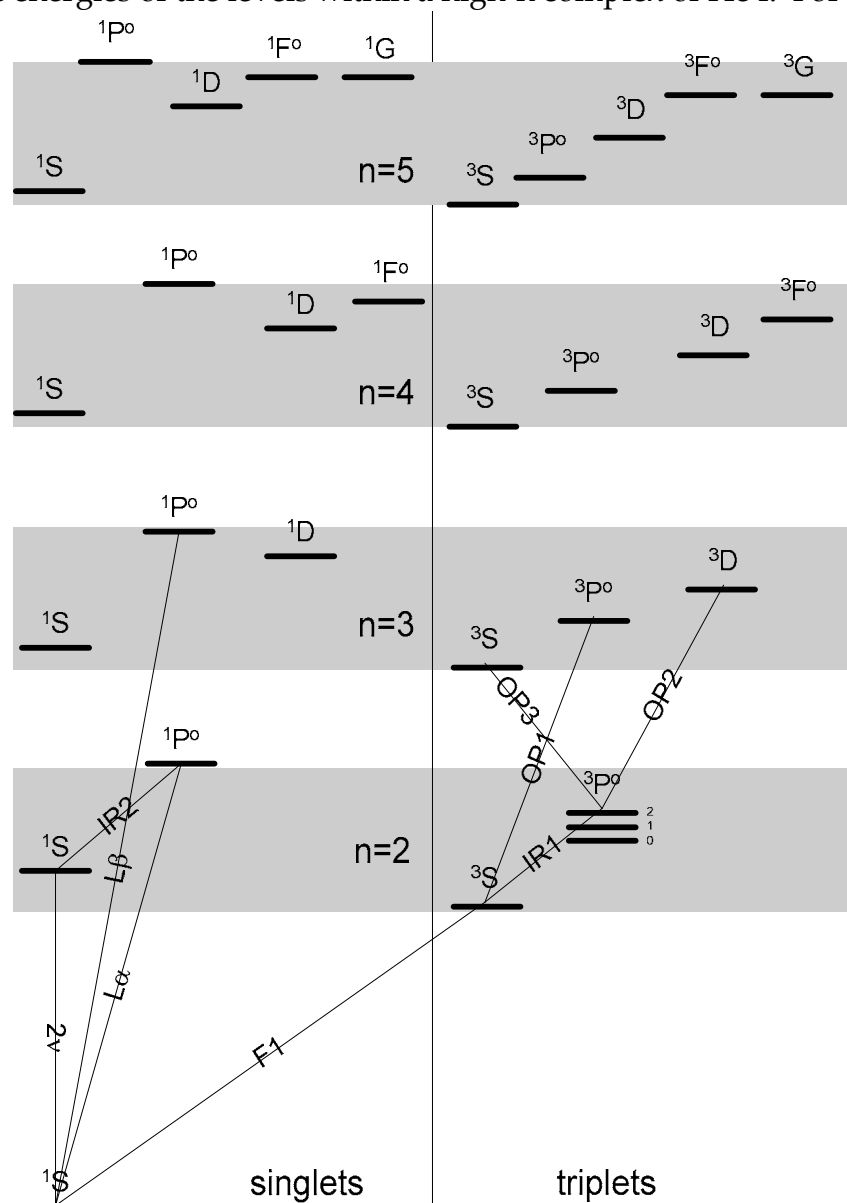


Figure 9 A partial Grotrian diagram for the helium iso-electronic sequence. helium

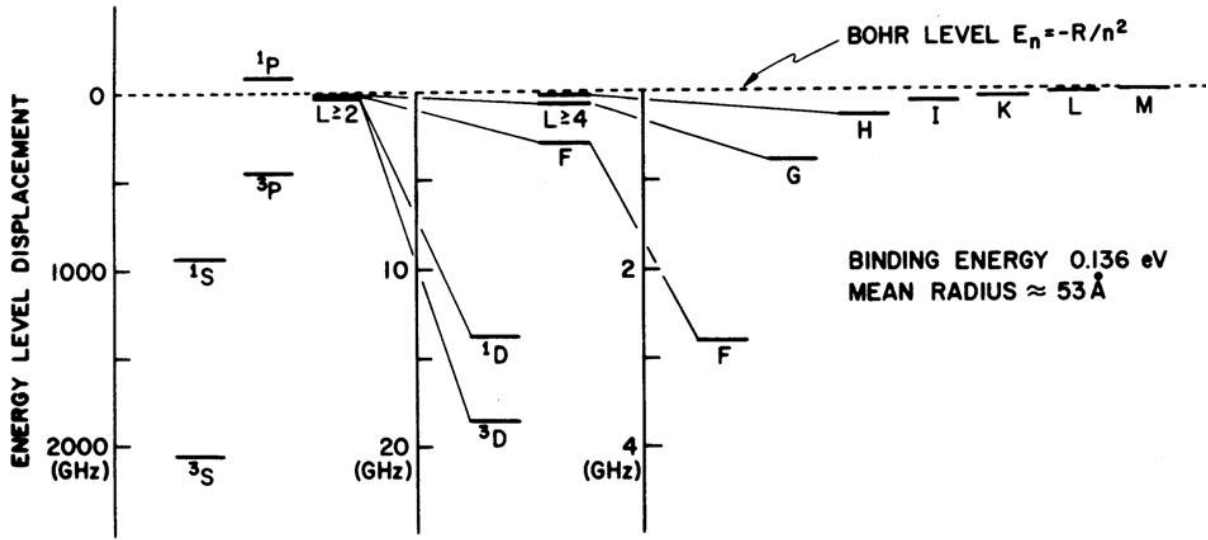


Figure 10 A comparison of energies of various states within a high-n state of He⁰ From Wino & McAdam (1978).

8.3 Collisional data

Bound-bound collision data for He⁰ come from Bray et al. (2000).

8.4 Net emission

8.5 The Helium Triplets

The population of the metastable 2s ³S level is determined including all processes that create and destroy the level. Processes that destroy 2s ³S include

photoionization and collisional ionization, radiative decays to ground, and collisional transitions to the singlets. Processes that create populations include three-body and radiative recombination and collisions to the triplets from the singlets. Including only radiative recombination, exchange collisions to the singlets, and radiative decays to ground, the relative population of the 2³S level of He⁰ can be written as

$$\frac{He(2^3S)}{He^+} = \frac{5.79 \times 10^{-6} t_4^{-1.18}}{1 + 3110 t_4^{-0.51} n_e^{-1}} \tag{218}$$

where t_4 is the electron temperature in units of 10^4 K.

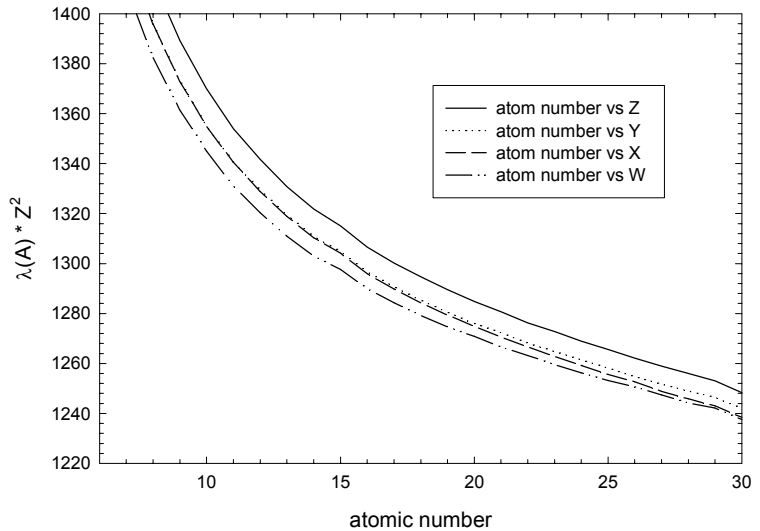


Figure 11 Wavelengths of lines from the n = 2 complex along the He iso-electronic sequence. helike_energies

8.6 Collapsed versus resolved levels

A level in which all of the spin and angular momentum states are explicitly determined individually is said to be resolved. One in which these are replaced by a single level, with the sublevels assumed to be populated according to their statistical weight, is said to be collapsed. Treating a level as a collapsed levels saves computer time and is appropriate if the density is high enough for collisions to make the state fully *l*-mixed.

Figure shows a plot of the density needed to *l*-mix a level (the y-axis) vs the principle quantum number (the x-axis). The data are taken from Pengelly & Seaton (1964). This can be used as a guide for adjusting what levels can be treated as the collapsed case.

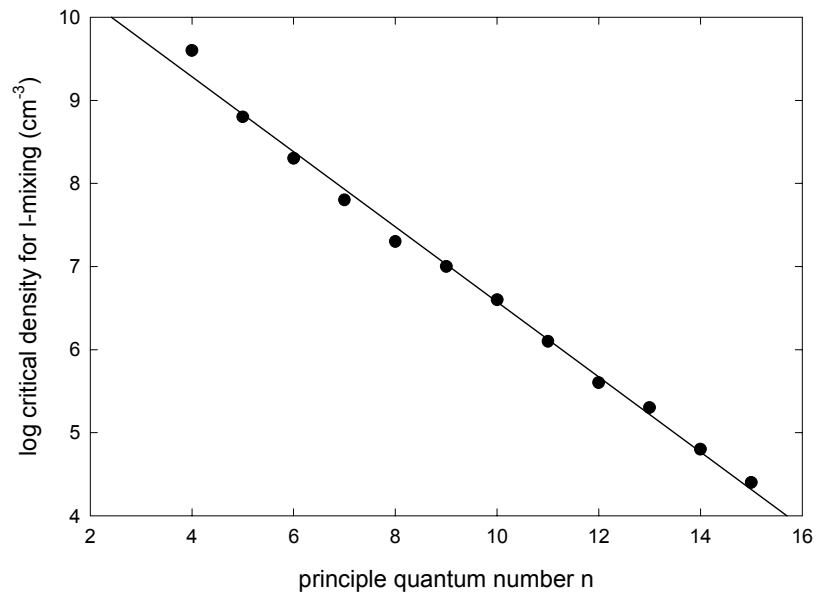


Figure 12 The lowest principle quantum number which can be treated as *l*-mixed (the x-axis) is shown versus the density for this to occur (the y-axis). Original data taken from Pengelly & Seaton (1964).

8.7 Ionization Equilibria

The ionization equilibria of the various ions/atoms is accurate for all photon and electron densities. Tests presented in Part III of this document show that the balance goes to LTE in the high photon and electron density limits.

Table 21
Wavelengths (\AA) of lines from the $n=2$
complex

Z		$2s\ ^3S$	$2p\ ^3P_1^o$	$2p\ ^3P_2^o$	$2p\ ^1P^o$
	Z	Y	X	W	
2	He	625.6	591.4	591.4	584.4
3	Li	210.3	202.2	202.2	199.3
4	Be	104.6	101.7	101.7	100.3
5	B	62.43	61.09	61.09	60.32
6	C	41.46	40.74	40.74	40.27
7	N	29.52	29.09	29.09	28.79
8	O	22.09	21.81	21.81	21.60
9	F	17.15	16.95	16.95	16.81
10	Ne	13.70	13.55	13.55	13.45
11	Na	11.19	11.08	11.08	11.00
12	Mg	9.317	9.232	9.229	9.169
13	Al	7.875	7.807	7.804	7.757
14	Si	6.744	6.688	6.685	6.648
15	P	5.845	5.799	5.796	5.767
16	S	5.104	5.065	5.062	5.039
17	Cl	4.499	4.466	4.463	4.444
18	Ar	3.996	3.967	3.964	3.948
19	K	3.572	3.547	3.544	3.531
20	Ca	3.212	3.190	3.187	3.177
21	Sc	2.904	2.885	2.881	2.872
22	Ti	2.637	2.620	2.617	2.610
23	V	2.406	2.391	2.387	2.381
24	Cr	2.203	2.190	2.186	2.181
25	Mn	2.025	2.013	2.009	2.005
26	Fe	1.867	1.856	1.853	1.850
27	Co	1.727	1.717	1.713	1.711
28	Ni	1.602	1.593	1.589	1.587
29	Cu	1.490	1.482	1.478	1.477
30	Zn	1.387	1.380	1.376	1.375

Table 22
Helium-like energy levels

index	desig	E(wn,He)	E(wn,O)	E(wn,Fe)
0	1 1S	0	0	0
1	2 3S	1.59867e+005	4.52637e+006	5.35554e+007
2	2 1S	1.66280e+005	4.58831e+006	5.38793e+007
3	2 3P ₀ ^o	1.69076e+005	4.58550e+006	5.39002e+007
4	2 3P ₁ ^o	1.69076e+005	4.58550e+006	5.39002e+007
5	2 3P ₂ ^o	1.69076e+005	4.58550e+006	5.39002e+007
6	2 1P	1.71135e+005	4.62917e+006	5.40690e+007
7	3 3S	1.83243e+005	5.33976e+006	6.34332e+007
8	3 1S	1.84866e+005	5.35628e+006	6.35220e+007
9	3 3P ₀ ^o	1.85562e+005	5.35599e+006	6.35302e+007
10	3 3D	1.86118e+005	5.36562e+006	6.35794e+007
11	3 1D	1.86118e+005	5.36562e+006	6.35794e+007
12	3 1P	1.86209e+005	5.36815e+006	6.35812e+007
13	4 3S	1.90301e+005	5.61633e+006	6.68519e+007
14	4 1S	1.90942e+005	5.62299e+006	6.68884e+007
15	4 3P ₀ ^o	1.91216e+005	5.62297e+006	6.68922e+007
16	4 3D	1.91452e+005	5.62701e+006	6.69134e+007
17	4 1D	1.91452e+005	5.62701e+006	6.69134e+007
18	4 3F	1.91452e+005	5.62701e+006	6.69134e+007
19	4 1F	1.91452e+005	5.62701e+006	6.69134e+007
20	4 1P	1.91493e+005	5.62798e+006	6.69142e+007
21	5 3S	1.93348e+005	5.74265e+006	6.84256e+007
22	5 1S	1.93664e+005	5.74591e+006	6.84432e+007
23	5 3P ₀ ^o	1.93800e+005	5.74592e+006	6.84452e+007
24	5 3D	1.93921e+005	5.74799e+006	6.84566e+007
25	5 1D	1.93921e+005	5.74799e+006	6.84566e+007
26	5 3F ₀ ^o	1.93921e+005	5.74799e+006	6.84566e+007
27	5 1F	1.93921e+005	5.74799e+006	6.84566e+007
28	5 3G	1.93921e+005	5.74799e+006	6.84566e+007
29	5 1G	1.93921e+005	5.74799e+006	6.84566e+007
30	5 1P	1.93943e+005	5.74849e+006	6.84568e+007

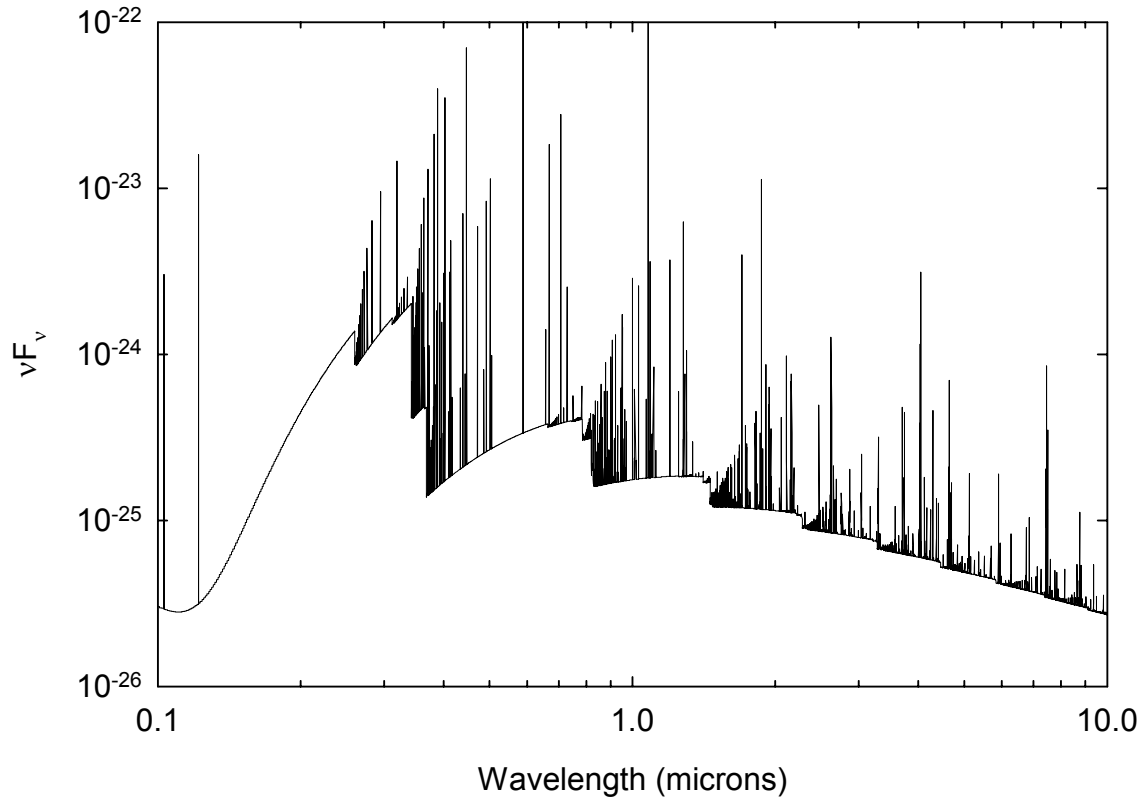


Figure 13 The net emission from a pure atomic helium gas at 10^4 K. This is from the calculation `heatomt10.in` in the test suite. .

9 H⁻ AND MOLECULES

9.1 Overview

An ion-molecule network, initially based on Black (1978) but heavily revised to include the networks described below, is included in Cloudy. The network presently includes H⁻, H₂, H₂⁺, H₃⁺, HeH⁺, OH, OH⁺, CH, CH⁺, O₂, O₂⁺, CO, CO⁺, H₂O, H₂O⁺, H₃O⁺, and CH₂⁺.

The treatment of the major hydrogen molecules (i.e., H₂, H₂⁺, H₃⁺ and H⁻) is discussed in the first subsection, and is based on Lambert and Pagel (1968); Black (1978); Lites and Mihalas (1984). The heavy element network is based on Hollenbach and McKee (1979; 1989; hereafter HM79 and HM89); Tielens and Hollenbach (1985a, b; hereafter TH85), Lenzuni, Chernoff, and Salpeter (1991; hereafter LCS91), and Wolfire, Tielens, and Hollenbach (1990); Crosas and Weisheit (1993); Puy et al (1993), Maloney, Hollenbach, & Tielens (1996), Hollenbach & Tielens (1999), and the UMIST database (<http://www.rate99.co.uk/>). This section is adapted from Ferland and Persson (1989) and Ferland, Fabian, and Johnstone (1994; 2002).

9.2 The Saha Equation for Arbitrary Systems

The Boltzmann equation relates the densities of related species by the expression

$$\frac{n_{final}}{n_{initial}} = \frac{\rho_{final}}{\rho_{initial}} \exp(-\Delta E / kT) \quad (219)$$

where $n_{initial}$ and n_{final} indicate the densities of the initial and final states, and the ρ 's are the densities of available states at a given energy. Consider the process $i \Rightarrow j+k$. The energy change during this process is

$$\Delta E = \chi_i + \frac{1}{2}mv^2 \quad (220)$$

where the first term is the ionization or dissociation potential of the initial system, and the second term represents the kinetic energy of the system in the final state. The sign of ΔE is related to the energies of the initial and final systems by

$$E_{final} = E_{initial} + \Delta E \quad (221)$$

The ρ 's entering equation 219 are the total densities of states accessible at an energy E . Since the initial state is a bound particle we can take it as at rest in the lab frame, and consider the final state consisting of two constituent particles moving with kinetic energy ΔE . The density of states of the final particles can be written as the product of densities of states due to electron spin and to motion of the particle. Nuclear spins are assumed to be uncorrelated, so nuclear statistical weights cancel out and are not carried through.

Considering only spin and motion (momentum) the total density of states is the spin statistical weight of the particle g_{spin} multiplied by the density of states due to momentum g_p (Mihalas 1978, p 112; Elitzur 1992, p 14):

$$\rho_{total} = g_{spin} g_p \quad (222)$$

where g_p is

$$g_p = \frac{dx dy dz dp_x dp_y dp_z}{h^3} . \quad (223)$$

The volume element can be removed from the problem by defining it as the volume containing one particle,

$$dx dy dz = (n_k / g_k)^{-1} \quad (224)$$

while the momentum volume element is given in terms of the particle's speed u by

$$dp_x dp_y dp_z = 4\pi p^2 dp = 4\pi m^3 u^2 du . \quad (225)$$

Combining these with equation 219 we find

$$\frac{n_{final} n_k}{n_{initial} n_i} = \frac{n_j n_k}{n_i} = \left(\frac{g_{spin,j} g_{spin,k}}{g_{spin,i}} \right) \left(\frac{g_{p,j} g_{p,k}}{g_{p,i}} \right) \exp(-\Delta E / kT) . \quad (226)$$

Shortening $g_{spin,x}$ to simply g_x , and using equation 225, we find

$$\frac{n_j n_k}{n_i} = \left(\frac{g_j g_k}{g_i} \right) \left(\frac{4\pi}{h^3} \frac{m_j^3 u_j^2 \exp(-\frac{1}{2} m_j u_j^2 / kT) du_j m_k^3 u_k^2 \exp(-\frac{1}{2} m_k u_k^2 / kT) du_k}{m_i^3 u_i^2 \exp(-\frac{1}{2} m_i u_i^2 / kT) du_i} \right) \exp(-\chi / kT) \quad (227)$$

Integrating each energy term over velocity, making the substitution

$$x \equiv \left(\frac{m}{2kT} \right)^{1/2} u , \quad (228)$$

we find

$$\int_0^\infty u_j^2 \exp(-\frac{1}{2} m_j u_j^2 / kT) du_j = \left(\frac{2kT}{m_j} \right)^{3/2} \int_0^\infty \exp(-x^2) x^2 dx = \left(\frac{2kT}{m_j} \right)^{3/2} \frac{\pi^{1/2}}{4} \quad (229)$$

where the root π over 4 is the value of the integral. The final form of the Saha equation, for an arbitrary system, is:

$$\begin{aligned} \frac{n_j n_k}{n_i} &= \left(\frac{g_j g_k}{g_i} \right) \left(\frac{2\pi kT}{h^2} \frac{m_j m_k}{m_i} \right)^{3/2} \exp(-\chi / kT) \\ &= 8.7819 \times 10^{55} \left(\frac{g_j g_k}{g_i} \right) \left(\frac{T m_j m_k}{m_i} \right)^{3/2} \exp(-\chi / kT) \end{aligned} \quad (230)$$

For the case of ionization producing an electron, the mass of the electron is neglected relative to the mass of the atom. If the atom and ion are i and j , then we have a mass ratio factor that is basically

$$\frac{m_j m_k}{m_i} = \frac{m_{ion} m_e}{m_{atom}} \approx m_e. \quad (231)$$

The most common final expression (Mihalas 1978) includes the assumption that m_i and m_k are nearly identical, and cancel out. In this case we obtain the form of the Saha equation most often encountered for hot gas, with the 2 being the spin statistical weight of the electron:

$$\frac{n_{ion} n_e}{n_{atom}} = \left(\frac{2g_j}{g_i} \right) \left(\frac{2\pi m_e kT}{h^2} \right)^{3/2} \exp(-\chi/kT). \quad (232)$$

In the case of molecular hydrogen

$$\frac{n_H n_H}{n_{H_2}} = 4 \left(\frac{\pi kT m_p}{h^2} \right)^{3/2} \exp(-\chi/kT). \quad (233)$$

9.3 The Hydrogen Network

The main hydrogen network includes H , H_2 , H_2^* , H_2^+ , H_3^+ , and HeH^+ .

The statistical weight of H_2^+ is 4 while that of H_2 is 1 and the dissociation energies are 2.647 eV and 4.477 eV respectively.

The set of balance equations for these species is solved simultaneously, using the matrix:

$$\begin{pmatrix} H \text{ conservation} \\ H^- \text{ balance} \\ H_2 \text{ balance} \\ H_2^+ \text{ balance} \\ H_3^+ \text{ balance} \end{pmatrix} \begin{pmatrix} n(H^0) \\ n(H^-) \\ n(H_2) \\ n(H_2^+) \\ n(H_3^+) \end{pmatrix} = \begin{pmatrix} n(H^0) \\ 0 \\ 0 \\ 0 \\ 0 \end{pmatrix}. \quad (234)$$

In the balance equations the process that destroy species x are entered as $c[x][x]$, (these are negative), while those which create x from y are entered as $c[x][y]$.

9.4 LTE Populations of Hydrogen Molecules

In much of the following discussion comparison and relationships will be made between the predicted hydrogen species populations and their LTE values.

The LTE relative population density of H^- is

$$P^*(H^-) = \frac{n^*(H^-)}{n_e n(H^0)} = \frac{g_{H^-}}{g_{H^0} g_e} \left(\frac{h^2}{2\pi m_e kT} \right)^{3/2} \exp(I(H^-)/kT) \text{ [cm}^3\text{]} \quad (235)$$

where g_i is the statistical weight of the constituents, ($g_{H^-} = 1$; $g_{H^0} = 2$; and $g_e = 2$), the binding energy of the negative hydrogen ion is $I(H^-) = 0.055502$ Ryd, and other constants have their usual meaning.

The LTE relative population density of H_2 is

$$P^*(H_2) = \frac{n^*(H_2)}{n(H^0)n(H^0)} = \frac{g_{H_2}}{g_{H^0}g_{H^0}} \left(\frac{h^2}{\pi m_p kT} \right)^{3/2} \exp(I(H^-)/kT) \text{ [cm}^3\text{]} \quad (236)$$

9.5 The H^- Balance; Radiative Processes

Although only a trace amount of hydrogen is in the form of H^- , the opacity provided by this ion is often dominant in the optical and near infrared, and it couples energy in the near infrared continuum to moderately ionized gas. The methods and approximations employed to include heating and cooling by H^- are described here. Other discussions can be found in Lambert and Pagel (1968), Vernazza, Avrett, and Loeser (1981), and Lites and Mihalas (1984). This section is based on Ferland and Persson (1989).

The equilibrium density of H^- is determined by assuming statistical equilibrium, and balancing production and destruction mechanisms. Great care is taken in including both forward and back reactions, to ensure that the present treatment of H^- is capable of going to LTE in the limit of high radiation or particle densities.

9.5.1 Radiative attachment

This is the most important creation mechanism for H^- at low densities, when three-body processes are negligible;



For temperatures greater than 10^4 K the rate coefficient is evaluated by numerically integrating the photodetachment cross section over frequency;

$$\alpha_{rad}(T) = P^*(H^-) \int_{\nu_0}^{\infty} \alpha_{\nu} \frac{8\pi\nu^2}{c^2} \exp(-h\nu/kT) d\nu \text{ [cm}^3 \text{ s}^{-1}\text{]} \quad (238)$$

where cross sections computed by Wishart (1979) and spline interpolation are used. These cross sections are in excellent agreement with the velocity operator bound-free cross sections tabulated by Doughty et al. (1966). The energy interval between the photodetachment threshold at 0.055502 Ryd and ~ 1.8 Ryd is divided into a large number of cells with logarithmically increasing width, and the integration is carried out as a straight forward sum.

This method is not numerically expedient for very low temperatures, where the energy bandwidth of the integral is small, and a much finer frequency grid would be required. Rather, the integration was carried out using spline interpolation and 32 point gaussian quadrature, integrating over factors of two in $h\nu/kT$. The results were then fitted with a set of power-laws. The rate coefficients can be approximated by:

$$\alpha(T_e) = \begin{cases} 8.934 \times 10^{-18} T^{0.505} & 1K \leq T < 31.62 \text{ K} \\ 5.159 \times 10^{-18} T^{0.664} & 31.62K \leq T < 90 \text{ K} \\ 2.042 \times 10^{-18} T^{0.870} & 90K \leq T < 1200 \text{ K} \quad [\text{cm}^3 \text{ s}^{-1}] \\ 8.861 \times 10^{-18} T^{0.663} & 1200K \leq T < 3800 \text{ K} \\ 8.204 \times 10^{-17} T^{0.393} & 3800K \leq T \leq 10^4 \text{ K} \end{cases} \quad (239)$$

These approximations fit the exact numerical results with a mean deviation of 0.7 percent, and the largest error of 2.05 percent, over the indicated temperature range.

Tests show that the numerical radiative attachment rates computed here are in very good agreement with the approximation given by Hutchings (1976), who used the cross sections computed by Doughty et al. (1966), for temperatures $500 \text{ K} \leq T \leq 2500 \text{ K}$. (Notice that there is a typographical error in the approximation for the radiative attachment rate given by Palla, Salpeter, and Stahler 1983.) It is also within 10% of the value given by Dalgarno and Kingston (1963), which was based on earlier calculations of the photodetachment cross section.

Continuum occupation numbers can be large in the infrared. The induced radiative attachment rate coefficient is

$$\alpha_{ind}(T) = P^*(H^-) \int_{\nu_0}^{\infty} \alpha_{\nu} \frac{4\pi J_{\nu}(\tau)}{h\nu} \exp(-h\nu/kT) d\nu \quad [\text{cm}^3 \text{ s}^{-1}] \quad (240)$$

where the mean intensity of the depth-dependent continuum is $J_{\nu}(\tau)$. This expression is used for all temperatures.

9.5.2 Photodetachment

Photodetachment,



is the dominant H- destruction mechanism for many conditions. The rate is evaluated in the standard manner;

$$\Gamma(H^-) = \int_{\nu_0}^{\infty} \alpha_{\nu}(bf) \frac{4\pi J_{\nu}(\tau)}{h\nu} d\nu \quad [\text{s}^{-1}] \quad (242)$$

The integral is evaluated as a sum over the numerically binned continuum. The incident continuum is then attenuated by optical depth increments

$$d\tau(H^-) = \alpha_{\nu}(bf) n(H^-) \left\{ 1 - \exp(-h\nu/kT) / b_{H^-} \right\} f(r) dr \quad (243)$$

where b_{H^-} is the departure coefficient for H-, $b_{H^-} \equiv n(H^-)/n^*(H^-)$, $f(r)$ is the filling factor, and $n^*(H^-)$ is the LTE H- density.

9.5.3 Photodetachment by hard photons

The H- photoabsorption cross section increases above $\sim 3/4$ Ryd, energies where excitation of $n \geq 2$ levels is possible. Cross sections that include this process are taken from Broad and Reinhardt (1976). These calculations do not extend to high energies,

so I scaled high-energy hydrogen cross sections by the ratio of H^- to H^0 cross sections at 18\AA in order to take absorption of x - and γ -rays into account.

The cross section for $(\gamma, 2e^-)$ absorption is much smaller than (γ, e^-) (Broad and Reinhardt 1976), and this latter process is neglected.

9.5.4 The approach to LTE; high radiation densities

As a test of the assumptions and methods, the approach to LTE under conditions determined by radiative attachment (spontaneous and induced) and photodetachment are first considered. Tests in which

gas with temperature T is exposed to black body radiation fields with color temperature T_{color} are computed. The color and gas temperatures are set equal, $T = T_{color}$, and the intensity of the radiation field is varied up to the black body limit. The intensity of the radiation field is parameterized by the equivalent energy density temperature $T_u = (u/a)^{1/4}$, where u is the energy density (erg cm^{-3} ; see above) and a is the Stefan's radiation density constant. The equilibrium population of H^- was computed, including all process mentioned below, but with the hydrogen density small enough (typically $\sim 10^5 \text{ cm}^{-3}$) for radiative processes to be most important. The H^- population is expressed as a departure coefficient, and the results are shown in Figure 14, for tests in which $T_{color} = 0.5, 1, \text{ and } 2 \times 10^4 \text{ K}$.

When $T_u = T_{color}$, and the radiation field is in strict thermodynamic equilibrium, radiative processes must hold H^- in LTE and departure coefficients of unity are expected. The computed departure coefficients for the three temperatures are 0.9998, 0.9996, and 1.0030, respectively. As the Figure shows, when T_u is lowered below T_{color} , the intensity of the radiation field falls below its thermodynamic equilibrium value, and the population of H^- increases. This is because the photodetachment rate (which is proportional to the intensity of the radiation field) is no longer in balance with the radiative attachment rate (which is proportional only to the electron density).

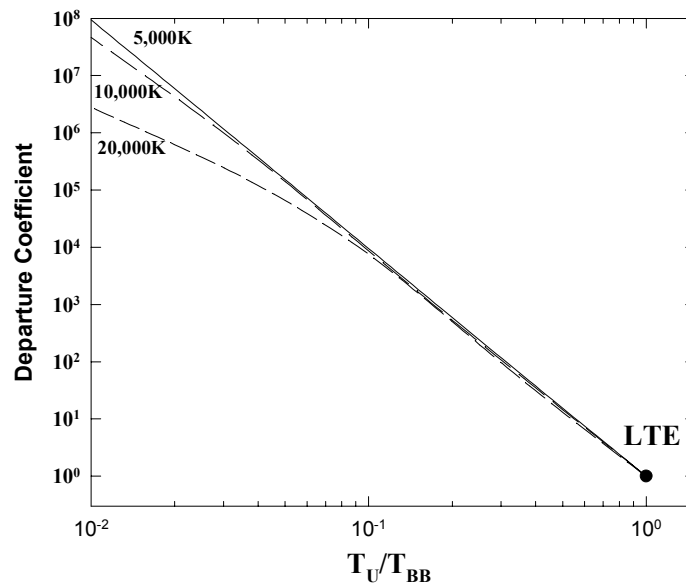


Figure 14 Departure coefficients for H^- . The figure shows tests in which the hydrogen density was held fixed at a low and the gas irradiated by black bodies with color temperatures of 5, 10, and $20 \times 10^3 \text{ K}$. Gas temperature and color temperatures were equal. The energy density temperature T_u was varied up to its LTE limit. The H^- departure coefficient is within 0.2% of unity when $T_u = T_{color}$. hmivsu

9.6 The H⁻ Balance; Collisional Processes

9.6.1 Associative detachment

The most important H₂ formation mechanism in grain-free environments, and a significant H⁻ destruction mechanism, is associative detachment,



where rate coefficients were originally from Bieniek and Dalgarno (1979) and have been updated to Launay et al. (1991). The rate is shown in Figure 15. The reverse reaction rate C_R , for electron collisional dissociation of H₂, is related to the forward rate coefficient C_F by detailed balance;

$$C_R = C_F \frac{P^*(H^-)}{P^*(H_2)} \quad [s^{-1}]. \quad (245)$$

9.6.2 Electron collisional detachment

For nebular temperatures ($\sim 10^4$ K) and moderate levels of ionization, the process



is a competitive H⁻ destruction mechanism. Rates taken from the compendium of Janev et al. (1987) are used. The reverse process, electron three-body recombination with neutral hydrogen, is included via detailed balance;

$$C_R = C_F \frac{P^*(H^-)}{P^*(H^0)} \quad [s^{-1}] \quad (247)$$

9.6.3 Collisional ionization by suprathermal electrons

The total suprathermal collisional ionization rate is computed using

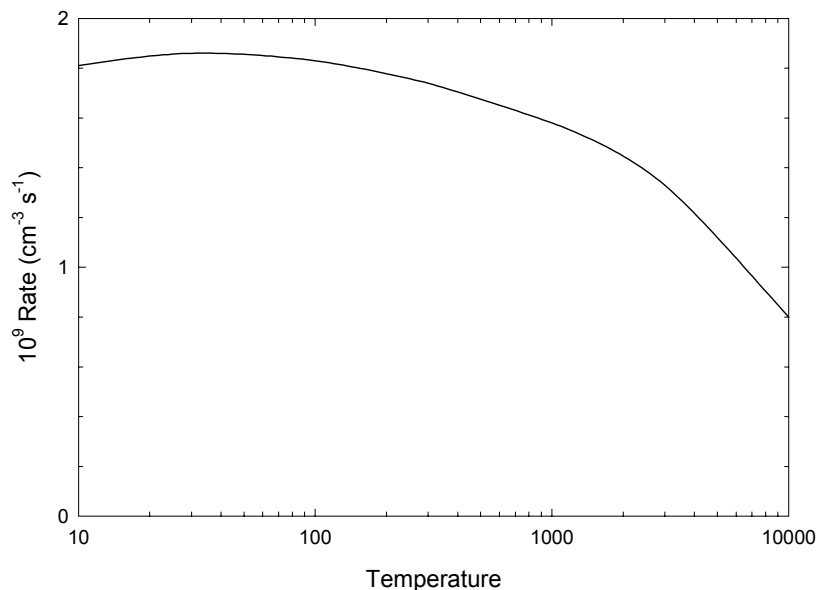
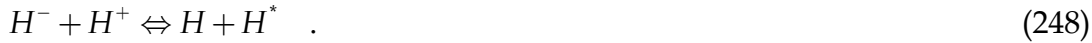


Figure 15 Rate coefficient for H⁻ → H₂. The rates are taken from Launay et al. (1991)

approximations from Shull and Van Steenberg (1985). Ionization of H⁻ by suprathermal electrons is scaled from the H⁰ rates using cross sections at 20 eV given by Janev et al. (1987). This energy was chosen as representative of the mean energy of the secondary electron shower. The majority of these collisions are of the form e⁻ + H⁻ → H(1s) + 2e⁻, although e⁻ + H⁻ → H⁺ + 3e⁻ collisions occur roughly 1% of the time.

9.6.4 Mutual neutralization

Neutral hydrogen can charge transfer with the negative ion through



The rate coefficients given in Janev et al. (1987) are used. By far the largest rate coefficients are for collisions that populate hydrogen in the $n=3$ level. These rates are based on both experimental and theoretical data (see, for example, Peart et al. 1985).

The reverse reaction is included using detailed balance. If the rate coefficient for the forward reaction is C_F then the reverse reaction rate, and its rate coefficient C_R , are given by

$$C_F P^*(H^-) P^*(H^+) = C_R P^*(H^0) P^*(H^0) \quad (249)$$

where n_i and b_i are the population and departure coefficient of hydrogen in the i^{th} level.

9.6.5 Charge neutralization with heavy elements

The process



is considered by Dalgarno and McCray (1973), who give rate coefficients for very low temperatures and ionization levels. Judging from the curves given by Peterson et al. (1971), upon which the Dalgarno and McCray rates are based, the approximation they give should still be valid (although very uncertain) at temperatures of general interest ($\sim 0.5 - 1.0 \times 10^4$ K). Here A^+ is all singly ionized species, which are assumed to be neutralized at the same rate.

9.6.6 Neglected processes

Collisional detachment by protons ($p^+ + H^- \rightarrow H + p^+ + e^-$), which has a negligible rate coefficient according to Janev et al. (1987), is neglected, as is collisional detachment by atomic hydrogen ($H^- + H \rightarrow 2H + e^-$), which has no reliable rate coefficient according to Lites and Mihalas (1984).

9.6.7 The approach to LTE; high hydrogen densities

A series of models in collisional equilibrium was computed. Radiative processes were also included, but the incident radiation field, a 10^4 K blackbody, was given a negligible intensity (an ionization parameter of 10^{-12}). Three temperatures, 0.5, 1, and 2×10^4 K, were considered to span the temperature range typical of regions with significant H⁻ population. The hydrogen density was varied between 10^8 and 10^{18} cm⁻³ to confirm the approach to LTE at high densities. The results of these calculations are shown in Figure 16.

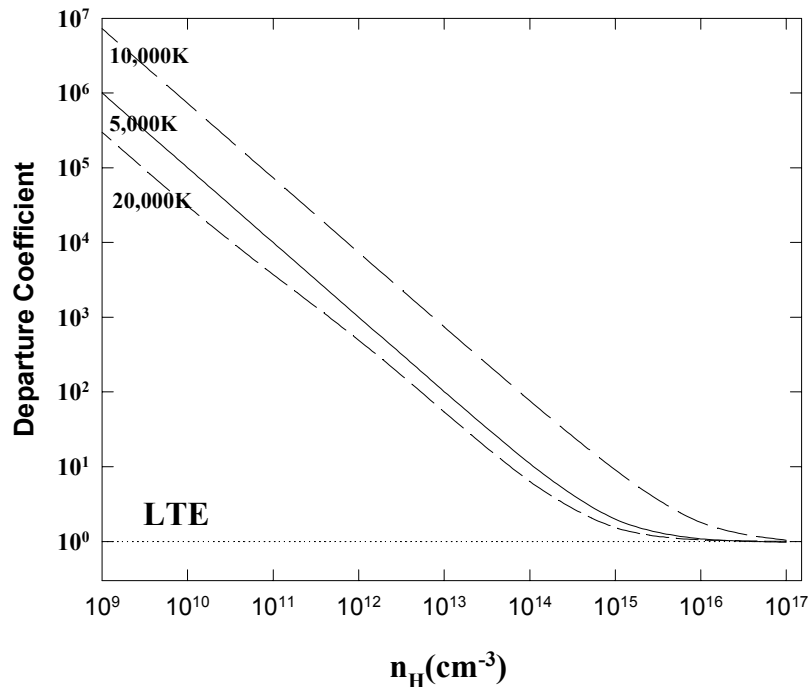


Figure 16 Departure coefficients for H⁻ are shown. The radiation density was low and the total hydrogen density varied. Three gas temperatures are shown. Collisions bring H⁻ to LTE at high densities. hmivsn

For the majority of the calculations hydrogen is largely neutral, and for the smaller temperatures a significant fraction of the hydrogen was in the molecular form (H₂ and H₂⁺). The calculation confirms that the departure coefficients are within 2% of unity at the highest densities computed.

9.7 The HeH⁺ Molecular Ion

Rates for radiative association of He and H⁺ to form HeH⁺ are taken from Zygelman and Dalgarno (1990).

9.8 The H₂ Molecule

The hydrogen chemistry network includes the ion-molecules H₂, H⁻, H₂⁺, and H₃⁺. All of the chemical reactions involving H₂ described by HM79, TH85, HM89, and LCS91 have been incorporated in the present treatment. Rather than go into these details, which are well presented in these papers, we only outline details of how some of the processes have been implemented.

9.8.1 Associative detachment of H⁻

The process



is the main H₂ formation mechanism in low-density grain-free regions, and is treated as described above. At temperatures of interest here (~10³ K) the rate for H₂

formation by this process is set by the rate for radiative association to form H^- , and is of order $10^{-15} \text{ cm}^3 \text{ s}^{-1}$ (see above).

9.8.2 Catalysis on grain surfaces

The process



is a competitive H_2 formation process when grains are present. The rate coefficient is taken from Hollenbach and McKee (1979) and Cazaux & Tielens (2002). Defining the fraction of atoms which form molecules as

$$f_a = \left(1 + 10^4 \exp(-600/T_{gr})\right)^{-1} \quad (253)$$

then the rate coefficient is given by

$$\alpha_{gr}(H_2) = 3 \times 10^{-18} \frac{\sqrt{T} A_{gr} f_a}{1 + 0.04 \sqrt{T_{gr} + T} + 0.002T + 8 \times 10^{-6} T^2} [\text{cm}^3 \text{ s}^{-1}] \quad (254)$$

where A_{gr} is the grain abundance relative to the ISM value, and T and T_{gr} are the electron and grain temperatures respectively. The grain temperature is determined self-consistently, including radiative and collisional heating and cooling, as described in the section "Grain Physics" beginning on page 307 below.

At $T=10^3 \text{ K}$ and $T_{gr}=100 \text{ K}$ (representative values of the gas and grain temperature in regions near a $H^0 - H_2$ interface) the rate coefficient for grain catalysis is $\sim 4 \times 10^{-18} \text{ cm}^3 \text{ s}^{-1}$. For most conditions where carbon is at least once ionized radiative association through H^- is at least a competitive H_2 formation mechanism. The ratio of the two processes (referred to as the H^- and grain H_2 formation routes) is then

$$\frac{r(H^-)}{r(\text{grain})} = \frac{n_e \alpha(H^-)}{n_H \alpha(\text{grain})} \approx \frac{n_e}{n_H} 250 \quad (255)$$

i.e., the H^- route is faster for conditions of moderate ionization ($n_e/n_H > 4 \times 10^{-3}$) even when grains are present. When grains are absent (or deficient) the H^- route dominates.

9.8.3 Excited atom radiative association

Rates for the process



are taken from Latter and Black (1991).

9.8.4 Excited molecular dissociation

Rates for the process



are given in Janev et al. (1987; their process 2.2.17), and these have been adopted by Lenzuni et al. (1991) and Crosas and Weisheit (1993) in their work on high density gas. Tests show that this process, if taken at face value, is by far the fastest destruction mechanism for molecular hydrogen under ISM conditions.

The process outlined by Janev et al. (1987) involves an electron capture by H₂ into vibrationally excited levels ($4 \leq v \leq 9$). The process is fast at low temperatures because the energy barrier is small, and the excited levels have large populations at laboratory densities. The process proceeds much more slowly at ISM densities, however, because excited levels have populations below their LTE value. This situation is thus similar to that described by Dalgarno and Roberge (1979). We have modified the Janev et al. (1987) rates using the physics outlined by Dalgarno and Roberge.

9.8.5 Discrete absorption into Lyman and Werner bands

Line absorption and excitation leading to dissociation through the vibrational continuum,



is the dominant H₂ destruction mechanism in regions where photodissociation (by photons with $h\nu > 14.7$ eV) and photo-ionization (with $h\nu > 15.4$ eV) do not occur (Stecher and Williams 1967).

Photodissociation through the Lyman-Werner bands occurs through a large number of transitions between 1109Å and the Lyman edge for a region shielded by atomic hydrogen (i.e., no radiation shortward of 912Å). Individual H₂ electronic transitions become optically thick for sufficient column densities, and eventually the H₂ becomes self-shielding. H₂ then becomes the dominant hydrogen species.

Photodissociation through the Lyman-Werner bands is included using the approximations outlined by TH85. The incident radiation field is taken as the mean over the energy interval 1109Å–912Å, (appropriate for photo-excitation into the $B^1 \Sigma_u^+$ electronic state). This quantity is then reposed in terms of the Habing (1968) radiation field, which is the quantity used by TH85. H₂ self-shielding is included using escape probabilities and the deduced optical depth, again using the approximations described by TH85.

9.8.6 Photo-ionization to H₂⁺

Photons with energies greater than 15.4 eV produce H₂⁺ via



This process both creates H₂⁺ and heats the gas. Photo-absorption cross sections are taken from the compendium of Janev et al. (1987).

9.8.7 Collisional dissociation by H⁰, He⁰, and e⁻

The rate coefficient for the forward process, collisional dissociation by the species S (one of H⁰, He⁰, or e⁻),



is taken from Dove and Mandy (1986; dissociation by H^0), Dove et al. (1987; dissociation by He^0) and Janev et al. (1987; dissociation by electrons). These can be important destruction mechanisms only for warm regions of the ISM because of the large binding energy of H_2 ($\sim 50,000$ K).

The reverse reactions are included via detailed balance. Three-body formation of H_2 is important only for very high densities ($n \gg 10^{10} \text{ cm}^{-3}$).

9.8.8 H_2 cooling

Cooling due to collisional excitation of vibration-rotation levels of H_2 is treated using the analytic fits given in Lepp and Shull (1983). Both $H_2 - H$ and $H_2 - H_2$ collisions are included.

9.8.9 H_2 heating

Many electronic excitations eventually decay to excited vibration-rotation levels within the ground electronic state, and these can then heat by gas following collisionally de-excitation. The scheme outlined by TH85 is again used.

9.9 Heavy Element Molecules

The heavy element molecule network described by Hollenbach and McKee (1989) has been incorporated into Cloudy.

The system of equations which are solved are as follows:

$$\begin{pmatrix} \text{C conservation} \\ \text{O conservation} \\ \text{CH balance} \\ \text{CH}^+ \text{ balance} \\ \text{OH balance} \\ \text{OH}^+ \text{ balance} \\ \text{CH}_2^+ \text{ balance} \\ \text{C}^+ \text{ balance} \\ \text{CO balance} \\ \text{CO}^+ \text{ balance} \\ \text{H}_2\text{O balance} \\ \text{H}_2\text{O}^+ \text{ balance} \\ \text{H}_3\text{O}^+ \text{ balance} \\ \text{O}_2 \text{ balance} \\ \text{O}_2^+ \text{ balance} \end{pmatrix}
 \begin{pmatrix} C \\ O \\ CH \\ CH^+ \\ OH \\ OH^+ \\ CH_2^+ \\ C^+ \\ CO \\ CO^+ \\ H_2O \\ H_2O^+ \\ H_3O^+ \\ O_2 \\ O_2^+ \end{pmatrix}
 =
 \begin{pmatrix} C_{total} \\ O_{total} \\ 0 \\ 0 \\ 0 \\ 0 \\ 0 \\ 0 \\ 0 \\ 0 \\ 0 \\ 0 \\ 0 \\ 0 \\ 0 \end{pmatrix}
 \quad (261)$$

The heavy element chemistry network includes the molecules CH, CH^+ , OH, OH^+ , CH_2^+ , CO, CO^+ , H_2O , H_2O^+ , H_3O^+ , O_2 , and O_2^+ . The heavy element network, the hydrogen network described above, and the hydrogen-helium ionization balance

network, are solved self-consistently. Of the 12 molecules in the heavy element network only CO develops a significant population under most circumstances.

9.9.1 Collisional Processes

The collision networks described by the references given at the start of the section are included. Their approximations for the temperature dependence of the rate coefficients are used.

Photodissociation by line absorption of CO was updated to the formalism given by Hollenbach, Takahashi, & Tielens, (1991; their equations 11 and 12), which was based on the work of van Dishoeck & Black (1988). Additionally the rate coefficients for the reaction network have been updated to the rates given in Hollenbach et al.

9.9.2 Photochemical processes and heating

Rates for photochemical reactions of the form $h\nu + XY \Rightarrow X + Y$ are largely taken from the compendium of Roberge et al. (1991). These are posed in terms of the average interstellar radiation field. They have been incorporated by taking the depth-dependent continuum, renormalizing this to the average interstellar radiation field, and then using the coefficients given by Roberge et al.

An exception to this prescription is CO, which can become a major opacity source. Photodissociation is treated by numerically integrating over the continuum (with a threshold of 12.8 eV) using the photodissociation cross section given by HM79.

Photodissociation heats the gas if the internal energy of the daughters is small. The kinetic energy is taken to be $\langle h\nu - DE \rangle$ where DE is the dissociation energy and the mean is over the portion of the Balmer continuum that is active. Again, an exception is CO (the most important since it is the only heavy molecule that becomes optically thick), where the heating is evaluated by numerically integrating over the attenuated incident continuum.

9.9.3 Cooling

Cooling due to collisional excitation of vibration-rotation levels of CH, OH, and H₂O is treated using the scheme outlined by HM79.

Of these CO is the most important. ¹²CO and ¹³CO are treated as multi-level rigid rotors, with the full spectrum of the ground vibration state predicted.

9.9.4 CO Lines

Table 23 lists the lowest rotation transitions of the ¹²CO and ¹³CO rotation ladder.

Label	λ	g_l	g_u	gf	A	Label	λ
¹² CO	2589m	1	3	2.24E-08	7.43E-08	¹³ CO	2475m
¹² CO	1294m	3	5	8.96E-08	7.14E-07	¹³ CO	1238m
¹² CO	863.0m	5	7	2.02E-07	2.58E-06	¹³ CO	825.0m
¹² CO	647.2m	7	9	3.58E-07	6.34E-06	¹³ CO	618.8m
¹² CO	517.8m	9	11	5.60E-07	1.27E-05	¹³ CO	495.0m

12CO	431.5m	11	13	8.07E-07	2.22E-05	13CO	412.5m
12CO	369.8m	13	15	1.10E-06	3.57E-05	13CO	353.6m
12CO	323.6m	15	17	1.43E-06	5.37E-05	13CO	309.4m
12CO	287.7m	17	19	1.81E-06	7.70E-05	13CO	275.0m
12CO	258.9m	19	21	2.24E-06	1.06E-04	13CO	247.5m
12CO	235.4m	21	23	2.71E-06	1.42E-04	13CO	225.0m
12CO	215.7m	23	25	3.23E-06	1.85E-04	13CO	206.3m
12CO	199.1m	25	27	3.79E-06	2.36E-04	13CO	190.4m
12CO	184.9m	27	29	4.39E-06	2.95E-04	13CO	176.8m
12CO	172.6m	29	31	5.04E-06	3.64E-04	13CO	165.0m
12CO	161.8m	31	33	5.74E-06	4.43E-04	13CO	154.7m
12CO	152.3m	33	35	6.48E-06	5.32E-04	13CO	145.6m
12CO	143.8m	35	37	7.26E-06	6.33E-04	13CO	137.5m
12CO	136.3m	37	39	8.09E-06	7.45E-04	13CO	130.3m
12CO	129.4m	39	41	8.96E-06	8.70E-04	13CO	123.8m

10 THE HEAVY ELEMENTS

10.1 Overview

The code considers all 465 atoms and ions of the lightest 30 elements. The treatment of the ionization equilibrium of ions with more than two electrons is fairly conventional (see, for instance, Halpern and Grindlay 1980; Kallman and McCray 1982). This treatment is more approximate than that of the H and He iso-sequences because the majority of ions are treated considering only the ground term and continuum for each ionization stage. In all cases, collisional ionization from ground (using data from Voronov 1997; and Xu and McCray 1991) and a net three-body recombination coefficient (see, for example, Burgess and Summers 1976; the actual code is taken from Cota 1987) are included. Photoionization rates are modified for induced recombination as described by equation 207. All published charge transfer rate coefficients are also included (Kingdon and Ferland 1996). Inner shell photoionization is treated using Auger yields given by Kaastra and Mewe (1993). Photoionization cross sections are from Verner et al. (1996).

This treatment is approximate at high densities for two reasons. First, net radiative recombination coefficients, which have been summed over all levels (Aldrovandi and Pequignot 1972; Aldrovandi and Péquignot 1974; Gould 1978; Verner and Ferland 1996), are used. These sums are correct only in the low-density limit. At high densities levels can undergo collisional ionization before radiative decays to the ground state occur. This brings high levels into LTE, which actually increases the recombination rate. A second problem is that substantial populations can build up in highly excited states when the density and temperature are high. When this occurs, the partition function of the atom or ion is no longer equal to the statistical weight of the ground state. As a result the ionization equilibrium of the heavy elements is approximate for very high densities ($n \gg 10^{10} \text{ cm}^{-3}$), with uncertainties increasing for higher densities. The statistical and thermal equilibrium of high-density gas is an area of on-going research.

Many exotic line transfer effects can influence certain lines due to coincidental

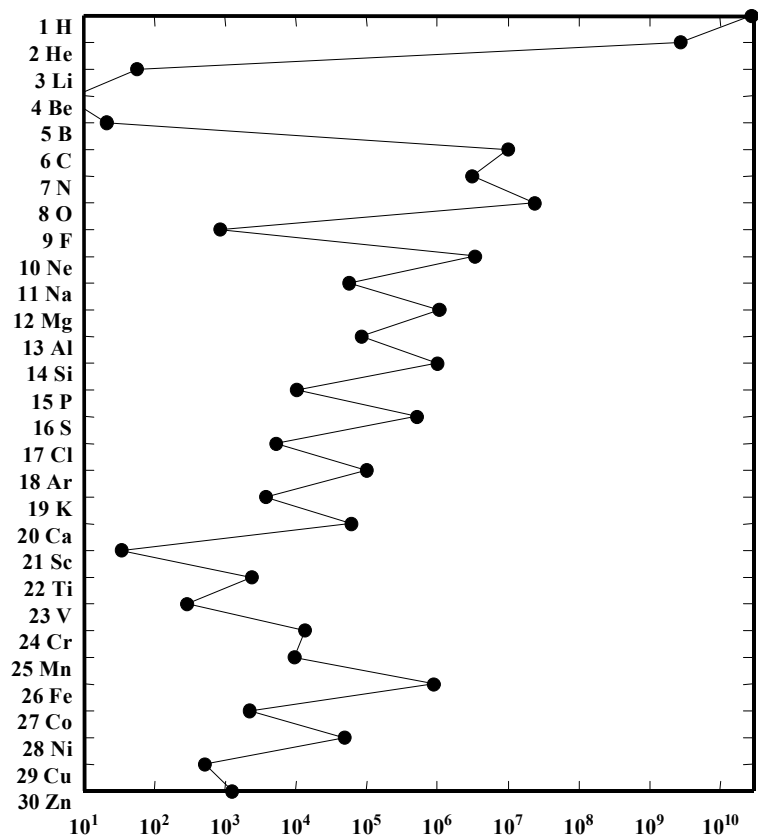


Figure 17 Solar system abundances are shown. ssystem

line overlap. A good general reference to a number of these processes is the paper by Swings and Struve (1940). All of these processes are included in the line formation processes for those lines that are predicted by the code. Morton, York, and Jenkins (1988) and Verner, Verner, and Ferland (1996) provide a line list for UV resonance lines, and Bowen's 1960 paper on forbidden lines remains a classic.

The effects of resonant structures often dominate collision strengths for infrared transitions. Oliva, Pasquali and Reconditi (1996) and van Hoof et al. (2000a) stress the uncertainties these may introduce.

10.2 Solar System Abundances

Figure 17 plots the solar system abundances of the elements, as tabulated by Anders and Grevesse (1989) and Grevesse and Noels (1993). The x-axis is the abundance by number relative to a scale where the abundance of silicon is 10^6 . The y-axis lists the atomic number and the chemical symbol for the element.

10.3 Periodic Table

A periodic table of the first 36 elements follows.

1 H																	2 He
3 Li	4 Be											5 B	6 C	7 N	8 O	9 F	10 Ne
11 Na	12 Mg											13 Al	14 Si	15 P	16 S	17 Cl	18 Ar
19 K	20 Ca	21 Sc	22 Ti	23 V	24 Cr	25 Mn	26 Fe	27 Co	28 Ni	29 Cu	30 Zn	31 Ga	32 Ge	33 As	34 Se	35 Br	36 Kr

10.4 Ionization Balance

10.4.1 Photoionization cross sections

Photoionization cross sections for all elements are evaluated using Dima Verner's routine *phfit*, which fits Opacity Project data where possible, and the best theoretical or experimental data for other cases. The fitting procedure is described in Verner Yakovlev, Band, and Trzhaskovshaya (1993), Verner and Yakovlev (1995), and Verner, Ferland, Korista, and Yakovlev (1996).

10.4.2 Auger multi-electron ejection

Many electrons may be ejected following removal of an inner electron. This is fully treated using electron yields taken from Kaastra and Mewe (1993), see page 281 for more details. This process couples non-adjacent stages of ionization. The code iterates on the ionization solution to keep the system of equations a bi-diagonal matrix (see page 291).

Figure 18 shows photoionization cross sections for each shell of singly ionized iron, along with plots of the electron yield, assuming data given by Kaastra & Mewe (1993). A single photoionization of the 1s shell can remove as many as 8 electrons.

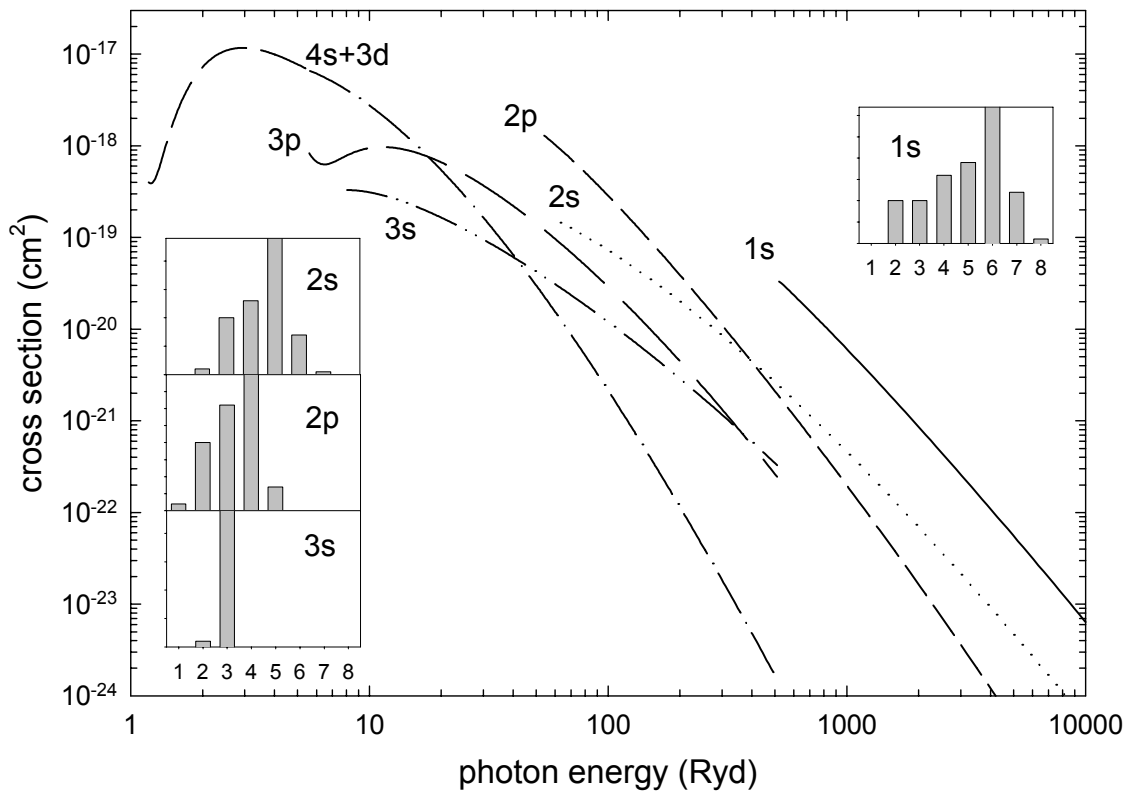


Figure 18 Photoionization cross sections and electron yields for singly ionized iron. Each subshell is shown along with the corresponding electron yield. IronPhoto

10.4.3 Compton scattering ionization of bound electrons

Ionization of outer valence electrons by Compton scattering is treated for all species by assuming that the cross section is the relativistic Compton cross section, multiplied by the number of valence electrons.

10.4.4 Collisional ionization rate coefficients

Fits to collisional ionization rate coefficients are evaluated in Dima Verner's routine *cfit*. These rates come mainly from Arnaud and Raymond (1992) and Arnaud and Rothenflug (1985), and by interpolation where rates are not given.

10.4.5 Radiative recombination rate coefficients

Radiative recombination rate coefficients are evaluated by Dima Verner's routine *rrfit*, which uses fits by Arnaud and Raymond (1992), Verner and Ferland (1996), Shull and van Steenberg (1982), and by Landini and Monsignori Fossi (1990, 1991).

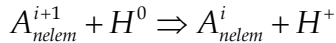
10.4.6 Low temperature dielectronic recombination

Dielectronic recombination through low-lying autoionizing states is known to be the dominant recombination mechanism for many ions of second-row elements (i.e., Nussbaumer and Storey 1983). Unfortunately, these have not been computed for most third row or higher elements. This constitutes a major uncertainty in understanding the ionization balance of these elements, and has been described, for

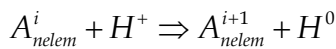
instance, by Ali et al. (1991) and Savin (2000). For those elements where a dielectronic recombination rate coefficient has not been computed and the parent ion is not a closed shell, the means of the rate coefficient for ions of C, N, O, and Ne are used instead. This assumption can be modified with the **dielectronic recombination** command described in Part I of this document.

10.4.7 Charge transfer

Rates for charge transfer between hydrogen and the heavy elements are evaluated using Jim Kingdon's routines *HCTIon* and *HCTRecom*. These rates are evaluated in routine *MakeCharTran*, which is called by routine *ionize*, and stored into master arrays, *HCharExcIon* and *HCharExcRec*. The rate coefficient for the process



is stored as *HcharExcRec[nelem][i]*. The rate coefficient for the process



is stored as *HCharExcIon[nelem][i]*.

For species more than 4 times ionized, a statistical estimate made by Alex Dalgarno (Ferland et al. 1997) is used. The rate coefficient for transfer between atomic hydrogen and a highly ionized species is given by $1.92 \times 10^{-9} \zeta \text{ cm}^3 \text{ s}^{-1}$, where ζ is the charge of the ion. Other atoms are treated analogously.

All of these include the thermal effects of charge transfer, as described by Kingdon & Ferland (1998).

10.5 Ionization Potentials

Table 24 lists ionization potentials for photoionization of the outer shell of the first thirty elements. These are given in Rydbergs for infinite mass nuclei.

Figure 19 shows the number of ions with valence shell ionization potentials within logarithmically increasing energy widths, as a function of the log of the ionization potentials in Rydbergs. Two large peaks occur, one near ~ 25 Ryd (~ 350 eV) and a second near ~ 160 Ryd (~ 2 keV). The continuum binning used in the code is designed to resolve these as separate features.

10.5.1 Ionization potential array indices

The vector *ipElement* contains array indices to thresholds of all valence and inner shell ionization edges of the elements. It has four dimensions. The first dimension is atomic weight of the element, and the second is the ionization stage, 1 for the atom, ranging up to the atomic number of the element. The third dimension is the shell

Table 24 Ionization Potentials of the Elements (Rydbergs)

	1 H	2 He	3 Li	4 Be	5 B	6 C	7 N	8 O	9 F	10 Ne
1	9.996(-1)	1.807	3.963(-1)	6.852(-1)	6.099(-1)	8.276(-1)	1.068	1.001	1.280	1.585
2		4.000	5.559	1.338	1.849	1.792	2.176	2.581	2.570	3.010
3			9.003	1.131(+1)	2.788	3.520	3.487	4.038	4.609	4.664
4				1.600(+1)	1.907(+1)	4.740	5.694	5.689	6.405	7.138
5					2.500(+1)	2.882(+1)	7.195	8.371	8.393	9.275
6						3.601(+1)	4.058(+1)	1.015(+1)	1.155(+1)	1.161(+1)
7							4.903(+1)	5.434(+1)	1.361(+1)	1.524(+1)
8								6.405(+1)	7.011(+1)	1.757(+1)
9									8.107(+1)	8.790(+1)
10										1.001(+2)

number, 1 for the K-shell, ranging up to 7. The fourth dimension is a set of pointers. One is the lower energy limit or threshold for the shell, 2 is the upper limit as set in routine *LimitSh*, and element three is the offset pointer to the opacity array.

A parallel two dimensional array, *nsShells [nelem][ion]*, contains the number of shells for the ionization stage *i* of the element with a given atomic weight. With this nomenclature, the pointer to the valence shell threshold of ionization stage *i* of an element *n* would be *ipElement[n,i, nsShells[n,I]]*. These valence pointers are also stored in the array *ipHeavy[nelem][nstag]*.

Table 24b Ionization Potentials of the Elements (Rydbergs)

	11 Na	12 Mg	13 Al	14 Si	15 P	16 S	17 Cl	18 Ar	19 K	20 Ca
1	3.777(-1)	5.620(-1)	4.400(-1)	5.991(-1)	7.710(-1)	7.614(-1)	9.533(-1)	1.158	3.191(-1)	4.493(-1)
2	3.476	1.105	1.384	1.202	1.450	1.715	1.750	2.031	2.325	8.724(-1)
3	5.264	5.890	2.091	2.461	2.220	2.560	2.911	2.994	3.367	3.742
4	7.270	8.033	8.820	3.318	3.781	3.477	3.930	4.396	4.477	4.944
5	1.017(+1)	1.039(+1)	1.130(+1)	1.226(+1)	4.780	5.342	4.985	5.514	6.075	6.211
6	1.266(+1)	1.371(+1)	1.400(+1)	1.507(+1)	1.620(+1)	6.471	7.131	6.689	7.309	7.996
7	1.532(+1)	1.653(+1)	1.774(+1)	1.812(+1)	1.934(+1)	2.065(+1)	8.393	9.136	8.643	9.349
8	1.942(+1)	1.955(+1)	2.092(+1)	2.228(+1)	2.274(+1)	2.412(+1)	2.560(+1)	1.055(+1)	1.137(+1)	1.082(+1)
9	2.204(+1)	2.412(+1)	2.426(+1)	2.580(+1)	2.732(+1)	2.786(+1)	2.941(+1)	3.105(+1)	1.292(+1)	1.384(+1)
10	1.077(+2)	2.701(+1)	2.935(+1)	2.950(+1)	3.120(+1)	3.286(+1)	3.349(+1)	3.518(+1)	3.703(+1)	1.553(+1)
11	1.212(+2)	1.295(+2)	3.249(+1)	3.499(+1)	3.525(+1)	3.710(+1)	3.890(+1)	3.961(+1)	4.150(+1)	4.350(+1)
12		1.443(+2)	1.533(+2)	3.848(+1)	4.119(+1)	4.150(+1)	4.351(+1)	4.544(+1)	4.627(+1)	4.830(+1)
13			1.693(+2)	1.792(+2)	4.497(+1)	4.790(+1)	4.827(+1)	5.043(+1)	5.253(+1)	5.341(+1)
14				1.965(+2)	2.070(+2)	5.198(+1)	5.511(+1)	5.555(+1)	5.782(+1)	6.010(+1)
15					2.256(+2)	2.370(+2)	5.949(+1)	6.283(+1)	6.329(+1)	6.575(+1)
16						2.568(+2)	2.689(+2)	6.747(+1)	7.115(+1)	7.162(+1)
17							2.900(+2)	3.029(+2)	7.607(+1)	7.989(+1)
18								3.253(+2)	3.389(+2)	8.504(+1)
19									3.626(+2)	3.770(+2)
20										4.020(+2)

Table 24c Ionization Potentials of the Elements (Rydbergs)

	21 Sc	22 Ti	23 V	24 Cr	25 Mn	26 Fe	27 Co	28 Ni	29 Cu	30 Zn
1	5.396(-1)	5.012(-1)	4.954(-1)	4.974(-1)	5.464(-1)	5.808(-1)	5.780(-1)	5.613(-1)	5.678(-1)	6.904(-1)
2	9.408(-1)	9.981(-1)	1.077	1.213	1.149	1.190	1.255	1.335	1.491	1.320
3	1.820	2.020	2.154	2.275	2.475	2.253	2.462	2.596	2.708	2.919
4	5.401	3.180	3.433	3.613	3.763	4.028	3.768	4.035	4.217	4.366
5	6.752	7.298	4.798	5.105	5.321	5.513	5.843	5.593	5.872	6.071
6	8.136	8.783	9.415	6.662	7.037	7.281	7.497	7.938	7.570	7.938
7	1.014(+1)	1.035(+1)	1.107(+1)	1.177(+1)	8.768	9.187	9.481	9.775	1.022(+1)	9.996
8	1.162(+1)	1.252(+1)	1.275(+1)	1.357(+1)	1.430(+1)	1.111(+1)	1.160(+1)	1.191(+1)	1.227(+1)	1.286(+1)
9	1.323(+1)	1.412(+1)	1.513(+1)	1.538(+1)	1.630(+1)	1.717(+1)	1.368(+1)	1.418(+1)	1.463(+1)	1.492(+1)
10	1.654(+1)	1.587(+1)	1.694(+1)	1.796(+1)	1.825(+1)	1.926(+1)	2.024(+1)	1.651(+1)	1.705(+1)	1.749(+1)
11	1.836(+1)	1.948(+1)	1.879(+1)	1.990(+1)	2.102(+1)	2.133(+1)	2.244(+1)	2.359(+1)	1.956(+1)	2.014(+1)
12	5.052(+1)	2.142(+1)	2.264(+1)	2.191(+1)	2.311(+1)	2.431(+1)	2.469(+1)	2.588(+1)	2.711(+1)	2.284(+1)
13	5.562(+1)	5.790(+1)	2.472(+1)	2.608(+1)	2.525(+1)	2.653(+1)	2.786(+1)	2.822(+1)	2.947(+1)	3.085(+1)
14	6.106(+1)	6.344(+1)	6.585(+1)	2.824(+1)	2.962(+1)	2.883(+1)	3.021(+1)	3.162(+1)	3.197(+1)	3.337(+1)
15	6.817(+1)	6.923(+1)	7.172(+1)	7.431(+1)	3.199(+1)	3.359(+1)	3.263(+1)	3.408(+1)	3.557(+1)	3.601(+1)
16	7.416(+1)	7.673(+1)	7.791(+1)	8.063(+1)	8.327(+1)	3.596(+1)	3.763(+1)	3.663(+1)	3.822(+1)	3.984(+1)
17	8.041(+1)	8.313(+1)	8.584(+1)	8.709(+1)	8.996(+1)	9.275(+1)	4.017(+1)	4.199(+1)	4.094(+1)	4.255(+1)
18	8.915(+1)	8.974(+1)	9.261(+1)	9.547(+1)	9.680(+1)	9.981(+1)	1.027(+2)	4.462(+1)	4.652(+1)	4.549(+1)
19	9.466(+1)	9.893(+1)	9.959(+1)	1.026(+2)	1.056(+2)	1.070(+2)	1.106(+2)	1.133(+2)	4.929(+2)	5.130(+1)
20	4.171(+2)	1.047(+2)	1.093(+2)	1.100(+2)	1.131(+2)	1.163(+2)	1.178(+2)	1.211(+2)	1.242(+2)	5.420(+1)
21	4.435(+2)	4.593(+2)	1.154(+2)	1.201(+2)	1.208(+2)	1.241(+2)	1.275(+2)	1.291(+2)	1.318(+2)	1.357(+2)
22		4.870(+2)	5.036(+2)	1.265(+2)	1.314(+2)	1.322(+2)	1.357(+2)	1.392(+2)	1.400(+2)	1.435(+2)
23			5.326(+2)	5.499(+2)	1.382(+2)	1.433(+2)	1.441(+2)	1.478(+2)	1.503(+2)	1.521(+2)
24				5.803(+2)	5.983(+2)	1.504(+2)	1.557(+2)	1.566(+2)	1.597(+2)	1.629(+2)
25					6.300(+2)	6.489(+2)	1.631(+2)	1.687(+2)	1.689(+2)	1.737(+2)
26						6.819(+2)	7.015(+2)	1.763(+2)	1.807(+2)	1.822(+2)
27							7.357(+2)	7.563(+2)	1.900(+2)	1.945(+2)
28								7.923(+2)	8.129(+2)	2.043(+2)
29									8.504(+2)	8.724(+2)
30										9.106(+2)

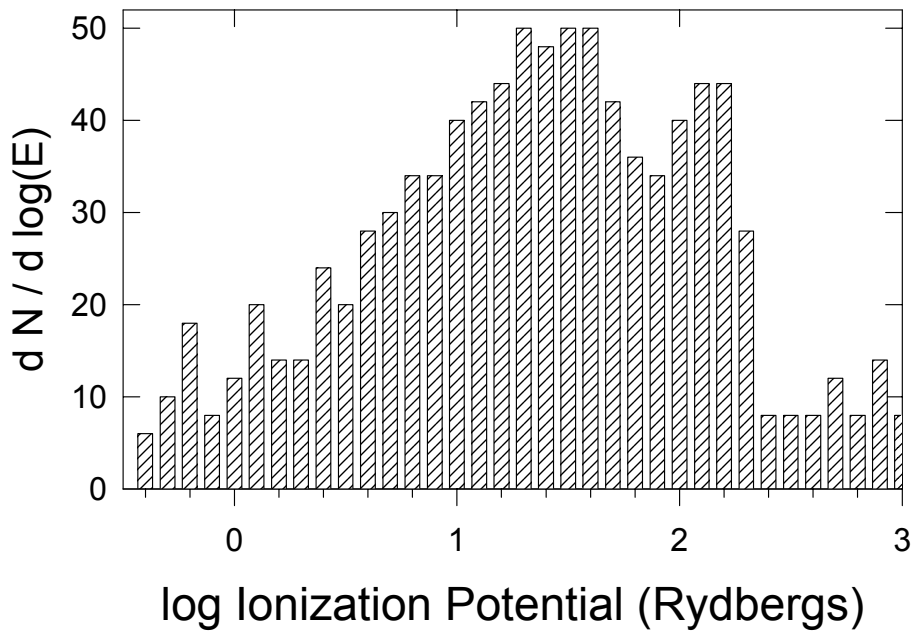


Figure 19 The number of elements with valence shell ionization potentials within logarithmically increasing energy widths is shown as a function of the log off the ionization potential. ipDen

10.6 Heavy Element Variables

10.6.1 Atomic weights

These are stored in atomic mass units, within the vector *AtomicWeight*. The mass (gm) of unit atomic weight m_{AMU} is stored as the *physcont.h*.

10.6.2 Ionic and total abundances

Information concerning the abundance of an element and the distribution of this abundance over the various stages of ionization is stored in the two dimensional real array *xIonDist*[atomic number][ionization stage]. The atomic number ranges from 0 for hydrogen through one less than LIMELM, currently 30. The ion stage ranges from 0 for the atom, through the atomic number plus one for the fully ionized species. All abundances have units cm^{-3} .

10.6.3 Element names

These are all contained in the *elementnames* structure, defined in the header file *elementnames.h*.

chElementSym Standard chemical symbols for all elements now in the code are stored within this 2-character variable.

chIonStage This is a two character vector *limelm*+1 long, containing the numbers from 1 through *limelm*+1. It is used for the spectroscopic designation of the spectrum produced by a level of ionization. C IV would be represented as C 4.

chIonRoman This is a two character vector *limelm*+1 long, containing the numbers from 1 through *limelm*+1 expressed as Roman numerals.

chElementName This is an eleven character vector *limelm* long with the names of the first *limelm* elements.

Finally, a series of macros are defined in *cddefines.h* that allows these arrays to be addressed in a simple manner. The elements have names like `ipHYDROGEN` or `ipHELIUM`, and are set to the proper indices, 0 and 1 in these cases.

chElementNameShort This is a four character vector *limelm* long with the first four letters of the names of the first *limelm* elements.

10.6.4 Photoionization rates

These are stored in the multidimensional vector *PhotoRate*. The first two dimensions give the atomic number of the element and the ionization stage, with the atom being zero. The second dimension is an index to the shell. These range from 0 to 6, and are 1s, 2s, 2p, 3s, 3p, 3d, 4s. Note that, for neutrals and ions of third row and heavier elements, some of the inner shells may be only partially filled. The last dimension contains the photoionization rate [0] the low-energy heating rate [1], and the high-energy (secondary ionizing) heat [3].

10.6.5 Fluorescence yields

These are taken from the compilation by Kaastra and Mewe (1993), and are stored in structure *yield*. The real variable *vyield* has 4 dimensions. Each element gives the fraction of electron holes that are filled by ejecting various numbers of electrons. For the latter, the index 0 will return the fraction of ionizations of that shell that eject only 1 electron. The second element is the shell number in Dima's notation (0 for the 1s shell), the atomic number (5 for carbon, etc) and the stage of ionization (1 for the atom) are the last two. The second variable in the structure is an integer array that indicates the most number of electrons that can be ejected.

10.6.6 Ionization potential pointers

These are set within routine *CreatePoint*, which calls routine *ipShells* to actually set the array index.

10.7 Isoelectronic Sequences

Figure 20 shows partial Grotrian diagrams for second row sequences. For sequences of elements heavier than K the ground configuration is correct for ions twice or more times ionized. For these heavier elements the atom and first ion may have non-standard configurations for the outer shell.

Table 25 lists all isoelectronic sequences for the first thirty elements. The bottom row on the table indicates the shell number, in the nomenclature used for the photoionization shell layering.

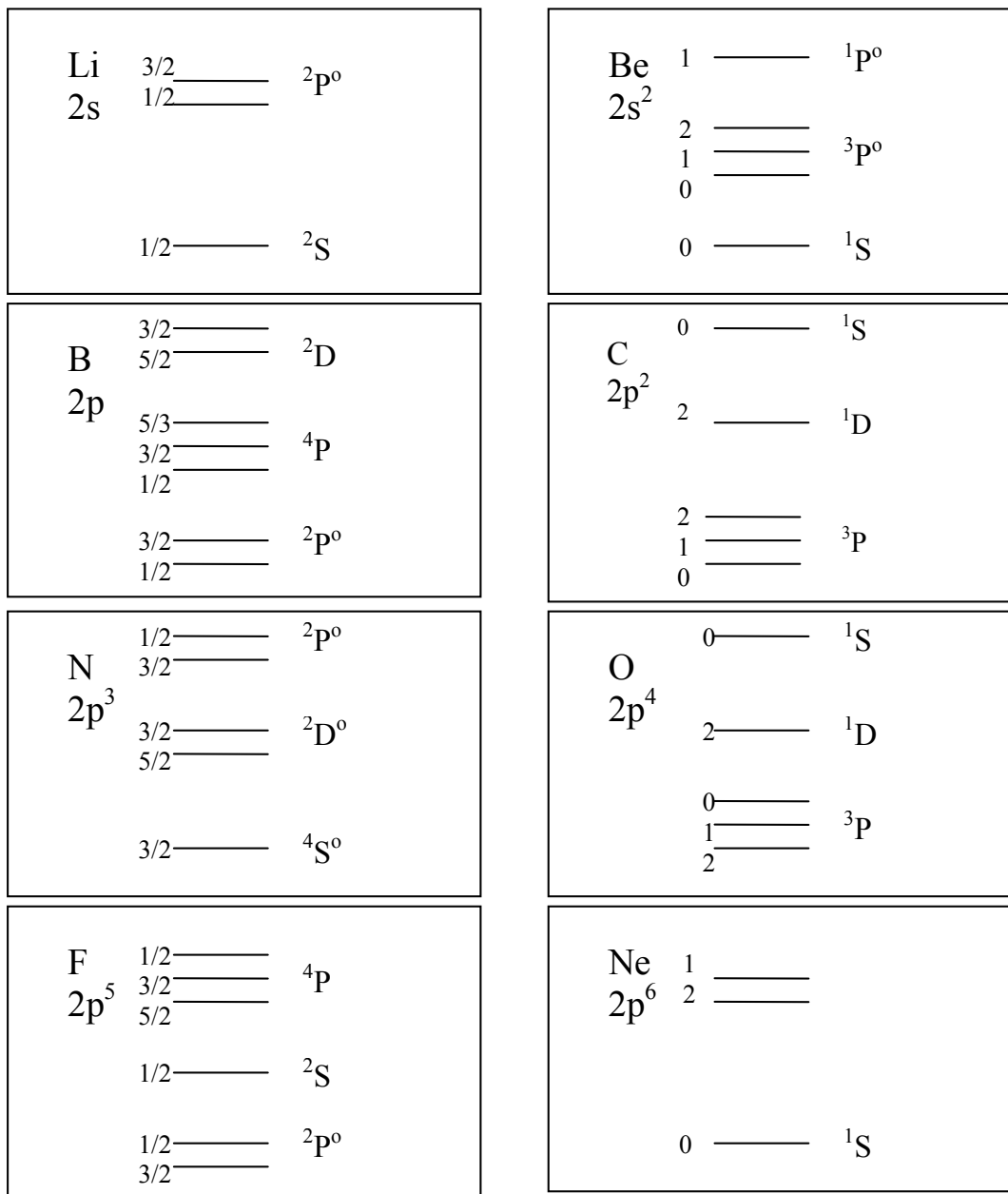


Figure 20 Partial Grotrian diagrams for the second row isoelectronic sequences. The levels are correct for first ion and higher, but may not be for some atoms, or for ions of elements with more mass than K.

10.8 Be-sequence

The model atom used for Be-like ions (CIII, NIV, OV, AlII, SiIII, SIV, etc) is shown in Figure 21.

10.9 Carbon

Low temperature dielectronic recombination rate coefficients are taken from Nussbaumer and Storey (1983).

Table 25 Isoelectronic Sequences

1 H	2 He	3 Li	4 Be	5 B	6 C	7 N	8 O	9 F	10 Ne
1s ² S	1s ² 1S	2s ² S	2s ² 1S	2p ² P	2p ² 3P	2p ³ 4S	2p ⁴ 3P	2p ⁵ 2P	2p ⁶ 1S
H 1	He 1	Li 1	Be 1	Bo 1	C 1	N 1	O 1	F 1	Ne 1
He 2	Li 2	Be 2	Bo 2	C 2	N 2	O 2	F 2	Ne 2	Na 2
Li 3	Be 3	Bo 3	C 3	N 3	O 3	F 3	Ne 3	Na 3	Mg 3
Be 4	Bo 4	C 4	N 4	O 4	F 4	Ne 4	Na 4	Mg 4	Al 4
Bo 5	C 5	N 5	O 5	F 5	Ne 5	Na 5	Mg 5	Al 5	Si 5
C 6	N 6	O 6	F 6	Ne 6	Na 6	Mg 6	Al 6	Si 6	P 6
N 7	O 7	F 7	Ne 7	Na 7	Mg 7	Al 7	Si 7	P 7	S 7
O 8	F 8	Ne 8	Na 8	Mg 8	Al 8	Si 8	P 8	S 8	Cl 8
F 9	Ne 9	Na 9	Mg 9	Al 9	Si 9	P 9	S 9	Cl 9	Ar 9
Ne10	Na10	Mg10	Al10	Si10	P 10	S 10	Cl10	Ar10	K 10
Na11	Mg11	Al11	Si11	P 11	S 11	Cl11	Ar11	K 11	Ca11
Mg12	Al12	Si12	P 12	S 12	Cl12	Ar12	K 12	Ca12	Sc12
Al13	Si13	P 13	S 13	Cl13	Ar13	K 13	Ca13	Sc13	Ti13
Si14	P 14	S 14	Cl14	Ar14	K 14	Ca14	Sc14	Ti14	V 14
P 15	S 15	Cl15	Ar15	K 15	Ca15	Sc15	Ti15	V 15	Cr15
S 16	Cl16	Ar16	K 16	Ca16	Sc16	Ti16	V 16	Cr16	Mm16
Cl17	Ar17	K 17	Ca17	Sc17	Ti17	V 17	Cr17	Mm17	Fe17
Ar18	K 18	Ca18	Sc18	Ti18	V 18	Cr18	Mm18	Fe18	Co18
K 19	Ca19	Sc19	Ti19	V 19	Cr19	Mm19	Fe19	Co19	Ni19
Ca20	Sc20	Ti20	V 20	Cr20	Mm20	Fe20	Co20	Ni20	Cu 20
Sc21	Ti21	V 21	Cr21	Mm21	Fe21	Co21	Ni21	Cu 21	Zn 21
Ti22	V 22	Cr22	Mm22	Fe22	Co22	Ni22	Cu 22	Zn 22	
V 23	Cr23	Mm23	Fe23	Co23	Ni23	Cu 23	Zn 23		
Cr24	Mm24	Fe24	Co24	Ni24	Cu 24	Zn 24			
Mm25	Fe25	Co25	Ni25	Cu 25	Zn 25				
Fe26	Co26	Ni26	Cu 26	Zn 26					
Co27	Ni27	Cu 27	Zn 27						
Ni28	Cu 28	Zn 28							
Cu 29	Zn 29								
Zn 30									
1	1	2	2	3	3	3	3	3	3

11 Na	12 Mg	13 Al	14 Si	15 P	16 S	17 Cl	18 Ar	19 K	20 Ca
3s ² S	3s ² 1S	3p ² P	3p ² 3P	3p ³ 4S	3p ⁴ 3P	3p ⁵ 2P	3p ⁶ 1S	3d ² D	3d ² 3F
Na 1	Mg 1	Al 1	Si 1	P 1	S 1	Cl 1	Ar 1	K 1 ³	Ca 1 ¹
Mg 2	Al 2	Si 2	P 2	S 2	Cl 2	Ar 2	K 2	Ca 2 ¹	Sc 2 ¹
Al 3	Si 3	P 3	S 3	Cl 3	Ar 3	K 3	Ca 3	Sc 3	Ti 3
Si 4	P 4	S 4	Cl 4	Ar 4	K 4	Ca 4	Sc 4	Ti 4	V 4
P 5	S 5	Cl 5	Ar 5	K 5	Ca 5	Sc 5	Ti 5	V 5	Cr 5
S 6	Cl 6	Ar 6	K 6	Ca 6	Sc 6	Ti 6	V 6	Cr 6	Mm 6
Cl 7	Ar 7	K 7	Ca 7	Sc 7	Ti 7	V 7	Cr 7	Mm 7	Fe 7
Ar 8	K 8	Ca 8	Sc 8	Ti 8	V 8	Cr 8	Mm 8	Fe 8	Co 8
K 9	Ca 9	Sc 9	Ti 9	V 9	Cr 9	Mm 9	Fe 9	Co 9	Ni 9
Ca 10	Sc 10	Ti 10	V 10	Cr 10	Mm 10	Fe 10	Co 10	Ni 10	Cu 10
Sc 11	Ti 11	V 11	Cr 11	Mm 11	Fe 11	Co 11	Ni 11	Cu 11	Zn 11
Ti 12	V 12	Cr 12	Mm 12	Fe 12	Co 12	Ni 12	Cu 12	Zn 12	
V 13	Cr 13	Mm 13	Fe 13	Co 13	Ni 13	Cu 13	Zn 13		
Cr 14	Mm 14	Fe 14	Co 14	Ni 14	Cu 14	Zn 14			
Mm 15	Fe 15	Co 15	Ni 15	Cu 15	Zn 15				
Fe 16	Co 16	Ni 16	Cu 16	Zn 16					
Co 17	Ni 17	Cu 17	Zn 17						
Ni 18	Cu 18	Zn 18							
Cu 19	Zn 19								
Zn 20									
4	4	5	5	5	5	5	5	6	6

21 Sc	22 Ti	23 V	24 Cr	25 Mm	26 Fe	27 Co	28 Ni	29 Cu	30 Zn
3d ³ 4F	3d ⁴ 5D	3d ⁵ 6S	3d ⁶ 5D	3d ⁷ 4F	3d ⁸ 3F	3d ⁹ 2D	3d ¹⁰ 1S	4s ² S	4s ² 1S
Sc 1	Ti 1	V 1	Cr 1	Mm 1	Fe 1	Co 1	Ni 1	Cu 1	Zn 1
Ti 2	V 2	Cr 2	Mm 2	Fe 2	Co 2	Ni 2	Cu 2	Zn 2	
V 3	Cr 3	Mm 3	Fe 3	Co 3	Ni 3	Cu 3	Zn 3		
Cr 4	Mm 4	Fe 4	Co 4	Ni 4	Cu 4	Zn 4			
Mm 5	Fe 5	Co 5	Ni 5	Cu 5	Zn 5				
Fe 6	Co 6	Ni 6	Cu 6	Zn 6					
Co 7	Ni 7	Cu 7	Zn 7						
Ni 8	Cu 8	Zn 8							
Cu 9	Zn 9								
Zn 10									
6	6	6	6	6	6	6	6	7	7

10.10 Nitrogen

Low temperature dielectronic recombination rate coefficients are taken from Nussbaumer and Storey (1983). Photoionization from the excited 2D level of N^0 is included, and can be the dominant ionization mechanism in well-shielded regions.

10.11 Oxygen

Low temperature dielectronic recombination rate coefficients are taken from Nussbaumer and Storey (1983).

Photoionization from the first two excited states of O^{2+} is included as a general ionization mechanism. This can dominate the ionization of the ion since it occurs

³ Neutral and first ion have non-standard filling.

behind the He⁺ - He⁺⁺ ionization front, which shields the region from 4 Ryd and higher radiation. Similarly, photoionization from the first excited state and all inner shells of O⁰ are included.

10.11.1 The O I model atom

A partial Grotrian diagram for the O I atom considered in the Lβ-O I fluorescence problem is shown in Figure 22. Multiplet averaged transition probabilities are taken from unpublished Opacity Project data, and the collision strengths are from the \bar{g} approximation for collisions between electrons and neutrals. Rates for fluorescence between the two transitions are computed as in Netzer et al. (1985).

Level populations including all physical processes are computed in routine *oilevl*. This routine is called by routine *p8446*, which is responsible for the interactions between the hydrogen and oxygen atoms.

10.12 Neon

Low temperature dielectronic recombination rate coefficients are taken from Nussbaumer and Storey (1987).

10.13 Magnesium

Low temperature dielectronic recombination rate coefficients for recombination to the atom are taken from Nussbaumer and Storey (1986). Rate coefficients have not been computed for recombination to the ions. Means of CNO are used.

Photoionization from the excited ²P^o level of Mg⁺ is included as a general Mg⁺

destruction mechanism using Opacity Project data retrieved from *TOPBase*. This can easily be the dominant Mg⁺ destruction mechanism in BLR calculations since the excited state has an ionization potential below 1 Ryd. The code will generate a comment at the end of the calculation if this is a competitive Mg⁺ destruction mechanism.

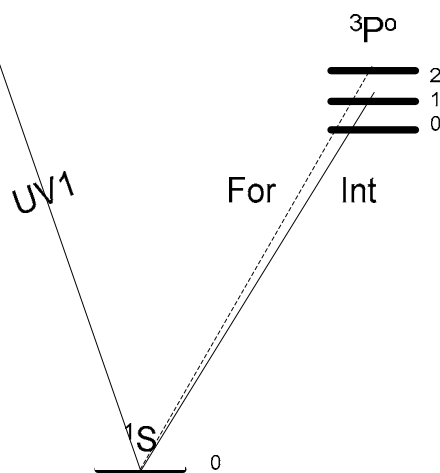


Figure 21 The Be-sequence model atom. The permitted transition is marked "UV1", while the forbidden and intercombination transitions are "For" and "Int".

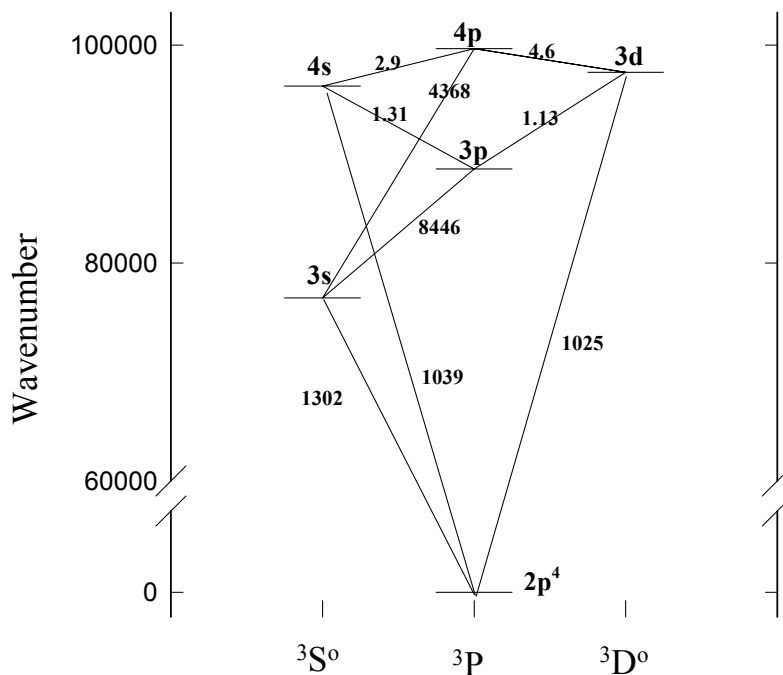


Figure 22 The levels of O⁰ included in the calculation of the OI-Lβ pumping problem are shown. oigrot

10.14 Aluminum

Low temperature dielectronic recombination rate coefficients for recombination to the atom and first ion are taken from Nussbaumer and Storey (1986). Rate coefficients have not been computed for recombination to other ions. Means of CNO are used.

10.15 Calcium

Low temperature dielectronic recombination rate coefficients have not been computed for this element. Means of CNO are used.

10.15.1 The Ca II model atom

The Ca II ion is treated as a five-level atom plus continuum. The model atom is shown in Figure 23, and is similar to that described by Shine and Linsky (1974). Collision strengths for j-mixing collisions are from Saraph (1970). Collision and radiative data for the $4s - 4p$ transition are taken from the compendium of Mendoza (1983), and all other collision data are from Chidichimo (1981) and Saraph (1970).

Radiative data for the $3d - 4p$ and $4s - 3d$ transitions are from Black, Weisheit, and Laviana (1972); these are in good agreement with the calculations of Osterbrock (1951). The compendium by Shine and Linsky (1974) provides photoionization cross sections for excited levels, which are adopted here. Photoionization of the excited 2D level by $\text{Ly}\alpha$ (Wyse 1941) and all other line or continuum sources is explicitly included.

Recombination contributions to the population of individual levels are included by dividing the excited state recombination coefficient among the excited levels considered, according to their statistical weight and the rules of LS coupling.

All Ca II transitions (including the forbidden lines) can become quite optically thick. Radiative transfer is treated with the escape probability formalism, assuming incomplete redistribution, including destruction by background opacities.

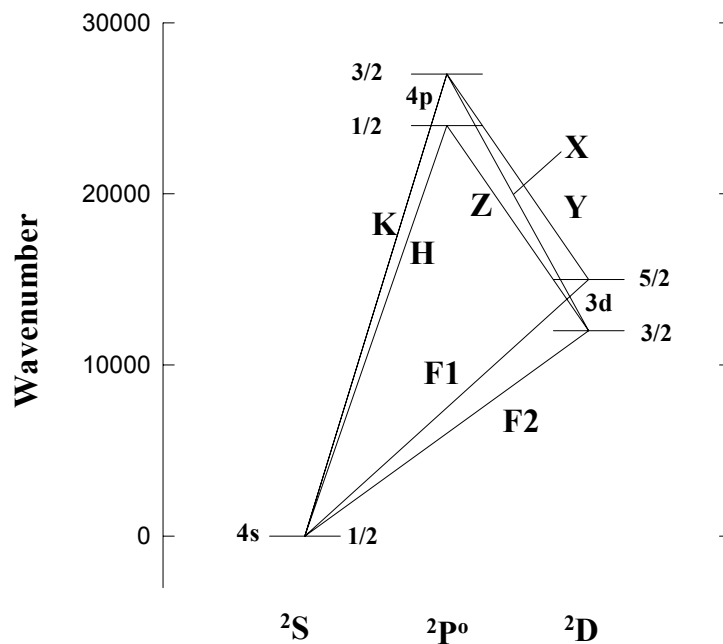


Figure 23 The five levels of Ca⁺ included in the calculations are shown. The wavelengths of the predicted lines are K (3934), H (3969), X (8498), Y (8542), Z (8662), F1 (7291), and F2 (7324). ca2grot

10.16 Iron

Low temperature dielectronic recombination rate coefficients have not been computed for this element. Means of CNO are used. Charge transfer rate coefficients are from Neufeld and Dalgarno (1989), Neufeld (1989) and Ferland, Korista, Verner, and Dalgarno (1997).

10.16.1 The FeII model atom

The Fe II ion is described by Verner et al. (1989) and in sections of Part I of this document. In the current implementation up to 376 levels can be included. This is an area of extensive activity. Figure 24 shows the lowest 16 levels of the atom and some of the lines predicted.

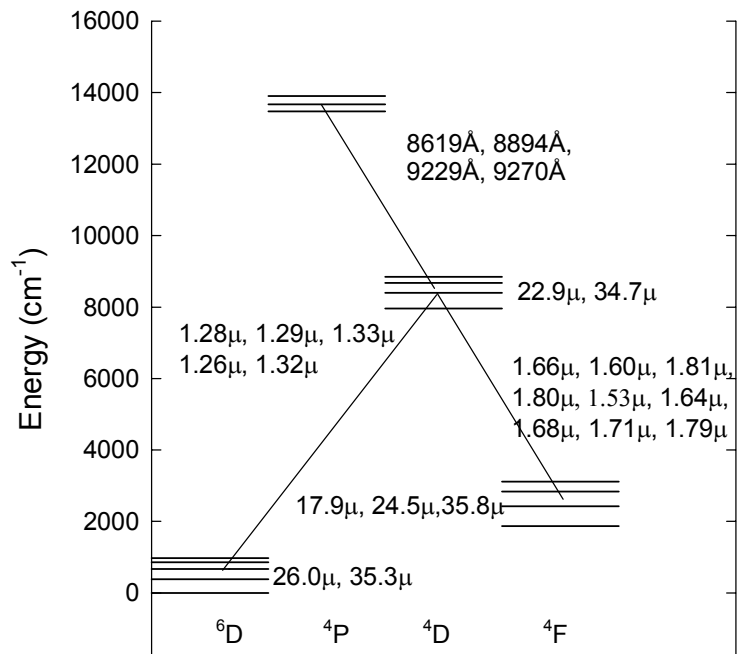


Figure 24 The sixteen level atom used to compute FeII IR emission. Lines predicted are indicated.

10.16.2 The FeIV model atom

FeIV is treated as a twelve-level atom, with energies from Sugar and Corliss (1985), transition probabilities from Garstang (1958), and collision strengths from Berrington and Pelan (1996). Figure 25 shows the model atoms with the lines predicted by the code indicated.

10.16.3 Fe $K\alpha$ emission

The intensity of the Fe $K\alpha$ line is predicted including both recombination and fluorescence. Figure 26 shows the fluorescence yield and $K\alpha$ energy. The line predictions are separated into “cold” iron (i.e., iron with M-shell electrons present) and “hot” iron (those ionization states producing lines with energies greater than ~ 6.4 keV). This includes the recombination and collisional contribution. The “TOTL” $K\alpha$ is the sum of the two.

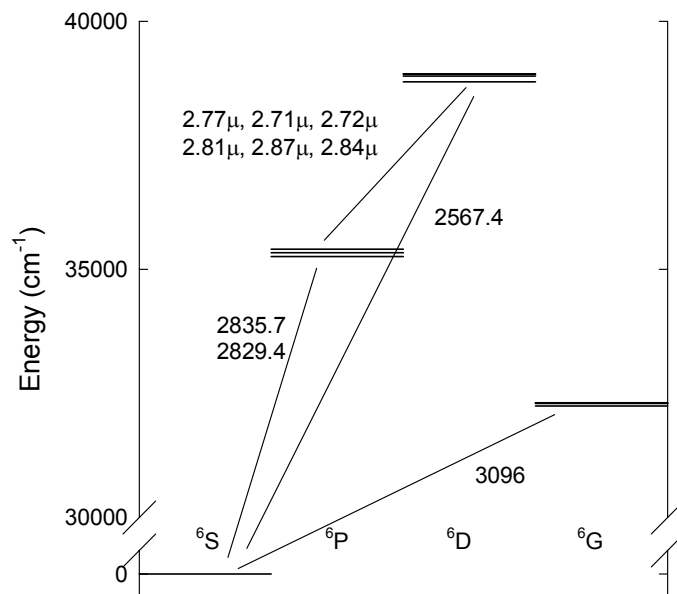


Figure 25 The twelve level atom used to compute FeIV emission. Lines predicted are indicated.

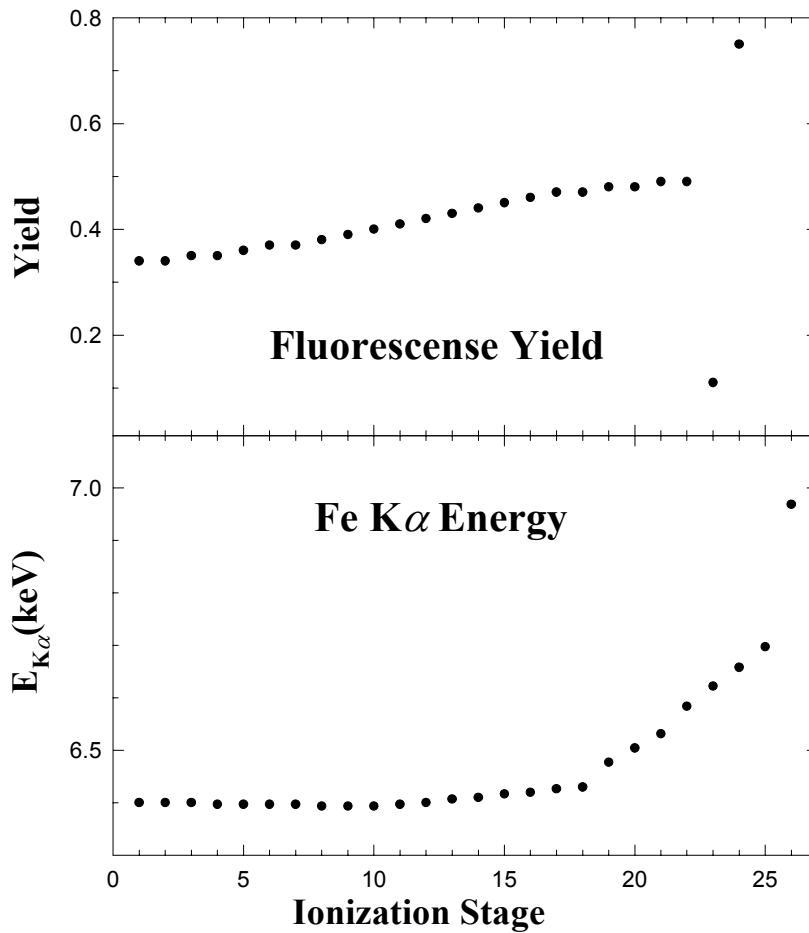


Figure 26 The fluorescence yield and energy of the emitted Fe K α photon are shown as a function of ionization stage. feka

10.17 Heavy Element Opacities

Figure 27 shows a calculation of the opacity of a solar gas with very low ionization.

10.18 Overall Reliability

Table 26
Ionization Balance Reliability

	1 H	2 He	3 Li	4 Be	5 B	6 C	7 N	8 O	9 F	10 Ne
1	A									
2		A								
3			A							
4				A						
5					A					
6						A				
7							A			
8								A		
9									A	
10										A

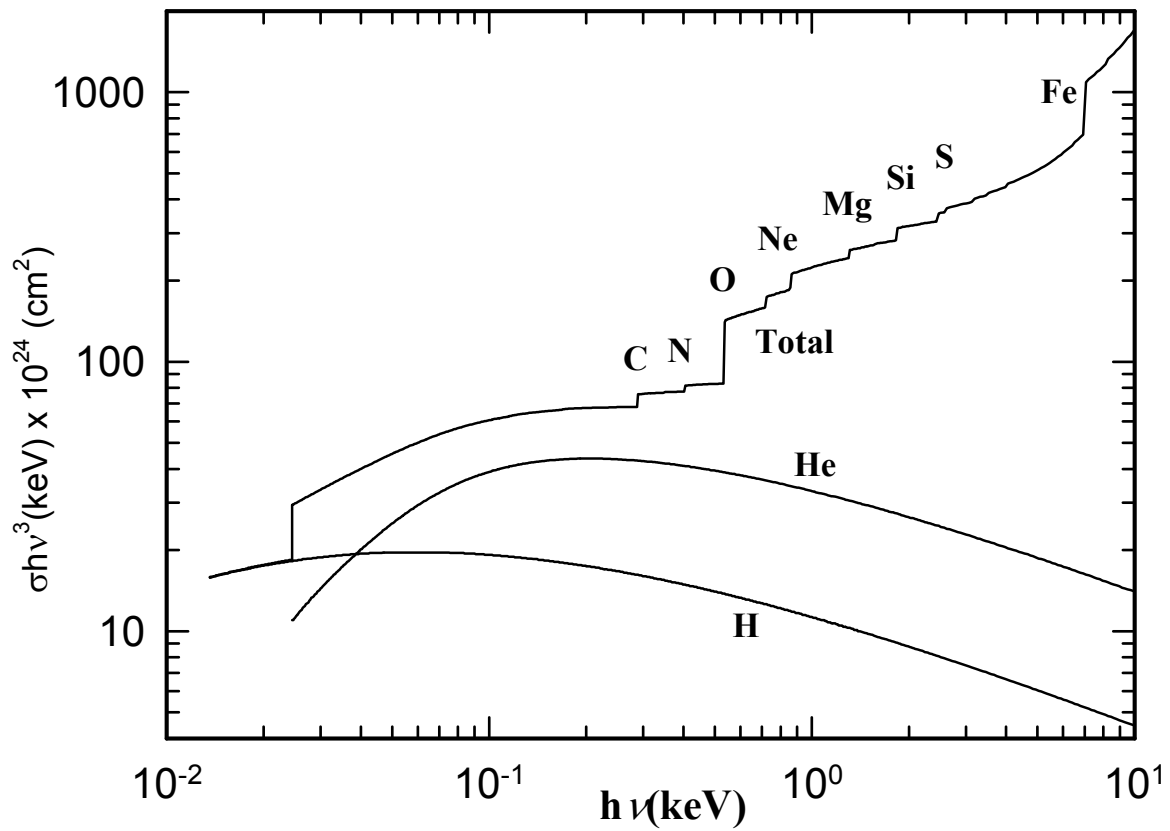


Figure 27 The opacity of a neutral gas with solar abundances is shown as a function of energy. The curve is scaled to allow direct comparison with conventional calculations of opacity at X-Ray energies (i.e., Morrison and McGammon 1983). hevopc

Ionization Balance Reliability Continued

	11 Na	12 Mg	13 Al	14 Si	15 P	16 S	17 Cl	18 Ar	19 K	20 Ca
1	A	A	A							
2		A	A							
3			A							
4				A						
5					A					
6						A				
7							A			
8								A		
9	A								A	
10	A	A								A
11	A	A	A							
12		A	A	A						
13			A	A	A					
14				A	A	A				
15					A	A	A			
16						A	A	A		
17							A	A	A	
18								A	A	A
19									A	A
20										A

Ionization Balance Reliability Continued

	21 Sc	22 Ti	23 V	24 Cr	25 Mn	26 Fe	27 Co	28 Ni	29 Cu	30 Zn
1										
2										
3										
4										
5										
6										
7										
8										
9										
10										
11	A									
12		A								
13			A							
14				A						
15					A					
16						A				
17							A			
18								A		
19	A								A	
20	A	A								A
21	A	A	A							
22		A	A	A						
23			A	A	A					
24				A	A	A				
25					A	A	A			
26						A	A	A		
27							A	A	A	
28								A	A	A
29								A		A
30										A

It is difficult to estimate the overall uncertainty present in an ionization balance calculation. The current photoionization cross-section data are based on accurate experiments or the Opacity Project (Verner et al. 1996). These should be accurate to roughly 10% except near resonances. Although resonances are included in the Opacity Project data, the positions of these resonances are uncertain by more than their width because the OP was not intended as an atomic structure calculation. Recombination coefficients including low temperature dielectronic recombination have yet to be computed for the majority of the stages of ionization of the elements now in Cloudy, but recombination from parent ions with closed shells is not affected, and good rates exist (Verner and Ferland 1996).

It is possible to make a subjective estimate of the uncertainty in the calculation of the ionization balance for nebular temperatures. Table 26 lists the elements now included in the calculations and gives this estimate of the uncertainty. For recombination from a closed shell autoionization resonances do not occur near threshold, recombination is primarily radiative, and the calculations should be virtually exact. Dielectronic recombination rates are also known for those species treated by Nussbaumer and Storey. These are given a quality weighting of A.

These uncertainties refer to the ionization balance of an optically thin cell of gas at nebular temperatures. The intensities of emission lines will be less uncertain than this for two reasons. First, the thermostat effect of any collisionally excited line prevents its intensity from changing by much. Second is the fact that the integrated column density in an ion is affected as much by (fairly exact) quantities such as the ionization structure of H or He, as by the atomic data of a particular ion. At coronal

temperatures the Burgess mechanism dominates, and the situation should be somewhat better.

10.19 The Bi-Diagonal Matrix

The ionization-recombination balance equations are written as a series of n equations coupling adjacent levels of ionization, i.e.,

$$n_z \Gamma_z^{eff} = n_{z+1} \sum n_x \alpha_{z+1} \quad . \quad (262)$$

where the effective photoionization rate Γ includes all ionization processes (photoionization of valence and inner shells, collisional ionization, charge transfer ionization, etc) and is modified to include the Auger effect. The total recombination rate coefficient $\sum n_x \alpha_{z+1}$ includes all recombination processes (dielectronic, radiative, 3-body, charge transfer). In much of the following this total recombination rate coefficient will be written simply as $n_e \alpha_e$, with the implicit understanding that all recombination processes are actually included.

The vector `ionrec.TotIonizRate[nelem][ion]` contains total destruction rates while `ionrec.TotRecomRate[nelem][ion]` contains the total creation rates. The resulting ionization balance is solved in routine *BiDiag*.

10.20 Ionization stage trimming

The code tries to not compute abundances of ions with trivial abundances. During a calculation it is constantly raising or lowering the lowest and highest stage of ionization that is considered. Those ions judged to have trivial abundances are given an abundance of zero, and the lower or upper limit is altered as appropriate. The logic used to describe whether an ionization stage has a trivial abundance is described where the `set trim` command is described in Part I of this document.

11 THERMAL EQUILIBRIUM

11.1 Overview

This section describes the system of equations setting the local thermal balance of a cloud. The electron temperature is the only thermodynamic quantity used to characterize a photoionized cloud. The electron velocity distribution is predominantly Maxwellian (Bohm and Aller 1947) although a trace constituent of non-thermal electrons may contribute when high-energy photons are present (Spitzer & Tomasko 1968). A kinetic temperature can then characterize most of the electron velocity distribution. This in turn is defined by the balance between processes that add energy (heat) and remove energy (cool) the electrons.

Heating or cooling can be defined relative to either the ground state or continuum, and this difference has caused some confusion in the literature. Cloudy defines heating and cooling relative to the continuum, as in Osterbrock (1989). Note that, in this scheme of bookkeeping, photoionization contributes an amount of heat given by $h(\nu - \nu_0)$, where $h\nu_0$ is the ionization potential of the atom or ion and ν is the photon energy. Emission of a recombination line *does not* constitute a cooling process. Heating and cooling rates are computed in cgs units (ergs, not Rydbergs) throughout Cloudy.

11.2 Thermal Stability

The criterion for thermal stability used by Cloudy is that the net cooling (i.e., cooling minus heating) has a positive temperature derivative (Field 1965). This can be expressed as

$$\frac{d(\Lambda - G)}{dT} > 0 \quad . \quad (263)$$

The code will print a “u” next to the temperature in the zone results, and make a comment at the end of the calculation, if possibly thermally unstable solutions were found. The criterion used by the code is that the derivative *at constant density* (isochoric) be positive. The more traditional criterion is that the derivative *at constant pressure* (isobaric) be positive (Field 1965).

The fact that the code identifies a region as possibly thermally unstable does not necessarily show that it is. The derivatives used in equation 263 are those found during the search for the thermal solution. As such they are evaluated out of equilibrium as part of the temperature solver. Their primary purpose was not to perform this thermal stability analysis. A section of Part III of this document goes into more detail about the stability check performed by the code, and how to do a better one.

11.3 Compton Energy Exchange

There are two parts to the Compton energy exchange problem. First, photons scatter off an electron at an angle θ , causing a change of photon energy due to Compton recoil given by

$$\frac{\Delta\varepsilon_-}{\varepsilon_o} = \left[1 - \frac{1}{1 + (\varepsilon_o / m_e c^2)(1 - \cos\theta)} \right] . \quad (264)$$

For isotropic scattering the median scattering angle corresponds to $\cos\theta = 0.5$. Scattering by thermal electrons crates a shift with a distribution centered at

$$\frac{\Delta\varepsilon_-}{\varepsilon_o} = \frac{4kT}{m_e c^2} \quad (265)$$

and a standard deviation given by

$$\frac{\sigma}{\varepsilon_o} = \sqrt{\frac{2kT}{m_e c^2}} \quad (266)$$

(see, e.g., Zycki et al. 1994).

The net volume-heating rate due to Compton energy exchange is given by

$$G_{Comp} - \Lambda_{Comp} = \frac{4\pi n_e}{m_e c^2} \left\{ \int \sigma_h J_\nu h\nu [1 + \eta_\nu] d\nu - 4kT \int \sigma_c J_\nu d\nu \right\} [\text{erg s}^{-1} \text{cm}^{-3}] \quad (267)$$

(see, for instance, Levich and Sunyaev 1970; and Krolik, McKee, and Tarter 1981). The two terms in braces are the heating and cooling terms respectively, while the factor in brackets in the first term accounts for heating due to both spontaneous and stimulated Compton scattering. Induced Compton heating is important when η_ν is large at frequencies where $h\nu \geq kT$. In fact it is, at most, a few percent effect in most circumstances.

The terms σ_h and σ_c appearing in equation 267 are the effective energy exchange (scattering) cross section for energy exchange, and differ from the Thomson cross section for energies $h\nu \sim m_e c^2$, where the Klein-Nishina cross section must be used. The numerical fits to Winslow's (1975) results, as used by Krolik, McKee, and Tarter (1981) and kindly provided by Dr. C.B. Tarter, are used. Defining

$$\alpha = \left\{ 1 + \nu_{Ryd} \left(1.1792 \times 10^{-4} + 7.084 \times 10^{-10} \nu_{Ryd} \right) \right\}^{-1} \quad (268)$$

and

$$\beta = \left\{ 1 - \alpha \nu_{Ryd} \left(1.1792 \times 10^{-4} + 2 \times 7.084 \times 10^{-10} \nu_{Ryd} \right) / 4 \right\} , \quad (269)$$

where ν_{Ryd} is the photon frequency in Rydbergs, the Compton energy-exchange rate coefficients are then $\sigma_h = \sigma_T \alpha$ and $\sigma_c = \sigma_T \alpha \beta$. Tests show that these are in excellent (much better than 1%) agreement with Guilbert's (1986) calculations for $h\nu < 10$ MeV, the energies where Guilbert's calculations are valid.

The total Compton heating-cooling rates are evaluated zone by zone in routine *highen*. The coefficients for the heating and cooling terms, i.e., α and the product $\alpha\beta$, are calculated at the beginning of the calculation and stored in the vectors *csigh*(v) and *csigc*(v). The heating is determined by summing over the continuum;

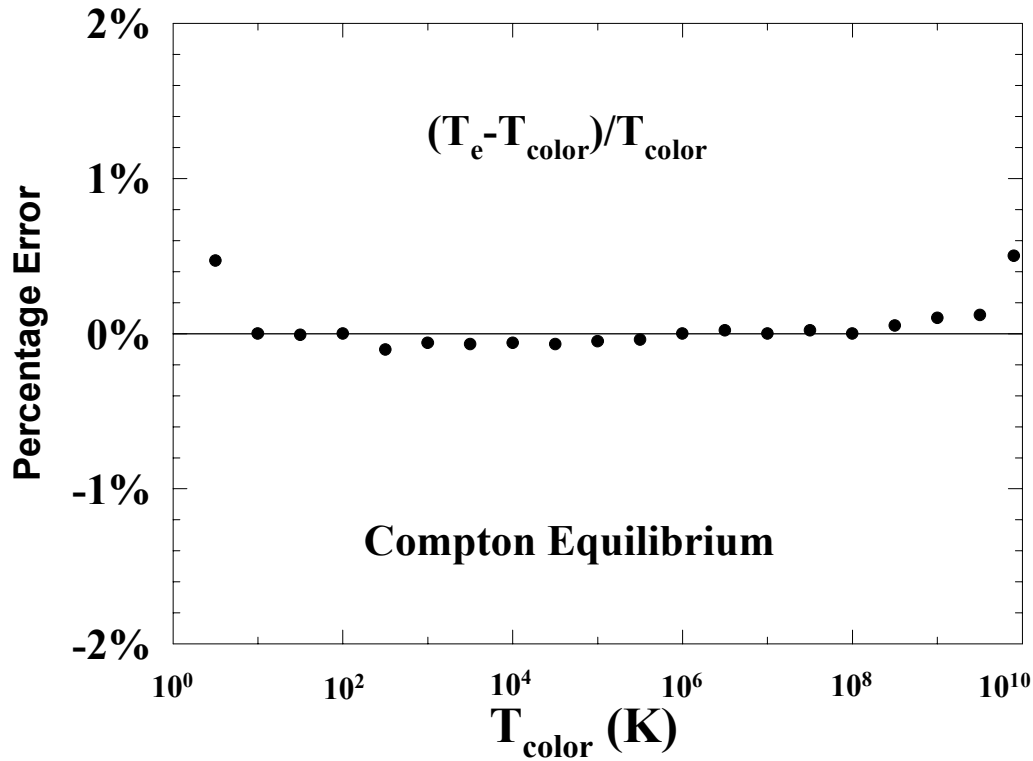


Figure 28 Thermal equilibrium in the Compton Limit. Calculations are for blackbody continua of various temperatures, given as T_{color} along the x-axis. The energy density temperature T_U is set equal to T_{color} . The density is adjusted to maintain ionization parameters $U \sim 10^{10}$, so that the thermal equilibrium equations are dominated by the Compton exchange problem. The deviation of the computed equilibrium temperature T_e from the asymptotic Compton temperature T_{color} is shown. Compton

$$G_{Comp} = \frac{n_e}{mc^2} \sigma_T (h\nu_{Ryd})^2 \sum \alpha_i \varphi_i \nu_i^2 (1 + \eta_i) \quad (270)$$

where φ_i is the photon flux, η_i is the photon occupation number, σ_T is the Thomson cross section, and ν_i is the photon energy in Rydbergs .

Figure 28 shows results of a series of calculations in which Compton energy exchange was the dominant physical process affecting the temperature. These are a series of models in which the gas was irradiated by black body continua in strict thermodynamic equilibrium (i.e., $T_u = T_{color}$) and various hydrogen densities. Over the temperature range $3 \text{ K} \leq T_{color} \leq 10^{10} \text{ K}$ the computed equilibrium electron temperature equaled the color temperature within much better than 1% ($\langle (T_e - T_{color}) \rangle / T_{color} = -0.00073 \pm 0.0019$).

which the energy density temperature was varied (this is shown as the x-axis), but the color temperature held fixed at 10^5 K.

Note also that when $T_u > T_{color}$ induced Compton heating drives T_e above T_{color} . Only when the color and energy density temperatures are equal do the equilibrium and color temperatures match.

11.4 Bound Compton Ionization, Heating

Compton scattering can ionize atoms for photons of sufficiently high energy (≈ 2.3 keV for hydrogen). Rates for bound Compton scattering are computed in routine *highen*. The energy given to an electron by a 90° scattering is found by rearranging equation 264 above

$$e = h\nu \left(1 - \frac{1}{1 + \frac{h\nu}{mc^2}} \right). \quad (271)$$

Setting this equal to the ionization potential of the species, $h\nu_o$, electrons will be removed by photons having an energy greater than

$$h\nu = \sqrt{h\nu_o mc^2}. \quad (272)$$

11.5 Expansion Cooling

Adiabatic cooling ($\text{erg cm}^{-3} \text{ s}^{-1}$) due to the hydrodynamic expansion of the gas is given by

$$L_{\text{exp}} = -\frac{DU}{Dt} = -\frac{p}{\rho} \frac{D\rho}{Dt} - U\nabla \cdot \mathbf{v} \approx kT \frac{dn}{dt} = nkT \left[\frac{a}{u} + \frac{2u}{r} \right] [\text{erg s}^{-1} \text{ cm}^{-3}] \quad (273)$$

where n , a , v , and r are the total particle density, acceleration, wind velocity, and radius respectively. This cooling term is only included when a wind geometry is computed.

11.6 Free-free Heating-Cooling

The volume free-free heating rate is given by

$$G_{\text{ff}} = 4\pi \int_{\nu_c}^{\infty} n_e \alpha_{\nu}(\text{ff}) J_{\nu} d\nu [\text{erg s}^{-1} \text{ cm}^{-3}] \quad (274)$$

where the free-free cross section is denoted by $\alpha_{\nu}(\text{ff})$ and ν_c is the critical frequency defined below, and J_{ν} is the sum of the attenuated incident radiation field and the OTS line fields. Diffuse reemission, mainly free-free emission, is *not* included in this integral, as discussed below.

The code works with the difference between cooling and heating, since this is numerically more stable than considering each term as an independent heat source or coolant.

Cooling due to diffuse continua are treated by defining a critical frequency ν_c as follows. Gas at a depth r into the cloud is transparent to photons with energies above a critical frequency ν_c such that

$$\tau_c = \int_0^r \kappa(\nu_c) f(r) dr = \int_0^r \alpha_\nu(ff, \nu_c) n_e f(r) dr = 1 \quad (275)$$

and optically thick at lower frequencies. The critical frequency ν_c is evaluated for each zone.

The free-free cooling rate is then given by

$$\Lambda_{ff}(\tau) = \int_{\nu_c}^{\infty} n_e \alpha_\nu(ff) 4\pi B_\nu(T_e) d\nu = \Lambda_{ff}(0) \times \exp(-h\nu_c / kT) \quad (276)$$

where $\Lambda_{ff}(0)$ is the optically thin cooling rate and $B_\nu(T)$ is Planck's function. This is equivalent to assuming that, for $\nu < \nu_c$, where the cloud is optically thick, free-free heating and cooling exactly balance, as suggested by Kirchhoff's law and detailed balance considerations. Energies below ν_c are not included in free-free heating or cooling. This critical frequency is not allowed to be less than the plasma frequency for the current conditions.

11.7 Photoelectric Heating, Recombination Cooling

The net heating rate due to photoelectric heating less spontaneous and induced recombination cooling of level n is given by

$$G = G_{n,\kappa} - \Lambda_{ind,n} - \Lambda_{spn,n} \text{ [erg s}^{-1} \text{ cm}^{-3}] \quad (277)$$

where the volume heating rate due to photoionization is

$$G_{n,\kappa} = n_n \int_{\nu_o}^{\infty} \frac{4\pi J_\nu}{h\nu} \alpha_\nu h(\nu - \nu_o) d\nu \text{ [erg s}^{-1} \text{ cm}^{-3}] , \quad (278)$$

the volume cooling rate due to induced recombination is

$$L_{ind,n} = n_e n_p 4\pi P_n^* \int_{\nu_o}^{\infty} \frac{J_\nu}{h\nu} \alpha_\nu \exp(-h\nu / kT) h(\nu - \nu_o) d\nu \text{ [erg s}^{-1} \text{ cm}^{-3}] \quad (279)$$

and the cooling rate due to spontaneous radiative recombination is

$$L_{spn,n} = n_e n_p kT \beta(T, n) \text{ [erg s}^{-1} \text{ cm}^{-3}] . \quad (280)$$

The cooling rate coefficient $\beta(T, n)$ is evaluated as described on page 243.

11.8 Collisional Ionization - Three-Body Recombination

The net volume-heating rate due to collisional ionization less three-body recombination is given by

$$G_{n,\kappa} - L_{n,\kappa} = \sum_n P_n^* n_e n_p C_{n,\kappa} h\nu_o (1 - b_n) \text{ [erg s}^{-1} \text{ cm}^{-3}] \quad (281)$$

where $C_{n,\kappa}$ is the collisional ionization rate, P^* are STE populations, and b_n is the departure coefficient. The term $(1 - b_n)$ is only large and positive for very low levels, in which $I_n > kT$. Far from thermodynamic equilibrium this is usually a net cooling process only for the ground term. This is because departure coefficients for excited states are nearly unity while the ground level usually has $b_n \gg 1$.

11.9 H⁻ Heating and Cooling

11.9.1 H⁻ bound-free

The volume-heating rate due to spontaneous absorption (photodissociation) is

$$G_{H^-} = n(H^-) \int_{\nu_0}^{\infty} \frac{4\pi J_{\nu}}{h\nu} \alpha_{\nu} h(\nu - \nu_0) d\nu \quad [\text{erg s}^{-1} \text{ cm}^{-3}] \quad (282)$$

where symbols have their usual meaning. The volume-cooling rate due to induced radiative attachment is

$$L_{ind, H^-} = n_e n_{H^0} P^*(H^-) \int_{\nu_0}^{\infty} \alpha_{\nu} \frac{4\pi J_{\nu}}{h\nu} \exp(-h\nu / kT) h(\nu - \nu_0) d\nu \quad [\text{erg s}^{-1} \text{ cm}^{-3}] \quad (283)$$

while the volume cooling rate for spontaneous radiative attachment is

$$L_{spn, H^-} = n_e n_{H^0} 8\pi P^*(H^-) \int_{\nu_0}^{\infty} \alpha_{\nu} \frac{\nu^2}{c^2} \exp(-h\nu / kT) h(\nu - \nu_0) d\nu \quad [\text{erg s}^{-1} \text{ cm}^{-3}]. \quad (284)$$

11.9.2 H⁻ free-free

Free-free heating and cooling by H⁻ is also significant, although less so than bound-free heating. This is included, making the appropriate correction for stimulated emission, using the cross sections given by Vernazza et al. (1981; see also Bates et al. 1975).

Under most circumstances H⁻ bound-free heating and cooling are much more important than H⁻ free-free processes. This is surprising at first sight, since standard opacity curves comparing bound-free and free-free opacities (Bates et al. 1975; Mihalas 1978) show that the two are comparable. These curves are for strict thermodynamic equilibrium, with H⁻ departure coefficients of unity. Like the ground state of hydrogen, the departure coefficient for H⁻ is often many orders of magnitude larger than unity, so that the H⁻ bound-free opacity and the resulting heating greatly exceed the H⁻ free-free opacity.

11.10 Line Heating and Cooling

11.10.1 Overview

All lines will be treated as data types *EmLine*. The following sections describe the major routines for computing heating and cooling for n -level atoms. Emission lines are often optically thick. All lines are transferred using escape probabilities, by

determining level populations including both collisional and radiative processes (see, for example, Elitzur 1991). Line masing can sometimes occur, and again is treated using escape probabilities.

In all cases the net cooling due to a transition is given as

$$L_{line} = h\nu_{u,l} (n_l C_{l,u} - n_u C_{u,l}) \quad [\text{erg cm}^{-3} \text{ s}^{-1}] \quad (285)$$

where the populations of levels are given by n_i and C_{ij} is the collision rate. This cooling is evaluated in routines *level2*, *level3*, *levelN*, and *beseq*. Each routine is responsible for evaluating the line intensity, cooling, and destruction rate, and entering these into the appropriate stacks. Each routine sets the following attributes.

Lines can act to *heat* rather than cool the gas when the gas is irradiated by a continuum with a brightness temperature greater than the gas temperature at the line energy. This is an important gas heating mechanism for PDRs, for instance (Tielens and Hollenbach 1985). If η is the photon occupation number of the attenuated incident continuum at the line frequency (see page 213 above), then the rate atoms are excited from the ground level is given by $\eta \varepsilon A_{ul}$ where ε is the line escape probability. A fraction $C_{ul}/(C_{ul} + \varepsilon A_{ul})$ of these radiative excitations is converted into heat by collisional de-excitation. The net heating due to this process is then

$$G_{FIR} = n_l \eta_\nu \varepsilon_{lu} A_{ul} \left(\frac{C_{ul}}{C_{ul} + \varepsilon_{lu} A_{ul}} \right) h\nu \quad [\text{erg cm}^{-3} \text{ s}^{-1}] \quad (286)$$

where n_l is the density of the ground level. This process is included for all transferred lines.

11.10.2 Two level atoms

Cooling due to collisional excitation of two level atoms of the heavy elements is evaluated in routine *level2*. This routine does the following: a) finds the abundance of the two levels by balancing collisional and radiative processes, subject to the sum $n_l + n_u = \text{abundance}$. b) adds the line cooling (or heating) to the total cooling, c) adds the line derivative to dC/dT , d) evaluates the fraction of the escaping line destroyed by background opacity, e) adds this to the local OTS radiation field, f) records the line opacity population $n_l - n_u g_l/g_u$. The populations of the atom are saved in the vector *PopLevls*.

11.10.3 Three level atoms

The level populations, cooling, and line destruction by background opacity sources are computed for three level atoms in routine *level3*.

Routine *level3* is called with three arguments, the three line structures. Levels are designated by the indices 0, 1, and 2, with 0 being the lowest level. The routine is called with three line structures, indicated by *t10*, *t21*, and *t20*, each representing the downward radiative transition between the indicated levels. Any one of these transitions may be a dummy transition, using the dummy line *TauDmmy* provided for this purpose. The total rates between any two levels $i \Rightarrow j$ is indicated by R_{ij} . This includes collisions, radiative decays (both photon escape and destruction by

background opacity), and induced transitions. If the total abundance of the parent ion is A , the three balance equations are

$$n_0 + n_1 + n_2 = A \quad (287)$$

$$n_0(R_{01} + R_{02}) = n_1R_{10} + n_2R_{20} \quad (288)$$

$$n_1(R_{10} + R_{12}) = n_2R_{21} + n_0R_{01} . \quad (289)$$

Setting n_0 to $A - n_1 - n_2$ equation 288 becomes

$$(R_{01} + R_{02})(A - n_1 - n_2) = n_1R_{10} + n_2R_{20} . \quad (290)$$

After gathering terms this equation becomes

$$A(R_{01} + R_{02}) = n_1(R_{10} + R_{01} + R_{02}) + n_2(R_{20} + R_{01} + R_{02}) . \quad (291)$$

Substituting for n_0 , equation 289 becomes

$$n_1(R_{10} + R_{12}) = n_2R_{21} + R_{01}(A - n_1 - n_2) . \quad (292)$$

Gathering terms this equation becomes

$$n_1(R_{10} + R_{12} + R_{01}) = AR_{01} + n_2(R_{21} - R_{01}) . \quad (293)$$

Solving 291 for n_1 we obtain

$$n_1 = \frac{A(R_{01} + R_{02})}{R_{10} + R_{01} + R_{02}} - \frac{n_2(R_{20} + R_{01} + R_{02})}{R_{10} + R_{01} + R_{02}} \quad (294)$$

and solving 293 we find

$$n_1 = \frac{AR_{01}}{R_{10} + R_{12} + R_{01}} + \frac{n_2(R_{21} - R_{01})}{R_{10} + R_{12} + R_{01}} \quad (295)$$

Equating the two and gathering terms we obtain

$$n_2 \left(\frac{R_{21} - R_{01}}{R_{10} + R_{12} + R_{01}} + \frac{R_{20} + R_{01} + R_{02}}{R_{10} + R_{01} + R_{02}} \right) = \frac{A(R_{01} + R_{02})}{R_{10} + R_{01} + R_{02}} - \frac{AR_{01}}{R_{10} + R_{12} + R_{01}} \quad (296)$$

with the solution

$$n_2 = A \left(\frac{(R_{01} + R_{02})}{R_{10} + R_{01} + R_{02}} - \frac{R_{01}}{R_{10} + R_{12} + R_{01}} \right) \bigg/ \left(\frac{R_{21} - R_{01}}{R_{10} + R_{12} + R_{01}} + \frac{R_{20} + R_{01} + R_{02}}{R_{10} + R_{01} + R_{02}} \right) . \quad (297)$$

In the code the term in the numerator in the previous equation is called *alpha*, and the denominator *beta*. Replacing n_2 in equation 294 we obtain

$$n_1 = \frac{[A(R_{01} + R_{02}) - n_2(R_{20} + R_{01} + R_{02})]}{(R_{10} + R_{01} + R_{02})} \quad (298)$$

Again the two terms are called *alpha* and *beta*.

11.10.4 N level atoms

The level populations, cooling, and line destruction by background opacity sources are computed for n level atoms in routine *LevelN*. There is no limit to the number of levels that can be considered.

Routine *LevelN* is called with 12 arguments. These are:

nlev This is the number of levels for the model atom. It is an integer and can be as large as the value of *limLevelN*, currently 20.

abund This is the total abundance of the ion. The total population of the *nlev* levels will add up to this quantity, which is a real variable.

g This is a real vector of dimension *nlev*. It contains the statistical weights of the levels.

ex This is a real vector of dimension *nlev*. It contains the excitation temperature (K) of the *nlev* levels *relative to ground*. The excitation temperature of the lowest level should be zero.

p This is a real vector of dimension *nlev* and is the computed population of the *nlev* atom. It will contain all zeros if *abund* is zero, and *p[0]* will equal *abund* if the temperature is so low that the Boltzmann factors are zero for the current cpu.

data This two dimensional real vector is *data[nlev][nlev]*. *Data[u][l]* is the effective transition probability (the product of the Einstein A and the escape probability) for the transition. *Data[l][u]* is the collision strength for the transition.

dest This two dimensional real vector is *dest[nlev][nlev]*. *Dest[u][l]* is the destruction rate (the product of the Einstein A and the destruction probability) for the transition. *dest[l][u]* is not used.

pump This two dimensional real vector is *pump[nlev][nlev]*. *pump[u][l]* is the upward pumping rate (the Einstein B_{lu}) for the transition.

ipdest This two dimensional integer vector is *ipdest[nlev][nlev]*. *ipdest[u][l]* is the pointer to the line in the continuum array. *LevelN* computes the local line destruction rate and includes this in the OTS field if the pointers are non-zero. If this vector contains zeros then no flux is added to the OTS field.

cooltl This real variable is the total cooling in ergs/s produced by the model atom.

chLabel This is a 4 character variable, and is a label for the ion.

negpop This logical variable is true if any of the level populations were negative.

11.10.5 Li Sequence

Table 27 gives the stronger lines of Li-sequence ions. *Level3* is used for this sequence.

Table 27 Lithium Sequence Lines

<i>N</i>	<i>Ion</i>	<i>j=3/2-1/2</i>	<i>j=1/2-1/2</i>	<i>j=3/2-1/2</i>	<i>j=1/2-1/2</i>
6	C IV	1548.195	1550.770	312.422	312.453
7	N V	1238.821	1242.804	209.270	209.303
8	O VI	1031.9261	1037.6167	150.088	150.124
10	Ne VIII	770.409	780.324	88.134	
12	Mg X	609.79	624.95	57.88	57.92
13	Al XI	550.03	568.15	48.30	48.34
14	Si XII	499.40	520.67	40.92	
16	S XIV	417.61	445.77	30.43	
18	Ar XVI	353.92	389.14	25.53	
20	Ca XVIII	302.215	344.772	18.69	18.73
26	Fe XXIV	192.017	255.090	10.62	10.66

11.10.6 Boron Sequence

Figure 31 shows levels within the lowest three configurations of the Boron sequence. These are calculated in routine *AtomSeqBoron*.

11.10.7 Beryllium sequence atoms

The level populations, cooling, and line destruction by background opacity sources are computed for a specialized four level atom in routine *AtomSeqBeryllium*.

Routine *beseq* is called with five arguments, the collision strengths between the excited triplet levels, the line optical depth array for the fast ($j=1$ to $j=0$) transition, and the transition probability for the slow ($j=2$ to $j=0$) transition. Induced processes are only included for the fast transition. The collision strength stored in the line array is the collision strength for the entire multiplet. Rates to levels within the term are assumed to scale as the ratio of level statistical weight to term statistical weight. The level populations for the ground and excited states, with no correction for

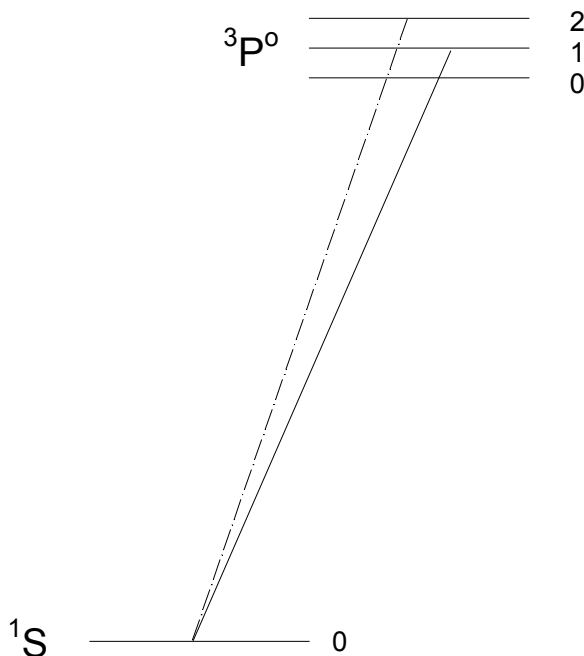


Figure 30 The four levels included in routine *beseq1*

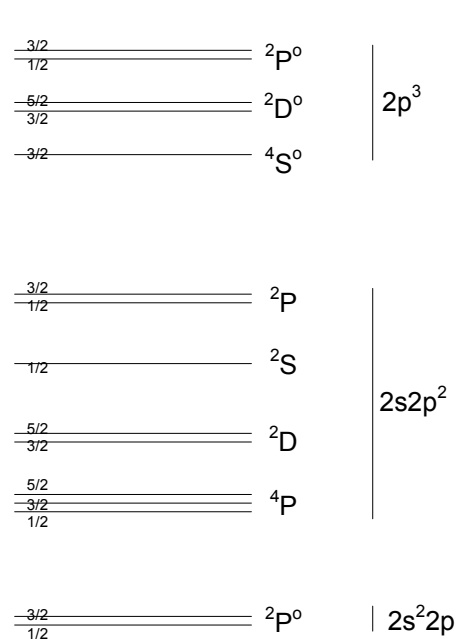


Figure 31 Energy Level Diagram for Boron Sequence. Boron

stimulated emission, are returned in the array *PopLevls*, contained in the common block of the same name.

The total rates between any two levels $i \Rightarrow j$ is indicated by R_{ij} . This includes collisions, radiative decays (for the fast transition, both photon escape and destruction by background opacity, and induced transitions). If the total abundance of the parent ion is A , the three balance equations are

$$n_0 + n_1 + n_2 + n_3 = A \quad (299)$$

$$n_0 (R_{01} + R_{02} + R_{03}) = n_1 R_{10} + n_2 R_{20} + n_3 R_{30} \quad (300)$$

$$n_1 (R_{10} + R_{12} + R_{13}) = n_3 R_{31} + n_2 R_{21} + n_0 R_{01} \quad (301)$$

$$n_2 (R_{20} + R_{21} + R_{23}) = n_3 R_{32} + n_1 R_{12} + n_0 R_{02} \quad (302)$$

Collisions are included in all these terms. R_{32} includes the slow downward line escape, while R_{02} and R_{20} includes escape, destruction by background opacity, and fluorescent excitation - deexcitation. In the code the terms on the LHS of equations 301, 302, and 300 are called α , β , and γ .

11.11 Evaluation of the Cooling Function

11.11.1 Total cooling

The cooling function is evaluated in routine *coolr*. This in turn calls other routines which compute cooling for individual elements. Each individual coolant is entered as a separate quantity in the array *cooling*. Under some extreme circumstances agents that are normally coolants can actually heat the gas. Negative coolants are stored in a parallel array, *heatnt*.

The total cooling is the sum of this array, referred to as the variable *ctot*, and evaluated in routine *SumCool*.

11.11.2 The cooling derivative

As the cooling is evaluated, its approximate temperature derivative is computed by making analytic expansions of the cooling for individual agents. For instance, collisionally excited lines of positive ions have collisional excitation rates that depend on the product

$$L_{line} \propto n_e n_{ion} T_e^{-1/2} \exp(-T_{exc} / T_e) \quad (303)$$

where T_{exc} is the excitation temperature of the line. In this case the derivative of the cooling function can be expressed as

$$\frac{dL_{line}}{dT} \propto n_e n_{ion} \frac{d}{dT_e} T_e^{-1/2} \exp(-T_{exc} / T_e) = L_{line} \left[\frac{T_{exc}}{T_e^2} - \frac{1}{2T_e} \right] \quad (304)$$

This derivative is used by the thermal predictor-corrector routine to make the initial guess at a new temperature. This is approximate since both electron and ionic densities also depend on the temperature.

The variable *tsq1* contains the value $1/T^2$, while *halfte* is $(2T)^{-1}$. Both are part of the structure *cooling*.

11.12 Evaluation of the Heating Function

Various contributions to the heating function are evaluated throughout the code. Each heating agent stores its contribution to the total heating within a cell of the two dimensional array *heating*. The total heating is always the sum of the total contents of the *heating* array.

Heating due to photoionization of all stages of ionization of the 30 elements now included in the code are stored as *heating[nelem][ion]*. Heating due to photoionization of ionization stage *i* (*i=0* for the atom) of element with atomic number *nelem* is stored as *heating[nelem][i]*. Other agents are stored in unused portions of this array. The total heating and its temperature derivative are deduced from this array in routine *SumHeat*. The heating is stored as the variable *htot*.

Line heating is treated as a special case since these usually cool rather than heat. The level population routines are supposed to sort lines into heating and cooling components, and put these into the *EmLine* structure. The entries stored as *ipLnHeat* are then added to the heating stack as *heating[22][0]* when the total line cooling is evaluated in routine *SumCool*. The entries stored as cooling are added to the cooling stack here too. Normally this will catch all negative coolants early. Attempts to add negative cooling to the cooling stack are trapped and stored in the array *heatnt*. This is added to the total heating in routine *SumCool*.

11.13 Equilibrium Calculations

11.13.1 Hydrogen only

Figure 32 shows the results of a series of calculations in which the full set of statistical and thermal equilibrium equations are solved for thin cells of pure hydrogen gas with various densities.

The ionizing continuum is, in all cases, a black body with $T_{color} = 5 \times 10^4$ K, and the energy density of the radiation field is varied, up to the thermodynamic equilibrium limit, $T_u = T_{color}$.

Although the gas temperature in the thermodynamic equilibrium limit does not depend on the gas density, the physical processes that drive the gas to this temperature do. Thermal equilibrium calculations were performed with three densities chosen to span a fairly wide range. For low densities ($n(H) = 10^5$ cm⁻³) the gas remains highly ionized for all values of T_u shown. The temperature in thermodynamic equilibrium is set by the balance between Compton and inverse-Compton scattering. The intermediate density case ($n(H) = 10^{10}$ cm⁻³) reaches thermodynamic equilibrium with $\sim 3/4$ of the heating-cooling set by Compton scattering and the remainder due to free-free and free-bound processes. The high-density ($n(H) = 10^{15}$ cm⁻³) case reaches its thermodynamic equilibrium temperature with a balance between free-free (1/3 of the total) and free-bound (2/3 of the total)

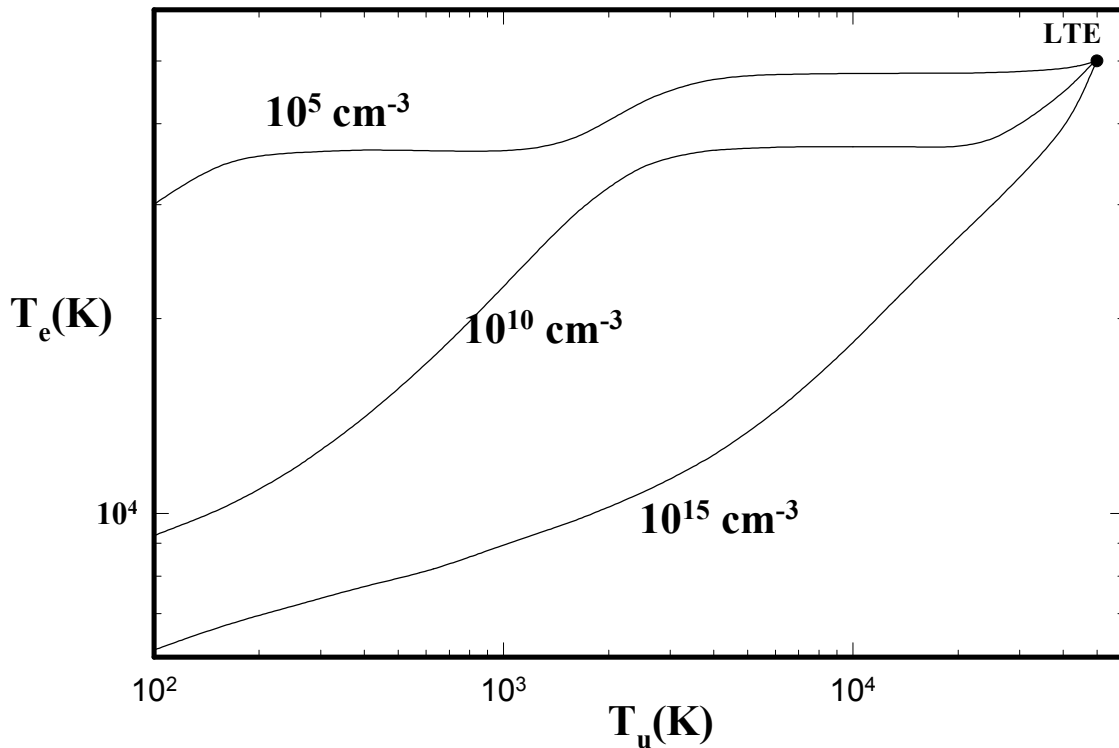


Figure 32 Thermal equilibrium calculations for an optically thin gas with 3 hydrogen densities are shown as a function of the radiation field energy density, parameterized as T_u . Ionization is by a 5×10^4 K black body. Various processes drive the gas to thermodynamic equilibrium when T_u reaches 5×10^4 K. hlte

processes. In all cases the level populations and electron temperature are within $\sim 1\%$ of their expected thermodynamic equilibrium values when $T_u = T_{color}$.

11.13.2 Helium-only gas

To do

11.13.3 Metal rich gas

Simulations of very metal rich gas is now a major emphasis of the code (Hamann & Ferland (1993; Ferland et al. 1996). In these cases the thermal and ionization balance is totally dominated by the heavy elements.

Figure 33 shows the results of a series of calculations in which gas with strongly enhanced abundances of the heavy elements is exposed to a series of black body radiation fields with different temperatures and energy densities. Ferland and Rees (1988) and Ferland and Persson (1989) gave analogous calculations for pure hydrogen clouds. The filled circles represent the cases where the energy densities of the radiation field are equal to the color temperature, and strict thermodynamic equilibrium is expected. This is indeed the case. The distribution of ionization for each color temperature is radically different, but the line interactions with the radiation field bring the gas to the expected equilibrium temperature. This tests both the ionization and thermal balance in this extreme environment.

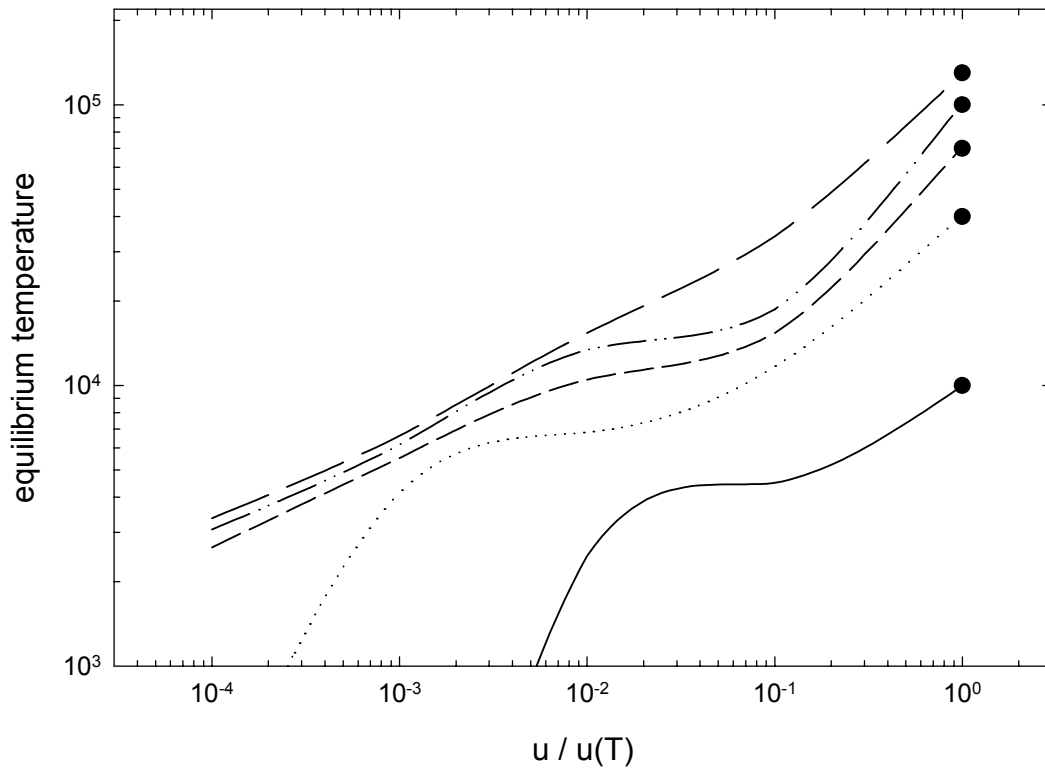


Figure 33 Equilibrium temperature of gas exposed to five black bodies with various energy density temperatures. The color temperatures of the blackbodies are 10,000K, 40,000K, 70,000K, 100,000K and 130,000K. The metallicity was 10 times solar (Hamann and Ferland 1993) so that heating cooling of thousands of heavy element emission lines dominates the thermal equilibrium. The simulation is of an optically thin cell of gas with density 10^{10} cm^{-3} (results do not depend on this density). The x-axis is the local energy density relative to the energy density in thermodynamic equilibrium at that temperature. The gas goes to thermodynamic equilibrium when the radiation field does (the color and energy density temperatures are equal). `high_z_te`

12 GRAIN PHYSICS

12.1 Overview

The following discussion outlines some physical processes relating to grains, as incorporated in Cloudy. It is adopted from Baldwin et al. (1991), and was written in close collaboration with P.G. Martin.

Several grain populations, types of graphite and “astronomical silicates”, are available. Usually one of each type, for a total of two, is selected, although there is no limit to the number of grain populations. Optical properties like opacity of the species are based on a realistic power-law size distribution. Other properties (like potential and temperature) are computed for a mean grain size rather than calculated for each individual size.

The following describes the “old”, default, grains that were originally incorporated into the code in the late 1980’s (Baldwin et al. 1991). These use optical properties that correspond to averages over the grain size distribution. The new (“pgains”) grains both resolves the grain size distribution and includes single photon heating for the smaller grains. This new treatment is described in van Hoof et al. (2001) and will be included in this document at a later time.

12.2 Grain Opacity

Grains are not included in the calculation by default. When enabled with the `grain` command the default mixture has interstellar medium (ISM) properties. Grains more similar to those seen in Orion or planetary nebulae are also available.

12.2.1 ISM grains

The optical constants for the default (ISM) grain species are from the calculations of Martin and Rouleau (1990). These extend the work of Draine and Lee (1984) to ionizing energies where the grains are strongly absorbing. These opacity calculations were based on the Mathis, Rumpl, and Nordsieck (1977) power-law size distribution to simulate interstellar extinction in diffuse clouds.

12.2.2 Orion grains

Grains within the Orion Nebula have a relatively large ratio of total to selective extinction R and an exceptionally gray opacity in the ultraviolet. These are both indicative of a deficiency in small grains and a larger mean grain size. To account for this, a second set of opacity functions is included, the Orion group. For this the value of the smallest size (a_s) in the Mathis et al. (1977) size distribution was increased from $0.0025\mu\text{m}$ to $0.03\mu\text{m}$. While this simple adjustment of the size distribution is not entirely adequate for explaining the details of the visible and near ultraviolet Orion extinction curve (Mathis and Wallenhorst 1981), it should be an improvement for the ionizing ultraviolet portion, which is most important.

The Orion extinction curve is designed to simulate the large R grains observed in this HII region. Relative to ISM standard grains the total amount of grain material was preserved, so that α_{abs} in the infrared and in the EUV and X-Ray regions remains

unchanged. The main differential effect is to lower the cross section through a broad peak at 1 Ryd.

12.2.3 PN grains

Infrared opacities for the silicate component are taken from unpublished work by K. Volk. Ultraviolet silicate cross sections, and the graphite constituent, are standard ISM.

12.2.4 Extinction

The ISM extinction properties, both effective scattering (subscript *scat*) and absorption (subscript *abs*), are shown in Figure 34.

The quantities plotted are cross sections (cm²) per H nucleon: $\sigma = \kappa/n(H)$, where κ (cm⁻¹) is the opacity due to grains and $n(H)$ (cm⁻³) is the local density of H in any form. Rather than the total scattering cross section σ_s an effective scattering cross section $\sigma_{scat} = \sigma_s (1-g)$ is plotted. This discounts the radiation scattered near the forward direction. The asymmetry parameter g approaches unity at high and low energies, particularly for larger grains, so that σ_{scat} becomes much less than α_{abs} .

The optical depth τ is σ times the hydrogen column density (or κ integrated over the path). Absorption attenuates the incident radiation field as $\exp(-\tau_{abs})$. The effects of scattering are more difficult to model. In an open geometry, scattering attenuates approximately as $(1+0.5 \tau_{scat})^{-1}$. However, in a closed geometry, to within factors of order unity, the scattered light is not lost from the beam, and the scattering opacity can be ignored. In either case, effective grain scattering optical depth is generally fairly small through the ionized nebula at ionizing energies.

12.3 Photoelectric Emission

As discussed below, photoelectric emission from grains contributes directly to heating the gas and, through the grain potential U_g established, affects radiative and collisional heating of the grains and the grain drift velocity.

The photoionization rate of a grain, per unit projected area, is

$$\Gamma_g = \int_{\nu_0}^{\infty} Q_{abs} \frac{4\pi J}{h\nu} \hat{Y} d\nu \quad (305)$$

where \hat{Y} is the effective photoelectric yield per absorbed photon, Q_{abs} is the absorption efficiency factor, and $4\pi J/h\nu$ symbolizes the photon flux of direct, diffuse, and OTS radiation fields. For the OTS line component, the integral is of course just a sum over the line photons that are sufficiently energetic. The threshold for photoemission, to be determined self-consistently, is given by $h\nu_0 = \max\{V_n + V_g, V_n\}$, where V_n is the photoelectric threshold for a neutral grain and $V_g = eU_g$.

V_g will depend on grain size through Q_{abs} and \hat{Y} . In the present implementation, a typical V_g is defined for each species by using Q_{abs} averaged over the size distribution: $Q_{abs} = \alpha_{abs}/\Sigma = \kappa_{abs}/n(H) \Sigma$. The projected grain area per H, Σ , is similar for each species: 2.1×10^{-22} cm² for graphite and 2.4×10^{-22} cm² for silicates.

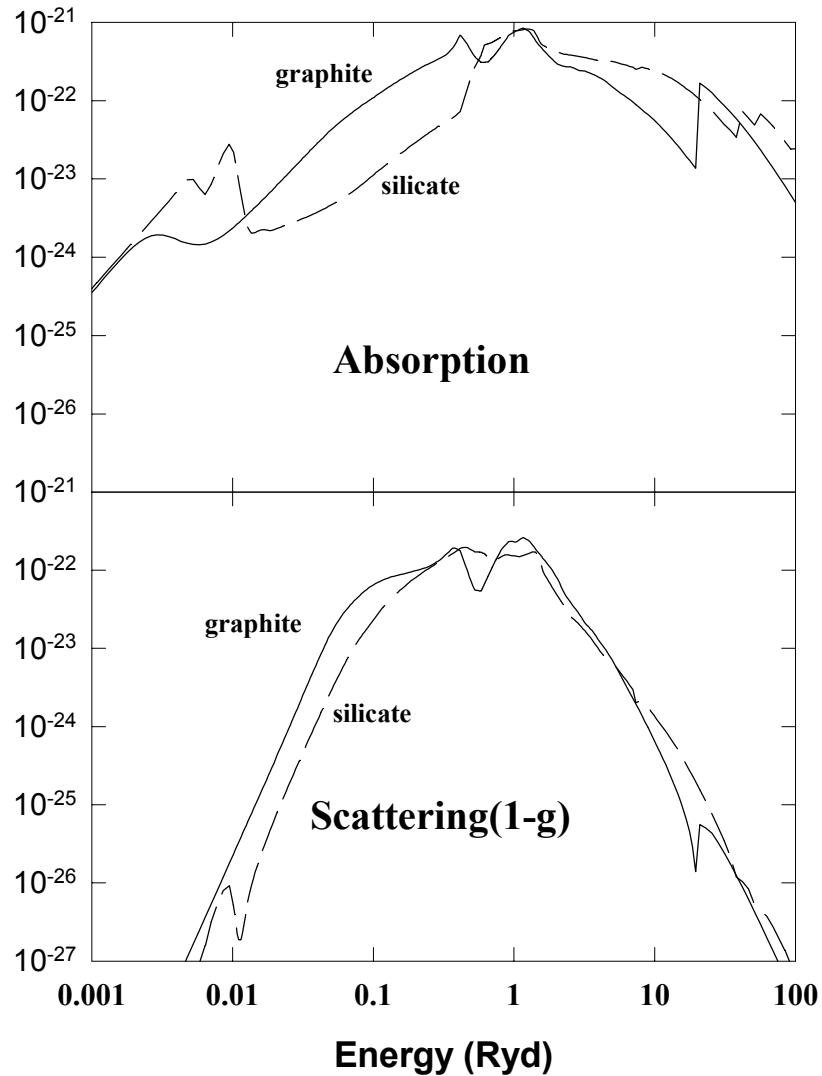


Figure 34 The absorption and scattering cross sections (cm^2 per hydrogen nucleon) for the two ISM grain populations, graphite and silicate, are shown. The effective scattering cross section is the scattering cross section multiplied by $1-g$, where g is the asymmetry parameter. grnopc

\hat{Y} is constructed as follows. The basic laboratory data measure the yield (per absorbed photon) for a neutral surface, Y_n . For each incident photon energy $h\nu$, the photoelectrons emerging from the neutral surface have varying energies E , with a probability distribution $p_n(E)$. To account for electron escape from finite sized grains, yields measured for semi-infinite sheets in the laboratory have to be corrected by a factor $f(E)$ (which introduces a size dependence). Such a correction would change the shape of the probability distribution as well as increase the integrated emission from a neutral surface (Draine 1978 gives an approximate expression for the overall increase). Then, formally

$$\hat{Y} = Y_n \int_{E_0}^{(h\nu - V_n)} f p_n dE \quad (306)$$

where $E_0 = \max\{0, V_g\}$ introduces the fact that the lowest energy photoelectrons do not escape from positively charged grains.

The form adopted is

$$Y_n = \min\{Y_0(1 - V_n/h\nu), Y_1\} \quad (307)$$

for $h\nu \geq V_n$, and $V_n = 8$ eV and $Y_0 = 0.5$ is assumed for both grain populations; according to Draine (1978) this combination gives about the right amount of photoelectric emission to heat neutral H I clouds in interstellar space ($h\nu \leq 13.6$ eV). For the higher energies a cap at $Y_1 = 0.2$ is introduced, which is suggested by experimental data. For p_n a simple form that is independent of E (Draine 1978) is adopted:

$$p_n = (h\nu - V_n)^{-1} \quad (308)$$

While only approximate, this induces the physically correct response (decrease) in \hat{Y} (and the photoelectric heating) when the grain is positively charged. Because the form of $f(E)$ is highly uncertain $f = 1$ is assumed (this again avoids a size dependency). Extension of the flat cap in Y_n to high energies also addresses this issue to some degree. With these assumptions, \hat{Y} is known in analytic form:

$$\hat{Y} = Y_n \min\{1, 1 - V_g/(h\nu - V_n)\} \quad (309)$$

12.4 Collisional Charging of a Grain

Per unit projected area of a grain, collisions with particles of space density n , mass m , and charge Z ($Z = -1$ for electrons) give an effective recombination rate

$$\alpha(gr) = -n \bar{v} S Z \eta, \quad (310)$$

where

$$\bar{v} = \sqrt{8kT/\pi m_e} \quad (311)$$

is the mean particle speed. In this expression, and for other collisional rates involving n below, it is implicit that there is a sum of similar terms over all species in the gas. For electrons S is the sticking probability which we take to be 1 (Spitzer 1948; Watson 1972; Draine 1978). For positively charged nuclei, SZ is the charge transfer efficiency, taken to be Z here. The last factor η , the correction for Coulomb interactions between the grain and the recombining particles of charge Z , is given in terms of

$$\psi = ZV_g/kT_e \quad (312)$$

by

$$\eta = \begin{cases} 1 - \psi & \text{if } \psi \leq 0 \\ \exp(-\psi) & \text{if } \psi > 0 \end{cases} \quad (313)$$

Terms for positively charged nuclei are included, but are usually small relative to the contribution from free electrons.

12.5 Grain Potential

The steady state grain potential is determined for each grain species independently by requiring charge balance. Expressed as a balance per unit area this is $\alpha_{gr} = \Gamma_{gr}$. Because of the many dependencies on V_{gr} , this is carried out numerically.

12.6 Grain Drift Velocity

The grain drift velocity is determined by balancing the radiative acceleration due to the direct attenuated radiation field with the drag forces given by equations 1-6 of Draine and Salpeter (1979). The equations are solved numerically for the drift velocity, including interactions with electrons and all ions present in the gas.

12.7 Radiative Heating and Cooling of a Grain

Once the grain potential is known, the rate of radiative heating of the grain per unit projected area is

$$G_{grain}(rad) = \int_0^{\nu_o} Q_{abs} 4\pi J d\nu + \int_{\nu_o}^{\infty} Q_{abs} \frac{4\pi J}{h\nu} (h\nu - EY) d\nu. \quad (314)$$

The last term represents the portion of the photon energy that does not heat the grain, but rather passes to the escaping electrons:

$$EY = Y_n \int_{E_o}^{(h\nu - V_n)} E f p_n dE. \quad (315)$$

With the above approximations for f and p_n this is given analytically by

$$EY = 0.5 Y_n \left[(h\nu - V_n)^2 - [\max(0, V_g)]^2 \right] / (h\nu - V_n) \quad (316)$$

The cooling of a grain by radiative losses, per unit projected area, is given by

$$\Lambda_{grain}(rad) = \int_0^{\infty} Q_{abs} 4\pi B_\nu(T_g) d\nu \quad (317)$$

where $B_\nu(T_g)$ is the Planck function for the grain temperature.

12.8 Collisional Heating of a Grain

Collisions with electrons, ions, and neutral particles also heat the grains. Per unit projected area of the grain, this heating rate may be written as

$$G_{grain}(col) = n \bar{v} S \left(2kT_e \xi - ZV_g \eta + I \eta - 2kT_g \eta \right). \quad (318)$$

The first term corresponds to kinetic energy extracted from the gas. The factor ξ makes adjustment for Coulomb interactions and is given by

$$\xi = \begin{cases} 1 - \psi/2 & \text{if } \psi \leq 0 \\ (1 + \psi/2) \exp(-\psi) & \text{if } \psi > 0 \end{cases}. \quad (319)$$

The second term in $G_{grain}(col)$ allows for the change of the particle's energy in the grain potential. In the third term, the product $I\eta$ is the average chemical energy released per impact. Here it is assumed that when impinging ions recombine the ionization energy released is deposited as heat in the grain (there is then no corresponding term for heating the gas in Λ_g below). The last term describes the effect of thermal evaporation of neutralized ions and thermally accommodated neutral particles (there is no corresponding term for electrons).

In implementing the above processes, S for electrons is again the sticking probability. For positively charged nuclei, S is the energy transfer efficiency, taken here to be unity (this process should be evaluated consistently with that for charge transfer). For neutral particles of mass m striking a grain whose typical atom has mass M , the accommodation coefficient $S \approx 2 m M / (m + M)^2$ (Draine 1978).

12.9 Grain Temperature

The equilibrium grain temperature is determined by the balance between cooling (Λ) and heating (G) by radiative and collisional processes. For the radiative terms, Q_{abs} averaged over the size distribution is used to obtain a typical temperature for each species.

As a test of the bandwidth of the code, and its behavior in a well-defined limit, tests were computed in which the grains were irradiated by black body radiation in strict thermodynamic equilibrium (i.e., the color and energy density temperatures were equal). Radiation temperatures between 10 K and 10^9 K, the temperature limits to the code, were used. These tests showed that the deduced grain equilibrium temperature was within much better than 1 percent of the blackbody temperature.

12.10 Photoelectric Heating of the Gas

Heating of the gas by photoemission from grains can be an important process in ionized regions (Spitzer 1948; Oliveira and Maciel 1986). For charged grains this heating rate ($\text{erg cm}^{-3} \text{ s}^{-1}$) is given by

$$G_{gas} = \int_{\nu_0}^{\infty} \kappa_{abs} \frac{4\pi J}{h\nu} (EY - V_g \hat{Y}) d\nu. \quad (320)$$

The first term describes the energy of the photoelectrons as they leave the surface, balancing the similar term in $G_{grain}(rad)$. The second term compensates for the grain potential, and can be seen to balance the related term in $G_g(col)$ when charge balance holds.

12.11 Collisional Cooling of the Gas

The gas is cooled as the gas particles hit the cooler grain surface. Per unit volume, this cooling rate may be written as

$$\Lambda_{gas} = n n(H) \Sigma \bar{v} S (2kT_e \xi - 2kT_{grain} \eta) , \quad (321)$$

the individual terms consistently balancing the corresponding ones in $G_g(col)$ (see equation 319).

12.12 Grain Sublimation

The code checks that grain survival is likely by comparing the highest grain temperature with the sublimation temperatures. These are taken to be 1400 K for silicates and 1750 K for graphite and are based on the paper by Laor and Draine (1993). These values are stored in the vector *sublimat* and initialized in block data *martin*. A warning will be printed at the end of the calculation if the grain temperature rises above the sublimation point. A caution will be printed if the temperature rises above 90% of the sublimation point.

12.13 Ionic Recombination on Grain Surfaces

Positive ion recombination on grain surfaces proceeds at a rate $n_{ion}n_H\alpha_{gr}$ where the recombination coefficient is taken from Draine and Sutin (1987; their equation 5.15). For a standard grain size distribution this rate coefficient is $\sim 5.8 \times 10^{-13} T_e^{-0.5} \text{ cm}^3 \text{ s}^{-1}$. This process is included for all ions included in the calculation when grains are present, but is not generally important. The rate coefficient is evaluated in routine *hmole* and stored as the variable *gionrc*.

12.14 Grain Variables

ndust The number of grain species. This variable appears in parameter statements throughout the code. Currently *ndust* is 20.

lgDustOn This logical variable is true if grains are enabled, and false otherwise. This is the variable to check to determine whether grains exist in the current model.

dqabs[energy][ndust] Absorption Q for this grain species as a function of energy.

dqscat[energy][ndust] Scattering Q for this grain species as a function of energy.

dston1[ndust] A logical variable that indicates whether this grain species is enabled.

dstab1[energy][ndust] Absorption cross section for this grain species

dstsc1[energy][ndust] Scattering cross section for this grain species.

dstab[ndust] Total absorption cross section for all grain species.

dstsc[energy] Total scattering cross section for all grain species.

dstq[ndust] The grain charge, in units of number of electrons.

dstpot[ndust] The grain potential, in Rydbergs.

dstdft[ndust] The grain species' drift velocity.

avdft[ndust] Variable used to derive average drift velocity of a grain species.

dustp[4][ndust] These are parameters describing the grain species, and are set in block data *martin*. They are defined in Peter Martin's program that computes grain optical parameters. The four elements of the array are the grain density, molecular weight, normalizing abundance, and depletion.

eev[limcrs][ndust] is an *limcrs* long array of energies (in Rydbergs, despite the variable name). *ndpts* of these are energies where the grain optical parameters are defined.

sab[limcrs][ndust] is an *limcrs* long array of absorption cross sections for the grain species, at the *ndpts* energy points. These are defined as the effective absorption cross section per hydrogen nucleon.

sse[limcrs][ndust] is an *limcrs* long array of scattering cross sections for the grain species, at the *ndpts* energy points. These are defined as the effective scattering cross section per hydrogen nucleon, multiplied by (1-g) where g is the grain asymmetry factor.

ndpts[ndust] is the number of energies where the grain optical properties are defined, for each species.

darea[ndust] is the grain surface area (cm²) per hydrogen nucleon.

dsize[ndust] is the grain radius (cm) per hydrogen nucleon.

dwork[ndust] Grain species neutral surface work function in Rydbergs.

dstfac[ndust] This is the log of the depletion scale factor for each grain species. It is equal to 0 for “normal” abundances, -1 for 1/10th of “normal”, etc. This is the first optional number that appears on the **grains** command. The number remains the log of the depletion throughout the calculation.

tedust[ndust] The equilibrium temperature for a grain species.

13 OTHER PHYSICAL PROCESSES

13.1 Overview

This section describes other physics processes that have been incorporated into Cloudy. Some of these are taken from published papers that have described the formalism used by Cloudy in detail. The original papers are cited in the beginning of each section.

13.2 Magnetic fields

Magnetic fields are not normally considered by the code, but can be included with the `magnetic field` command.

Cooling due to electron cyclotron emission, using equations from Fabian, Pringle, and Rees (1976; these assume optically thin emission) are included when the field is specified. The volume-cooling rate is given by

$$\Lambda_{\text{cyclotron}} = n_e \frac{B^2}{8\pi} \frac{4}{3} \sigma_{\text{Thom}} c \left(\frac{v_e}{c} \right)^2 = 4.5433 \times 10^{-25} n_e B^2 T_e \text{ [erg cm}^{-3} \text{ s}^{-1}] \quad (322)$$

where σ_T is the Thomson cross-section and

$$u_e = \left(\frac{8kT_e}{\pi m_e} \right)^{1/2} = 6.2124 \times 10^5 T_e^{1/2} \text{ [cm s}^{-1}] \quad (323)$$

is the mean electron speed. See, however, Masters, Pringle, Fabian, and Rees (1977). They show that this emission process is likely to be optically thick under some circumstances. Cyclotron optical depth effects are not now treated, so this cooling rate is likely to be an overestimate.

Magnetic pressure is included in the gas equation of state⁵. The magnetic pressure in the general case will be

$$P_{\text{mag}} = \frac{B_{\text{tangled}}^2}{8\pi} + \frac{B_{\text{tangential}}^2 - B_{\text{parallel}}^2}{8\pi} \text{ [dynes cm}^{-2}] \text{ [erg cm}^{-3}]. \quad (324)$$

and the enthalpy density is

$$w_{\text{mag}} = \frac{\gamma}{\gamma - 1} \frac{B_{\text{tangled}}^2}{8\pi} + \frac{B_{\text{tangential}}^2 + B_{\text{parallel}}^2}{4\pi} \text{ [dynes cm}^{-2}] \text{ [erg cm}^{-3}]. \quad (325)$$

The field strength is determined from local conditions across the cloud. A tangled field will have a strength that is related to the local density by equation 325. To force a constant magnetic field specify $\gamma = 0$. An ordered field is assumed to have constant strength if the gas is stationary. If the gas is moving (a wind solution is being

⁵ The pressure associated with the magnetic field was not included in the total pressure in versions 95 and earlier of the code.

performed) then the component in the radial direction (the parallel component) is constant and the transverse field has a strength that is given by (Cowling 1976)

$$B_t = B_i^0 \frac{u_o^2 - u_A^2}{uu_0 - u_A^2} . \quad (326)$$

where u_A is the Alfvén velocity at illuminated face,

$$u_A^2 = \frac{B_{parallel}^2}{4\pi\rho_0} \quad [\text{cm}^2 \text{ s}^{-2}]. \quad (327)$$

For reference, a tangled field will have a pressure equivalent to the thermal pressure of a gas with density n and temperature T when

$$P_{mag}/k = \frac{B^2}{8\pi} \frac{1}{k} = B^2 2.882 \times 10^{14} \approx nT \quad [\text{cm}^{-3} \text{ K}]. \quad (328)$$

In the ISM this magnetic pressure is often roughly equal to the ram or turbulent pressure

$$P_{ram}/k = \rho u^2 / 2k = 60.14 \quad n u_{\text{km s}^{-1}}^2 \approx nT \quad [\text{cm}^{-3} \text{ K}]. \quad (329)$$

where the last velocity is in km/s and n is the nucleon density (cm^{-3}). For comparison, the Alfvén velocity, the speed at which magnetic fields convey information, is

$$u_A = \frac{B}{(4\pi\rho)^{1/2}} \approx 2.19 \times 10^6 B \quad n^{-1/2} \quad [\text{km s}^{-1}]. \quad (330)$$

Cosmic rays should not be included when a magnetic field is specified, since the effects of a field on cosmic ray transport are not now treated. A warning will be printed if both are included.

13.3 Cosmic Ray Interactions

The implementation of cosmic rays was done in collaboration with Richard Mushotzky. This section is taken from Ferland and Mushotzky (1984).

Synchrotron radio sources are usually modeled in terms of an interaction between a magnetic field and a relativistic gas with a typical energy per electron of a few hundred MeV (see Pacholczyk 1970; Longair 1981). The spectral index of the radio emission for radio-loud active galaxies is usually ~ -0.7 , and this suggests that the electrons, which make the dominant contribution to synchrotron emission, have a density (per unit energy interval) given by $n(cr, E) \sim E^{-2.4}$ (Kellerman 1966). The total relativistic electron density is sensitive to the lower bound of the energy distribution, which is typically of order 10–100 MeV, corresponding to relativistic factor of $\gamma \sim 10$ –100 (Lee and Holman 1978).

The cosmic ray density used by Cloudy is defined as

$$n(cr) = \int_{E_{\min}}^{E_{\max}} n(cr, E) dE \quad [\text{cm}^{-3}] \quad (331)$$

with the lower bound set to $E_{\min} = 5 \text{ MeV}$, corresponding to $\gamma \sim 10$. The density is only weakly sensitive to the upper limit $E_{\max} \approx 10 \text{ GeV}$ because of the strong convergence of the electron density function, although uncertainties in the lower energy bound introduce a fundamental uncertainty. Cosmic ray protons should have much smaller effects than the electrons, so the total cosmic ray electron density $n(\text{cr})$ is the only parameter.

The code assumes that the gas is “optically thin” to the energetic electrons. Serious and fundamental uncertainties afflict detailed treatments of the penetration of energetic particles into gas, particularly if magnetic fields are present. In the simplest case penetration is impeded only by ionization and heating losses resulting from two-body collisions. In this case the ability to heat an entire cloud is determined by the range of a particle, or the column density of gas required to stop it (see Rossi 1952). Relativistic electrons have a range that is given to within 15% by (Berger and Seltzer 1965)

$$R_e = 10^{25} \left(\frac{E}{100 \text{ MeV}} \right)^{0.8} \text{ [cm}^{-2}\text{]} \quad (332)$$

for a gas composed of neutral hydrogen. The range of a 100 MeV electron in a fully ionized gas, in which bremsstrahlung and Coulomb losses are more important than ionization, would be some 10 times smaller.

The relativistic particles both heat and ionize the gas. The main concern is for the rate with which energy is transferred to the cold gas (Lea and Holman 1978; Ginzberg and Syrovatskii 1964). In the H^+ zone the main interaction will be with free electrons. Kinetic energy is passed to the cold electrons at a rate

$$G_{cr} = 8.5 \times 10^{-19} n_e n(\text{cr}) \text{ [erg cm}^{-3} \text{ s}^{-1}\text{]} \quad (333)$$

by direct Coulomb interactions (Jackson 1975; Spitzer 1962; Ginzburg and Syrovatskii 1964; Pacholczyk 1970). Here n_e is the thermal electron density, and the integration is over the electron distribution given above.

In regions where hydrogen is neutral the main interaction between thermal and relativistic gases is through ionization of the cold gas. For large neutral fractions very little of the energy of secondary electrons goes into actually heating the gas (Rossi 1952; Spitzer and Tomasko 1968). Calculations show that secondary electrons have typical energies of $\sim 40 \text{ eV}$, and that there is roughly one ionization per 15 eV deposited. Using the Bethe-Bloch approximation (Ginzburg and Syrovatskii 1964) the neutral heating rate is

$$G_{cr} = 3.7 \times 10^{-20} n(H^0) n(\text{cr}) \text{ [erg cm}^{-3} \text{ s}^{-1}\text{]} \quad (334)$$

and the H^0 ionization rate is

$$\Gamma = 1.5 \times 10^{-8} n(\text{cr}) n(H^0) \text{ [erg cm}^{-3} \text{ s}^{-1}\text{]}. \quad (335)$$

This ionization rate was scaled through Lotz's (1967) curves to include collisional ionization of heavy elements in the calculation of heavy element ionization equilibria.

If cosmic rays are not included, and the hydrogen ground state photoionization rate falls below the galactic background cosmic ray ionization rate, then a comment will be generated warning that the cosmic ray background should perhaps be included. According to Spitzer (1978), the background cosmic ray ionization rate is very uncertain, but of the order of $2 \times 10^{-17} \text{ s}^{-1}$ for neutral hydrogen. According to the equations above, this rate corresponds to a cosmic ray density of $\sim 2 \times 10^{-9} \text{ cm}^{-3}$, the value used as the “background” cosmic ray density option for the **cosmic ray** command.

The discussion above, as well as the code, includes only two-body Coulomb interactions, and *does not* include collective effects, such as those discussed by Scott et al. (1980). Rephaeli (1987) notes that collective effects may not be important in most circumstances.

13.4 Line Radiation Pressure

Line radiation pressure was implemented in Cloudy in collaboration with Moshe Elitzur. The following was written in collaboration with Moshe, and is adopted from Elitzur and Ferland (1986).

13.4.1 Formalism

For radiation intensity I_ν the standard expression for the radiation pressure per unit frequency, P_ν , is (e.g. Schwarzschild 1965)

$$P_\nu = \frac{1}{c} \int I_\nu \mu^2 d\Omega \text{ [dynes cm}^{-2}; \text{ erg cm}^{-3}], \quad (336)$$

where $\mu = \cos(\theta)$ and θ is the direction of propagation of the radiation. When the radiation field is isotropic, its pressure and energy density,

$$u_\nu = \frac{1}{c} \int I_\nu d\Omega \text{ [dynes cm}^{-2}; \text{ erg cm}^{-3}], \quad (337)$$

are related by the familiar expression

$$P_\nu = \frac{1}{3} u_\nu \text{ [dynes cm}^{-2}; \text{ erg cm}^{-3}]. \quad (338)$$

This relation holds for a rather wide range of circumstances. If the angular distribution of I_ν is expanded in a power series in μ , then only powers higher than the second will lead to violations of equation 338. However, the successive coefficients of this expansion are decreasing approximately like the optical depth (e.g. Schwarzschild 1965, p 40), so deviations from equation 338 will only be proportional to $1/\tau^2$. Hence, when the medium is optically thick at the frequency ν equation 338 is an excellent approximation for the radiation pressure.

The only radiative quantity we need to know in order to calculate the radiation pressure is the angle-averaged flux, J_ν , since

$$u_\nu = \frac{1}{c} 4\pi J_\nu \text{ [dynes cm}^{-2}\text{; erg cm}^{-3}\text{]}. \quad (339)$$

The integrated radiation pressure is then

$$P(\nu) = \frac{4\pi}{3c} \int J_\nu d\nu \text{ [dynes cm}^{-2}\text{; erg cm}^{-3}\text{]}. \quad (340)$$

Introducing the line-width, defined by

$$\Delta\nu = \frac{1}{\bar{J}_{u,l}} \int J_\nu d\nu \text{ [Hz]} \quad (341)$$

where

$$\bar{J}_{u,l} = \int J_\nu \Phi(\nu) d\nu \text{ [erg cm}^{-2}\text{ s}^{-1}\text{ sr}^{-1}\text{]} \quad (342)$$

is the integrated mean intensity in the line and $\Phi(\nu)$ is the normalized line profile $\left[\int \Phi(\nu) d\nu = 1 \right]$. The quantity \bar{J} is readily available in the escape probability approximation because it is related directly to the source function S by

$$\bar{J}_{u,l} = S(1 - P_{u,l}) \text{ [erg cm}^{-2}\text{ s}^{-1}\text{ sr}^{-1}\text{]} \quad (343)$$

where $P_{u,l}$ is the photon escape probability. The line source function S is simply $B_\nu(T_{exc})$, the Planck function of the line excitation temperature. The final expression for the pressure due to a line at frequency ν is therefore

$$P(\nu) = \frac{4\pi}{3c} B_\nu(T_{exc}) \Delta\nu (1 - P_{u,l}) \text{ [dynes cm}^{-2}\text{; erg cm}^{-3}\text{]}. \quad (344)$$

Combining equation 344 with equation 153 on page 226 we obtain the final form of the line radiation pressure,

$$P(\nu) = \frac{8\pi h\nu^3}{3c^3} \frac{n_u/g_u}{(n_l/g_l - n_u/g_u)} \Delta\nu (1 - P_{u,l}) \text{ [dynes cm}^{-2}\text{; erg cm}^{-3}\text{]}. \quad (345)$$

In these expressions the line width is given in frequency units. Within the code the line width is given in velocity units, and the line pressure is given as

$$\begin{aligned} P(\nu) &= \frac{8\pi h\nu^4}{3c^4} \frac{n_u/g_u}{(n_l/g_l - n_u/g_u)} \Delta\nu (1 - P_{u,l}) = \frac{8\pi h}{3\lambda^4} \frac{n_u/g_u}{(n_l/g_l - n_u/g_u)} \Delta\nu (1 - P_{u,l}) \\ &= 6.872 \times 10^{-68} \nu^4 \frac{n_u/g_u}{(n_l/g_l - n_u/g_u)} \Delta\nu (1 - P_{u,l}) \\ &= 5.551 \times 10^{-26} \lambda^{-4} \frac{n_u/g_u}{(n_l/g_l - n_u/g_u)} \Delta\nu (1 - P_{u,l}) \end{aligned} \quad (346)$$

13.4.2 Line width

The line width is a crucial parameter in the calculations since the line radiation pressure is directly proportional to it. For lines with a moderate optical depth (i.e., $\tau \leq 10^4$) the damping wings are optically thin, and the line emission profile is essentially identical to the absorption profile. Then $\Phi(\nu)$ is simply described by the Doppler profile $\pi^{1/2} \exp(-x^2)$, where $x = (\nu - \nu_0) / \Delta\nu_{Dop}$ is the dimensionless frequency shift from line center and $\Delta\nu_{Dop} = (2kT/m)^{1/2} \nu_0/c$ is the Doppler width. The line full width is then

$$\Delta\nu = \Delta\nu_{Dop} \times 2(\ln \tau)^{1/2} \quad [\text{Hz}] \quad (347)$$

for $\tau \gg 1$.

The situation when the line optical depth exceeds $\sim 10^4$ is much more complicated. This is because scattering in the damping wings becomes significant, and the frequency dependence of the emission profile is not known before the entire radiative transfer problem is solved. In general, it is known that, for $L\alpha$ (generally the most important source of line radiation pressure) and large optical depths, the line width (in dimensionless units) is

$$x = k(a\tau)^{1/3} \quad , \quad (348)$$

(Adams 1972; Harrington 1973; Bonilha et al. 1979). In this expression a is the damping constant ($a \approx 4.72 \times 10^{-4} t_4^{-1/2}$ for $L\alpha$), τ is the line center optical depth, t_4 is the temperature in units of 10^4 K, and k is a number of order unity.

The frequency width required here is the value that will provide a rectangular profile with the same area as the proper integral of the source function. The results of Adams (1972) are adopted, and the resulting expression for the full line width in the case of large optical depths ($\tau \gg 1$) is

$$\Delta\nu = \Delta\nu_{Dop} 2.3 (a\tau)^{1/3} \quad (349)$$

An important point, evident from the plots provided by Adams for the source function as a function of frequency (his Fig 3), is that the width of the frequency distribution varies very little with position in the slab. This is also evident from the mean intensity plots of Harrington, as mentioned above, and is a result of the strong coupling between distant regions caused by scattering in the line wings. The expression provided in equation 349 for all locations in the slab, with τ being half the total slab thickness.

13.4.3 Background opacity and thermalization

Background opacity is included in the determination of the level populations using the formalism outlined in the section on line radiative transfer. Its main effect is to lower the line excitation temperature by providing a second “escape” (actually destruction) route for trapped photons. This is assumed to be the only effect background opacity has on radiation pressure. Balmer continuous absorption typically has an optical depth only of order unity, while the line optical depths are

many orders of magnitude larger. Absorption in the Balmer continuum can only compete with line scattering in the extreme wings, at frequency shifts exceeding $\sim (a\tau)^{1/2}$, which are much larger than the line width predicted by equation 349.

Collisional de-excitation can also break the assumption of pure scattering because a photon will be lost to the thermal pool before the radiative process can take place. This will happen when the density is high enough that the rate for collisional de-excitation, C_{ul} , exceeds the probability for the effective rate for the transition, $P_{ul} A_{ul}$, where P_{ul} is the line escape probability and A_{ul} is the Einstein coefficient. Because at large optical depths P_{ul} is essentially equal to τ^{-1} , the “effectively thin” assumption breaks down when

$$\tau \approx A_{ul} / C_{ul} \quad . \quad (350)$$

Once the line optical depth exceeds $\sim A/C$, a “thermalization limit” is encountered, and the assumption of a purely scattering nebula does not apply anymore. Therefore, in evaluating the optical depth for the line width expression (equation 349) the minimum of the actual line optical depth and the one prescribed by A/C is used. This is a conservative estimate of the effect of collisions on photon scattering. This is probably the most poorly understood part of the calculation of the line radiation pressure.

13.5 Radiative Acceleration

The radiative acceleration due to the direct attenuated continuum flux F_ν , for density ρ , is given by

$$a_{rad} = \frac{1}{\rho c} \int F_\nu \bar{\kappa}_\nu d\nu + \frac{1}{\rho c} \sum_l F_\nu(l) \kappa_l \gamma_l B_{l,u} \quad [\text{cm s}^{-2}]. \quad (351)$$

Here $\bar{\kappa}_\nu$ is the effective continuous opacity. The radiative acceleration includes the usual photoelectric and free-free absorption in the gas, and Compton and Rayleigh scattering. In addition it includes the term $\kappa_{abs} + (1-g)\kappa_s$ for the grain contributions if grains are present. The integral is over all energies considered by the code (from $\lambda \approx 10$ m to $h\nu \approx 100$ MeV).

The second term is a sum is over all transferred lines (typically 10^4 to 10^5 transitions). Here κ_l is the line opacity, $B_{l,u}$ is the Einstein coefficient, and γ_l is the escape probability in the direction towards the source of ionizing radiation (Ferland and Rees 1988).

13.6 Pressure Laws

13.6.1 Units

Pressure is force per unit area. The unit of force in the cgs system is the dyn, which is 10^{-5} N. The fundamental units of the dyn are g cm s^{-2} . For pressure these are dyn cm^{-2} or $\text{gm cm}^{-1} \text{s}^{-2}$.

13.6.2 Ideal gas laws

For a non-relativistic non-degenerate gas the energy density is

$$u = \frac{3}{2} n_{tot} k T_e \text{ [dyne cm}^{-2}; \text{ erg cm}^{-3}] \quad (352)$$

and the pressure is

$$P_{gas} = n_{tot} k T_e = \frac{2}{3} u \text{ [dynes cm}^{-2}; \text{ erg cm}^{-3}]. \quad (353)$$

n_{tot} is the total particle density (cm⁻³). For a relativistic non-degenerate gas the energy density is

$$u = 3 n_{tot} k T_e \text{ [dynes cm}^{-2}; \text{ erg cm}^{-3}] \quad (354)$$

and the pressure is

$$P_{gas} = n_{tot} k T_e = \frac{1}{3} u \text{ [dynes cm}^{-2}; \text{ dynes cm}^{-2}]. \quad (355)$$

13.6.3 Equation of state

When the pressure is held constant (with the **constant pressure** command) the pressure law is given by

$$P(r) = P_{gas}(r_o) + \int a_{rad} \rho dr = P_{gas}(r) + P_{line}(r) \quad (356)$$

where

$$P_{gas}(r_o) = n_{tot} k T \quad (357)$$

is the gas pressure at the illuminated face of the cloud, the total particle density is n_{tot} and r is the radius of the current position.

13.6.4 Turbulent pressure?

Turbulence can be included as a line broadening mechanism. It modifies line opacities and the resulting optical depths, and adds a component of ram pressure to the total pressure, given by

$$P_{turb}(r_o) = \frac{1}{2} \rho u_{turb}^2 = 5.8 \times 10^6 \left(\frac{n}{10^5 \text{ cm}^{-3}} \right) \left(\frac{u_{turb}}{1 \text{ km s}^{-1}} \right)^2 \text{ [dynes cm}^{-2}; \text{ cm}^{-3} \text{ K}] \quad (358)$$

where n is the density and u_{turb} is the turbulent velocity. Turbulent pressure is not included in the constant pressure law since it would be either negligible, or so large that it would not be possible to determine the gas pressure.

13.6.5 Ram or dynamic pressure

Pressure associated with energy of bulk motion can be referred to as ram or dynamic pressure. Ram pressure is given by ρu^2 .

13.6.6 Pressure variables and routines

TotalPressure This routine evaluates the sum of the gas and line radiation pressures. This routine *does not* evaluate the force term due to the attenuation and reflection of the incident continuum. The function has a single dummy argument, and returns the total pressure in dynes/cm².

PresInit This is the gas pressure at the illuminated face of the cloud.

pgas This is the gas pressure, nkT , with units dynes/cm²., and is evaluated in routine **TotalPressure**.

prad This is the line radiation pressure, evaluated as described on page 318. It is also evaluated in **TotalPressure**.

pinteg The integrated radiative force on the gas is evaluated in routine **radinc** and is stored as the variable **pinteg**. This is kept separate from the local gas pressure since it is really a global quantity, unaffected by changes at the current position.

pnow This is the current sum of gas and local line radiation pressure.

presur This routine obtains the current total pressure, and ratios that with the desired total pressure. This scale factor is then applied to various physical quantities.

perror This is the fractional error allowed in the pressure convergence. It currently is set in a data statement within **presur**.

presok **presur** will set the variable **presok** to false if the change in the local conditions was too large, and so capped, and to true if a good final pressure was achieved. The pressure is declared converged by **presur** when **pnow** (the local pressure) is within **perror** of being equal to the sum of **PresInit** and **pinteg**.

Plonte This routine calls **presur**.

13.7 Wind Geometry

Cloudy will do a simple hypersonic wind geometry if the **wind** command is specified with a positive velocity. The effective acceleration is written as $a_{\text{eff}} = a_{\text{rad}} - g_{\text{grav}}$, where a_{rad} is computed in equation 351 above, and g_{grav} is the inward gravitational acceleration due to the central object. By default the mass of the central object is one solar mass. The velocity is computed assuming that the acceleration is constant across the zone. In this case the change in the wind velocity v between the inner and outer edges of a zone of thickness dr will be

$$u^2 - u_o^2 = 2 a_{\text{eff}} dr \quad [\text{cm}^2 \text{ s}^{-2}] \quad (359)$$

where u_o is the velocity at the inner edge. The calculation will stop if the velocity ever falls below zero.

All calculations involving the velocity and density associated with this wind are performed in routine *presur*. The density at the illuminated face of the cloud is entered with the **hden** command. The density is varied across the model to conserve mass flux (i.e., the product $\rho(r) r^2 u(r)$ is kept constant). Because of this, a filling factor would not make physical sense, and should not be used. Note also that it is usually necessary to set an outer radius when a wind model is computed to stop the calculation from extending to infinity.

A simple Sobolev or large velocity gradient (LVG) approximation is used for line transfer when a wind is computed. In the constant expansion velocity case the effective optical depth is given by;

$$\tau_{l,u}(r) = \alpha_{l,u} \left(n_l - n_u \frac{g_l}{g_u} \right) r \frac{u_{th}}{\max(u_{th}, u_{exp})} \quad (360)$$

where r is the smaller of the radius or depth and u_{th} and u_{exp} are the thermal and expansion velocities respectively. The choice of the smaller of the radius or depth is not in strict keeping with the Sobolev approximation, but is necessary since calculations often begin at very large radii from the central object. The optical depths would have unphysically large values were this choice not made.

In the case where the code actually solves for the velocity, which is then not

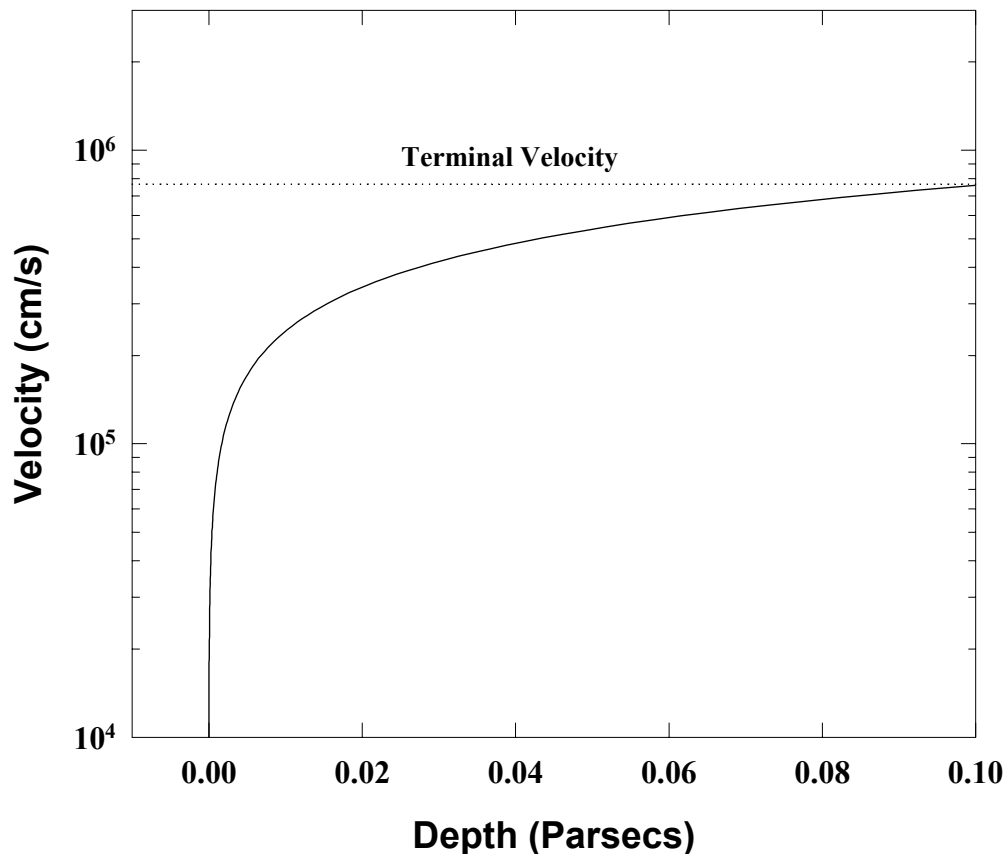


Figure 35 The wind velocity is computed using the input stream shown in one of the test cases in the last section. Parameters were chosen to have a readily computed final velocity. The velocity at the outer edge of the slab is within 1 percent of its expected value. wind

constant, the effective optical depth is given by (Castor, Abbott, & Klein 1975)

$$\tau_{l,u}(r) = \alpha_{l,u} \left(n_l - n_u \frac{g_l}{g_u} \right) v_{th} \left| \frac{dv}{dr} \right|^{-1} \quad (361)$$

where dv/dr is the acceleration.

Figure 35 shows a test case in which a wind is driven in the plane parallel electron scattering limit. As can be seen the numerical solution is in excellent agreement with the analytically predicted result.

The negative velocity case is currently under development.

13.8 Secondary Ionization

13.8.1 Ionization, heating, and cooling

Although the electron velocity distribution is predominantly Maxwellian (Bohm and Aller 1947), a small constituent of non-thermal secondary electrons may be present when high-energy radiation is present. Secondary ionizations by supra-thermal electrons are treated following Xu and McCray (1991) and Dalgarno et al. (1999). All sources of energetic electrons, including both Auger and primary electrons, are considered in the initial input of high-energy electrons into the gas. The resulting coefficient giving the rate of non-thermal electrons is stored as the variable *csupra*, which has units s^{-1} . A typical energy of an electron in the non-thermal shower is ~ 20 eV; this energy is used to evaluate collisional ionization and excitation cross sections. Secondary ionization is included among the general ionization processes considered for all species. The coefficient giving the rate for excitations of $\text{L}\alpha$ is given as *x12*.

13.8.2 Evaluation of rate of hot electron energy input

The variable *ipSecIon* points to the lowest photon energy (100 eV) where a photoelectron can produce secondary ionization. Below this energy photoelectrons are assumed to produce 100% heat with no secondary ionization.

Each of the routines that evaluate photoionization or Comptonization rates records the total energy input by photons with energy greater than this. These are saved with units Rydbergs per photoionization per atom, ε_{Ryd}^* .

13.8.3 Secondary rates per atom

Three variables, the heating efficiency *heatef*, the ionization efficiency *efionz*, and the efficiency for exciting $\text{L}\alpha$ *exctef*, are defined. In the following equations ε_{Ryd}^* is the initial energy of the hot photoelectron.

heatef This is a fraction (between 0 and 1) of the energy of the photoelectron that goes into heating the Maxwellian electron bath. The heat actually deposited in the free electrons ($\text{Ryd cm}^3 \text{ s}^{-1}$) is given by

$$L_{\text{sec}} = \varepsilon_{Ryd}^* \times \text{HEATEF} \quad [\text{erg cm}^{-3} \text{ s}^{-1}]. \quad (362)$$

efionz This is the number of hydrogen ionizations produced per Rydberg of heat input by suprathermal electrons. The number (s^{-1}) of knock-on secondary ionizations is given by

$$r_{ion} = CSUPRA = \varepsilon_{Ryd}^* \times EFIONZ \text{ [s}^{-1}\text{]}, \quad (363)$$

exctef This is the energy in Rydbergs that goes into $L\alpha$ excitations. The number of excitations of $L\alpha$ is given by

$$r_{Ly\alpha} = SECLA = \varepsilon_{Ryd}^* \times EXCTEF \times 4/3 \text{ [s}^{-1}\text{]}, \quad (364)$$

13.8.4 Total interaction rates

The interaction rates per unit volume are given by the rates per atom and the density of the atom. This results in the total number of secondary interactions per unit volume. This total rate is converted into a rate per target atom by dividing the volume rate by the number of *atoms* per unit volume. The results are the rates (with units s^{-1}) referred to by the variable

csupra (secondary ionization rate) and *x12* (secondary rate of excitation of Lyman lines).

Table 28 Secondary Ionization Efficiencies

Electron fraction	Secondary Ionization	Heating Efficiency	Ly α Excitations	sum
1.00E-04	3.75E-01	1.11E-01	4.19E-01	9.06E-01
3.16E-04	3.66E-01	1.51E-01	3.99E-01	9.15E-01
1.00E-03	3.51E-01	2.03E-01	3.71E-01	9.25E-01
3.16E-03	3.28E-01	2.73E-01	3.35E-01	9.36E-01
1.00E-02	2.92E-01	3.66E-01	2.87E-01	9.45E-01
3.16E-02	2.39E-01	4.87E-01	2.25E-01	9.51E-01
1.00E-01	1.64E-01	6.40E-01	1.50E-01	9.54E-01
3.16E-01	6.98E-02	8.24E-01	6.50E-02	9.59E-01
1.00E+00	0.00E+00	9.97E-01	0.00E+00	9.97E-01

13.8.5 Rates during the hydrogen balance solution

In deep regions of x-ray ionized clouds the dominant source of secondaries is often inner shell ionization of the heavy elements, especially oxygen. Often secondary ionization is the dominant ionization source of hydrogen, and in this case the secondary ionization rate changes as the electron density changes, during searches for the ionization balance. It would not be computationally expedient to reevaluate all heavy element ionization rates during the search for the hydrogen ionization balance, so, during this search an effective secondary ionization rate, given by a simple scaling law using the current electron fraction, and the secondary rate and electron fraction where it was last evaluated. The effective suprathermal rate is referred to as *csupeff*.

13.8.6 Molecules and Suprathermal Electrons

The collisional and heating effects of the suprathermal secondary electrons following inner-shell photoionization are treated using standard assumptions (Bergeron and Souffrin 1971; Shull and van Steenberg 1985; Voit 1991).

8 eV of heat is deposited for each H_2 ionization by a cosmic ray (Tielens and Hollenbach 1985). Relative rates are taken from HM89.

The result of this is a secondary ionization rate that must then be multiplied by scale factors that account for the relative collision cross section for each species relative to hydrogen. These are taken from HM89 and TH85.

Secondary electrons also produce a diffuse background of electronic H₂ lines that can photodissociate most molecules. This is treated using the scaling rule of Gredel, Lepp, and Dalgarno (1987) and Gredel et al. (1989).

13.9 Eddington Limit

The Eddington limit is given by

$$L_{Edd} = \frac{4\pi GcM}{\kappa} = 1.45 \times 10^{38} \frac{M}{M_{\odot}} \frac{\kappa_T}{\kappa} \text{ [erg s}^{-1}\text{]} \quad (365)$$

where κ_T is the Thomson opacity and κ is the actual gas opacity (generally several orders of magnitude above Thomson).

13.10 Jeans Length and Mass

The Jeans length and mass are computed for each zone in the calculation. The smallest computed Jeans length and mass are saved, and a note is printed at the end of the calculation if the computed structure is Jeans unstable.

The expression for the Jeans length is

$$\lambda_J = \left(\frac{\pi kT}{\mu m_p G \rho} \right)^{1/2} = 6.257 \times 10^7 \left(\frac{T}{\mu \rho} \right)^{1/2} \text{ [cm]} \quad (366)$$

where μ is the mean mass per particle

$$\mu = \frac{\sum n_i m_i}{\sum n_i} \text{ [gm]} \quad (367)$$

of the.

The Jeans mass is then given by

$$M_J = \frac{4\pi}{3} \rho \left(\frac{\lambda_J}{2} \right)^3 \text{ [gm]} \quad (368)$$

where the mass is that of a sphere with radius $\lambda_J/2$.

The minimum Jeans mass is evaluated in routine *tauinc* as the calculation progresses. The code will generate a comment if the computed structure is Jeans unstable.

13.11 Luminosity Distance

The luminosity distance D_L is given by equation 369.

$$D_L = \begin{cases} \frac{cz}{H_o}(1+z/2) & q_o = 0 \\ \frac{c}{H_o q_o^2} \left\{ q_o z + (q_o - 1) \left[(2q_o z + 1)^{1/2} - 1 \right] \right\} & q_o > 0 \quad [\text{cm}] \\ \frac{2c}{H_o} \left[1 + z - (1+z)^{1/2} \right] & q_o = 1/2 \end{cases} \quad (369)$$

For $q_o=1/2$ and $H_o = 70 \text{ km/s/Mpc}$ the luminosity distance is

$$D_L = 2.643 \times 10^{26} \left[1 + z - (1+z)^{1/2} \right] \quad [\text{cm}] \quad (370)$$

The proper distance D_P is given by $D_P = D_L (1+z)$.

Liske (2000) provides expressions giving the cosmological distance and redshift between any two objects.

14 GLOSSARY OF SYMBOLS

As far as possible, the notation used by HAZY follows standard texts (Osterbrock 1989; Mihalas 1978). This is a summary of some of the symbols used. Page references to Part II of HAZY or the numerical quantity are listed in the third column of this glossary.

The fundamental constants now used by the code are from a variety of revisions of the basic data, some dating back to the 1970's. An effort is now underway to convert the constants to the 1986 CODATA recommended values (see <http://physics.nist.gov/PhysRefData/codata86/codata86.html>).

Symbol	Description	Units	Notes
a	Stefan radiation density	$\text{erg cm}^{-3} \text{K}^{-4}$	7.56464×10^{-15}
a	damping constant	-	page 227
a_0	Bohr radius	cm	0.5291775×10^{-8}
a_{rad}	radiative acceleration	cm s^{-2}	page 318
A_{ul}	radiative rate from level u to l	s^{-1}	
b_n	departure coefficient	-	page 241
B	magnetic field	esu	
B_ν	Planck function	$\text{erg cm}^{-2} \text{s}^{-1} \text{Hz}^{-1} \text{sr}^{-1}$	
c	speed of light	cm s^{-1}	2.997925×10^{10}
C	collisional rate	s^{-1}	
C_{ul}	line collision rate	s^{-1}	
D_{ul}	line destruction probability	-	page 227
f	oscillator strength		
f(r)	filling factor	-	
f_ν F_ν	flux density	$\text{erg cm}^{-2} \text{s}^{-1} \text{Hz}^{-1}$	
g	grain asymmetry factor	-	page 308
g_i	statistical weight	-	
g_{III}	T aver free-free gaunt factor	-	
G	energy gains	heating	$\text{erg cm}^{-3} \text{s}^{-1}$
I	integrated intensity	$\text{erg s}^{-1} \text{sr}^{-1} \text{Hz}^{-1}$	
I_n	ionization potential of level n	erg; Ryd	
I_ν	intensity	$\text{erg s}^{-1} \text{sr}^{-1} \text{Hz}^{-1}$	
h	Planck's constant	erg s	6.62620×10^{-27}
J	integrated mean intensity	$\text{erg s}^{-1} \text{sr}^{-1}$	
J_ν	mean intensity	$\text{erg s}^{-1} \text{sr}^{-1} \text{Hz}^{-1}$	
k	Boltzmann constant	eV deg^{-1}	8.6171×10^{-5}
k	Boltzmann constant	erg deg^{-1}	1.38062×10^{-16}
L_\odot	luminosity of sun	erg s^{-1}	3.826×10^{33}
m_A	mass of atom A	gm	
m_{AMU}	atomic mass unit	gm	$1.6605402 \times 10^{-24}$
m_e	electron mass	gm	9.10956×10^{-28}
$m_e c^2$	electron energy	Ryd	3.75584×10^4

m_p	proton mass	gm	$1.6726231 \times 10^{-24}$
M_J	Jeans' mass	gm	page 327
M_\odot	mass of the sun	gm	1.989×10^{33}
M_\oplus	mass of the Earth	gm	5.977×10^{27}
n_e	electron density	cm^{-3}	
n_j	population of level j	cm^{-3}	
n_p	proton density	cm^{-3}	
$n(\text{H})$	total H density, all forms	cm^{-3}	
$n(x)$	density of species x	cm^{-3}	
$n(\text{cr})$	cosmic ray density	cm^{-3}	page 316
n	atom's level		
$N(x)$	column density of species x	cm^{-2}	
$N(\text{H})$	total H col den, all forms	cm^{-2}	
N_{eff}	effective H column density	cm^{-2}	
$P^*(x)$	LTE relative population	cm^3	page 241
P_{gas}	gas pressure	dyn cm^{-2}	page 322
P_{lines}	line radiation pressure	dyn cm^{-2}	page 322
P_{tot}	total pressure	dyn cm^{-2}	page 322
P_{ul}	line escape probability	-	page 227
$P_{\tau_x}(n)$	continuum escape prob	-	
pc	parsec	cm	3.085678×10^{18}
q_{ij}	line collisional rate coefficient	$\text{cm}^3 \text{s}^{-1}$	
q_n	collisional rate coefficient	$\text{cm}^3 \text{s}^{-1}$	
q_e	electron charge	esu	4.80325×10^{-10}
Q_{abs}	grain absorption efficiency	-	page 308
$Q(\text{H})$	hydrogen ionizing photons	s^{-1}	
r	radius	cm	
$r_{l,u}$	rate	s^{-1}	
r_o	inner radius	cm	
R	total to selective extinction	-	
R_{H}	Rydberg unit for H	-	page 213
R_∞	Rydberg unit for inf mass	-	page 213
R_{AU}	radius of Earth's orbit	cm	1.4959×10^{13}
R_\oplus	radius of the Earth	cm	6.378×10^{18}
R_\odot	radius of the sun	cm	6.9599×10^{10}
T_e	electron temperature	cm^{-3}	
$T_{\text{eff}}(\odot)$	Sun's effective temperature	K	5770
T_{exc}	excitation temperature	K	page 237
T_{color}	color temperature	K	
T_{low}	lowest temp allowed	K	2.8 K
T_u	energy density temperature	K	page 247
u	energy density	erg cm^{-3}	

U_g	grain potential	volt	page 311
u	velocity (mean or projected)	cm s^{-1}	
\bar{u}	mean particle speed	cm s^{-1}	page 310
u_{Dop}	Doppler velocity	cm s^{-1}	page 222
u_{exp}	expansion velocity	cm s^{-1}	
u_{th}	thermal velocity	cm s^{-1}	page 222
u_{turb}	turbulent velocity	cm s^{-1}	page 222
V_g	grain potential	eV	page 311
V_n	grain work function	eV	page 311
W	geometric dilution factor	-	
x	relative shift from line center	-	page 223
X_c	continuous to total opacity	-	page 227
\hat{Y}	grain photoelectric yield	-	
z	redshift	-	
Z	nuclear charge	-	
$\alpha(n, T)$	recombination coefficient	$\text{cm}^3 \text{s}^{-1}$	page 242
$\bar{\alpha}(n, T)$	effec recomb coefficient	$\text{cm}^3 \text{s}^{-1}$	page 216
α_v	continuous abs cross section	cm^2	
α_{lu}	line absorption cross section	cm^2	page 222
β	recombination cooling coef	$\text{cm}^3 \text{s}^{-1}$	page 250
η_v	photon occupation number	-	page 213
δr	zone thickness	cm	
Δr	depth into cloud	cm	
$\gamma_{u,1}$	cont pumping probability		page 229
Γ_n	photoionization rate	s^{-1}	page 246
Γ	reciprocal lifetime of up level	s^{-1}	page 227
Γ_{OTS}	OTS photoionization rate	s^{-1}	page 217
κ	absorption opacity	cm^{-1}	
κ_{lu}	line absorption opacity	cm^{-1}	
κ_s	continuous scattering opacity	cm^{-1}	
κ_v	continuous absorption opacity	cm^{-1}	
λ_J	Jeans' length	cm	page 327
Λ	energy loss, cooling	$\text{erg cm}^{-3} \text{s}^{-1}$	
μ	mean molecular weight	-	page 327
Ω	energy specific collision strength		page 231
Ω	shell coverage	sr	
$\Omega/4\pi$	covering factor	-	
$\Phi(H)$	flux of ionizing photons	$\text{cm}^{-2} \text{s}^{-1}$	
ϕ_v	photon flux density	$\text{cm}^{-2} \text{s}^{-1} \text{Ryd}^{-1}$	
ϕ_{OTS}	flux of OTS photons	$\text{cm}^{-2} \text{s}^{-1}$	page 217
ρ	mass density	gm cm^{-3}	
πa_0^2	area of first Bohr orbit	cm^2	87.9737×10^{-18}

14 GLOSSARY OF SYMBOLS

σ_T	Thomson cross section	cm ²	6.6524×10 ⁻²⁵
σ_v	scattering cross section	cm ²	
σ_{Ray}	Rayleigh scat cross section	cm ²	page 219
Σ	projected grain area	cm ²	page 308
τ	optical depth	-	
τ_{abs}	absorption optical depth	-	
τ_{scat}	scattering optical depth	-	
$\tau_{u,l}$	line optical depth	-	
Y	thermal averaged collision strength		page 231
ν	frequency	Hz	
ν_{Ryd}	frequency	Ryd	
$\delta\nu$	line width	Hz	
$\delta\nu_{Dop}$	Doppler width	Hz	
χ_n	$h\nu/kT$	-	

15 REFERENCES

- Abbott, D. C. 1982, ApJ, 259, 282
- Adams, T. 1972, ApJ, 174, 439
- Aldrovandi, S., & Pequignot, D. 1972, A&A, 17, 88
- Aldrovandi, S., & Pequignot, D. 1974, Revista Brasileira de Fisica, 4, 491
- Ali, B., Blum, R. D., Bumgardner, T. E., Cranmer, S. R., Ferland, G. J., Haefner, R. I., & Tiede, G. P. 1991, PASP, 103, 1182
- Allen, C. W. 1976, *Astrophysical Quantities*, Third Edition (London: Athlone Press)
- Allende Prieto, C., Lambert, D.L., & Asplund, M., 2001, ApJ, 556, L63
- Allende Prieto, C., Lambert, D.L., & Asplund, M., 2002, ApJ, 573, L137
- Aller, L. H. 1984, in *Physics of Thermal Gaseous Nebulae*, (Dordrecht: Reidel)
- Aller, L. H., & Czyzak, S. J. 1983, ApJS, 51, 211.
- Anderson, H., Ballance, C.P., Badnell, N.R., & Summers, H.P., 2000, J Phys B, 33, 1255
- Arimoto, N., & Yoshii, Y. 1987, A&A, 173, 23
- Armour, Mary-Helen, Ballantyne, D.R., Ferland, G.J., Karr, J., & Martin, P.G., 1999, PASP 111, 1251-1257
- Arnaud, M., & Raymond, J. 1992, ApJ, 398, 394
- Arnaud, M., & Rothenflug, R. 1985, A&AS, 60, 425
- Avni, Y., & Tananbaum, H. 1986, ApJ, 305, 83
- Avni, Y., Worrall, D. M., & Morgan, W. A. ApJ, 1995, 454, 673
- Avrett, E. H., & Loeser, R. 1988, ApJ, 331, 211
- Bahcall, J.H., & Kozlovsky, B.-Z. 1969, ApJ, 155, 1077
- Bajtlik, S., Duncan, R. C., & Ostriker, J. P. 1988, ApJ, 327, 570
- Balbus, S. A., & McKee, C. F. 1982, ApJ, 252, 529
- Baldwin, J., Ferland, G. J., Martin, P. G., Corbin, M., Cota, S., Peterson, B. M., & Slettebak, A. 1991, ApJ, 374, 580
- Baldwin J. A., Ferland, G. J., Korista, K. T., Carswell, R., Hamann, F., Phillips, M., Verner, D., Wilkes, B., & Williams, R. E. 1996, ApJ, 461, 683
- Baldwin, J. A., Ferland, G. J., Korista K. T., & Verner, D. 1995, ApJ, 455, L119
- Baldwin, J.A., Verner, E.M., Verner, D.A., Ferland, G.J., Martin, P.G., Korista, K.T., & Rubin, R. H., 2000, ApJS, 129, 229-246
- Baldwin, J., Wampler, J., & Gaskell, C. M. 1989, ApJ, 338, 630
- Balick, B., Gammon, R. H., & Hjellming, R. 1974 PASP, 86, 616
- Ballantyne, D.R., Ferland, G.J., & Martin, P.G., 2000, ApJ 536, 773-777
- Bässgen, G., Bässgen, M., & Grewing, M. 1988, A&A, 200, 51
- Bates, D. R., Kingston, A. E., & McWhirter, R. W. P. 1962, Proc R Soc, A267, 297
- Bechtold, J., Weymann, R. J., Lin, Z., & Malkan, M. A. 1987, ApJ, 315, 180
- Behar, E., Sako, M, Kahn, S.M., 2001, ApJ, 563, 497-504
- Behar, E., & Netzer, H., 2002, ApJ, 570, 165-170
- Bell, K. L., Kingston, A. E., & McIlveen, W. A. 1975, J. Phys. B 8, 358
- Benjamin, Robert A., Skillman, Evan D., & Smits, Derek P., 1999, ApJ, 514, 307
- Berger, M. J., & Seltzer, S. M. 1965, NASA SP-3012
- Bergeron, J., & Collin-Souffrin, S. 1971, A&A, 14, 167
- Berrington, K., & Pelan, A. 1995, A&AS, 114, 367
- Bertoldi, F., & Draine, B. T. 1996, ApJ, 458, 222
- Bethe, H. 1930, Ann. Phys. 5, 325
- Bica, E. 1988, A&A, 195, 76
- Bieniek, R. J., & Dalgarno, A. 1979, ApJ, 228, 635
- Binette, L., Prieto, A., Szuszkiewicz, E., & Zheng, W. 1989, ApJ, 343, 135
- Black, J. H. 1978, ApJ, 222, 125
- Black, J. H. 1987, in *Interstellar Processes*, ed. D.J. Hollenbach & H.A. Thronson, (Dordrecht: Reidel), p 731
- Bohm, D., & Aller, L. H. 1947, ApJ, 105, 131

- Bonihala, J. R. M., Ferch, R., Salpeter, E. E., Slater, G., & Noerdlinger, P. 1979, ApJ, 233, 649
- Borkowski, K. J., & Harrington, J. P. 1991, ApJ, 379, 168
- Bottorff, M., Lamothe, J., Momjian E., Verner, E., Vinkovic, D. & Ferland, G. 1998 PASP, 110, 1040
- Bottorff, M. C., Ferland, & Gary J., 2000, MNRAS 316, 103-106
- Bottorff, Mark & Ferland, Gary 2001a, ApJ, 549, 118-132
- Bottorff, M. C., Ferland, & Gary J., 2002, ApJ 568, 581-591
- Bottorff, Mark, Ferland, Gary, Baldwin, Jack, & Korista, Kirk, 2000, ApJ, 542, 644-654
- Boyd, R., & Ferland, G.J. 1987, ApJ, 318, L21
- Bowen, I. S. 1960, ApJ, 132, 1
- Bray, I., Burgess, A., Fursa, D.V., & Tully, J.A., 2000, A&AS, 146, 481
- Bregman, J. D., Allamandola, L. J., Tielens, A. G. G. M., Geballe, T. R., & Witteborn, F. C. 1989, ApJ, 344, 791
- Broad, J. T., & Reinhardt, W. P. 1976, Phys Rev A 14, 2159
- Brocklehurst, M., 1970, MNRAS, 148, 417
- Brocklehurst, M., 1972, MNRAS, 157, 211
- Brooks, Frederick P., 1995, *The Mythical Man-Month, Essays on Software Engineering*, Reading: Addison-Wesley)
- Brown, R. L., & Mathews, W. G. 1970, ApJ, 160, 939
- Burgess, A. 1965, ApJ, 141, 1588
- Burgess, A., & Summers, H. P. 1969, ApJ, 157, 1007
- Burgess, A., & Summers, H. P. 1976, MNRAS, 174, 345
- Burgess, A., & Tully, J. A. 1992, A&A, 254, 436
- Butler, S. E., Bender, C. F., & Dalgarno, A. 1979, ApJ, 230, L59
- Butler, S. E., & Dalgarno, A. 1979, ApJ, 234, 765
- Butler, S. E., Heil, T. G., & Dalgarno, A. 1980, ApJ, 241, 442
- Butler, S. E., & Dalgarno, A. 1980, ApJ, 241, 838
- Callaway, J. 1994, At Dat Nuc Dat Tab 57, 9
- Cameron, A.G.W. 1982, in *Essays in Nuclear Astrophysics*, ed CA Barnes, DD Clayton, & DN Schramm, (Cambridge: Cambridge Univ Press)
- Canfield, R. C., & Puetter, R. C. 1980, ApJ, 236, L7
- Cardelli, J. A. 1994, Science 264, 209
- Cardelli, J. A., et al. 1991, ApJ, 377, L57
- Castor, J.I., Abbott, D.C., & Klein, R.I., 1975, ApJ, 195, 157-174
- Carswell R. F. & Ferland, G. J. 1988, MNRAS, 235, 1121
- Castor, J. I. 1970, MNRAS, 149, 111
- Cazaux, S., & Tielens, A.G.G.M., 2002, ApJ, 575, L29-L32
- Chaffee, F. H., & White, R. E. 1982, ApJS, 50, 169
- Chamerlain, J.W., 1956, ApJ, 124, 390
- Chan, E. S., Avrett, E. H., & Loeser, R. 1991, A&A, 247, 580
- Chapman, R. D., & Henry, R. J. W. 1971, ApJ, 168, 169
- Chidichimo, M. C. 1981, J. Phys. B., 14, 4149
- Clavel, J., & Santos-Lleo, M. 1990, A&A, 230, 3
- Clegg, R. E. S. 1987, MNRAS, 229, 31p
- Clegg, R. E. S., & Harrington, J. P. 1989, MNRAS, 239, 869
- Clegg, R.E.S., Storey, P.J., Walsh, J.R., & Neale, L. 1997, MNRAS, 284, 348
- Cohen, E. R., & Taylor, B. N. 1987, Rev Mod Phys 57, 1121
- Cota, S. A. 1987, Ph.D. Thesis, OSU
- Cota, S. A., & Ferland, G. J. 1988, ApJ, 326, 889
- Cowie, L. L., & Songaila, A. 1986, ARA&A 24, 499
- Cowling, T.G., 1976, *Magnetohydrodynamics*, (Hilger; Bristol)
- Craig, I.J.D., & Brown, J.C., 1986, *Inverse Problems in Astronomy* (Adam Hilger: Bristol)
- CrinkLaw, G., Federman, S. R., & Joseph, C. L. 1994, ApJ, 424, 748
- Crosas, M., & Weisheit, J.C. 1993, MNRAS, 262, 359
- Cruddace, R., Paresce, F., Bowyer, S., & Lampton, M. 1974, ApJ, 187, 497
- Cunto, W., Mendoza, C., Oksenbein, F., Zeippen, C. J. 1993, A&A 275, L5

- Dalgarno, A., & Kingston, A. E. 1963, *Observatory*, 83, 39
- Dalgarno, A., & McCray, R. A. 1973, *ApJ*, 181, 95
- Dalgarno, A., & Roberge, W. G. 1979, *ApJ*, 233, L25
- Dalgarno, A., Yan, Min, & Liu, Weihong 1999, *ApJS*, 125, 237
- Davidson, K. 1972, *ApJ*, 171, 213
- Davidson, K. 1975, *ApJ*, 195, 285
- Davidson, K. 1977, *ApJ*, 218, 20
- Davidson, K., & Netzer, H. 1979, *Rep. Prog. in Physics* 51, 715
- Davidson, K., & Fesen, R.A. 1985, *ARA&A*, 23, 119
- de Jong, T., Chu, S-I., & Dalgarno, A. 1975, *ApJ*, 199, 69
- Desert, F.-X., Boulanger, F., & Puget, J. L. 1990, *A&A*, 237, 215
- Dove, J. E., Rush, A., Cribb, P., & Martin, P. G. 1987, *ApJ*, 318, 379
- Dove, J. E., & Mandy, M. E. 1986, *ApJ*, 311, L93
- Draine, B. T. 1978, *ApJS*, 36, 595
- Draine, B.T., & Bertoldi, Frank, 1996, *ApJ*, 468, 269-289
- Draine, B. T., & Lee, H. M. 1984, *ApJ*, 285, 89
- Draine, B. T., & Salpeter, E. E. 1979, *ApJ*, 231, 77
- Draine, B. T., & Sultin, B. 1987, *ApJ*, 320, 803
- Drake, G., 1993, Chapt 3 in *Long Range Casimir Forces, theory and recent experiments on atomic systems*, edited by Levin & Mihca, Plenum Press
- Drake, G., 1996, *Atomic Molecular Physics Handbook*, ed by Gordon Drake (AIP Press,)
- Drake, S. A., & Ulrich, R.K. 1980, *ApJS*, 42, 351
- Elitzur, M. 1982, *Rev. Mod. Phys* 54, 1125
- Elitzur, M. 1984, *ApJ*, 280, 653
- Elitzur, M, 1992, *Astronomical Masers*, (Dordrecht: Kluwer)
- Elitzur, M., Ferland, G. J., Mathews, W. G., & Shields, G. 1983, *ApJ*, 272, L55
- Elitzur, M., & Ferland, G. J. 1986, *ApJ*, 305, 35
- Elvis, M. et al. 1994, *ApJS*, 95, 1
- Fabian, A. C., Pringle, J. E., & Rees M. J. 1976, *MNRAS*, 175, 43
- Federman, S. R., et al. 1993, *ApJ*, 413, L51
- Fenley, J.A., Taylor, K.T., & Seaton, M.J. 1987, *J. Phys. B.* 20, 6457-6476
- Ferguson, J. W., Ferland, G. J., & A. K. Pradhan, 1995, *ApJ*, 438, L55
- Ferguson, J. W., & Ferland, G.J. 1997, *ApJ*, 479, 363
- Ferguson, J. W., Korista, K. T., Baldwin, J. A., & Ferland, G. J. 1997, *ApJ*, 487, 122
- Ferguson, J W., Korista, Kirk. T., and Ferland, Gary J., 1997, *ApJS* 110, 287-297
- Ferguson, J W., Korista, Kirk. T., Verner, D.A., & Ferland, Gary J., 2001, *ASP Conference Series, Vol 247, Spectroscopic Challenges of Photoionized Plasmas*, G Ferland & D Savin, editors.
- Ferland, G. J. 1977, *ApJ*, 212, L21
- Ferland, G. J. 1979, *MNRAS*, 188, 669
- Ferland, G. J. 1980a, *MNRAS*, 191, 243
- Ferland, G. J. 1980b, *BAAS*, 12, 853
- Ferland, G. J. 1980c, *PASP*, 92, 596
- Ferland, G. J. 1986, *PASP*, 98, 549
- Ferland, G. J. 1986, *ApJ*, 310, L67
- Ferland, G. J. 1992, *ApJ*, 389, L63
- Ferland, G. J. 1993, *ApJS*, 88, 49
- Ferland, G. J. 1999, *PASP*, 111, 1524
- Ferland, G. J. 1999a, in *ASP 162, Quasars and Cosmology*, ed G Ferland & J Baldwin
- Ferland, G. J., 1999b, *ApJ* 512 247-249
- Ferland, G.J., 2000, *RMxAC*, 9, 153
- Ferland, G.J., 2001a, *PASP*, 113, 41
- Ferland, G.J., 2001b, *ASP Conference Series, Vol 247, Spectroscopic Challenges of Photoionized Plasmas*, G Ferland & D Savin, editors (astro-ph/0210161)
- Ferland, G. J., Baldwin J. A., Korista, K. T., Hamann, F., Carswell, R., Phillips, M., Wilkes, B., & Williams, R. E. 1996, *ApJ*, 461, 683

- Ferland, G., Binette, L., Contini, M., Harrington, J., Kallman, T., Netzer, H., Pequignot, D., Raymond, J., Rubin, R., Shields, G., Sutherland, R., & Viegas, S. 1995, in *The Analysis of Emission Lines*, Space Telescope Science Institute Symposium Series, R. Williams & M. Livio, editors (Cambridge: Cambridge University Press)
- Ferland, G. J., & Elitzur, M. 1984, ApJ, 285, L11
- Ferland, G. J., Fabian, A. C., & Johnstone, R.M. 1994, MNRAS, 266, 399
- Ferland, G. J., Fabian, A. C., & Johnstone, R.M. 2002, MNRAS, 333, 876
- Ferland, G. J., Korista, K.T. & Peterson, B.M. 1990, ApJ, 363, L21
- Ferland, G. J., Korista, K.T., Verner, D. A., & Dalgarno, A. 1997, ApJ, 481, L115
- Ferland, G. J., Korista, K.T., Verner, D.A., Ferguson, J.W., Kingdon, J.B., Verner, & E.M. 1998, PASP, 110, 761
- Ferland, G. J., Lambert, D. L., Netzer, H., Hall, D. N. B., & Ridgway, S. T. 1979a, ApJ, 227, 489
- Ferland, G. J., Lambert, D. L., Slovak, M., Shields, G. A., & McCall, M. 1982, ApJ, 260, 794
- Ferland, G. J., & Mushotzky, R. F. 1982, ApJ, 262, 564
- Ferland, G. J., & Mushotzky, R. F. 1984, ApJ, 286, 42
- Ferland, G. J., & Netzer, H. 1979, ApJ, 229, 274
- Ferland, G. J., & Netzer, H. 1983, ApJ, 264, 105
- Ferland, G. J., Netzer, H., & Shields, G. A. 1979, ApJ, 232, 382
- Ferland, G. J., Peterson, B. M., Horne, K., Welsh, W. F., & Nahar, S. N. 1992, ApJ, 387, 95
- Ferland, G. J., & Persson, S. E. 1989, ApJ, 347, 656
- Ferland, G. J., & Rees, M. J. 1988, ApJ, 332, 141
- Ferland, G. J., & Shields, G. A. 1978, ApJ, 226, 172
- Ferland, G. J., & Shields, G. A. 1985, in *Astrophysics of Active Galaxies & Quasi-stellar Objects*, J.S. Miller, Ed.
- Ferland, G. J., & Truran, J. W. 1981, ApJ, 244, 1022
- Ferland, G. J., Williams, R. E., Lambert, D. L., Shields, G. A., Slovak, M., Gondhalekar, P. M., & Truran, J. W. 1984, ApJ, 281, 194
- Field, G. B. 1965, ApJ, 142, 431
- Francis, P. J. 1993, ApJ, 407, 519
- Fuhr, J. R., Martin, G. A., & Wiese, W. L. 1988, J. Phys. Chem. Ref. Data, 17, Suppl. 4
- Gaetz, T. J., & Salpeter, E. E. 1983, ApJS, 52, 155
- Garstang, R.H. 1958, MNRAS, 118, 57
- Gavrila, M. 1967, Phys Rev 163, 147, also JILA Report #86, Sept 19, 1966
- Ginzburg, V. I., & Syrovatskii, S. I. 1964, *The Origin of Cosmic Rays*, (Oxford: Pergamon)
- Gould, R. S. 1978, ApJ, 219, 250
- Grandi, S.A., 1975, ApJ, 196, 465
- Grandi, S.A., 1975, ApJ, 199, 43
- Grandi, S.A., 1976, ApJ, 206, 658
- Gredel, R., Lepp, S., & Dalgarno, A. 1987, ApJ, 323, L137
- Gredel, R., Lepp, S., Dalgarno, A., & Herbst, E. 1989, ApJ, 347, 289
- Greenhouse, M., et al. 1993, ApJS, 88, 23
- Grevesse, N., & Anders, E. 1989, *Cosmic Abundances of Matter*, AIP Conference Proceedings 183, p. 1, Ed. C. J. Waddington, (New York: AIP)
- Grevesse, N. & Noels, A. 1993 in *Origin & Evolution of the Elements*, ed. N. Prantzos, E. Vangioni-Flam, & M. Casse p. 15 (Cambridge: Cambridge Univ. Press)
- Grevesse, N., & Sauval, A.J., 2001, Space Science Review, 85, 161-174
- Guhathakurta, P., & Draine, B. T. 1989, ApJ, 345, 230
- Guilbert, P. W. 1986, MNRAS, 218, 171
- Guilbert, P., & Rees, M. J. 1988, MNRAS, 233, 475
- Habing, H. J. 1968, Bull. Astr. Inst. Netherlands 19, 421
- Halpern, J. P., & Grindlay, J. E. 1980, ApJ, 242, 1041
- Hamann, F., & Ferland, G. J. 1992, ApJ, 391, L53
- Hamann, F., & Ferland, G. J. 1993, ApJ, 418, 11
- Hamann, F., & Ferland, G. J. 1999, ARAA, 37, 487
- Harrington, J. P. 1969, ApJ, 156, 903

- Harrington, J. P. 1973, MNRAS, 162, 43
- Hauschildt, P.H., & Baron, E., 1999, J. Comp. Appl. Math, 109, 41-63
- Heitler, W. 1954, *The Quantum Theory of Radiation* (Oxford: Oxford University Press)
- Hjellming, R. M. 1966, ApJ, 143, 420
- Hollenbach, D., & McKee, C. F. 1979, ApJS, 41, 555
- Hollenbach, D., & McKee, C. F. 1989, ApJ, 342, 306
- Hollenbach, D.J., Takahashi, T., & Tielens, A.G.G.M., 1991, ApJ, 377, 192-209
- Hollenbach, D.J., & Tielens, A.G.G.M. 1999 Rev Mod Phys 71, 173
- Holweger, H., 2001, Joint SOHO/ACE workshop "Solar and Galactic Composition". Edited by Robert F. Wimmer-Schweingruber. Publisher: American Institute of Physics Conference proceedings vol. 598 location: Bern, Switzerland, March 6 - 9, 2001., p.23
- Hubbard, E. N., & Puetter, R. C. 1985, ApJ, 290, 394
- Hummer, D. G. 1962, MNRAS, 125, 21
- Hummer, D. G. 1968, MNRAS, 138, 73
- Hummer, D. G. 1988, ApJ, 327, 477
- Hummer, D. G, Berrington, K. A., Eissner, W., Pradhan, A. K., Saraph H. E., Tully, J. A. 1993, A&A, 279, 298
- Hummer, D. G., & Kunasz, 1980, ApJ, 236, 609
- Hummer, D. G., & Seaton, M. J. 1963, MNRAS, 125, 437
- Hummer, D. G., & Storey, P. J. 1987, MNRAS, 224, 801
- Hummer, D. G., & Storey, P. J. 1992, MNRAS, 254, 277
- Hutchings, J.B. 1976, ApJ, 205, 103
- Ikeuchi, S., & Ostriker, J. P. 1986, ApJ, 301, 522
- Jackson, J. D. 1975, *Classical Electrodynamics* (New York: Wiley)
- Kaler, J., & Jacoby, G. 1991, ApJ, 372, 215
- Janev, R. K., Langer, W. D., Post, D. E., & Evans, K. 1987, *Elementary Processes in Hydrogen-Helium Plasmas* (Berlin: Springer-Verlag)
- Jenkins, E. B. 1987, in *Interstellar Processes*, D. Hollenbach & H. Thronson, Eds, (Dordrecht: Reidel), p.533
- Johnson, L. C. 1972, ApJ, 174, 227
- Johnstone, R. M., Fabian, A. C., Edge, A. C., & Thomas, P. A. 1992, MNRAS, 255, 431
- Jones, A.P., Tielens, A. G. G. M., & Hollenbach, D.J. 1996, 469, 740-764
- Jura, M., 1974, ApJ, 191, 375-379
- Kaler, J., 1978, ApJ, 220, 887
- Kallman, T. R., & McCray, R. 1982, ApJS, 50, 263
- Karzas, W. J., & Latter, R. 1961, ApJS, 6, 167
- Kaastra, J. S., & Mewe, R. 1993, A&AS, 97, 443
- Kato, T. 1976, ApJS, 30, 397
- Kellerman, K. I. 1966, ApJ, 146, 621
- Khromov, G. S. 1989, Space Science Reviews 51, 339
- Kingdon, J. B., & Ferland, G. J. 1991, PASP, 103, 752
- Kingdon, J. B., & Ferland, G. J. 1993, ApJ, 403, 211
- Kingdon, J. B., & Ferland, G. J. 1995, ApJ, 450, 691
- Kingdon, J. B., & Ferland, G. J. 1996, ApJS, 106, 205
- Kingdon, J. B., Ferland, G. J., & Feibelman, W.A. 1995, ApJ, 439, 793
- Kingdon J.B., & Ferland, G.J., 1998, ApJ 506, 323-328
- Kingdon, J. B., & Ferland, G. J. 1998, ApJ, 516, L107-109
- Korista, K. T., Baldwin, J. A., & Ferland, G. J. 1998, ApJ, 507, 24
- Korista, K. T., & Ferland, G. J. 1989, ApJ, 343, 678
- Korista, K. T., & Ferland, G. J. 1998, ApJ, 495, 672
- Korista, K. T., Ferland, G. J., & Baldwin, J. 1997, ApJ, 487, 555
- Krolik, J., McKee, C. M., & Tarter, C.B. 1981, ApJ, 249, 422
- Kurucz, R. L. 1970, SAO Special Reports 309
- Kurucz, R. L. 1979, ApJS, 40, 1

- Kurucz, R. L. 1991, in *Proceedings of the Workshop on Precision Photometry: Astrophysics of the Galaxy*, ed. A. C. Davis Philip, A. R. Upgren, & K. A. James, (Schenectady: Davis), 27
- Kwan, J., & Krolik, J. 1981, *ApJ*, 250, 478
- Lambert, D. L., & Pagel, B. E. J. 1968, *MNRAS*, 141, 299
- La Franca, Franceshini, A., Cristiani, S., & Vio, R. 1995, *A&A*, 299, 19
- Lame N. J., & Ferland, G. J. 1991, *ApJ*, 367, 208
- LaMothe, J., & Ferland, G.J., 2001, *PASP*, 113, 165
- Landini, M., & Monsignori Fossi, B. 1990, *A&AS*, 82, 229
- Landini, M., & Monsignori Fossi, B. 1991, *A&AS*, 91, 183
- Lanzafame, A., Tully, J. A., Berrington, K. A., Dufton, P. L., Byrne, P. B., & Burgess, A. 1993, *MNRAS*, 264, 402
- Laor, A., & Draine, B. T. 1993, *ApJ*, 402, 441
- Latter, W. B., & Black, J. H. 1991, *ApJ*, 372, 161
- Lea, S., & Holman, G. 1978, *ApJ*, 222, 29
- Lennon, D. J., & Burke, V. M. 1991, *MNRAS*, 251, 628
- Lenzuni, P., Chernoff, D. F., & Salpeter, E. E. 1991, *ApJS*, 76, 759
- Levich, E. V., & Sunyaev, R.A. 1970, *Astrophysical Letters* 7, 69
- Lepp, S., & Shull, J. M. 1983, *ApJ*, 270, 578
- Lightman, A. P., & White, T.R. 1988, *ApJ*, 335, 57
- Liske, J., 2000, *MNRAS*, 319, 557-561
- Lites, B. W., & Mihalas, D. 1984, *Solar Physics* 93, 23
- Liu, X.-W., Storey, P. J., Barlow, M. J., & Clegg, R. E. S. 1995, *MNRAS*, 272, 369
- Longair, M. S. 1981, *High Energy Astrophysics*, (Cambridge: Cambridge University Press)
- Lotz, W. 1967, *ApJS*, 14, 207
- Launay, J.R., Le Dourneuf, M., & Zeippen, C.J., 1991, *A&A*, 252, 842-852
- MacAlpine, G. M. 1971, *ApJ*, 175, 11
- Maguire, S. 1993, *Writing Solid Code*, (Redmond: Microsoft Press)
- Maguire, S. 1994, *Debugging the Development Process*, (Redmond: Microsoft Press)
- Mallik, D. C. V., & Peimbert, M. 1988, *Rev Mexicana* 16, 111
- Maloney, P.R., Hollenbach, D.J., & Tielens, A. G. G. M., 1996, *ApJ*, 466, 561
- Martin, P. G. 1979, *Cosmic Dust* (Oxford: Clarendon Press)
- Martin, P. G. 1988, *ApJS*, 66, 125
- Martin, P. G., & Ferland, G. J. 1980, *ApJ*, 235, L125
- Martin, P.G., & Rouleau, F., 1991, in Malina R.F., Bowyer S., eds, *Extreme Ultraviolet Astronomy*, Pergamon Press, Oxford, p. 341
- Martin, P. G., & Whittet, D. C. B. 1990, *ApJ*, 357, 113
- Masters, A. R., Pringle, J. E., Fabian, A. C., & Rees, M. J. 1977, *MNRAS*, 178, 501
- Mathews, W. G., Blumenthal, G. R., & Grandi, S. A. 1980, *ApJ*, 235, 971
- Mathews, W. G., & Ferland, G. J. 1987, *ApJ*, 323, 456
- Mathis, J. S. 1982, *ApJ*, 261, 195
- Mathis, J. S. 1985, *ApJ*, 291, 247
- Mathis, J. S., Ruml, W., & Nordsieck, K. H. 1977, *ApJ*, 217, 425
- Mathis, J. S., & Wallenhorst, S. G. 1981, *ApJ*, 244, 483
- Matteucci, F., & Tornambe, A. 1987, *A&A*, 185, 51
- Matteucci, F., & Greggio, A. 1986, *A&A*, 154, 279
- Mazzotta, P., Mazzitelli, G., Colafrancesco, C., & Vittorio, 1998, *A&AS* 133, 403-409
- McKee, C. F. 1999, preprint, Astro-ph 9901370
- Mendoza, C. 1983, in *Planetary Nebulae*, IAU Sym 103, D. R. Flower, Ed., p 143, (Dordrecht: Reidel)
- Meyer, D.M., Jura, M., & Cardelli, J.A. 1998, *ApJ*, 493, 222-229
- Mewe, R. 1972, *A&A*, 20, 215
- Mihalas, D. 1972, *Non-LTE Model Atmospheres for B & O Stars*, NCAR-TN/STR-76
- Mihalas, D. 1978, *Stellar Atmospheres*, 2nd Edition (San Francisco: W.H. Freeman)
- Mihalszki, J. S., & Ferland, G. J. 1983, *PASP*, 95, 284
- Mohr P.J. & Taylor B.N., 1998 *Codata*, see *Reviews of Modern Physics*, Vol. 72, No. 2, 2000
- Morrison, R., & McCammon, D. 1983, *ApJ*, 270, 119

- Morton, D. C., York, D. G., & Jenkins, E. B. 1988, ApJS, 68, 449
- Nahar, S. N., & Pradhan, A. K. 1992, ApJ, 397, 729
- Netzer, H. 1990, in *Active Galactic Nuclei, Saas-Fee Advanced Course 20*, Courvorsier, T.J.-L., & Mayor, M., (Springer-Verlag; Berlin)
- Netzer, H., Elitzur, M., & Ferland, G. J. 1985, ApJ, 299, 752
- Netzer, H., & Ferland, G. J. 1984, PASP, 96, 593
- Neufeld, D. A. 1989, Harvard Research Exam
- Neufeld, D.A., 1990, ApJ, 350, 216
- Neufeld, D. A., & Dalgarno, A. 1989, Phys Rev A, 35, 3142
- Novotny, Eva, 1973, *Introduction to Stellar Atmospheres*, (New York; Oxford University Press)
- Nussbaumer, H., & Storey, P. J. 1983, A&A, 126, 75
- Nussbaumer, H., & Storey, P. J. 1984, A&AS, 56, 293
- Nussbaumer, H., & Storey, P. J. 1986, A&AS, 64, 545
- Nussbaumer, H., & Storey, P. J. 1987, A&AS, 69, 123
- O'Dell, C.R., 2001, ARAA, 39, 99
- Oliveira, S., & Maciel, W. J. 1986, Ap&SS, 126, 211
- Oliva, E., Pasquali, A., & Reconditi, M. 1996, A&A, 305, 210
- Olive, K.A., Steigman, G., & Walker, T.P., 2000, Physics Reports, 333-334, 389-407
- Osterbrock, D. E. 1951, ApJ, 114, 469
- Osterbrock, D. E. 1989, *Astrophysics of Gaseous Nebulae & Active Galactic Nuclei*, (Mill Valley; University Science Press)
- Osterbrock, D. E., & Flather, E. 1959, ApJ, 129, 26
- Osterbrock, D. E., Tran, H. D., & Veilleux, S. 1992, ApJ, 389, 305
- Ostriker, J. P., & Ikeuchi, S. 1983, ApJ, 268, L63
- Pacholczyk, A. G. 1970, *Radio Astrophysics* (San Francisco: Freeman)
- Pagel, B. E. J. 1997, *Nucleosynthesis and Chemical Evolution of Galaxies*, (Cambridge: Cambridge University Press)
- Palla, F., Salpeter, E. E., & Stahler, S. W. 1983, ApJ, 271, 632
- Peebles, P. J. E. 1971, *Physical Cosmology*, (Princeton: Princeton U. Press)
- Peimbert, M. 1967, ApJ, 150, 825
- Pengelly, R. M. 1964, MNRAS, 127, 145
- Pengelly, R.M., & Seaton, M.J., 1964, MNRAS, 127, 165
- Péquignot, D. 1986, *Workshop on Model Nebulae*, (Paris: l'Observatoire de Paris) p363
- Péquignot, D., & Aldrovandi, S.M.V. 1986, A&A, 161, 169
- Péquignot, D., Ferland, G.J., et al., in ASP Conference Series, Vol 247, *Spectroscopic Challenges of Photoionized Plasmas*, G Ferland & D Savin, editors
- Péquignot, D., Petitjean, P., & Boisson, C. 1991, A&A, 251, 680
- Péquignot, D., Stasinska, G., & Aldrovandi, S. M. V. 1978, A&A, 63, 313
- Percival, I.C., & Richards, D., 1978, MNRAS, 183, 329
- Peterson, J. R., Aberth, W., Moseley, J., & Sheridan, J. 1971, Phys Rev A, 3, 1651
- Pettini, M., & Bowen, D.V., 2001, ApJ, 560, 41
- Porquet, D., & Dubau, J. 2000, A&AS, 143, 495
- Prasad, S.S., & Huntress, W.T., 1980, ApJS, 43, 1-35
- Press W. H., Teukolsky, S.A., Vetterling, W. T., & Flannery, B. P. 1992, *Numerical Recipes*, (Cambridge; Cambridge University Press)
- Puetter, R. C. 1981, ApJ, 251, 446
- Puy, D., Alecian, G., Le Bourlot, J., Leorat, J., & Pineau des Forets, G. 1993, A&A, 267, 337
- Puy, D., Grenacher, L., & Jetzer, P., 1999, A&A, 345, 723
- Rauch, T. 1997 A&A, 320, 237
- Rauch, T. 2002, H-Ni grid, available at <http://astro.uni-tuebingen.de/~rauch>
- Raymond, J. C., Cox, D. P., & Smith, B. W. 1976, ApJ, 204, 290
- Rees, M. J., Netzer, H., & Ferland, G. J. 1989, ApJ, 347, 640
- van Regemorter, H. 1962, ApJ, 136, 906
- Rephaeli, Y. 1987, MNRAS, 225, 851
- Reilman, R. F., & Manson, S. T. 1979, ApJS, 40, 815, errata 46, 115; 62, 939

- Roberge, W. G., Jones, D., Lepp, S., & Dalgarno, A. 1991, *ApJS*, 77, 287
- Rossi, B. 1952, *High-Energy Particles* (New York; Prentice-Hall)
- Rouleau, F., & Martin, P.G. 1991, *ApJ*, 377, 526
- Rowan, T. 1990, *Functional Stability Analysis of Numerical Algorithms*, Ph.D. Thesis, Department of Computer Sciences, University of Texas at Austin
- Rubin, R. H. 1968, *ApJ*, 153, 671
- Rubin, R. H. 1983, *ApJ*, 274, 671
- Rubin, R. H. Martin, P. G. Dufour, R. J. Ferland, G. J Baldwin, J. A. Hester, J. J. & Walter, D. K. 1998, *ApJ*, 495, 891
- Rubin, R. H., Simpson, J. R., Haas, M. R., & Erickson, E. F. 1991, *ApJ*, 374, 564
- Rutten, Rob, 2002, Radiative transfer in stellar atmospheres, at <http://www.fys.ruu.nl/~rutten/node20.html>
- Rybicki, G. B., & Hummer, D. G. 1991, *A&A*, 245, 171
- Rybicki, G. B., & Hummer, D. G. 1992, *A&A*, 262, 209
- Rybicki, G. B., & Hummer, D. G. 1994, *A&A*, 290, 553
- Rybicki, G. B., & Lightman, A.P. 1979, *Radiative Processes in Astrophysics* (New York: Wiley)
- Sanders, D. B., et al. 1989, *ApJ*, 347, 29
- Saraph, H. E. 1970, *J.Phys.B.*, 3, 952
- Savage, B. D., & Sembach, K. R. 1996, *ARA&A*, 34, 279
- Savin, Daniel Wolf, 2000, *ApJ*, 533, 106
- Savin, D. W.; Kahn, S. M.; Linkemann, J.; Saghiri, A. A.; Schmitt, M.; Grieser, M.; Repnow, R.; Schwalm, D.; Wolf, A.; Bartsch, T.; Brandau, C.; Hoffknecht, A.; Müller, A.; Schippers, S.; Chen, M. H.; Badnell, N. R., 1999, *ApJS*, 123, 687
- Sciortino, S., et al. 1990, *ApJ*, 361, 621
- Scott, J. S., Holman, G. D., Ionson, J. A., & Papadopoulos, K. 1980, *ApJ*, 239, 769
- Schaerer D., de Koter, A., Schmutz, W., & Maeder, A. 1996ab, *A&A*, 310, 837, & *A&A*, 312, 475
- Schaerer D., & de Koter A. 1997, *A&A*, 322, 592
- Schuster, A. 1905, *ApJ*, 21, 1
- Schutte, W. A., Tielens, A. G. G. M., & Allamandola, L. J. 1993, *ApJ*, 415, 397
- Schwarzschild, M. 1965, *Structure & Evolution of the Stars*, (New York: Dover)
- Seaton, M. J. 1959, *MNRAS*, 119, 81
- Seaton, M. J. 1959, *MNRAS*, 119, 90
- Seaton, M. J. 1987, *J.Phys. B*, 20, 6363
- Sellgren, K., Tokunaga, A. T., & Nakada, Y. 1990, *ApJ*, 349, 120-125
- Sellmaier, F. H., Yamamoto, T., Pauldrach, A. W. A., & Rubin, R. H. 1996, *A&A*, 305, L37
- Shields, G. A. 1976, *ApJ*, 204, 330
- Shine, R. A., & Linsky, J. L. 1974, *Solar Physics* 39, 49
- Shull, J. M. 1979, *ApJ*, 234, 761
- Shull, J. M., & Van Steenberg, M. E. 1982, *ApJS*, 48, 95
- Shull, J. M., & Van Steenberg, M. E. 1985, *ApJ*, 298, 268
- Sellgren, K., Tokunaga, A. T., & Nakada, Y. 1990, *ApJ*, 349, 120
- Sellmaier, F.H., Yamamoto, T., Pauldrach, A.W.A., Rubin, R.H 1996, *A&A*, 305, 37
- Sikora, M., Begelman, M. C., & Rudak, B. 1989, *ApJ*, 341, L33
- Simonyi, C. 1977, *Meta-Programming: A Software Production Method*, Thesis, Stanford University
- Simpson, J. P. 1975, *A&A*, 39, 43
- Smits, D.P., 1996, *MNRAS*, 278, 683
- Snow, T. P., & Dodger, S. L. 1980, *ApJ*, 237, 708
- Snow, T. P., & York, D. G. 1981, *ApJ*, 247, L39
- Snow, T.P., & Witt, A. 1996, *ApJ*, 468, L65
- Spitzer, L. 1948, *ApJ*, 107, 6
- Spitzer, L. 1962, *Physics of Fully Ionized Gasses*, (New York: Interscience)
- Spitzer, L. 1978, *Physical Processes in the Interstellar Medium*, (New York: Wiley)
- Spitzer, L. 1985, *ApJ*, 290, L21
- Spitzer, L., & Tomasko, M. G. 1968, *ApJ*, 152, 971
- Stecher, T. P., & Williams, D. A. 1967, *ApJ*, 149, 29

- Stoy, R. H. 1933, MNRAS, 93, 588
Storey, P. J. 1981, MNRAS, 195, 27p
Storey, P. J. 1994, A&A, 282, 999
Storey, P. J., & Hummer, D. G. 1991, Comput. Phys. Commun. 66, 129
Storey, P. J., & Hummer, D. G. 1995, MNRAS, 272, 41 (on the web at <http://adc.gsfc.nasa.gov/adc-cgi/cat.pl?catalogs/6/6064/>)
Swings, P., & Struve, O. 1940, ApJ, 91, 546
Tarter, C. B., & McKee, C. F. 1973, ApJ, 186, L63
Tarter, C.B., Tucker, W.H., & Salpeter, E.E., 1969, ApJ, 156, 943
Tielens, A. G. G. M., & Hollenbach, D. 1985a, ApJ, 291, 722
Tielens, A. G. G. M., & Hollenbach, D. 1985b, ApJ, 291, 746
Tinsley, B. 1979, ApJ, 229, 1046
Tout, C. A., Pols, O. R., Eggleton, P. P. & Han, Z. 1996, MNRAS, 281, 257
Turner, J., & Pounds, K. 1989, MNRAS, 240, 833
Van Blerkom, D., & Hummer, D. G. 1967, MNRAS, 137, 353
Veigele, WM. J. 1973, Atomic Data Tables, 5, 51
van Dishoeck, E.F., & Black, J.H., 1988, ApJ, 334, 771
van Hoof, P. A. M. 1997, PhD Thesis, University of Groningen
van Hoof, P.A.M., Beintema, D.A., Verner D.A., & Ferland, G.J., 2000a, A&A 354, L41-L44
van Hoof, P.A.M., Van de Steene, G.C., Beintema, D.A., Martin, P.G., Pottasch, S.R., Ferland, G. J., 2000b, ApJ 532, 384-399
van Hoof, P.A.M., Weingartner, J.C., Martin, P.G., Volk, K., & Ferland, G.J., 2001, in *Challenges of Photoionized Plasmas*, (G Ferland & D. Savin, eds) ASP Conf Ser 247, 363-378 (astro-ph/0107183)
van Regemorter, H. 1962, ApJ, 136, 906
Vedel, H., Hellsten, U., & Sommer-Larsen, J. 1994, MNRAS, 271, 743
Vernazza, J. E., Avrett, E. H., & Loeser, C. B. 1981, ApJS, 45, 635
Verner, D. A., Yakovlev, D. G., Band, I. M., & Trzhaskovshaya, M. B. 1993, ADNDT, 55, 233
Verner, D. A., & Yakovlev, 1995, A&AS, 109, 125
Verner, D. A., & Ferland, G. J. 1996, ApJS, 103, 467
Verner, D. A., Ferland, G. J., Korista, K., & Yakovlev D. G. 1996, ApJ, 465, 487
Verner, D. A., Verner, K., & Ferland, G. J. 1996, ADNDT, 64, 1
Verner, E.M. Verner, D.A. Korista, K.T. Ferguson, J.W. Hamann, F. & Ferland, G.J. 1999, ApJS 120, 101
Voronov, G. S. 1997, ADNDT, 65, 1
Voit, G. M. 1991, ApJ, 377, 1158
Volk, K., and Kwok, S. 1988, ApJ, 331, 435
Vriens, L., & Smeets, A. H. M. 1980, Phys Rev A, 22, 940
Watson, W. D. 1972, ApJ, 176, 103
Weingartner, J.C., & Draine, B.T., 2001a, ApJS, 134, 263
Weingartner, J.C., & Draine, B.T., 2001b, ApJ, 548, 296
Weisheit, J. C. 1974, ApJ, 190, 735
Weisheit, J. C., & Collins, L. A. 1976, ApJ, 210, 299
Weisheit, J. C., & Dalgarno, A. 1972, Astrophysical Letters, 12, 103
Weisheit, J., Shields, G. A., & Tarter, C. B. 1981, ApJ, 245, 406
Wen, Z., & O'Dell, C.R. 1995, ApJ, 438, 784-793
Werner, K., & Heber, U. 1991, in *Stellar Atmospheres: Beyond Classical Models*, p 341, NATO ASI Series C, eds. L. Crivellari, I. Hubney, & D. G. Hummer, (Dordrecht: Kluwer)
White, R. E. 1986, ApJ, 307, 777
Wiese, W.L., Fuhr, J.R., & Deters, T.M., 1996, J Phys Chem Ref Data, Monograph 7
Wiese, W. L., Smith, M. W., & Glennon, B. M. 1966, NSRDS-NBS 4
Wilkes, B. J., Ferland, G. J., Truran, J., & Hanes, D. 1981, MNRAS, 197, 1
Wilkes, et al 1994, ApJS, 92, 53
Wilkinson, D. T. 1987, in *13th Texas Symposium on Relativistic Astrophysics*, M. P. Ulmer, ed., (Singapore: World Scientific), p209
Williams, R. E. 1967, ApJ, 147, 556
Williams, R. E. 1992, ApJ, 392, 99

15 REFERENCES

- Wills, B., Netzer, H., & Wills, D. 1985, *ApJ*, 288, 94
- Wing, W.H., & MacAdam, K.B., 1978, in *Progress in Atomic Spectroscopy*, Part A, W. Hanle & H. Kleinpopper, eds
- Winslow, A. M. 1975, Lawrence Livermore Lab. report UCID-16854
- Wishart, A. W. 1979, *MNRAS*, 187, 59p
- Wolfire, M. G., Tielens, A., & Hollenbach, D. 1990, *ApJ*, 358, 116
- Worral et al. 1987, *ApJ*, 313, 596
- Wyse, A. B. 1941, *PASP*, 53, 184
- York, D. G., Meneguzzi, M., & Snow, T. 1982, *ApJ*, 255, 524
- Xu, Y., & McCray, R. 1991, *ApJ*, 375, 190
- Zamorani, G., et al. 1981, *ApJ*, 245, 357
- Zheng, W., Kriss, G.A., Telfer, R.C., Grimes, J.P. & Davidsen, A.F. 1997, *ApJ*, 475, 469
- Zuckerman, B. 1973, *ApJ*, 183, 863
- Zycki, P. T., Krolik, J. H., Zdziarski, A. A., & Kallman, T. R. 1994, 437, 597
- Zygelman, B., & Dalgarno, A. 1990, *ApJ*, 365, 239

16 INDEX

— A —

abundances
 ionic, 280
 acceleration. see radiative
 acceleration
 adiabatic cooling. see expansion
 cooling
 age command, 202
 air vs vacuum wavelengths, 226
 Alfvén velocity, 316
 aluminum, 286
 astronomical unit, 330
 atomic mass, 224
 atomic weight, 224, 280
 AU
 radius, 330
 Auger effect, 276, 281
 averaging over terms, 233

— B —

b parameter, 223
 background
 cosmic ray, 318
 Be-sequence cooling, 302
 Bethe-Block approximation, 317
 blackbody
 definition, 213
 evaluated, 213
 Bohr radius, 231, 329
 Boltzmann factor
 continuum, 210
 line, 222
 Born approximation, 231
 bound-free
 opacity, 220
 Bowen OI, 285
 bremsstrahlung
 cooling, 296
 heating, 296
 opacity, 219

— C —

calcium, 286
 carbon, 282
 charge transfer
 heavy element, 278
 Cloudy
 charge transfer uncertainties, 204
 continuous opacity, 204
 density range, 205
 molecules, 205
 radiative transport, 206
 recombination uncertainties, 203
 temperature range, 205
 time steady assumption, 202
 uncertainties, 203
 validity range, 202
 collision rate, 231
 detailed balance, 244
 ionization, 277
 collision strengths
 averaging, 233
 defined, 231
 g-bar, 232
 Compton

bound heating, 296
 bound ionization, 246, 296
 cooling
 calculated, 293
 energy exchange
 accuracy, 294
 methods, 293
 heating
 calculated, 293
 continuous heavy element
 opacity, 288
 continuum
 arrays, 210
 binning, 209, 278
 Boltzmann factor, 210
 cell width, 211
 changing resolution, 209
 ConLocInter, 211
 ConOutInter, 211
 described, 209
 emission, 252
 energy bounds, 209
 energy pointer, 210
 fluorescence, 228
 frequencies saved, 210
 frequency array, 210
 generation, 212
 high energy limit, 209
 ionization edge pointers, 210
 low energy limit, 209
 mesh defined, 209
 occupation number, 211
 opacity, 217
 optical depth, 212
 OTS, 212, 216
 outward only, 217
 photon flux, 211, 212
 plasma frequency, 220
 pointers, 210
 range, 209
 summed, 212
 conversion factors, 214
 cooling
 adiabatic, 296
 Be-sequence atoms, 302
 collisional, 298
 Compton, 293, 295
 cyclotron, 315
 definition, 292
 derivative, 303
 evaluation, 303
 expansion, 296
 free-free, 297
 grain, 311, 312
 H-, 298
 heavy elements, 299
 hydrodynamic, 296
 hydrogen recombination, 243
 induced, 297
 n level atoms, 301
 recombination, 242, 297
 tests, 304
 three level atoms, 299
 two level atoms, 299
 cosmic ray, 316

background, 318
 physics, 316
 range, 317
 cosmic ray command, 318
 cosmological distance, 328
 cosmology
 distance, 327
 critical density, 232

— D —

damping constant
 defined, 227
 stored, 236
 density
 cosmic ray, 316
 H-, 264
 LTE, 263
 H2
 LTE, 264
 hydrogen
 LTE, 241
 molecules, 263
 range, 205
 wind law, 324
 derivative
 cooling, 303
 heating, 304
 destruction probability
 line
 complete, 227
 diffuse fields
 evaluated, 211
 diffuse OTS command, 216
 diffuse outward command, 217
 dissociation energy
 H-, 264
 H2, 263
 H2+, 263
 distance
 from redshift, 327
 Doppler b parameter, 223
 Doppler width
 computed, 223
 dumping
 line, 237
 dust. see grain
 dyn, 321

— E —

Earth
 radius, 330
 Eddington limit, 327
 Einstein coefficients, 224
 electron
 mean speed, 315
 non-thermal secondaries, 325
 secondary ionization, 325
 supra-thermal, 325
 temperature. see temperature
 element
 abundances stored, 280
 chemical symbols, 280
 ionization stage symbols, 280
 names, 280, 281

periodic table, 276
 energy density
 gas, 322
 magnetic, 315
 escape probability
 heavy element, 235
 line, 226
 complete, 227
 incomplete, 227
 maser, 228
 excitation energy, 222
 excitation temperature, 237
 expansion cooling, 296

— F —

filling factor, 324
 fluorescence
 continuum, 228
 yields, 281
 free-free
 cooling, 296
 H-, 298
 gaunt factor, 219
 heating, 296
 H-, 298
 opacity, 219
 free-free cooling
 plasma frequency, 297

— G —

gas
 energy density, 322
 equation of state, 322
 heat content, 322
 pressure, 322
 gaunt factor
 free-free, 219
 g-bar approximation, 232, 235
 geometry
 closed expanding, 230
 closed static, 230
 open, 230
 wind, 230
 glossary
 symbols, 329
 grain, 307
 absorption efficiency factor, 308
 area, 308
 collisional charging, 310
 drift velocity, 311
 exist?, 313
 gas cooling, 312
 gas heating, 312
 heating and cooling, 311
 ionic recombination, 313
 opacity, 307
 photoelectric emission, 308
 potential, 311
 temperature, 312
 variables, 313

— H —

Hartree, 214
 heating
 bound Compton, 296
 bremsstrahlung, 296
 collisional ionization, 297
 Compton, 293, 295
 continuum, 209
 cosmic ray, 317

definition, 292
 derivative, 304
 evaluated, 304
fine structure lines, 299
 free-free, 296, 297
 grain, 308, 310, 311, 312
 H-, 298
 heating array, 304
 line, 304
 photoelectric, 297
 tests, 304
 total
 evaluated, 304
 heavy element
 abundances stored, 280
 atomic weights, 280
 Auger ejection, 276, 281
 charge transfer, 278
 chemical symbols, 280
 collisional ionization, 277
 fluorescence yields, 281
 ionization pointers, 278, 281
 ionization potentials, 278
 ionization stored, 280
 labels for lines, 237
 limits, 205
 line transfer, 235
 molecules, 272
 names, 280, 281
 number of subshells, 279
 opacity offsets, 278
 overview, 275
 photoionization cross section, 276
 photoionization rates
 stored, 281
 recombination
 dielectronic, 277
 grain surface, 313
 radiative, 277
 reliability, 290
 shell number, 281
 helium
 statistical weight, 252
 hydrodynamic cooling, 296
 hydrogen
 balance equations, 244
 Boltzmann factors, 242
 collisional ionization, 245
 collisional rate equations, 244
 density
 LTE, 241
 emission, 252
 H-, 264
 H₂, 269
 HeH⁺, 269
 induced recombination, 246
 ionization energies, 242
 ionization solution, 244
 level energies, 242
 molecules, 263
 negative ion, 264
 oscillator strengths, 251
 overview, 204
 radiative rate equations, 246
 recombination coefficients, 242
 elements defined, 244
 recombination cooling, 242
 statistical weight, 241, 252
 three body recombination, 245

transition probabilities, 251
 hydrogenic line, 235

— I —

induced emission probability, 225
 induced recombination, 246
 infinite loop. see unending loop
 ionic abundances, 280
 ionization potential
 density, 278
 elements, 278
 pointers, 278
 ionization stage trimming, 291
 iron, 287
 isoelectronic sequence, 281

— J —

Jeans length, 327
 Jeans mass, 327

— L —

labels for lines, 237
 level 1 line, 235, 237
 level 2 line, 235, 237
 levels
 averaging, 233
 line
 adding level 1 lines, 238
 air vs vacuum wavelengths, 226
 array
 printing, 237
 Boltzmann factor, 222
 closed expanding geometry, 230
 closed static geometry, 230
 correction for stimulated
 emission, 222
 dumping, 237
 energy pointer, 210
 escape probability, 226
 excitation temperature, 237
 fine structure heating, 299
 g-bar approximation, 235
 heating, 304
 hydrogenic, 235
 label
 generating, 237
 level 1, 235, 237
 level 1 data file, 238
 level 2, 235, 237
 masing, 299
 open geometry, 230
 optical depth, 222
 optical depth arrays, 230
 outward, 211
 pointer, 210
 radiation pressure, 318
 redistribution function, 235
 reflected, 211
 source function, 226
 spectroscopic designation, 237
 thermalization length, 233
 width, 223
 wind geometry, 230
 line cooling. see cooling
 loop. see infinite loop
 LTE
 H- density, 263
 H departure coefficient, 241
 H level population, 241
 H₂ density, 264

- luminosity
 distance, 327
 Eddington, 327
 sun, 329
- M —
- magnesium, 285
 magnetic field
 pressure, 315
 maser
 correction for stimulated
 emission, 222
 escape probability, 228
 mass
 AMU, 329
 electron, 329
 Jeans', 330
 proton, 330
 sun, 330
 mean speed
 electron, 315
 Milne relation, 242, 252
 molecules, 205, 261
 heavy element, 272
 hydrogen, 263
- N —
- neon, 285
 nitrogen, 284
- O —
- occupation number
 array, 211
 continuum, 234
 defined, 211
 definition, 213
 pumping rate, 225
 summed continuum, 212
 OI fluorescence, 285
 opacity, 217
 absorption array, 212
 arrays, 217
 background line, 227
 bound-free, 220
 free-free, 219
 heavy element continuous, 288
 permitted line, 225
 pointers, 217
 Rayleigh scattering, 219
 scattering array, 212
 stimulated emission, 222
 optical depth
 arrays, 230
 closed geometry, 230
 continuum, 212, 220
 correction for stimulated
 emission, 222
 grain, 308
 line, 222
 line center, 222
 line center vs mean, 224
 mean vs line center, 224
 open geometry, 230
 stimulated emission, 222
 wind, 230
 oscillator strength, 222
 absorption, 222
 emission, 222
 OTS fields
 described, 216
- outward-only approximation, 217
 oxygen, 284
- P —
- parsec, 330
 periodic table, 276
 photoionization
 cross sections, 276
 fluorescence yields, 281
 rates evaluated, 218
 rates stored, 281
 Planck function. *see* blackbody
 plasma frequency, 220
 free-free cooling, 297
 pointers
 generating, 210
 heavy element continua, 278
 pressure
 compared, 316
 convergence, 323
 dynamic, 322
 gas, 322, 323
 integrated continuum, 323
 magnetic, 315
 radiation, 323
 ram, 316, 322
 total, 322
 turbulent, 322
 units, 321
 variables and routines, 323
 proper distance, 328
- R —
- radiation pressure, 323
 line, 318
 radiative acceleration
 computed, 321
 radiative transport
 methods, 206
 radius
 AU, 330
 Earth, 330
 sun, 330
 ram pressure, 316
 Rayleigh scattering, 219, 321
 recombination
 arrays, 244
 coefficients, 244
 cooling, 242
 efficiency, 244
 grain surface, 313
 hydrogenic, 242, 244
 induced, 246
 radiative rates, 277
 redshift
 distance, 327
 reliability, 207
 routine
 abscf, 223
 AddOpac, 217
 beseq, 302
 BiDiag, 291
 boltgn, 210
 cfit, 277
 chIonLbl, 237
 chLineLbl, 237
 ColStrGBar, 232
 ContCreatePointers, 209
 coolr, 303
- CreateData, 239
 CreatePoint, 281
 csphot, 218
 DumpLine, 237
 eina, 225
 EinstA, 251
 escmase, 228
 ffun, 212
 ffun1, 212
 fosc, 251
 GammaBn, 218
 GammaK, 218
 GammaPrt, 218
 gffsub, 219
 HCTIon, 278
 HCTRecom, 278
 highen, 293, 296
 hmole, 263, 313
 hrcf, 251
 ipContEnergy, 210
 ipFindLevLine, 239
 ipLineEnergy, 210
 ipoint, 210
 ipShells, 281
 level2, 299
 level3, 299
 LevelN, 301
 LimitSh, 279
 MakeCharTran, 278
 MakeLevLines, 239
 oilevl, 285
 OpacityCreateAll, 217
 p8446, 285
 phfit, 276
 Plonte, 323
 Plankf, 213
 presur, 323, 324
 PutCS, 239
 PutLine, 239
 radinc, 323
 rrfit, 277
 RTDiffuse, 211
 RTMake, 235
 RTMakeStat, 235
 RTMakeWind, 235
 SumContinuum, 212
 SumCool, 303, 304
 SumHeat, 304
 tauff, 297
 TexcLine, 237
 TotalPressure, 323
 velset, 223
 Rydberg unit, 213
- S —
- Saha equation
 arbitrary species, 261
 ions, 263
 molecular hydrogen, 263
 secondary ionization
 physics, 325
 routines, 325
 variables, 325
 shell number, 281
 Sobolev approximation, 324
 solar luminosity, 329
 solar mass, 330
 solar radius, 330
 speed

electron, 315
 stability
 thermal, 292
 Stark broadening, 229
 statistical weight
 H-, 264
 H2, 263
 H2+, 263
 helium, 252
 Ho, 264
 hydrogen, 252
 stimulated emission
 optical depths corrected for, 222
 sun
 effective temperature, 330
 luminosity, 329
 mass, 330
 radius, 330
 supra-thermal ionization. *See*
 secondary ionization

— T —

temperature
 excitation, 237
 grain, 312
 line excitation, 237
 LTE limit, 304
 range, 205
 sun effective, 330
 terms
 averaging, 233
 thermal stability, 292
 thermalization length, 233
 three level atoms, 299
 time dependent command, 202
 timescale
 H2 formation, 202
 recombination, 202
 transition probability, 224
 averaging, 233
 turbulence, 223
 two level atoms, 299

— U —

unending loop. *see* loop

— V —

van Regemorter approximation,
 232
 variable
 amu, 280
 anu, 210, 294
 AnuOrg, 210
 AovTot, 237
 AtomicWeight, 224, 280
 Aul, 237
 avdft, 313
 boltzmann, 215
 chargt, 291
 chContLabel, 210
 chElementName, 280
 chElementNameShort, 281
 chElementSym, 280
 chIonRoman, 280
 chIonStage, 280
 chLineLabel, 210
 ColOvTot, 236
 ColUL, 235
 ConLocInter, 211
 ConOutInter, 211

ConOutNoInter, 211
 ContBoltz, 210
 cooling, 303
 create, 291
 cs, 236
 csigc, 293
 csigh, 293
 csupeff, 326
 csupra, 325
 ctot, 303
 damp, 236
 damprel, 236
 darea, 314
 destroy, 291
 doppler, 223
 dsize, 314
 dstab1, 313
 dstdft, 313
 dstfac, 314
 dston1, 313
 dstpot, 313
 dstq, 313
 dstsc, 313
 dstsc1, 313
 dTau, 236
 dustp, 313
 dwork, 314
 e2TauAbs, 212
 eev, 314
 efionz, 325, 326
 egamry, 209
 emm, 209
 en1ryd, 215
 EnergyErg, 236
 EnergyK, 236
 EnergyRyd, 236
 EnergyWN, 236
 eVdegK, 215
 evRyd, 215
 exctef, 325, 326
 ExpmTau, 212
 ExpZone, 212
 flux, 211, 294
 FluxFaint, 209
 Fraclnwd, 236
 gf, 236
 gHi, 236
 gionrc, 313
 gLo, 236
 halfte, 304
 hcbolt, 242
 HCharExclon, 278
 HCharExcRec, 278
 heat, 236
 heatef, 325
 heating, 304
 heatnt, 303
 hgamnc, 246
 hlbolt, 242
 hrec, 244
 htot, 304
 HydroLines, 235
 IonStd, 235
 ipCont, 235
 ipElement, 278
 ipHeavy, 279
 ipLnCS1, 232, 237
 ipLnCS2, 237
 ipSeclon, 325

IgDustOn, 313
 limLevelN, 301
 ndpts, 314
 ndust, 313
 nelem, 235
 nflux, 209
 nsShells, 279
 nupper, 209
 OccNumbDiffCont, 211
 OccNumbIncidCont, 211
 OccNumbIncidCont, 211
 opac, 212, 217
 opacity, 236
 OpacStack, 217
 ophf, 244
 ots, 237
 otscon, 212, 217
 otslin, 212, 217
 outline, 211
 Pdest, 236
 perror, 323
 Pesc, 236
 pgas, 323
 PhotoRate, 281
 photos, 236
 pinteg, 323
 pnow, 323
 PopHi, 236
 PopLevels, 303
 PopLo, 236
 PopOpc, 236
 prad, 323
 presok, 323
 pump, 236
 RecomRate, 291
 reflin, 211
 sab, 314
 scatop, 212, 217
 sqabs, 313
 sqscat, 313
 sse, 314
 sublimat, 313
 SummedCon, 212
 SummedDif, 212
 SummedOcc, 212
 TauAbsFace, 212
 TauCon, 235
 TauDmmy, 299
 TauIn, 235
 TauLine2, 235
 TauLines, 235
 TauScatFace, 212
 TauScatFace, 212
 TauTot, 235
 TauTotalGeo, 212
 te1ryd, 215
 tedust, 314
 tmn, 219
 tsq1, 304
 WavnNKelv, 215
 WavnNRyd, 215
 widflx, 211
 WLAng, 236
 x12, 325
 xIntensity, 236
 xIonFrac, 280
 yield, 281
 velocity
 Alfvén, 316

average speed, 223
b parameter, 223
Doppler width, 223
electron, 315
mean speed, 310
most probable speed, 223
stored, 223

thermal, 223
Voigt function, 224
— W —
wavenumber, 231
wind, 323
density vs radius, 324

line transfer, 324
— Z —
zone
attenuation, 217